

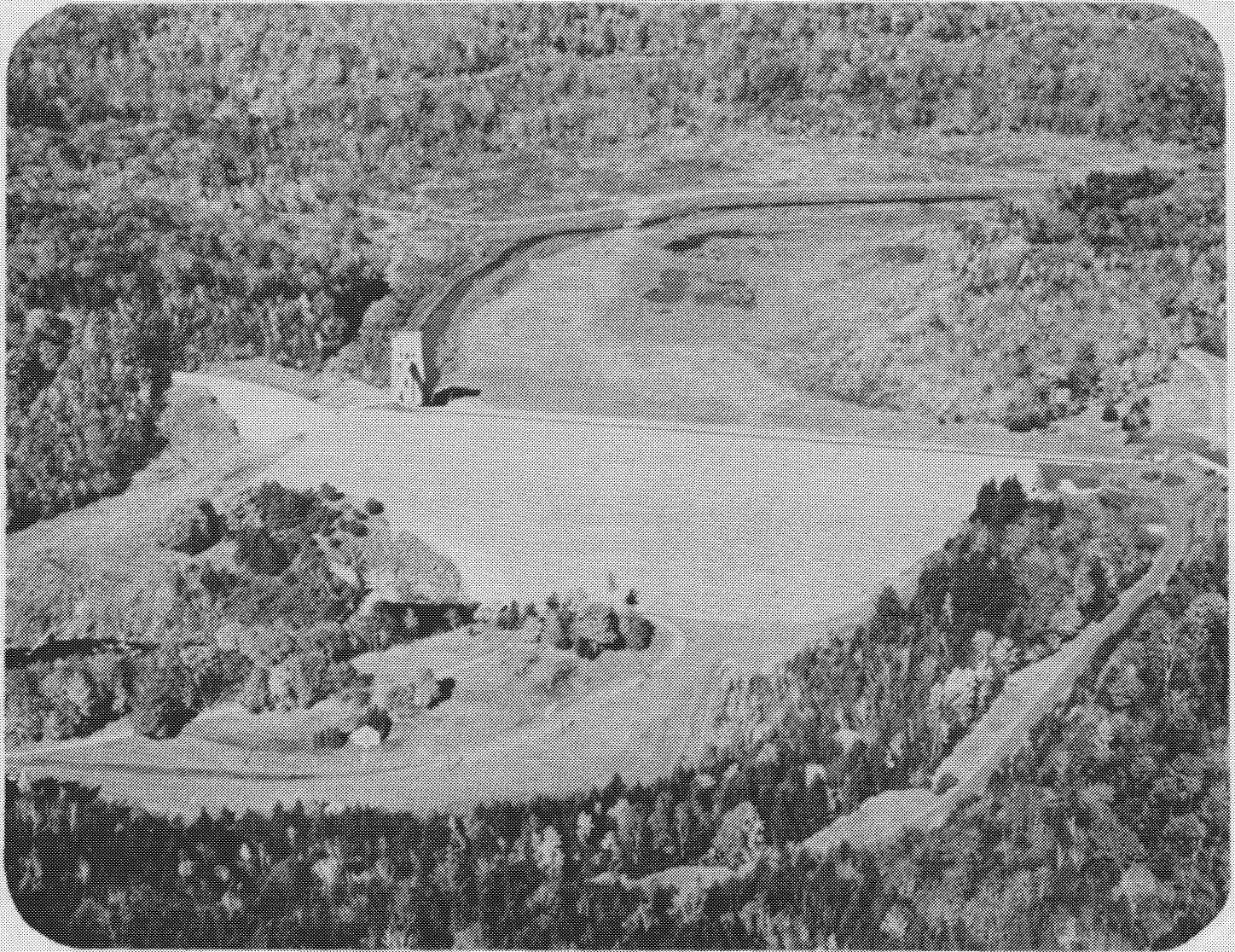


U.S. Army
Corps of Engineers
New England Division

DYNAMIC ANALYSIS OF KNIGHTVILLE DAM

FINAL REPORT

DECEMBER, 1982



Knightville Dam, Huntington, Massachusetts

DYNAMIC ANALYSIS OF KNIGHTVILLE DAM

FINAL REPORT

**PREPARED FOR
U.S. ARMY CORPS OF ENGINEERS
NEW ENGLAND DIVISION**



DECEMBER, 1982

VOLUME 1

FINAL REPORT
DYNAMIC ANALYSIS
OF KNIGHTVILLE DAM

<u>CONTENTS</u>	<u>PAGE</u>
LIST OF TABLES	vi
LIST OF PLATES	vii
LIST OF SYMBOLS	xi
SUMMARY	1
I. INTRODUCTION	
A. AUTHORIZATION.....	I-1
B. PURPOSE AND SCOPE.....	I-2
II. DESCRIPTION OF PROJECT	
A. GENERAL	II-1
B. EMBANKMENT	II-1
C. OUTLET WORKS	II-4
1. Intake Channel	II-4
2. Intake Tower	II-6
3. Service Bridge	II-6
4. Tunnel and Outlet Portal	II-6
D. SPILLWAY	II-8
E. PERTINENT DATA	II-8
III. FIELD TESTING PROGRAM	
A. GENERAL	III-1
B. EXPLORATION AND SAMPLING PROGRAM	III-1
1. Exploration	III-1
2. Sampling	III-5
3. Subsurface Conditions	III-8
C. SEISMIC WAVE VELOCITY MEASUREMENT INVESTIGATION	III-12
1. General	III-12
2. Procedure and Measurement	III-12
a. Cross-hole	III-12
b. Down-hole	III-15
c. Surface waves	III-16
3. Results of Wave Velocity Measurement Investigation	III-17

IV.	GEOLOGICAL AND SEISMOLOGICAL INVESTIGATION	
A.	REGIONAL GEOLOGY	IV-1
1.	Physiography	IV-1
2.	Surficial Geology	IV-4
3.	Bedrock Geology	IV-5
a.	Paleozoic Rocks	IV-7
b.	Igneous Intrusions	IV-9
4.	Structural Geology	IV-10
a.	Folding	IV-10
b.	Faulting	IV-12
5.	Regional Seismicity	IV-12
B.	SITE GEOLOGY	IV-13
1.	Physiography	IV-13
2.	Surficial Geology/Foundation Conditions .	IV-15
3.	Bedrock Geology	IV-17
a.	Mica Schist	IV-17
b.	Quartzitic Schist	IV-20
c.	Pegmatite	IV-20
4.	Structural Geology	IV-21
5.	Local Seismicity	IV-22
V.	SELECTION OF DESIGN EARTHQUAKE	
A.	SEISMIC HAZARD ANALYSIS	V-1
1.	Regional Events (50 to 215 km)	V-2
a.	Maximum Credible Earthquake	V-2
b.	Operating Basis Earthquake	V-4
2.	Local Events (\leq 50 km)	V-5
a.	Maximum Credible Earthquake	V-5
b.	Implications of the Strong Motion Data from the Gaza, New Hampshire Earthquake (January, 1982)	V-5
c.	Operating Basis Earthquake	V-9
B.	DESIGN EARTHQUAKES	V-9
1.	Regional Event	V-9
a.	Ground Motions	V-9
b.	Strong Motion Record	V-10
2.	Local Event	V-13
a.	Ground Motions	V-13
b.	Strong Motion Record	V-13

VI. STATIC AND DYNAMIC LABORATORY TESTING PROGRAM

A. GENERAL	VI-1
B. SOIL CLASSIFICATION AND INDEX PROPERTIES	VI-2
1. Soil Classification	VI-2
2. Index Properties	VI-3
a. Hydraulic Core	VI-3
b. Hydraulic Shell	VI-6
C. STATIC TESTING PROGRAM	VI-7
1. General	VI-7
2. Sample Preparation	VI-9
a. Hydraulic Core	VI-9
b. Hydraulic Shell	VI-9
3. Consolidated-Undrained Triaxial Compression (R) Tests	VI-10
a. General	VI-10
b. Procedure	VI-10
c. Results	VI-12
4. Consolidated-Drained Triaxial Compression (S) Tests	VI-17
a. General	VI-17
b. Procedure	VI-17
c. Results	VI-17
5. One-Dimensional Consolidation Tests	VI-19
D. DYNAMIC TESTING PROGRAM	VI-20
1. General	VI-20
2. Sample Preparation	VI-20
a. Hydraulic Core	VI-20
b. Hydraulic Shell	VI-20
3. Cyclic Triaxial ($C\bar{R}-\bar{R}$ and $C\bar{R}$) Tests	VI-21
a. General	VI-21
b. Procedure	VI-21
c. Results	VI-23
4. Resonant Column (RC) Tests	VI-36
a. General	VI-36
b. Procedure	VI-36
c. Results	VI-37
5. Small Strain Triaxial Tests	VI-41
a. General	VI-41
b. Procedure	VI-41
c. Results	VI-42

CONTENTS (Cont'd)

PAGE

VII. STATIC STATE OF STRESS ANALYSIS

A. GENERAL	VII-1
B. METHOD OF ANALYSIS	VII-1
C. SECTIONS ANALYZED	VII-1
D. STRESS-STRAIN AND MATERIAL PROPERTIES	VII-4
E. RESULTS OF STATIC ANALYSIS	VII-14

VIII. DYNAMIC ANALYSIS

A. GENERAL	VIII-1
B. FAILURE CRITERION	VIII-1
C. SIMPLIFIED ANALYSIS - SEED AND IDRIS PROCEDURE	VIII-2
1. General	VIII-2
2. Method of Analysis	VIII-3
3. Results of Simplified Analysis	VIII-4
D. ONE-DIMENSIONAL ANALYSIS	VIII-8
1. General	VIII-8
2. Method of Analysis	VIII-8
3. K ₂ (Max) Determination	VIII-9
4. Results of One-Dimensional Analysis ...	VIII-11
E. TWO-DIMENSIONAL FINITE ELEMENT ANALYSIS	VIII-18
1. General	VIII-18
2. Method of Analysis	VIII-18
3. Input Parameters	VIII-19
4. Results of Two-Dimensional Analysis ...	VIII-20

IX. SEISMIC STABILITY AND PERMANENT
 DEFORMATION ANALYSIS

A. GENERAL	IX-1
B. MAKDISI AND SEED SIMPLIFIED METHOD	IX-3
1. General	IX-3
2. Step #1: Critical Yield Acceleration Determination	IX-4
3. Step #2: Determination of Earthquake Induced Acceleration	IX-6
4. Step #3: Determination of Permanent Displacement	IX-7
C. SARMA STABILITY/COE DEFORMATION ANALYSIS ...	IX-10
1. General	IX-10
2. Sarman Stability Analysis	IX-10
3. Permanent Deformation	IX-14

CONTENTS (Cont'd)

PAGE

X.	SUMMARY, CONCLUSIONS AND RECOMMENDATIONS	
A.	SUMMARY AND CONCLUSIONS	X-1
1.	Liquefaction Potential	X-1
2.	Permanent Deformation	X-1
B.	RECOMMENDATIONS	X-2
XI.	REFERENCES	XI-1
APPENDICES		

LIST OF TABLES

<u>No.</u>		<u>Page No.</u>
1.	Summary of Pertinent Data	II-10
2.	Summary of Borehole Locations	III-4
3.	Summary of Exploration and Sampling Quantities	III-7
4.	Significant Earthquakes within the Knightville Dam Study Area	IV-26
5.	Acceleration for Maximum Credible Earthquakes within the Knightville Dam Study Area	V-3
6.	Strong Motion Records from Gaza, N.H. Earthquake	V-6
7.	Summary Table of Recommended Free-Field Rock Ground Motions	V-11
8.	Summary of Cyclic Load Triaxial Test Data (Hydraulic Core)	VI-24
9.	Summary of Cyclic Load Triaxial Test Data (Hydraulic Shell)	VI-26
10.	Summary of the Hyperbolic Parameters (From Duncan, Wong and Ozawa, 1980)	VII-7
11.	Soil Parameters Used in Non-linear Static Analysis - FEADAM	VII-12
12.	Determination of $K_2(\max)$ from Field Data and Laboratory Test Data for SHAKE Analyses	VIII-10
13.	Selected Strength Parameters	IX-11

LIST OF PLATES

<u>Plate No.</u>	<u>Title</u>	<u>Page No.</u>
1	Vicinity Map	II-2
2	General Project Features	II-3
3	Photographs of Embankment Section	II-5
4	Photographs of Outlet Works	II-7
5	Photographs of Spillway Section	II-9
6	Results of Pre-Construction Field Testing Program	III-2
7	Boring Location Plan	III-3
8	Results of Field Testing Program: Crest	III-9
9	Results of Field Testing Program: Downstream Slope	III-11
10	Layout for Seismic Investigation	III-13
11	Regional Physiographic Provinces	IV-2
12	Regional Bedrock Geology	IV-6
13	Regional Structural Geology	IV-8
14	Regional Seismicity Map	IV-14
15	Geologic Section and Test Data	IV-16
16	Site Outcrop Map	IV-18
17	Historical Seismicity (1568 to 1975) of Study Area	IV-23
18	Instrumental Seismicity (1975 to 1981) of Study Area	IV-24
19	Gaza, N.H. Earthquake Data	V-8
20	Puddingstone Reservoir Strong Motion Record	V-12
21	Golden Gate Park Strong Motion Record	V-14

LIST OF PLATES (Cont'd)

<u>Plate No.</u>	<u>Title</u>	<u>Page No</u>
22	Response Spectrum, $A_{\max} = 0.204g$	V-16
23	Response Spectrum, $A_{\max} = 0.086g$	V-17
24	Engineering Properties of Hydraulic Core	VI-4
25	Gradation Limits of Hydraulic Shell Material	VI-8
26	Typical Results of \bar{R} Tests	VI-13
27	Results of Static Strength Tests on "Undisturbed" Core Material	VI-14
28	Results of Static Strength Tests on Compacted Shell Material	VI-15
29	Typical Results of S Tests	VI-18
30	Typical $\bar{C}R$ Test Results (Hydraulic Core)	VI-29
31	Typical $\bar{C}R$ Test Results (Hydraulic Shell)	VI-30
32	Cyclic Stress Conditions Causing 5% and 10% Axial Strain (Hydraulic Core)	VI-32
33	Cyclic Stress Conditions Causing 5% and 10% Axial Strain (Hydraulic Shell)	VI-33
34	Comparison of Laboratory Test Results	VI-35
35	Shear Modulus and Damping Versus Strain (Hydraulic Core)	VI-39
36	Shear Modulus and Damping Versus Strain (Hydraulic Shell)	VI-40
37	Embankment Cross-Section Used for Dynamic Analysis	VII-3
38	Finite Element Grid Used for FEADAM and FLUSH, Station 8+50	VII-5
39	Finite Element Grid Used for FEADAM and FLUSH, Station 4+82	VII-6
40	Transformed Stress-Strain Data	VII-9
41	Determination of Elastic Parameters	VII-10
42	Determination of Bulk Modulus Parameters	VII-11

LIST OF PLATES (Cont'd)

<u>Plate No.</u>	<u>Title</u>	<u>Page No.</u>
43	Results from FEADAM, Station 8+50	VII-15
44	Results from FEADAM, Station 8+50	VII-16
45	Results from FEADAM, Station 4+82	VII-17
46	Results from FEADAM, Station 4+82	VII-18
47	Charts for Determination of Liquefaction Potential Using Simplified Method	VIII-5
48	Liquefaction Potential of Core Based on Simplified Procedure	VIII-6
49	Results of One-Dimensional Analysis Using SHAKE, Station 8+50; Crest	VIII-12
50	Results of One-Dimensional Analysis Using SHAKE, Station 8+50; Upstream Slope	VIII-13
51	Results of One-Dimensional Analysis Using SHAKE, Station 4+82; Crest	VIII-14
52	Results of One-Dimensional Analysis Using SHAKE, Station 4+82; Upstream Slope	VIII-15
53	Average Superimposed Shear Stress Versus Cyclic Shear Resistance at Elevation 555, Station 8+50	VIII-22
54	Average Superimposed Shear Stress Versus Cyclic Shear Resistance at Elevation 575, Station 8+50	VIII-23
55	Average Superimposed Shear Stress Versus Cyclic Shear Resistance at Elevation 590, Station 8+50	VIII-24
56	Average Superimposed Shear Stress Versus Cyclic Shear Resistance at Elevation 567, Station 4+82	VIII-25
57	Average Superimposed Shear Stress Versus Cyclic Shear Resistance at Elevation 585, Station 4+82	VIII-26
58	Zone of Liquefaction Determined from FLUSH, Stations 8+50 and 4+82	VIII-28
59	Elements of The Newmark Sliding Block Analysis	IX-2

LIST OF PLATES (Cont'd)

<u>Plate No.</u>	<u>Title</u>	<u>Page No.</u>
60	Seismic Stability Analysis Using Makdisi and Seed Simplified Procedure	IX-5
61	Induced Permanent Deformation, Simplified Analysis	IX-8
62	Permanent Deformation Analysis Using Sarma Method, Station 8+50	IX-12
63	Permanent Deformation Analysis Using Sarma Method, Station 4+82	IX-13
64	Displacement Versus $k_y g/A_{max}$	IX-16
65	Maximum Accelerations Through Embankment, Station 8+50	IX-18
66	Maximum Accelerations Through Embankment, Station 4+82	IX-19

LIST OF PERTINENT SYMBOLS

A	=	coefficient of acceleration of a rectangular pulse
A _{max}	=	maximum acceleration at the center of the potential sliding mass
B	=	Skempton's pore pressure coefficient; also bulk modulus
C _c	=	compression index
c _v	=	coefficient of consolidation
CR	=	consolidated-undrained cyclic load triaxial test with pore pressure measurement
CR-R	=	consolidated-undrained cyclic load triaxial test followed by undrained monotonic load triaxial test - both phases with pore pressure measurement
C _N	=	correction factor for effective overburden pressure
D	=	damping ratio or total height of embankment section
E	=	consolidated-undrained small strain cyclic triaxial test
E _i	=	initial Young's modulus
f	=	subscript used to denote that stress is on the specimen failure plane
{F}	=	forces acting at ends of slice analyzed in 2-D dynamic analysis
G	=	shear modulus
G _{max}	=	maximum shear modulus

LIST OF PERTINENT SYMBOLS
(continued)

G_s	=	specific gravity of solids
g	=	acceleration of gravity
h	=	total height of embankment
Hz	=	Hertz (cycles per second)
K	=	horizontal earthquake acceleration coefficient or modulus number for static state of stress analysis, or effective principal stress ratio, or stiffness matrix for 2-D dynamic analysis
K_b	=	bulk modulus number for static state of stress analysis
K_c	=	principal stress ratio at end of consolidation
K_{max}	=	maximum average yield acceleration of sliding mass for Makdisi and Seed's simplified analysis
KW	=	pseudo-static earthquake force
k	=	coefficient of yield acceleration of sliding block for Newmark's sliding block analysis
k_y	=	critical yield acceleration
K_{2max}	=	maximum stiffness coefficient for computing G_{max}
LL	=	liquid limit
LIR	=	load increment ratio
MMI or M	=	Modified Mercalli earthquake Intensity
m_b	=	body magnitude of earthquake

LIST OF PERTINENT SYMBOLS
(continued)

$[M]$	= mass matrix for 2-D dynamic analysis
m	= bulk modulus exponent
$\{m\}$	= vector related to mass matrix for 2-D dynamic analysis
n	= modulus exponent
N	= number of cycles or SPT blow counts
N_{eq}	= equivalent number of cycles
\bar{N}_{eq}	= average equivalent number of cycles
N_1	= modified penetration resistance - blows/ft
p_{ga}	= peak ground acceleration
P_a	= atmospheric pressure
PI	= plasticity index
R_f	= failure ratio
\bar{R}	= consolidated-undrained, monotonic load triaxial test with pore pressure measurement
RC	= resonant column test
S	= consolidated-drained, monotonic load triaxial test with volume change measurements
T_o	= first natural period of embankment
$\{T\}$	= forces related to energy transmission for FLUSH program
u	= pore pressure
u_c	= pore pressure at completion of consolidation (same as back pressure)

LIST OF PERTINENT SYMBOLS
(continued)

U	= permanent displacement
\ddot{U}_{\max}	= maximum crest acceleration
$\{u\}$	= nodal point displacement for 2-D dynamic analysis
$\{\ddot{u}\}$	= nodal point acceleration for 2-D dynamic analysis
V_s	= shear wave velocity
V_p	= compression wave velocity
V_R	= Rayleigh wave velocity
$\{V\}$	= forces originating from viscous boundaries analyzed in 2-D dynamic analysis
y	= distance to failure surface in Sarma/COE analysis and vertical distance to center of gravity of sliding mass in Makdisi-Seed analysis
\ddot{y}	= input acceleration time history for 2-D dynamic analysis
β	= angle measured from horizontal to assumed sliding surface of wedge
ϵ_a	= axial strain
γ_d	= dry unit weight
γ_t	= total unit weight of soil
γ'	= submerged unit weight
γ_{sa}	= single amplitude shear strain
λ	= damping factor
c	= value of shear stress at zero total stress

LIST OF PERTINENT SYMBOLS
(continued)

c'	=	value of shear stress at zero effective stress
ϕ	=	angle of shearing resistance in terms of total stress
ϕ'	=	angle of shearing resistance in terms of effective stress
$\bar{\sigma}_c$	=	effective isotropic consolidation stress
$\bar{\sigma}_1$	=	effective major principal stress
$\bar{\sigma}_3$	=	effective minor principal stress
$\bar{\sigma}_{1c}$	=	consolidated, effective major principal stress
$\bar{\sigma}_{3c}$	=	consolidated, effective minor principal stress
$\sigma_1 - \sigma_3$	=	applied deviator stress
$\bar{\sigma}_{ff}$	=	effective normal stress on failure surface at failure
$\bar{\sigma}_{fc}$	=	effective normal stress on failure surface at end of consolidation
σ_d	=	cyclic deviator stress
τ_f	=	shear stress on failure surface
τ_{fc}	=	consolidated shear stress on failure surface
τ_{fy}	=	cyclic shear resistance on failure plane
ρ	=	mass density
ν	=	Poisson's ratio

FINAL REPORT
DYNAMIC ANALYSIS OF
KNIGHTVILLE DAM

SUMMARY

Knightville Dam is located on the Westfield River, approximately 4½ miles north of the town of Huntington, Massachusetts. This dam is a 1200-foot long hydraulic fill structure having a maximum height of 160 feet. The embankment consists primarily of three earth zones: a central relatively fine grained core zone, upstream and downstream hydraulic shell zones, and an upper impervious fill zone. The dam is owned and operated by the U.S. Army Corps of Engineers, New England Division and is considered to be a high hazard dam.

In 1977 Knightville Dam was investigated for seismic stability, since the embankment materials were considered to be highly susceptible to liquefaction under earthquake shaking. The investigation was completed in 1981; recommendations included that a comprehensive dynamic analysis utilizing state-of-the-art procedures be performed. The results of this comprehensive analysis are presented herein.

For this work, a field testing program was performed in order to determine the characteristics of the embankment and foundation, to obtain soil samples for laboratory testing and to perform a seismic wave velocity measurement survey. The program consisted of exploration and sampling and a cross-hole, down-hole and surface wave measurement survey at crest and downstream borehole locations. Disturbed and "undisturbed" samples were obtained for laboratory testing using split-spoon, stationary piston and Pitcher-type samplers. Due to the coarse nature of the shell material, few undisturbed samples were obtained in this material.

The results of the seismic survey were used to compute the in situ dynamic soil properties, including shear modulus (G) and Poisson's Ratio (ν). Because of difficulties experienced during the survey, only values of shear moduli could be computed. These values were assumed as the maximum values (G_{\max}) in the dynamic analysis.

Static and dynamic laboratory tests were performed on disturbed, but representative, and "undisturbed" samples. Both programs included standard index tests. For the static testing program, both isotropic and anisotropic stress-controlled consolidated-undrained (\bar{R}) and drained (S) triaxial compression tests were performed. The dynamic laboratory testing program included isotropic and anisotropic cyclic load triaxial ($C\bar{R}$) tests, resonant column (RC) tests, and small strain triaxial (E) tests.

Test specimens for both testing programs consisted of "undisturbed" core samples and compacted shell specimens. Due to the few number of "undisturbed" shell samples available for testing, it was necessary to reconstitute the samples in the laboratory for strength testing.

A seismic hazard analysis was performed by Prof. Nafi Toksoz, TAMS Seismological Consultant, in order to establish earthquake parameters to be used in the dynamic analysis. Based on the regional and local studies performed, Prof. Toksoz concluded that the Maximum Credible Earthquake would occur at Cape Ann, Massachusetts and would have a body magnitude of 6.5 and a peak base rock acceleration of 200 cm/sec^2 . For the Operating Basis Earthquake, Prof. Toksoz concluded that the event would also occur at Cape Ann and would have a body magnitude of 5.5 and a peak base rock acceleration of 84 cm/sec^2 .

On January 19, 1982 an earthquake of $m_b = 4.7$ occurred in Gaza, New Hampshire. This earthquake was useful in this study because for the first time strong motion records became available

for an earthquake of known magnitude in New England. The available information was used by Prof. Toksoz during his study.

The earthquake record which was chosen for the analysis is the Puddingstone Reservoir record which was recorded in southern California during the 1971 San Fernando earthquake. The use of this record was recommended by TAMS Earthquake Engineering Consultant, Prof. Robert Whitman, and was scaled for use as the Operating Basis (0.086g) and Maximum Credible (0.204g) earthquake events. The record has a duration and frequency consistent with those recommended by Prof. Toksoz.

In order to perform a comprehensive dynamic response analysis, it was first necessary to evaluate the stress in the dam prior to earthquake shaking. A finite element computer procedure entitled FEADAM was used to evaluate these stresses. For this study the static stresses were computed at two embankment cross sections; Station 8+50 and Station 4+82. The former station was selected since it represents the approximate maximum section; the latter section was selected in order to evaluate the effects of the thick glacial till foundation on the dynamic response of the dam.

For the dynamic analysis, simplified procedures developed by Seed et. al. were used for the preliminary evaluation of the embankment behavior during the design earthquakes. The liquefaction potential of the dam was evaluated on the basis of standard penetration test (SPT) data obtained during the field testing program and a one-dimensional model of the materials comprising the dam and foundation. The dynamic stability and permanent deformation of the dam was then assessed using simplified analytical procedures which considered the predominant period of vibration, spectral acceleration, yield acceleration and an idealized rigid block representing a potential sliding mass of the embankment.

The next step in the analysis was to utilize more sophisticated computer techniques to determine the liquefaction potential, embankment stability and permanent deformation. The computer programs used included: (1) SHAKE - a one-dimensional dynamic analysis, (2) FLUSH - a two-dimensional finite element dynamic analysis, (3) STRAIN - a post processor program for FLUSH, (4) SAM4 - seismic stability procedure utilizing Sarma's stability analysis, and (5) YDBH9 - a permanent deformation procedure developed by TAMS.

The results of the study indicate that portions of the hydraulic core could liquefy under the Operating Basis and Maximum Credible earthquake events, and that in the core liquefaction is most likely to occur in the section of the embankment underlain by the thick glacial deposits. The results also indicate that the hydraulic shells, which are considered to be relatively free-draining, would remain stable (i.e., not liquefy) under the earthquake events. The results of the seismic stability and permanent deformation analyses, which assumed that no post-earthquake shear resistance was available in the core, indicate that the permanent deformation in the dam would not exceed one-inch.

The analytical techniques used for the assessment of dynamic dam behavior involve the use of mathematical models that are based on simplifying assumptions. In addition, the significant properties of the soil used in the analytical methods are determined on the basis of an incomplete knowledge of soil behavior. It would be hardly worthwhile to utilize more exact mathematical models in view of the difficulty in determining non-linear properties of the materials comprising the embankment. However, in view of the valid assessment of the seismic stability of earth dams as obtained from analytical procedures during recent years, it is reasonable to expect that the results obtained for Knightville Dam are representative of the probable performance of the dam during future earthquakes.

FINAL REPORT
DYNAMIC STABILITY ANALYSIS
OF KNIGHTVILLE DAM
HUNTINGTON, MASSACHUSETTS

I. INTRODUCTION

A. AUTHORIZATION

The engineering services reported herein were authorized by the U.S. Army Corps of Engineers, New England Division (NED), under Contract DACW 33-81-C-0121, Dynamic Stability Analysis of Knightville Dam, Huntington, Massachusetts, dated 18 September 1981. The authority for this project is derived from Public Law 96-367, Public Works Appropriation Act for FY-1981, approved 1 October 1980.

B. PURPOSE AND SCOPE

Knightville Dam is located on the Westfield River in Huntington, Massachusetts. The dam is a hydraulic fill structure having a maximum height of 160 feet above the riverbed and a total length of about 1,200 feet. According to the Corps of Engineers screening criteria, the dam is considered to be high hazard.

In 1977 the dam was selected as one of six Corps of Engineer's dams located in New England to be investigated for seismic stability. The embankment materials at Knightville Dam were considered to be highly susceptible to liquefaction under earthquake shaking. The investigation was performed in two phases and included preliminary field, laboratory and office investigations. Recommendations based on these investigations, which were completed in 1981, included that a comprehensive dynamic analysis utilizing state-of-art procedures be performed in order to assess the seismic stability of the hydraulic fill embankment at Knightville Dam.

In order to perform a comprehensive dynamic analysis, it is necessary to obtain and/or select the important soil and earthquake parameters which characterize the embankment and the geotectonics of the area. For this work these parameters were determined from a series of investigations performed by TAMS, and the results were presented to NED in separate milestone reports, as follows:

- Field Testing Program Report (January 1982)
- Geology and Seismicity Report (April 1982)
- Laboratory Testing Report (May 1982)

The results of these three investigations were then used to perform a dynamic analysis. The results of the analysis were presented in the final milestone report entitled, Dynamic Response Analysis dated September 1982. An attachment to this report was also submitted and included a listing of sample input and output for all computer programs used in the dynamic analysis.

The FINAL REPORT presented herein is a compilation of each of the aforementioned milestone reports. The REPORT is submitted in two volumes: the FINAL REPORT (Volume 1) and the APPENDIX to the FINAL REPORT (Volume 2).

II. DESCRIPTION OF PROJECT

A. GENERAL

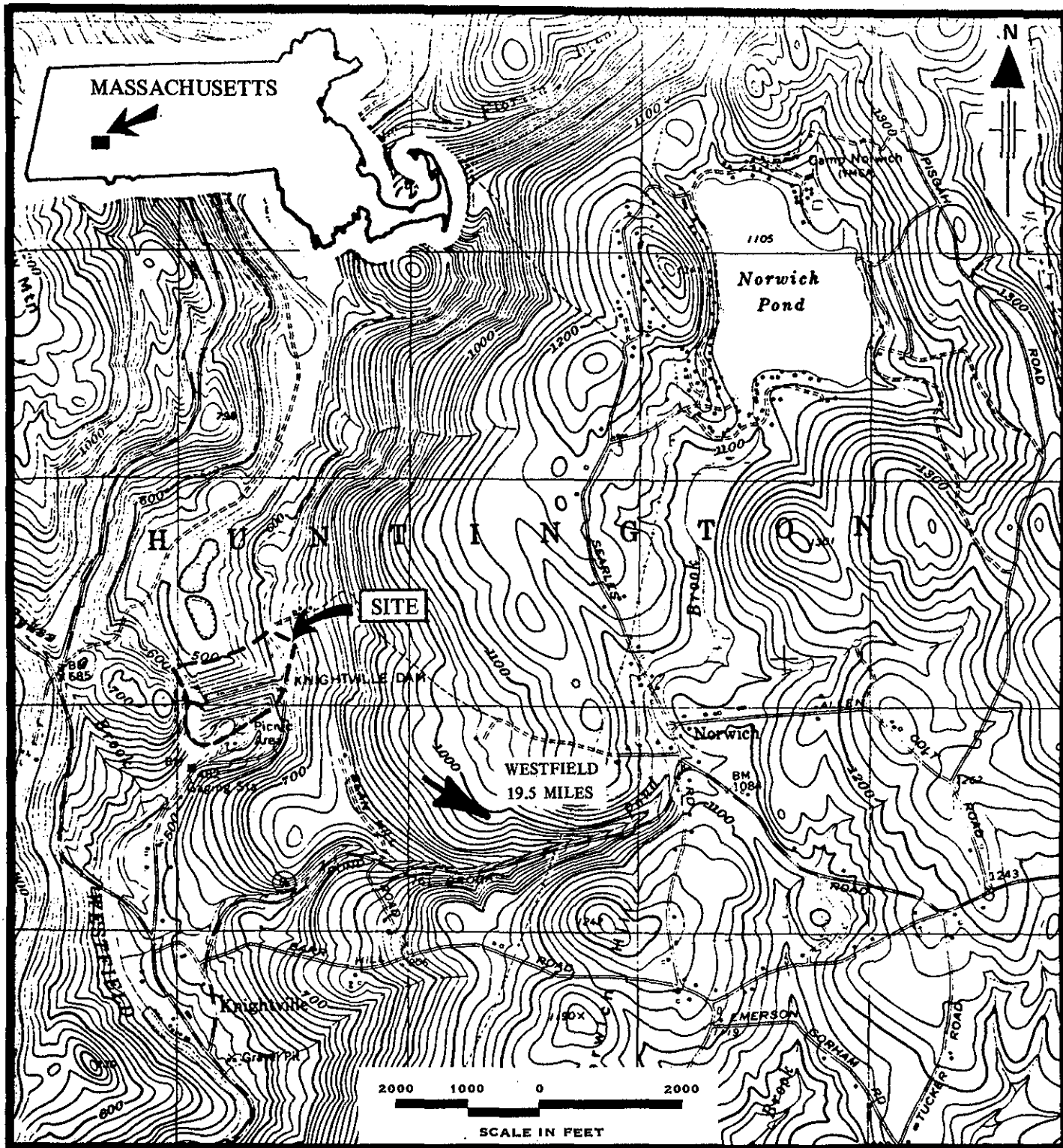
Knightville Dam is located on the Westfield River, approximately 4-1/2 miles north of the town of Huntington, Hampshire County, Massachusetts, at latitude 42° 17.4'N and longitude 72° 51.7'W. (West Hampton Quadrangle, Massachusetts, U.S.G.S., see Plate 1). The dam was constructed between September 1939 and December 1941 as authorized by the "Revised 1936 Flood Control Act for the Connecticut River Valley," and is one in a system of dams constructed in the Connecticut River Basin under this Act. The dam is owned and operated by the U.S. Army Corps of Engineers.

Knightville Dam is a hydraulic earth fill type structure with a downstream rock toe. The outlet works are located at the right abutment and consist of an intake channel, an intake structure with trash racks, a combined wet-well type intake tower and superstructure and a 16-foot diameter tunnel through rock. The flow through the tunnel is controlled by gates mechanically operated from the gatehouse above. The spillway is located on the right abutment adjacent to the dam and has a fixed crest at elevation 610 feet (NGVD)*. The important project features are shown on Plate 2, and a more detailed description of these features is presented below.

B. EMBANKMENT

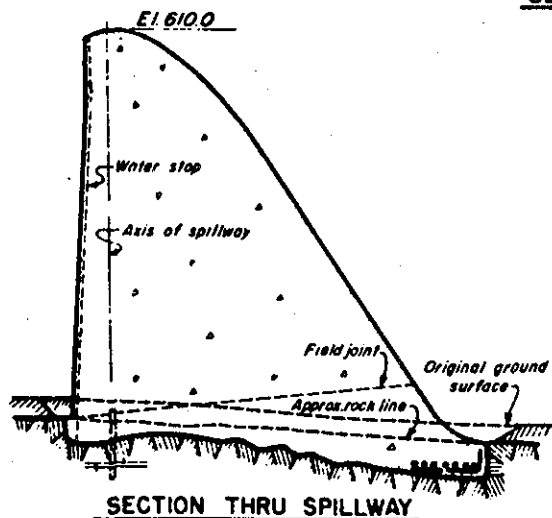
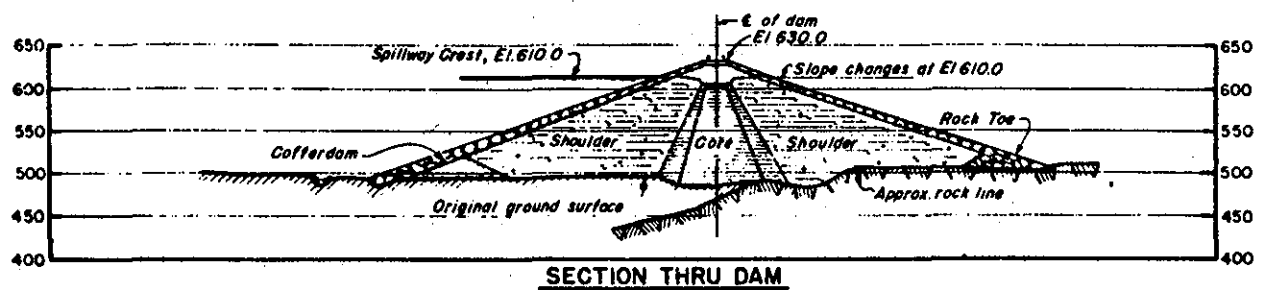
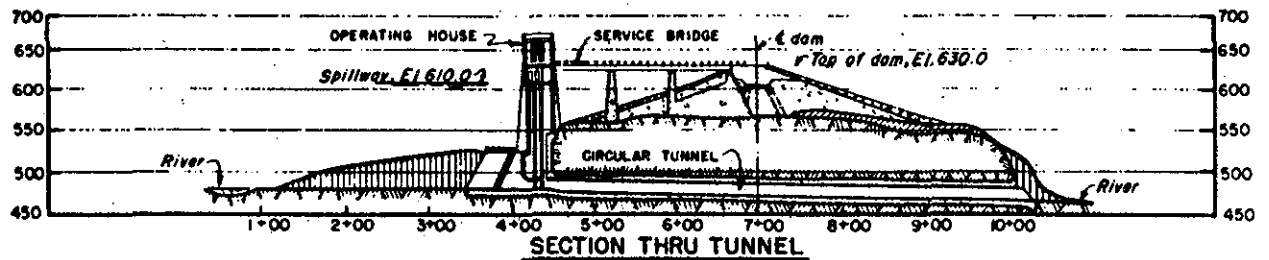
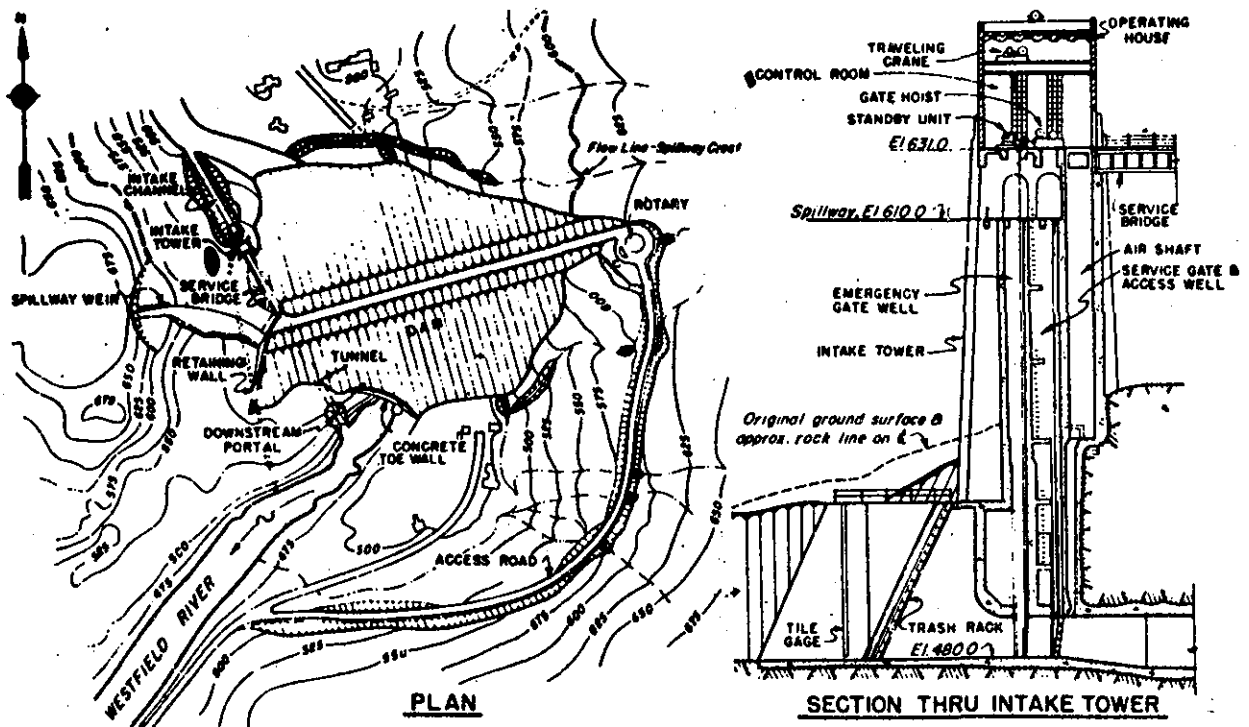
The embankment is a 1200-foot long hydraulic fill structure having a maximum structural height of approximately 160 feet. The crest of the dam is at approximate El 630 and is 30± feet wide. The upstream and downstream slopes are 1 Vertical to 3 Horizontal (1V:3H) from the foundation to El 610,

* Unless otherwise noted, all elevations are with respect to National Vertical Geodetic Datum (NGVD)



FROM: USGS West Hampton Quadrangle, Massachusetts

DYNAMIC STABILITY ANALYSIS OF
KNIGHTVILLE DAM
NEW ENGLAND DIVISION, COE
VICINITY MAP



**DYNAMIC STABILITY ANALYSIS OF
KNIGHTVILLE DAM
NEW ENGLAND DIVISION, COE
GENERAL PROJECT FEATURES**

FROM: U. S. Army Corps of Engineers (1973)

and 1V:2.5H from El 610 to El 630. The slopes are protected with riprap which varies in thickness from approximately 3 feet at the crest to 9 feet at the toe. The downstream embankment toe is supported by a 70-foot high concrete retaining wall; there is a rock toe at all other locations along the base of the upstream and downstream slopes. Plate 3 shows overview photographs of the embankment.

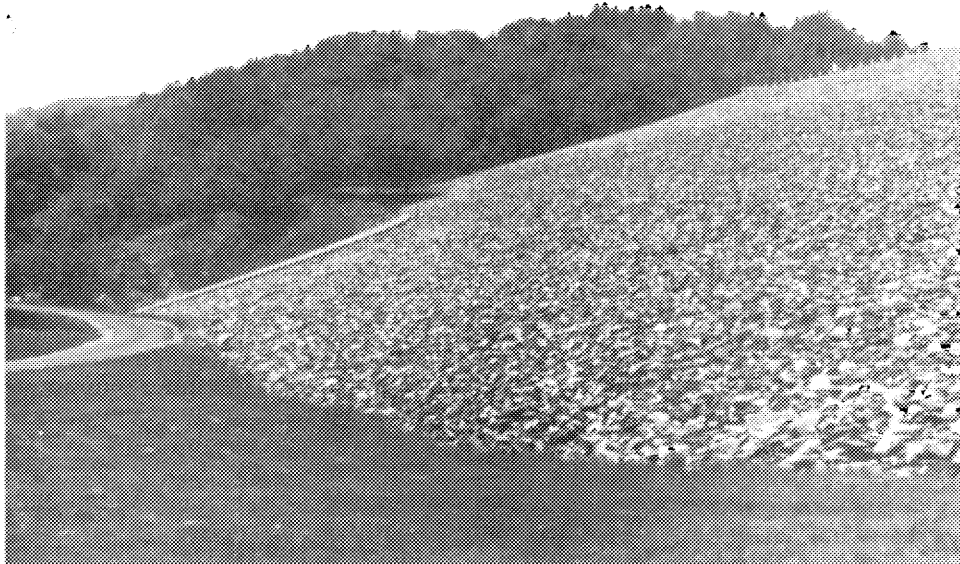
The embankment consists primarily of three earth zones: a central hydraulic core, outer hydraulic shoulders (or shells) and an upper cap section. The core and shoulders were constructed to approximate El 605 using the hydraulic fill method of construction. This method was used to separate the fine and coarse fractions of the borrow materials for the central core and outer shells, respectively. The upper cap, between El 605 and El 630 (top of dam), consists of an impervious rolled fill directly above the core; the cap is flanked by a compacted pervious material on each side. According to the U.S. Army Corps of Engineers (1941), a layer of boulders was placed on top of the hydraulic core to serve as a working mat for placement of the overlying rolled fill material.

C. OUTLET WORKS

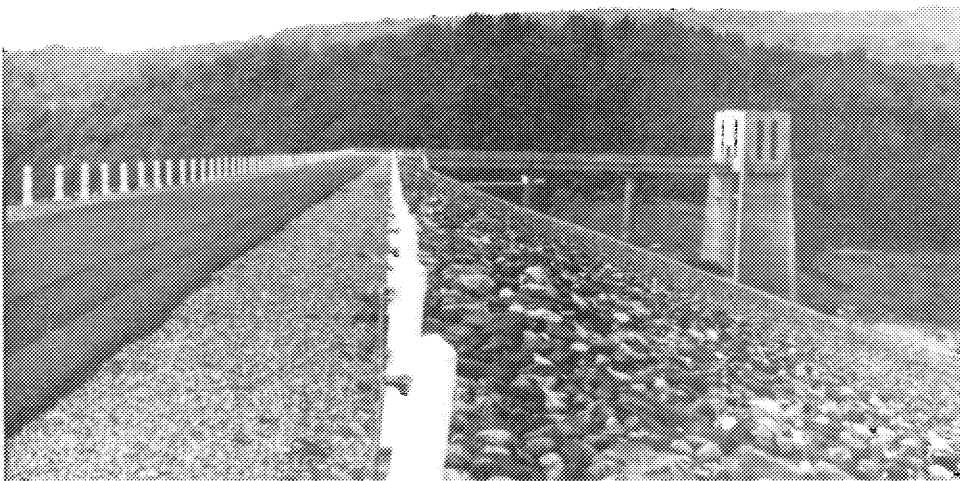
The outlet works, which are located on the right abutment of the dam, consist of an intake channel, an intake structure with trash racks, a tunnel section and an outlet portal, as described below.

1. Intake Channel

The intake channel is 30 feet wide and 250 feet long. The channel is excavated in rock with side slopes of 4 on 1 and has a bottom elevation of 480 feet. (See Plate 4). As previously mentioned, the winter pool is maintained at El 520 feet.



Downstream rock fill slope with top of concrete toe wall at left.



Top of dam, upstream slope and intake tower.

2. Intake Tower

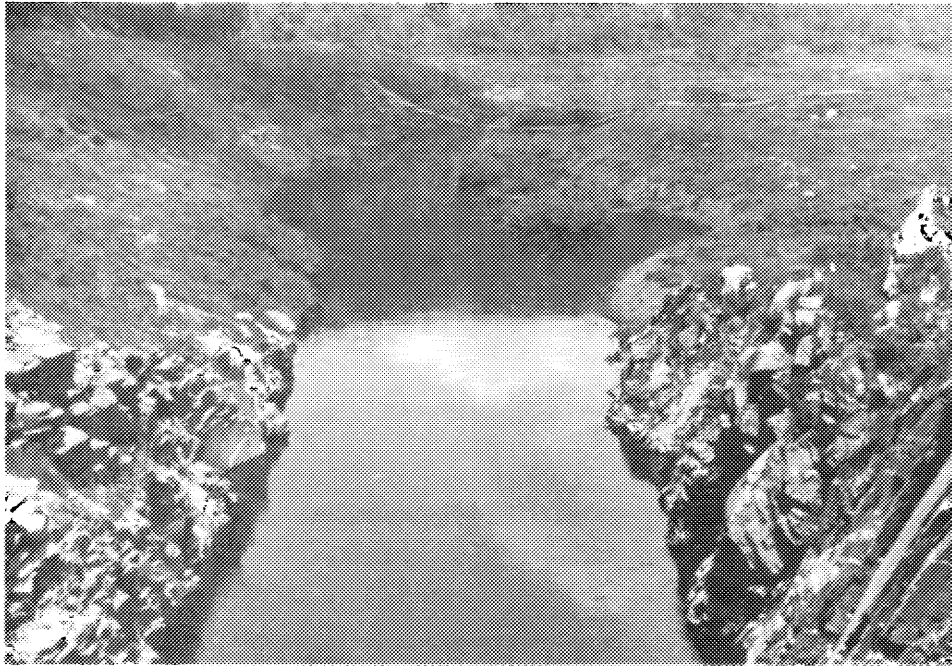
The intake tower is located on the upstream slope of the dam over the outlet works (See Plate 3). The intake structure has trash racks and a bell-mouth inlet which leads into the gate section and is concrete lined throughout. Flow through the tunnel is controlled by three self-closing caterpillar type service gates (Broome Gates), each 6 feet wide by 12 feet high. Emergency gate slots are provided immediately upstream of the service gates. The gate section is lined with semi-steel conduits from the emergency gate to a point 12 feet downstream of the service gates. The gate tower is reached from the embankment by a 3 span service bridge. Individual electrically powered cable hoists are located at the operating floor level over each of the gate wells for raising and lowering the service gates. An overhead electric traveling crane, 65-ton capacity, is used for the operation of the single emergency gate.

3. Service Bridge

Access to the control tower is provided by a service bridge with three 70'-0" spans. Each span consists of two plate girders, 5 feet deep and 71 feet long. The bridge has a length of about 214 feet, a roadway width of 12 feet between curbs.

4. Tunnel and Outlet Portal

Flow from the 3 gated sections passes into a 52-foot long transition section which leads into a 16-foot diameter concrete lined circular tunnel that is 500 feet long and ends with a 30-foot long transition section to the outlet portal. The last 30 feet of the tunnel forms a gradual transition from the 16-foot tunnel section to a round-topped, trapezoidal bottom portal. The concrete lining is carried 15 feet beyond the portal and the section changes to open rock cut with side slopes of 4 on 1. The discharge



Intake channel.



Outlet portal.

channel is 14.5 feet wide at the end of concrete lining with a bottom El 468. (See Plate 4)

D. SPILLWAY

The spillway is an ungated chute type located in a natural saddle in the right abutment of the dam. (See Plate 5) The spillway approach channel was excavated in rock to El 590 feet. The valley extending from the saddle down to the river provides a suitable channel in which the spillway discharge can return to the river with only a small area at the west end of the spillway bucket that required excavation. The spillway weir is an overflow ogee gravity section that is convexed upstream with a crest elevation of 610 feet and a length of 400 feet. The weir is constructed on solid rock with a grout curtain provided. A retaining wall is required on the east side of the spillway to separate the earth fill embankment from the spillway weir.

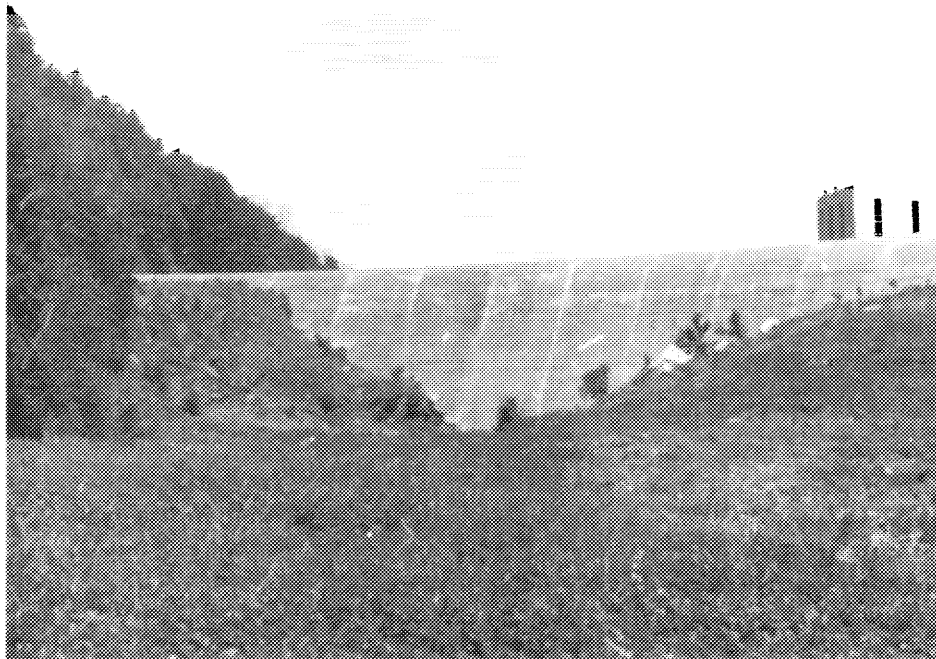
According to the U.S. Army Corps of Engineers (1973), the maximum impoundments recorded at the damsite have been as follows:

<u>Year</u>	<u>Date</u>	<u>Max. Water Surface Elev.</u>	<u>Storage Acre-Ft.</u>	<u>Use % of Total</u>
1948	24 Mar	597.2	24,500	50
1949	2 Jan	610.2	49,400	100
1951	4 Apr	574.7	21,800	44
1953	30 Mar	592.2	34,000	68
1955	22 Aug	585.0	28,500	57
1955	18 Oct	607.8	47,200	95
1960	8 Apr	587.0	29,800	60

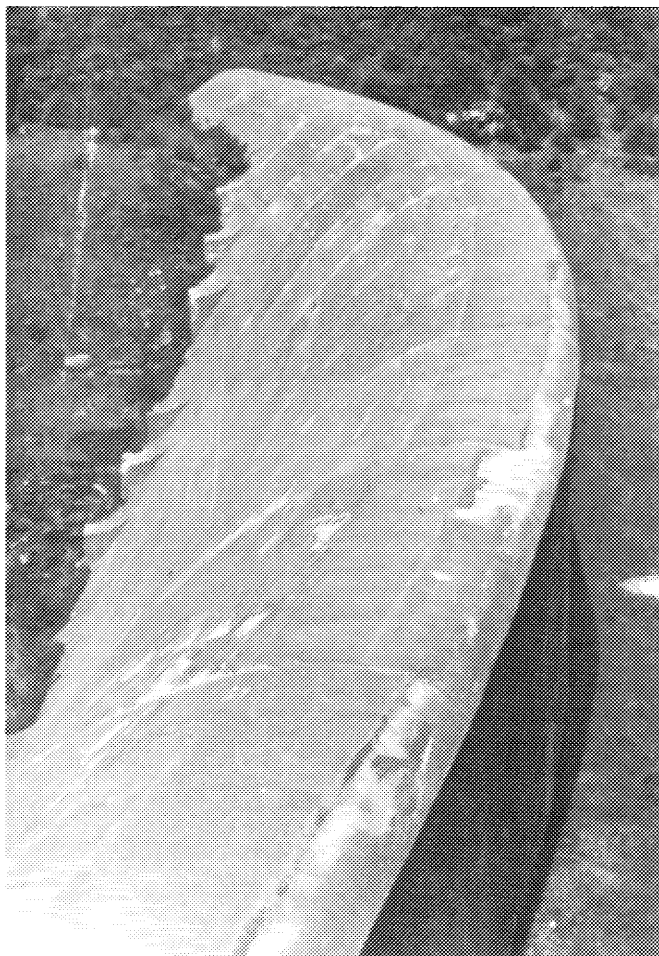
Normal operations at the project require that the reservoir be drained immediately after filling.

E. PERTINENT DATA

Table 1 provides a summary of the pertinent structural and hydrologic/hydraulic data for the project.



Downstream face of spillway weir and spillway discharge channel.



Spillway weir from left (east) end.

Table 1
SUMMARY OF PERTINENT DATA

(From U.S. Army Corps of Engineers, 1973)

Location: Westfield River, Huntington, Massachusetts

Drainage Area: 162 Square Miles

DAM

Type.....Hydraulic earth fill
 Length.....1200 feet
 Maximum height above streambed160 feet
 Top elevation.....630 feet NGVD
 Top width.....30 feet
 Embankment slopes
 (Upstream and Downstream).....Above El 610 1 on 2.5
 Below El 610 1 on 3.0

OUTLET WORKS

Type.....Upstream intake tower, wet well type, with outlet tunnel in rock
 Service gates.....Three Broome 6'x12' each
 Emergency gate.....One Broome 6'x12'
 Outlet capacity.....14,400 c.f.s.
 Inside diameter of tunnel.....16 feet
 Length of tunnel from centerline of gates.....605 feet
 Invert elevation.....480.0 feet NGVD

SPILLWAY

Type.....Uncontrolled, curved concrete ogee weir
 Crest length.....400 feet
 Crest elevation.....610.0 feet NGVD
 Design discharge.....41,000 c.f.s.

RESERVOIR DATA

	<u>Elevation</u> (Ft. NGVD)	<u>Storage</u> (Feet)	<u>Area</u> (Acres)	<u>Capacity</u> (Acre-Feet)	<u>Runoff</u> (Inches)
Winter Pool	520	40.0	30.0	270	0.03
Spillway Crest	610	130.0	960.0	49,000	5.6

material. In all of these boreholes, the casing was advanced to the bottom of the hole and a plastic inclinometer casing (3.34-inch outside diameter) was installed for seismic survey measurements. The plastic casing was grouted in the hole as the steel casing was removed. Special drilling procedures were used during grout operations to insure good grout contact with the surrounding soil and to prevent the fracturing of loose embankment soils. A description of this procedure is presented in Appendix A (Volume 2).

Boreholes K-1 on the crest and K-4 on the slope were 3-inch and 4-inch diameter cased holes, respectively. These boreholes were the last to be drilled in their respective arrays since they were used as shot holes for the seismic wave measurement investigation.

2. Sampling

Soil samples were obtained at both borehole array locations to determine the nature and condition of the embankment materials and to obtain samples for static and dynamic laboratory testing. In general, two types of soil samples were obtained: disturbed, but representative samples for classification tests, and relatively undisturbed samples suitable for laboratory static and dynamic strength and compressibility testing. A summary of the exploration and sampling quantities is presented in Table 3.

In the crest boreholes, disturbed soil samples of the impervious rolled fill and the hydraulic core were obtained using a 1-3/8 inch diameter (I.D.) split spoon sampler driven by a 140 pound hammer falling 30 inches. Split spoon sampling was performed generally at 5 to 10-foot intervals, except at the rolled fill/hydraulic core interface, where continuous sampling was performed. Blow counts were recorded for each 6 inches of penetration.

Relatively "undisturbed" soil samples of the fine-grained hydraulic core material were taken in crest borehole K-2 using a 2.8-inch diameter thin-walled stationary piston sampler. These samples were taken at 5-ft intervals within the upper part and 10-ft intervals within the lower part of the core. Each sample was handled with extreme care and stored in a heated shelter provided by Corps project personnel. The description of the procedure used for stationary piston sampling operations is presented in Appendix A (Volume 2).

At the downstream borehole locations, K-4, K-5, K-6, 1-3/8-inch and 3-inch diameter split spoon samples were taken in the shell material, either continuously or at 2 to 5-foot intervals. The 3-inch diameter sampler was driven 24-inches by a 300-lb hammer falling 18 inches. The larger sampler (3-inch) was used to obtain more representative samples of the shell material for laboratory testing. Also due to the coarse gravel and cobbles in this material, use of the smaller (1-3/8-inch) sampler would give excessively high resistance values which could lead to misinterpretation of the results.

Undisturbed sampling of the shell material was attempted using a Pitcher-type and a double tube (Christensen NX-D3) core barrel sampler. The Pitcher-type sampler consisted of a rotating outer metal barrel having a saw-tooth lower cutting edge, and an inner, stationary, thin-walled Shelby tube (2.8 inch I.D.). The double tube core barrel was NX-size and contained an outer rotating barrel with a diamond bit at its cutting edge, and an inner split barrel.

Undisturbed sampling of the shell materials proved to be extremely difficult due to the presence of coarse gravel and cobbles (6-inch maximum diameter) within the material. During sampling operations the larger outer barrel of the Pitcher sampler would cut the coarse fraction component, which would then enter the outer barrel, and catch the

Table 3
SUMMARY OF EXPLORATION
AND SAMPLING QUANTITIES

NUMBER OF SAMPLES						
<u>DISTURBED</u>				<u>"UNDISTURBED"</u>		
<u>Borehole Number</u>	<u>Total Depth (Feet)</u>	<u>1-3/8" Split Spoon</u>	<u>3" Split Spoon</u>	<u>2.8" Station- ary Piston</u>	<u>2.8" Pitcher- Type</u>	<u>NW-Size Double Tube</u>
<u>Crest</u>						
K-1	159.1	31	---	---	---	---
K-2*	158.3	10	---	17	---	---
K-3*	158.5	13	---	---	---	---
<u>Downstream Slope</u>						
K-4	69.2	---	17	---	---	---
K-5*	73.7	---	18	---	10	3
K-6*	77.2	9	1	---	4	2

*Plastic (3.34 inch outside diameter) inclinometer casing installed to bottom of borehole for seismic survey.

smaller diameter inner thin-walled barrel at its lower edge causing it to "crimp" and/or "crush". To eliminate this problem, the Christensen sampler was substituted. However, the drilling fluid, which is discharged between the inner and outer barrels, eroded the relatively non-plastic fine fraction component before the sample could advance into the inner barrel. During these sampling operations, adjustments were made in the speed of sampler rotation and drilling fluid pressure to maximize the number of undisturbed samples which could be obtained in the coarse, cohesionless shell material.

3. Subsurface Conditions

The borings at the crest location encountered approximately 32 feet of rolled impervious fill, underlain by approximately 123 feet of hydraulic core, which, in turn, is underlain by bedrock. The impervious fill consists of gravelly, silty, coarse to fine sand with cobbles and/or boulders, which appears to be medium dense to very dense. The hydraulic core consists of silty fine sand and fine sandy silt, with traces of clay and organic matter; this material appears to range from a loose to medium dense degree of compactness.

Standard penetration resistance values (N-values) for each of the crest boreholes are plotted versus depth and elevation (See Plate 8). The N-values for the rolled impervious fill generally range between 40 and 100 blows per foot. High N-values (over 100 blows/ft.) were encountered at a depth of 28 to 32 feet. In the hydraulic core the N-values generally range between 3 and 5 blows per foot above El 560 and 5 to 10 blows per foot below El 560.

A soil profile at the downstream slope borehole locations consists of approximately 7.5 feet of riprap, underlain by hydraulic shell material which, in turn, is underlain by bedrock. The shell materials consist of dense to very

III. FIELD TESTING PROGRAM

A. GENERAL

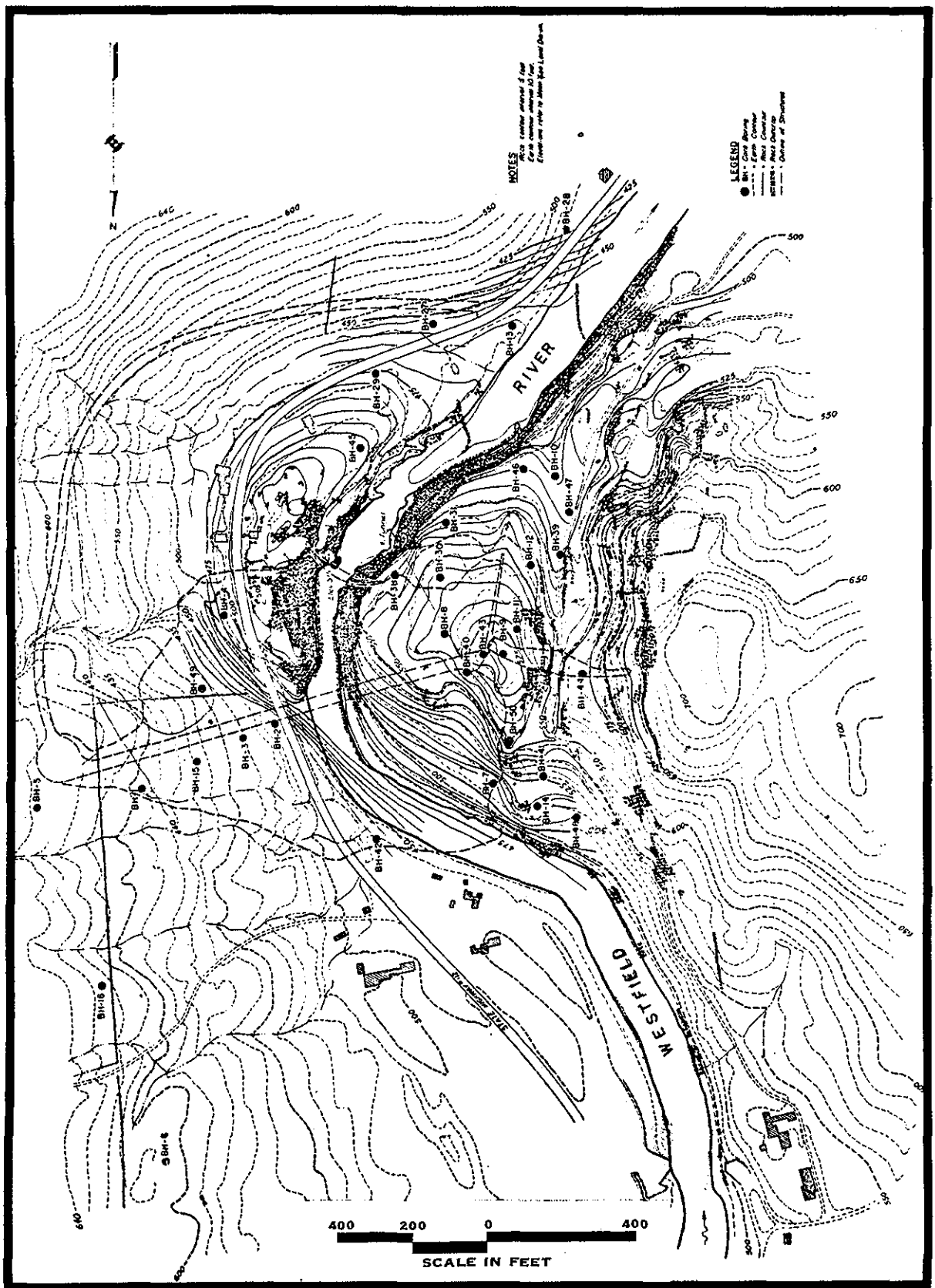
Prior to construction of the project, a program of exploration and sampling was conducted by Corps personnel at the damsite and in the reservoir area. According to the U.S. Army Corps of Engineers (1939), the field testing program included 50 boreholes, 98 test pits and two hand excavated open cuts. The results of this program are presented in Plate 6.

In 1980, another exploration and sampling program was performed at the site to investigate the liquefaction and cyclic mobility potential of the embankment. For the work, two deep boreholes were made at crest locations (Stations 8+50 and 6+00) and penetrated the impervious rolled fill and hydraulic core. Laboratory tests were performed on disturbed and "undisturbed" soil samples; these tests included visual classification, Atterberg limits, water content and grain-size determinations. The results of this program are presented in U.S. Army Corps of Engineers (1981).

B. EXPLORATION AND SAMPLING PROGRAM

1. Exploration

For this work, six boreholes were drilled through the embankment to determine the characteristics of the embankment materials and the underlying foundation, to obtain soil samples for laboratory testing and to perform a seismic wave velocity measurement survey. An array of three boreholes each was made at the crest and on the downstream slope. The boreholes were spaced approximately 15 feet on center within each array; their locations are summarized in Table 2 and shown on Plate 7. The field testing program was performed between October and December 1981.



AFTER: U.S. Army Corps of Engineers (1939)

**DYNAMIC STABILITY ANALYSIS OF
KNIGHTVILLE DAM
NEW ENGLAND DIVISION, COE
RESULTS OF PRE-CONSTRUCTION
FIELD TESTING PROGRAM**

The three crest boreholes, K-1, K-2 and K-3, were drilled through the impervious rolled fill and hydraulic core materials to the underlying bedrock foundation. Boreholes K-4, K-5 and K-6 were drilled along the downstream slope through the shell material also to the underlying bedrock. To facilitate drilling on the downstream slope, a timber platform was constructed and the riprap was hand-excavated to the depth of underlying hydraulic fill material prior to exploration and sampling.

Table 2

SUMMARY OF BOREHOLE
LOCATIONS

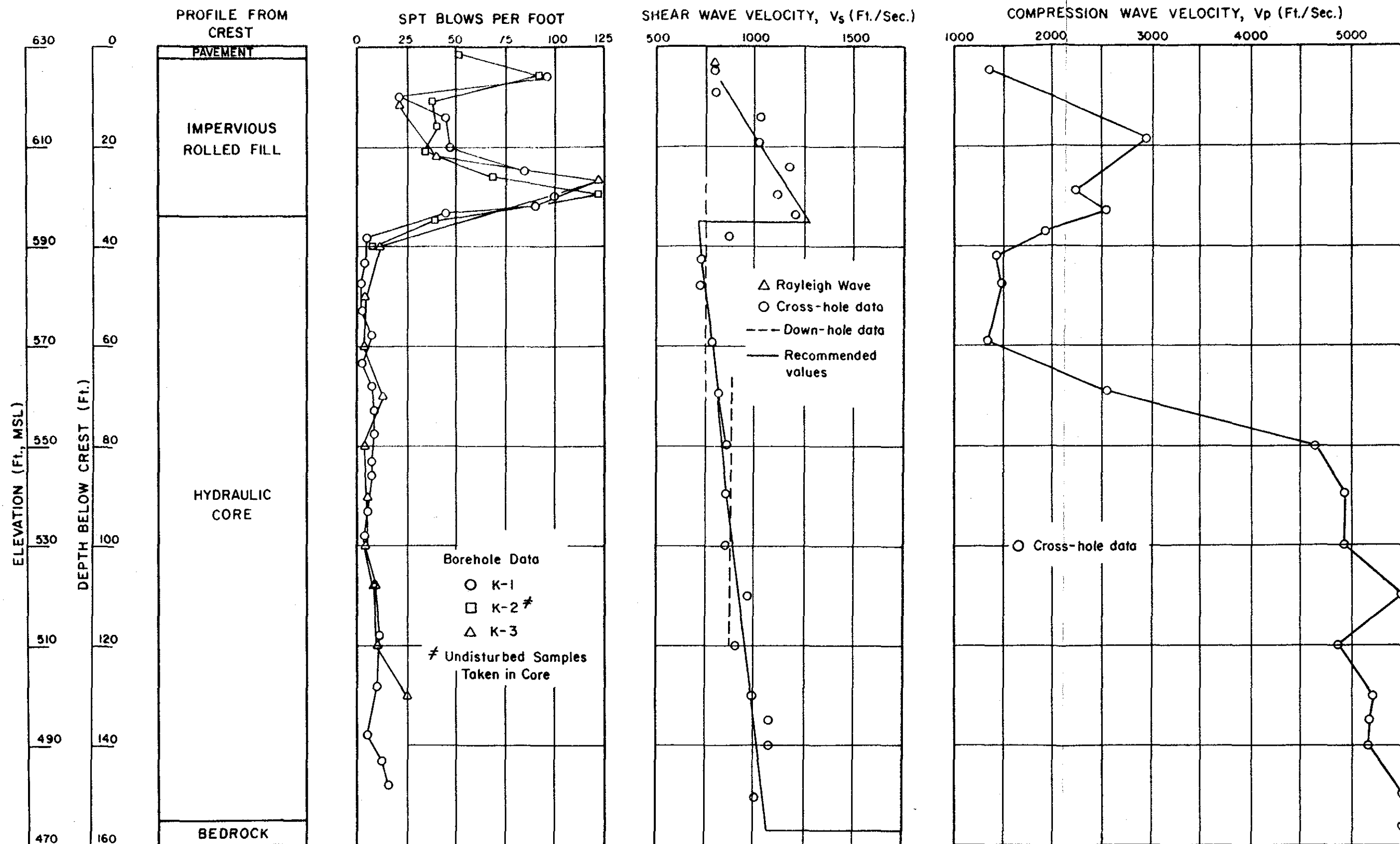
Boring Number

<u>Crest</u>	<u>Station**</u>	<u>Offset*</u>	<u>Surface Elevation (Ft., MSL)</u>
K-1	7+75.0	3.2L	629.76
K-2	7+60.2	3.0L	629.78
K-3	7+45.0	2.8L	629.86
<u>Downstream Slope</u>			
K-4	7+76.1	180.0L	571.84
K-5	7+59.6	180.0L	571.77
K-6	7+43.6	180.0L	571.75

* Offset from Centerline of Dam.

** Stationing as on Original Design Drawings.

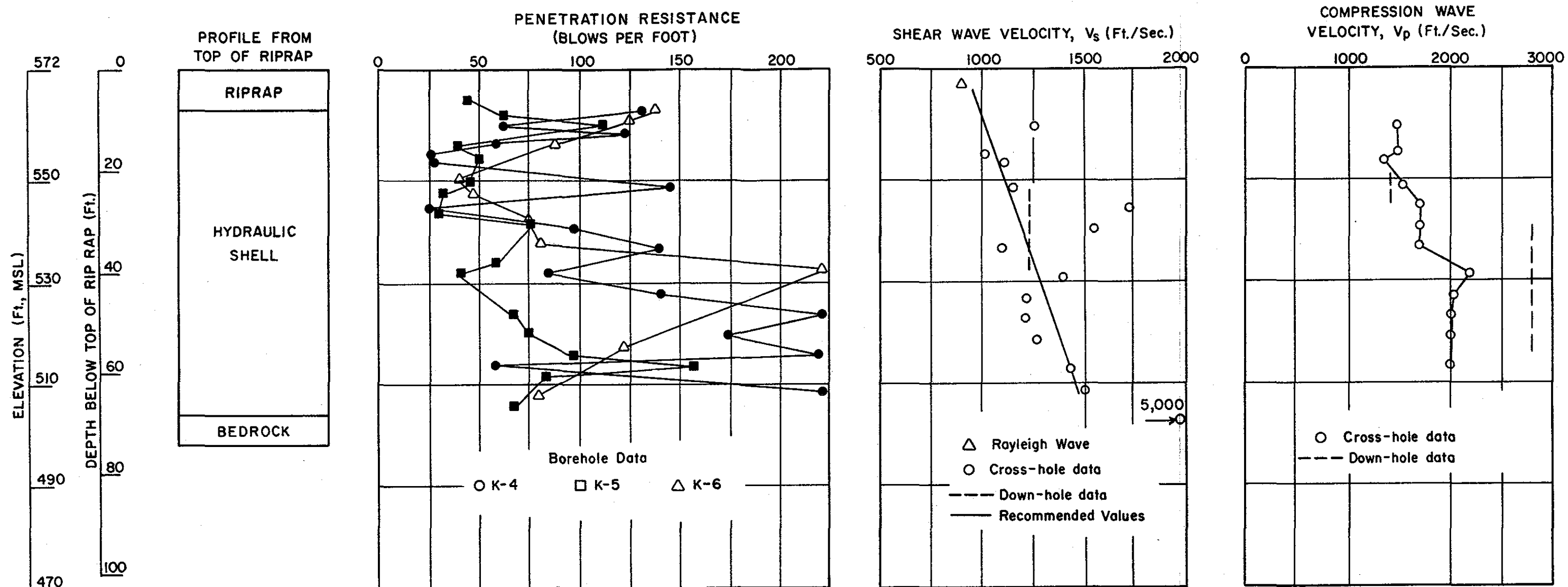
Borings K-2 and K-3 on the crest and K-5 and K-6 on the downstream slope were advanced using 5-inch and 6-inch diameter flush coupled steel casing, respectively. The larger size casing was required at slope borehole locations due to the cobble and coarse gravel-size particles of the shell



dense gravelly sands to sandy gravels, with varying amounts of silt. The N-values for this material are plotted versus depth in Plate 9; the large range in recorded N-values indicates the heterogeneity of the shell material.

Bedrock encountered at the crest and downstream borehole locations consisted of unweathered dark-gray micaceous schist and pegmatite composed principally of quartz, feldspar and muscovite. The elevation of the bedrock at the downstream slope borehole locations was found to be approximately 25 feet higher than at the crest locations (El 500 vs 475). This rise in bedrock surface was observed during pre-construction investigations as shown in Plate 6. A more detailed description of the local bedrock is included in Section IV of this Report.

Water level readings could not be obtained in the the hydraulic core fill or shell materials during exploration and sampling, since a bentonitic drilling fluid (mud) was used to advance the boreholes. Previous investigations (1980) indicate water levels at a depth of 55 feet (El 575) in the central core. The results of the seismic survey performed for this work and discussed in a following section, indicate soil saturation at a depth of approximately 70 feet (El 560). Water level data from the observation wells located along the upstream and downstream slopes of the dam exist for the project; the data recorded for these wells indicate that the upstream and downstream shells are unsaturated when the winter pool (El 520) is maintained.



NOTE:
Hollow circles are SPT N-values (i.e., 140lb. hammer dropping 30 inches); All darkened circles are for 300lb. hammer dropping 18 inches.

C. SEISMIC WAVE VELOCITY MEASUREMENT INVESTIGATION

1. General

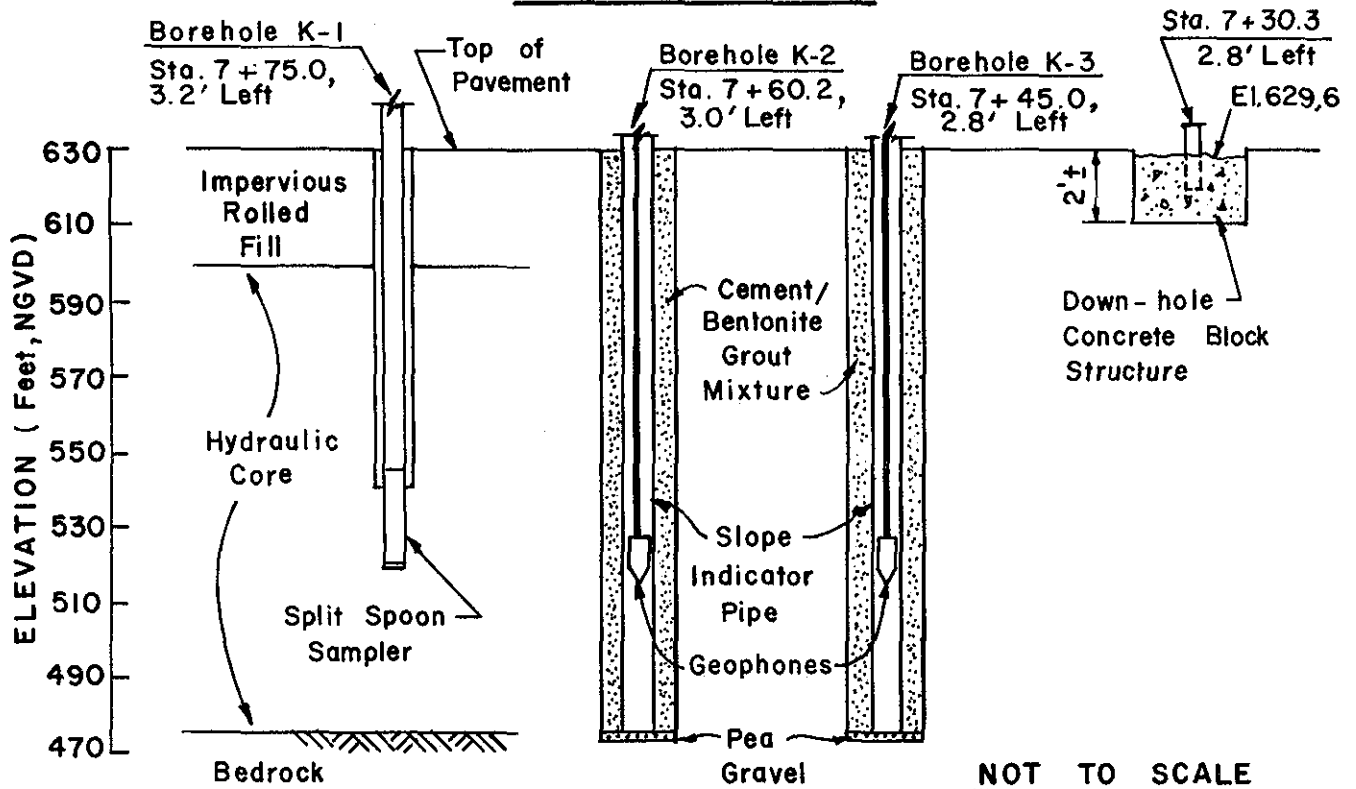
A seismic wave velocity survey was performed in the crest and downstream slope boreholes to determine shear (S), compression (P) and surface (R or Rayleigh) wave velocities throughout a range of depths in the impervious rolled fill, hydraulic core and hydraulic downstream shoulder. The investigation included cross-hole, down-hole and surface wave seismic survey techniques.

Each of the techniques used in this investigation measures the time for seismic waves to travel between two points in a soil mass. In the cross-hole technique, P- and S-wave travel time is measured horizontally between two points; in the down-hole technique, P- and S-wave travel time is measured on an incline from the surface to a point at some depth and distance away from the source. Surface wave (R) travel time is measured between two points on the ground surface. The measured travel times and distance between the respective points in the soil mass are used to compute the P-, S-, and R-wave velocities; these velocities are then used to compute values of shear moduli at very low shear strain levels for use in the dynamic stability analyses.

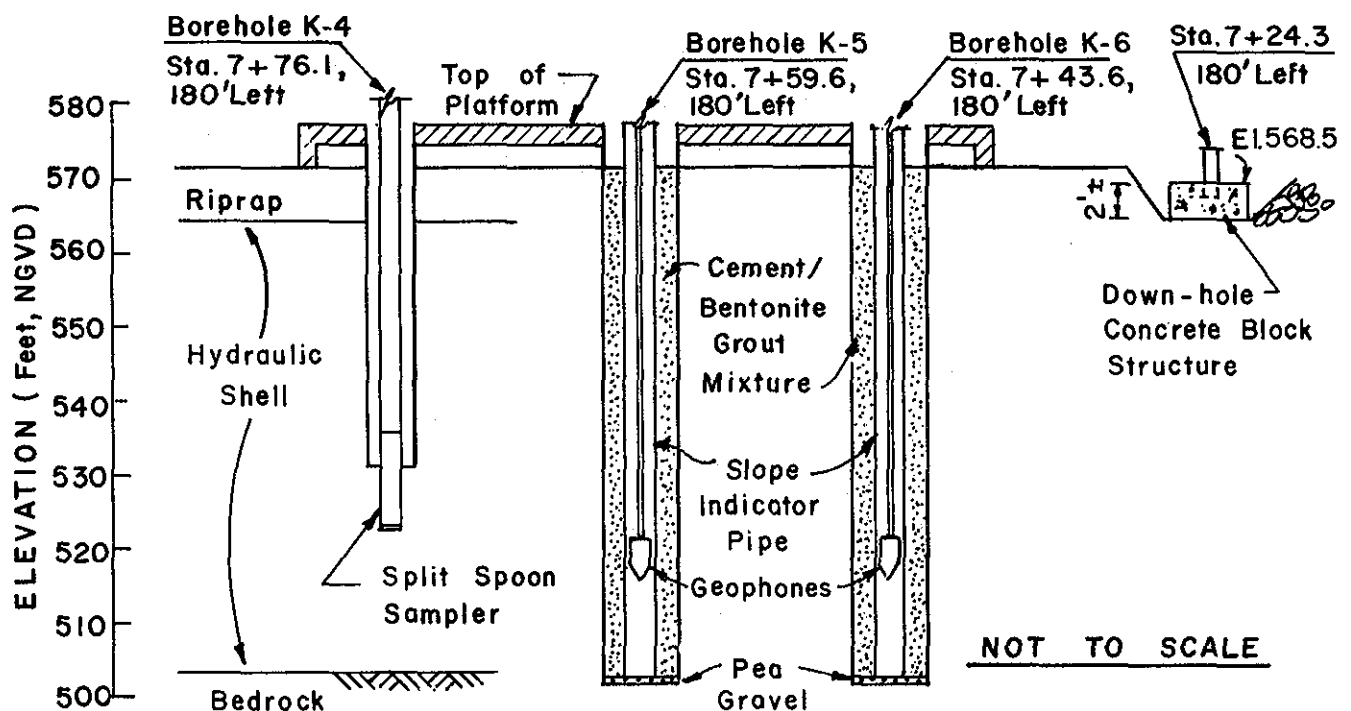
2. Procedure and Measurement

a. Cross-hole - A drill rig was positioned at the location of Borehole K-1 on the crest to advance a 3 inch diameter steel cased borehole. After the borehole was advanced to a depth of about 5 ft, standard penetration test equipment was inserted and the sampler was driven 12 inches. A geophone containing vertical and horizontal velocity transducers was wedged in each of the plastic inclinometer casings in Boreholes K-2 and K-3 at the same depth as the sampling spoon tip. (See Plate 10). The seismic test was then performed using a short drop (about 3-inch) of the 140-lb hammer

CREST OF DAM



DOWNSTREAM SLOPE



DYNAMIC STABILITY ANALYSIS OF
KNIGHTVILLE DAM
NEW ENGLAND DIVISION, COE
LAYOUT FOR
SEISMIC INVESTIGATION

as the impulse. Each time the 140-lb hammer was dropped, a compression wave traveled downward along the drill rod. The compression wave was coupled with the soil via the sampling spoon at the bottom of the rod. Compression and shear waves were generated in the soil and their arrivals at the velocity transducer in Boreholes K-2 and K-3 were recorded on a storage oscilloscope. A transducer which was attached to the drill rod was used to trigger the oscilloscope. The vertically-oriented shear waves generated by the sampler penetrating the soil were most discernible using the vertically-oriented transducer within the geophone. Compression waves were generally most discernible using one of the two orthogonal, horizontal transducers within the geophone. The procedure of dropping the hammer and recording the arrivals was done several times at the same depth in order to establish the optimum oscilloscope settings and to verify the reproducibility of the test. The entire procedure was repeated at about 5 ft intervals to a depth of 50 ft and at 10 ft intervals from this depth to bedrock at the crest borehole locations.

At the downstream slope location, the procedure was performed using Borehole K-4 as the signal hole and Boreholes K-5 and K-6 as the receiving holes. The depth interval used for testing the outer shell material was about 4 feet (See Plate 10).

The verticality of Boreholes K-2 and K-3 on the crest and K-5 and K-6 on the slope were determined using a slope inclinometer torpedo. Since the measured time for the seismic waves to travel between boreholes was on the order of 10^{-3} seconds, precise distances between the inclinometer casing were required at all depths. By combining these measurements with the center-to-center spacing of the boreholes at the ground surface, horizontal distances between the cased boreholes at all cross-hole measurement depths were determined. The following formulas were used to calculate the compression wave velocity (V_p) and shear wave velocity (V_s) by the cross-hole technique:

$$V_p = \frac{(\text{horizontal distance between geophones})}{(\text{P-wave travel time})}$$

$$V_s = \frac{(\text{horizontal distance between geophones})}{(\text{S-wave travel time})}$$

The P- and S-wave travel times is the difference between P- and S-wave arrival times from the first geophone to the second, respectively.

b. Down-hole - A concrete block was cast-in-place at each of the boring array locations; each block was approximately a 2-ft cube. (See Plate 10). At the crest location, the block was embedded about 2 ft into the rolled fill. At the downstream location, the block rested on the surface of the hydraulic shell material, after a small area was excavated of rip-rap. The blocks were located about 15 feet east of and in line with their respective arrays. Three short sections of 2-inch angle iron were placed in the block at the time of casting. One section extended vertically about 7-in. out from the center of the block. The other two sections made a 45° angle with the vertical, extended out of the concrete block about 18-in., in the plane of the section oriented perpendicular to the centerline of the boreholes.

The concrete blocks were used as wave sources in the down-hole tests. The tests were performed by first wedging a geophone in the cased borehole nearest the block (K-3 at the crest location and K-6 at the downstream slope location) at the desired depth. The seismic test was performed by striking one of the angle irons with a 2-lb. sledge hammer. The angle irons and hammer were wired to form an electrical circuit which triggered the oscilloscope when the two pieces touched. The hammer blow also caused a slight movement of the concrete block which generated body waves (P- and S-waves) in the soil; their arrivals at the geophone in the cased borehole were recorded on the storage oscilloscope. The test was repeated using combinations of strike

directions, afforded by the three angle irons, and combinations of transducer orientation until the clearest definition of arrival for both wave types was obtained.

The entire procedure was repeated from just below ground surface to the bottom of the borehole, at intervals of about 10 ft at the crest location and 5 ft at the downstream slope location. The depth at which down-hole data were obtained was measured each time. The verticality of each borehole was determined as previously described.

The determination of shear wave arrivals was facilitated by the use of polarization of the signal generated. Two traces were compared which were caused by hammer blows in opposite directions generating waves for which the initial particle movements were opposite in direction. The initial shear wave arrival was identified as the beginning of this reversal of particle movement. Similarly, compression waves were polarized by hammer blows in the opposite direction. Since particles oscillate parallel to the direction of travel during P-wave propagation, polarization was obtained by applying hammer blows directly (or near directly) oriented toward and away from the receiving geophone.

A plot of travel distance vs travel time allowed the determination of velocities for a given depth interval by approximating the data with a straight line. The velocity is given by the slope of the straight line. For these measurements, wave propagation was not truly vertical but was inclined because the source was not directly above the geophone in the borehole.

c. Surface waves - Rayleigh wave velocities were measured on the surface at each location using the same equipment as used in the down-hole tests. To measure R-waves, a geophone was wedged into one of the cased boreholes at the ground surface elevation (K-2 at the crest location and K-6 at the downstream slope location) and the concrete block was struck in a combination of directions. Due to the direction of particle

motion caused by Rayleigh waves, vertically and/or longitudinally directed blows coupled with the vertical transducer most clearly displayed the R-wave arrival. Rayleigh wave velocity (V_R) was computed using the following formula:

$$V_R = \frac{\text{(horizontal distance between geophone and block)}}{\text{(travel time)}}$$

3. Results of Wave Velocity Measurement Investigation

The results of this investigation are summarized in Plates 8 and 9. Plate 8 shows the compression (V_p) and shear (V_s) wave velocities measured in the impervious rolled fill and the hydraulic core. Plate 9 shows these velocities for the shell material. Also included in both Plates are the Rayleigh wave velocities (V_R) measured at the surface elevations, and V_s and V_p measurements in the bedrock foundation. Tabulations of these data are presented in Appendix A.

In general, the results of the cross-hole and down-hole tests were consistent and repeatable. On occasion, however, wave arrivals were difficult to interpret and, in a few instances, the interpretation of wave arrivals produced results which were not reasonable. Five typical oscilloscope photographs taken for the cross-hole and down-hole investigation are presented in Appendix A.

No compression wave results for the down-hole survey are plotted in Plate 8. In most cases, the down-hole compression wave energy was not detected in the hydraulic core fill; this is likely due to the reflection of waves at the boundary between the impervious rolled fill and the underlying core.

The down-hole shear and compression wave velocity measurements in the rolled fill gave erratic results. These results did not appear to be consistent with the cross-hole data. Two reasons for these erratic readings are as follows:

(a) Interpretation of the down-hole measurements involves a comparison of the interval travel path length to the interval travel time between wave arrivals at two successive depths. This analysis works well when the total travel paths are nearly coincident but of different lengths. This is the case for the deeper measurements. However, at shallow depths, the successive travel paths are quite different. Thus, at shallow depths the potential for error in the down-hole measurements is greater.

(b) The signal generated by the down-hole test is not as distinct as the signal generated during the cross-hole technique. The arrival of this complex signal in the borehole is sometimes difficult to interpret. The shape of the wave form as it travels through the soil may change due to a variety of reasons including unusual boundary conditions, non-uniform soil properties, horizontal layering, etc. Hence, the selection of arrival times for the compression and shear waves is sometimes difficult.

Plate 9 shows that there are inconsistencies in the measured V_p -values for the cross-hole and down-hole techniques. In general, the two methods should compare well if the soil was homogeneous and isotropic in the zone being evaluated. However, the down-hole technique is essentially measuring the velocity of propagation of vertical waves, and the cross-hole technique is measuring the velocity of propagation of horizontal waves. The difference may be significant in some soils. Secondly, the inherent problems with the down-hole technique discussed above may lead to inaccuracies in the interpretation of the down-hole test results. Hence, the variation between the two techniques may be a result of the anisotropic properties of the shell material and the test errors discussed above. The cross-hole data for V_p is believed to be more reliable.

Interpretation of Rayleigh wave measurements was complicated by the effects of surface conditions at each of the locations. At the crest location, the road surface is underlain by several inches of a crushed stone base course over the rolled fill. At the downstream slope location, the surface of the downstream shell is overlain by about 8 ft of riprap. Best estimates of surface wave velocities are plotted in Plates 8 and 9 and are believed to represent wave velocities for the rolled fill and shell materials for the crest and downstream slope locations, respectively. The velocities have been plotted at depths corresponding to one half of the computed wave length, which represents the average depth of soil through which most of the energy of the surface waves travel.

Based on the results of the cross-hole, down-hole, and surface wave measurements, recommended values of shear wave velocity (V_s) and compression wave velocity (V_p) vs elevation are presented as solid lines on Plates 8 and 9. The recommended value of V_s will be used to compute shear moduli (G); the computed values will represent shear moduli (G_{max}) at very small shear strains. Values of Poisson's Ratio (ν) could be computed using values of V_s and V_p at each testing elevation; however, due to the variability of the data as previously discussed, values of Poisson's Ratio were not based on the results of the velocity measurements investigation. The values of G_{max} and ν used in the dynamic and static analyses are discussed in a following section.

IV. GEOLOGICAL AND SEISMOLOGICAL INVESTIGATION

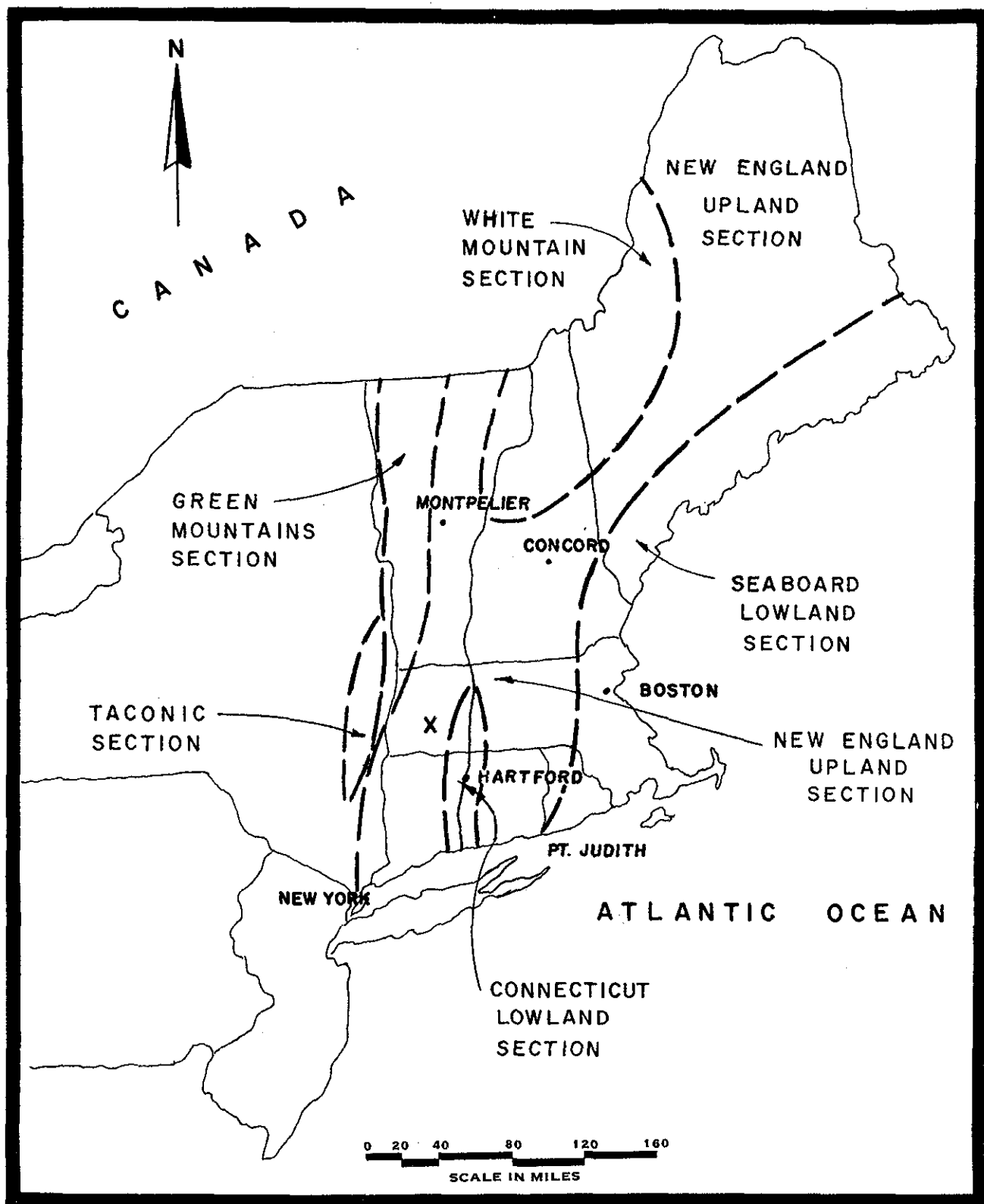
A. REGIONAL GEOLOGY

1. Physiography

Knightville Dam is located in the New England Upland Section of the New England Maritime physiographic province (Roberts, 1976). The Upland Section is an extensive area which extends from Maine to New York City, and is flanked by the Seaboard Lowland Section at its eastern boundary, and the Green Mountain and Taconic Mountain Sections at its northern and western boundaries, respectively. (See Plate 11).

The topography of the New England Upland Section is that of a maturely dissected peneplain which has been modified by continental glaciation. The most recent occurred approximately 8,000 to 10,000 years ago during the Wisconsin glacial stage. During this time the land surface was altered by glacial erosion of the hilltops and the formation of broad open-valley straths. Since this time, the post-glacial rivers and streams have dissected and eroded the glacial deposits and sediments creating a broadly undulating plain (Fenneman, 1938).

The drainage in the Upland Section is controlled by some major rivers and numerous small streams which are short and have steep gradients. In the western Massachusetts area, the Connecticut River is the major feature which controls the drainage. Its three western tributaries include the Deerfield, Mill and Westfield Rivers. The course of these rivers changed over time and formed the initial Connecticut River drainage system. Evidence of their "ancient" drainage courses



X - Approximate Location of Knightville Dam

DYNAMIC STABILITY ANALYSIS OF
KNIGHTVILLE DAM
NEW ENGLAND DIVISION, COE
REGIONAL PHYSIOGRAPHIC
PROVINCES

are the broad, mature valleys which were carved in the hard crystalline rocks of the highlands east of the Connecticut Valley.

The Seaboard Lowland Section of the province (See Plate 11) includes the relatively low coastal border of New England. The Section extends from Narragansett Bay at the south to the Gulf of St. Lawrence at the north (Roberts, 1976). The Lowland is lower in altitude and smoother in relief than the adjacent Upland Section. Drainage in the Lowland Section is controlled by the major rivers which include the Charles and Mystic, the Merrimack, and the Piscataqua.

The Connecticut Valley Section extends along a north-south strip from the Long Island Sound to northern Massachusetts, and is bordered by the New England Upland Section on either side. The width of the Valley Section is approximately 20 miles and includes the Connecticut River Valley. The topography is moderately level at the valley floor, and at its northern end is approximately 400 feet below the crest of the lateral escarpment (Fenneman, 1938).

The Green Mountain Section extends along the western boundary of the Upland Section from Canada to northern Massachusetts. The topography of the Mountain Section is rugged and altitudes range to over 4000 feet above sea level, but are typically less than 3000 feet.

Located to the west and south of the Green Mountain Section is the Taconic Section. This Section extends from near Poughkeepsie, New York to Brandon, Vermont. Elevations of the Taconics range from 1200 feet in the south to 2000 feet in the north. The limestone valley of Vermont lies between the Taconic Mountains and the Green Mountains; the valley is part of the Taconic Section and includes Rutland, Vermont.

2. Surficial Geology

The bedrock in the northeastern United States is overlain by a blanket of glacial drift which varies up to 100 feet in thickness. These deposits were laid down in late Pleistocene time during and after the Wisconsin glaciation, and include: (1) glacial till or "hardpan", (2) glaciofluvial deposits, (3) glacio-lacustrine deposits, and (4) other alluvial, organic and aeolian deposits.

The glacial till or "hardpan" forms a relatively thin mantle and encompasses the ground moraine covering most of the northeastern region. According to Fenneman (1938), the till averages between five and fifteen feet in thickness in Massachusetts and Connecticut. Two layers of till are known to exist: a lower blue-gray layer and an upper yellow-red-brown layer (Pessl and Schafer, 1968). In general, the lower till is more compact and less coarse than the upper till. Both till layers consist of varying amount of cobbles, gravels, sands, silts and clays which were deposited as either ground moraines and/or drumlins during the advance and retreat of the glaciers.

The glaciofluvial deposits are scattered throughout the Section and consist of stratified gravels, sands, silts and clays. These materials were deposited by glacial streams and meltwaters in the form of kames, kame terraces, esker and outwash plains (Thornbury, 1965).

Glacio-lacustrine deposits are found at the location of old glacial lakes. Lake Hitchcock, an old glacial lake, occupied the present Connecticut River Valley. It was formed during the retreat of the late Pleistocene ice sheet and extended from a natural dam at Rocky Hill, Connecticut northward to Lyme, New Hampshire. Streams feeding into the lake and

meltwater from the glacier contributed large quantities of sediment. The coarse sands and gravels from the streams formed delta deposits and the finer silts and clays were sedimented over the lake bottom forming deposits of varved clay over 100 feet thick (Ladd, 1975). Other glacial lakes which were formed in the Section experienced similar depositional sequences.

3. Bedrock Geology

The bedrock of northeastern United States is commonly exposed through the glacial till mantle on the upper slopes of stream valleys and occasionally in the present valleys where the streams have cut through the outwash and till and have exposed rock spurs along the sides of the pre-glacial valleys.

The greater part of the New England Upland Section is underlain by metamorphic rocks of Paleozoic Age. (See Plate 12). In general, these rocks are at a lower elevation than the Precambrian granites and gneisses which form the ridges and hilltops, but higher than the Paleozoic sedimentary rocks which form the structural basin, e.g., Boston and Narragansett Basins, along the coast.

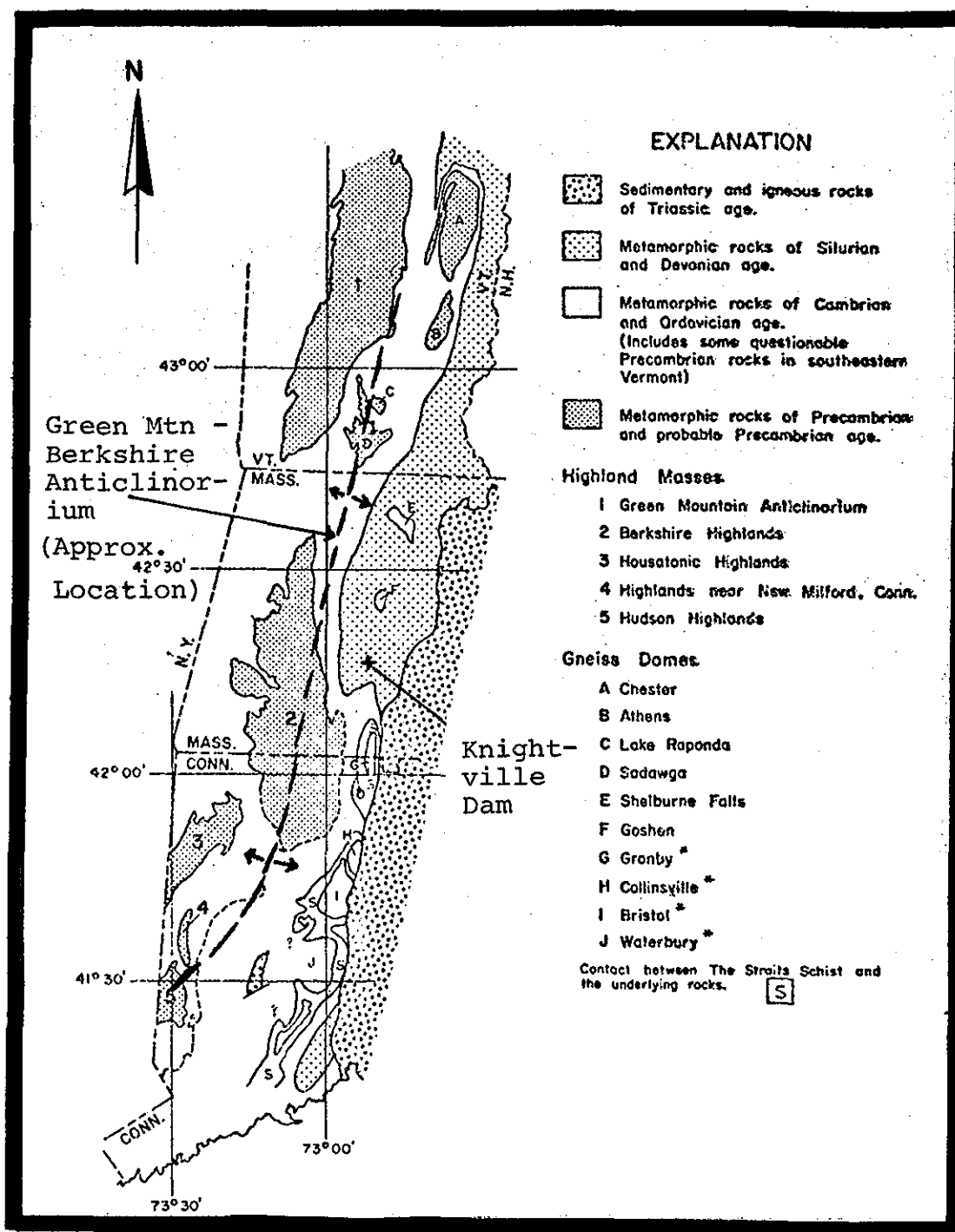
The Green Mountains in western Vermont, the Hoosic Mountains in western Massachusetts, and the Hudson Highlands consist of gneissic rocks of Precambrian Age. The Taconic Mountains consist of strongly metamorphosed schists. The narrow valley which is located between the Taconic Mountains and the western boundary of the Upland Section is composed of limestone and marble. The Connecticut Valley Section is underlain by Triassic shales, sandstones and conglomerates which abruptly give way to the schists and granites of the New England Upland Section.

The bedrock geology of the New England area is complex due to the long sequence of deposition, folding, faulting, intrusion and erosion which has occurred during its geologic history. However, a depositional pattern exists with respect to the series of anticlinoria and synclinoria found in the region (Johnson, 1977). The major folds trend north and east and are designated as follows: (1) Green Mountain - Berkshire Hills Anticlinorium, (2) Connecticut Valley - Gaspé Synclinorium, (3) Bronson Hill Anticlinorium, and (4) the Merrimack Synclinorium.

The east limb of the Green Mountain - Berkshire Anticlinorium forms the western boundary of the New England Upland Section in Massachusetts as evidenced by the Berkshire, Housatonic and Hudson Highlands. The eastern limb is chiefly underlain by metamorphosed sedimentary and volcanic rocks, and local granitic and pegmatitic intrusions. (See Plate 13). The metamorphic rocks are of Lower to Middle Paleozoic age and overlie a basement complex of Precambrian igneous rocks and gneisses. Knightville Dam is located on the eastern limb of this structural feature; a discussion of the bedrock of this limb follows.

a. Paleozoic rocks - The metamorphic rocks which outcrop within the eastern limb in western Massachusetts are of Ordovician and Silurian age. The Ordovician rocks make a continuous succession of related formations which are distinct from the overlying Silurian rocks. The Ordovician rocks are free of carbon and largely free of iron, whereas the Silurian rocks are very graphitic and iron rich (Emerson, 1917).

1. Savory Schist - The lowermost Paleozoic rock of Ordovician age in Western Massachusetts is the Savory Schist. The schist is light gray, but generally appears greenish when



AFTER: Stanley (1968)

weathered due to the presence of chlorite. Thick beds of sugary limestone are intercalated with the schist and are penetrated by large hornblende crystals. Thin beds of pyroxene limestone are also locally scattered throughout the formation.

2. Hawley Schist - The Hawley Schist is the next oldest formation in the western Massachusetts area. Its mineral constituents vary with location throughout the area. The southern member is a chlorite and sericite schist, whereas the northern member is more of a hornblende schist. The southern member is exposed at various locations.

3. Goshen Schist - The Goshen Schist is a dark gray, graphitic muscovite schist of Silurian age. The Taconic Unconformity exists between this formation and the overlying formations. This rock is commonly arenaceous, containing numerous red garnets and small black mica flakes, and frequently splits into flags.

4. Conway Schist - The Conway Schist is the youngest Silurian member outcropping on the eastern limb of the Anticlinorium. The formation consists of a quartzofeldspathic schist and a dark graphitic muscovite schist. These rocks have been subjected to a medium to high degree of metamorphism.

Common primary minerals are present in the mica schist and the quartzitic schist but both have their own predominant mineral constituents. The primary constituents of the mica schist are quartz, muscovite, biotite and feldspar, while accessory minerals include graphite, manganese garnet, and staurolite. In the quartzofeldspathic schist, quartz and albite are the dominant minerals (Williams et al, 1954).

b. Igneous Intrusions - Igneous rocks, chiefly granite and pegmatite, from dikes and veins throughout the

aforementioned metamorphic rocks of the region. The coarse grained, muscovite-biotite-quartz-feldspar bearing intrusions occur as long, tabular or sheet-like sills aligned parallel to the schistosity, or as dikes which cut across the schistosity of the adjacent rock. The intrusions are highly muscovitic, which indicate that the granite melted the surrounding schists to some extent and incorporated some of the constituents of the schist into the mass (Emerson, 1917).

Throughout the region, most of the intrusions do not seem to have been forcefully injected into the schists, because a majority of the bedrock inclusions within the granite rock maintain the regional trends of the surrounding stratified rocks (Billings, 1941).

4. Structural Geology

a. Folding - Major regional structural trends and minor structural features present in the local strata have been used as evidence to suggest at least four phases of folding in the geologic history of the western Massachusetts area (Jackson, 1975 and Hatch, 1968).

The earliest phase of regional deformation formed north-northeast trending isoclinal folds in Devonian and older rocks. The isoclinal folds are gently to moderately plunging with axial schistosity that generally is the major plane feature of the region. The regional schistosity of the rock units is parallel to the axial surfaces of the north-trending folds formed during this stage of folding. Since these folds are isoclinal, the schistosity is parallel or sub-parallel to the bedding except in axial regions of the folds.

The local intersections of bedding and schistosity throughout the region represent the axis of the early-stage isoclinal folds as evidenced by the parallel schistosity

to the axial surface of the folding stage. The granite and pegmatitic intrusions found throughout the metamorphic rocks are commonly parallel to the axial traces of the early isoclinal folds and are subsequently deformed by all three later stages of folding. The alignment may indicate that the dikes and sills intruded the schists during or following the early stage of folding.

The second stage of deformation did not significantly alter the map pattern of the region, but produced gentle to moderately plunging, tight to open folds with a well developed axial plane slip cleavage.

The third stage of folding influenced the structural map pattern of the region by producing a large, overturned syncline with a well developed northeast-trending, northwest-dipping slip cleavage. This stage, called the Huntington stage of deformation, formed the Huntington syncline which refolded the large early isoclinal folds and changed their north-south axial trends to east-west trends near Huntington, Massachusetts.

The minor folds produced by the Huntington stage of deformation have axial plane slip cleavage which deformed the schistosity of the early stage of folding. The slip cleavage is parallel to the axial surface of small crinkle folds present in the schists. The rocks tend to break parallel to the slip cleavage in zones where it is the dominant planar feature. In the fringe areas at many young minor folds, the slip cleavage has evolved into a schistosity that truncates the bedding and a weakly preserved, early stage schistosity.

The final stage of folding produced large, north-trending open folds which warped the Taconic unconformity separating the Ordovician and Silurian rocks.

b. Faulting - Slemmons and Glass (1978) performed a regional evaluation of the faults and lineaments, basement plutons, topographic lineaments, and major geophysical anomalies of New England. Their work was based on remote sensing and fault compilation data obtained for the study. Their report presents a series of 1:250,000 scale maps for the entire New England and eastern New York region, which show the lineaments detected in the study.

In a later study, Slemmons, Sanders and Whitney (1980) performed a study of active faults in southern New England. Their study included a series of low-sun angle aerial reconnaissance examination of major faults, lineaments, and seismic zones. The region covered in the study included the Connecticut Lowland area, the Moodus earthquake area, faults of the Clinton-Newbury fault system, the Cape Ann area, the Ossipee earthquake area, and the Ammonoosuc fault zone. Their study concluded that all of the faults investigated were inactive or "dead", and are relics of a Paleozoic to Mesozoic Tectonic regime.

5. Regional Seismicity *

A study of the regional seismicity has been conducted and based on historical and instrumental data which have been collected for the northeastern United States and eastern Canada. The historic data go back almost 450 years and are based primarily on "felt" reports. Instrumental data have been collected from a network of more than 100 seismic stations which have been in operation in the northeastern United States since 1975.

Information collected from the more recent instrumental data indicates that, unlike the seismicity pattern

* This is a summary of Professor Toksoz's Work which is presented in Appendix B (Volume 2).

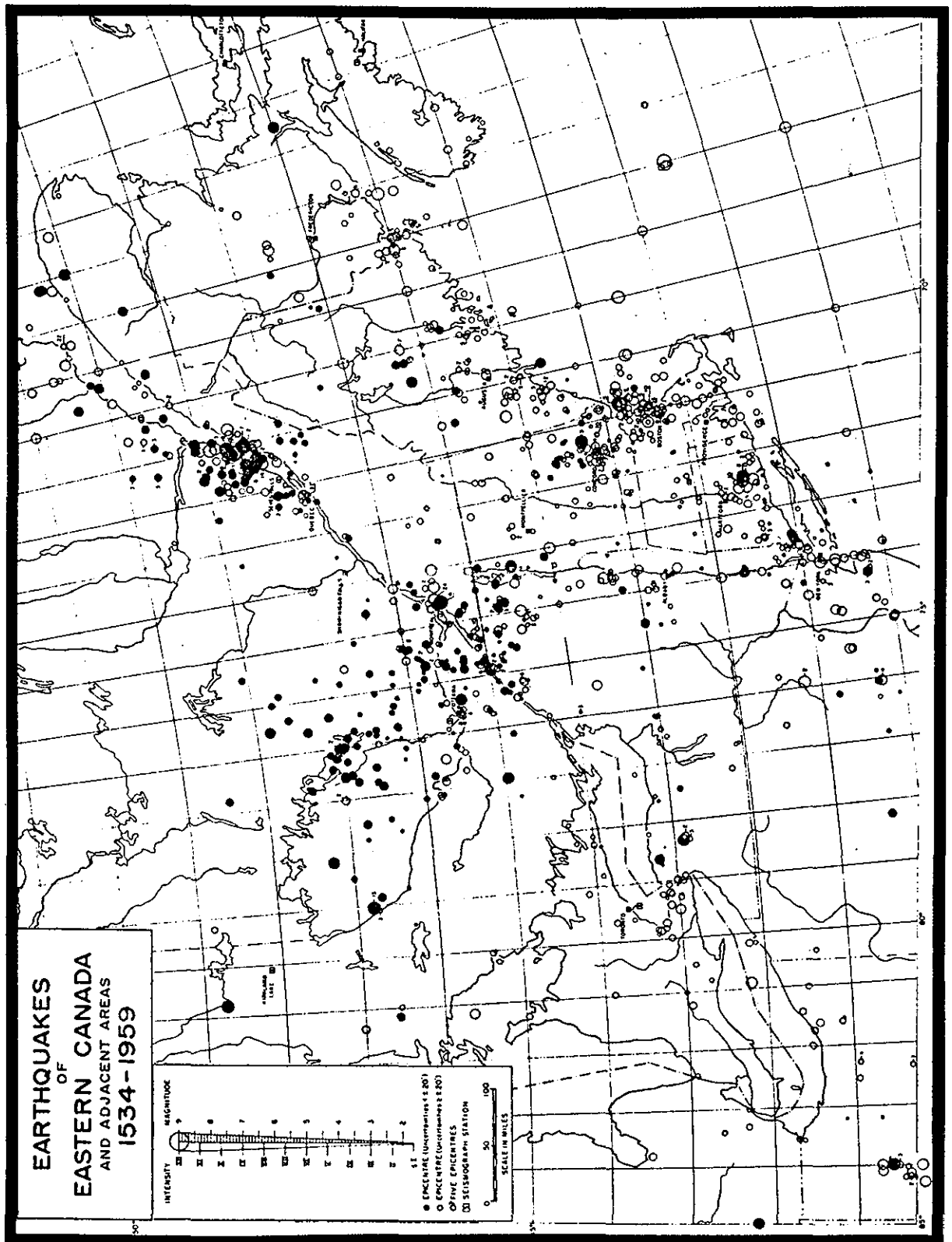
of the western United States, epicenters in the northeast are scattered, and define regional patterns of seismicity rather than well-defined active fault zones. For this reason fault activity is not a primary measure of seismic risk in this region.

Plate 14 shows all regional epicenter data collected for the period 1534 - 1959. The areas which appear to have the most seismic activity include southern Quebec, eastern Massachusetts, central New Hampshire, southern Connecticut and the New York - northern New Jersey area. In general, the vast majority of earthquakes are small, with magnitudes of less than four to five and intensities less than VI to VII. However, moderate to large events have occurred and include the 1727 and 1755 Cape Ann, Massachusetts, 1737 and 1907 New York, New York, 1940 Ossipee, New Hampshire and 1954 Lake George, New York events.

B. SITE GEOLOGY

1. Physiography

Knightville Dam is located on the Westfield River approximately 4-1/2 miles north of the town of Huntington, Hampshire County, Massachusetts. The dam is constructed in the Connecticut River Basin. The Westfield River, which is a major river within the Basin, currently flows through a narrow and steep-sided valley in the vicinity of the damsite. This valley becomes relatively broad and shallow as it approaches the lowlands of the Connecticut River Valley.



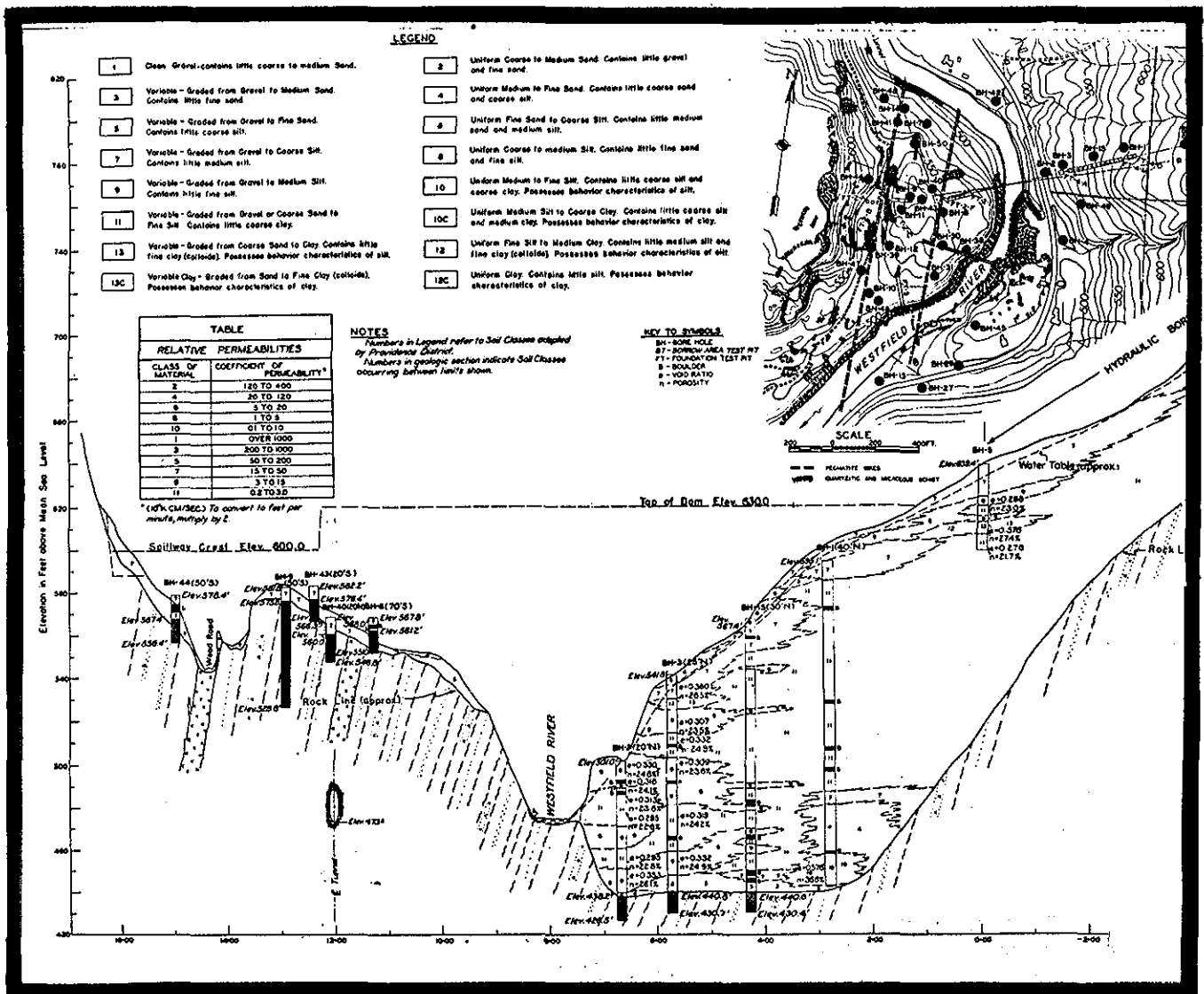
At the damsite, the Westfield River flows through the west side of a buried pre-glacial valley. The river has cut through the thick accumulation of glacial outwash and till which was deposited during the last glacial retreat. Evidence of glacial erosion is seen at the west abutment, where bed-rock is abundantly exposed, and in the present upstream river channel which forms a small box-type rock canyon.

The west bank of the river rises precipitously from the river channel to a maximum height of 60 ft above the stream. A relatively flat plain is located at the top of the cliff which presently serves as the spillway channel. Above the plain, the valley wall rises almost vertically to a height of 170 ft above the spillway channel. The valley floor upstream of the dam has a shallow gradient, gradually rising east of the river channel to approximately the east abutment of the dam. The valley wall steepens in gradient at this point, until it rises to nearly 200 ft above the dam crest.

2. Surficial Geology/Foundation Conditions

During design of the dam, a program of subsurface exploration and sampling was made to investigate the geologic conditions at the site. The program was accomplished by means of auger and wash borings, rock coring and test pits. The location of the boreholes, a description of the foundation materials which were found to exist at the damsite and some of the engineering properties of the overburden materials are shown on Plate 15.

In general, the soils which form the foundation of the dam consist of an unstratified, well-compacted glacial till formation consisting of gravels, sand and silts. Few clay size particles were found to exist in the till. The



AFTER: U.S. Army Corps of Engineers (1939)

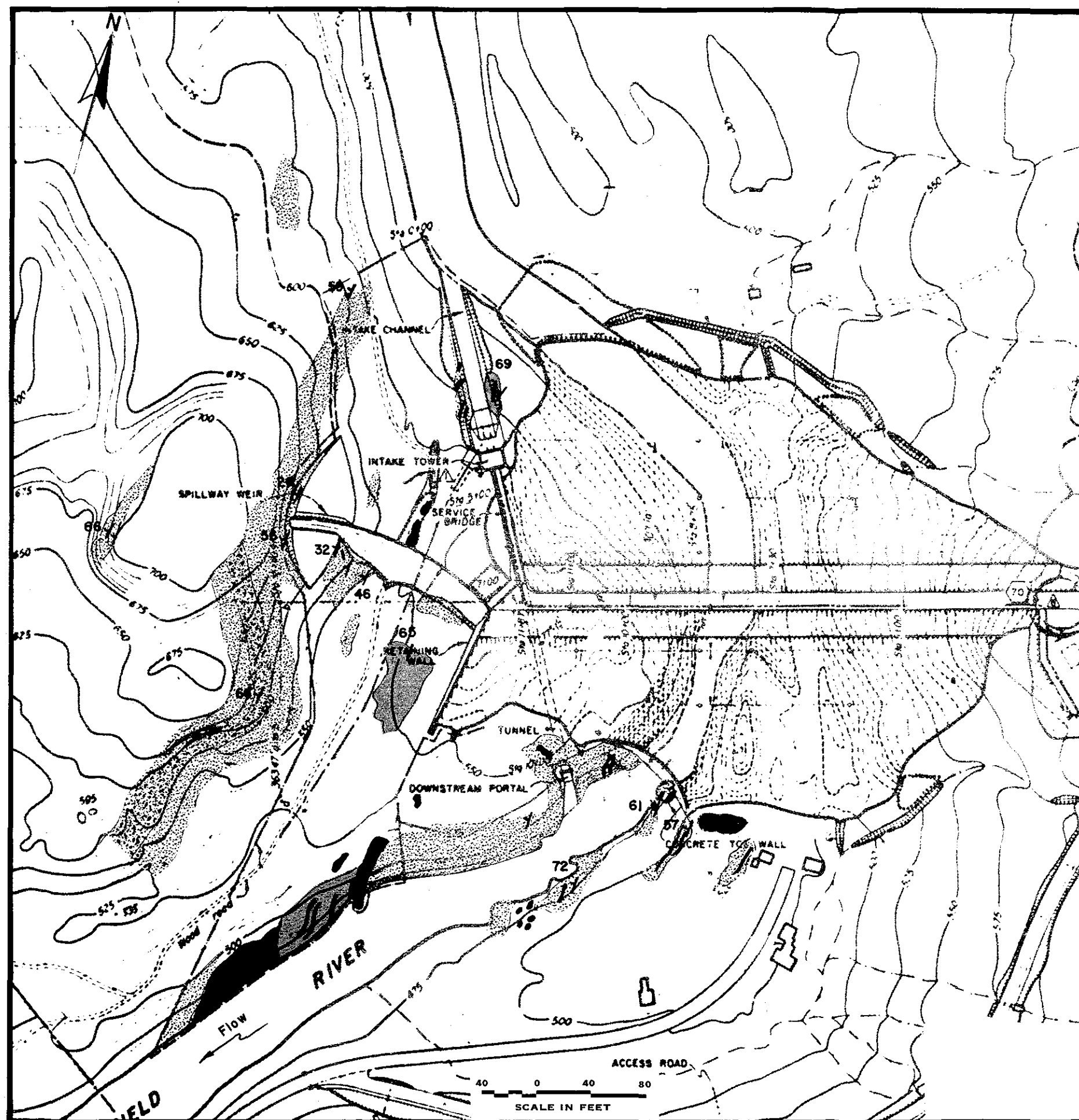
maximum thickness of the till is approximately 160 ft and exists beneath the extreme left abutment of the dam. (See Plate 15). It is uncertain whether the full depth of till was deposited at once or during successive glacial stages. During the exploration and sampling, the till was found to be essentially impervious. Artesian pressures were found to exist in deeply buried more pervious strata usually located directly above rock.

Bedrock was found to exist beneath the dam at the right abutment as shown on Plate 15. The bedrock exists below a thin mantle of till and consists of crystalline quartzitic and micaceous schist. The boreholes made during the field testing program of this work verify the existence of this rock below the embankment. The granite and pegmatite veins beneath the dam and its appurtenant structures form intrusive dikes and veins. These bodies which are located at the west abutment are also shown on Plate 15.

3. Bedrock Geology

The bedrock exposed at the damsite is composed of a series of mica and quartzitic schists with intrusions of pegmatite veins and sills. The exposed metamorphic rocks are the constituents of the Conway Schist Formation. This Formation is continuously exposed along the western wall of the Westfield River valley above the spillway channel, and intermittently exposed along both sides of the intake channel and the downstream river channel immediately adjacent to the dam. (See Plate 16). The rock types which exist at the dam are discussed below.

a. Mica Schist - The principal rock type exposed at Knightville Dam is a finely corrugated muscovite schist. This



LEGEND



Conway Schist: dark gray, finely corrugated graphitic muscovite schist, with biotite, garnet and zoisite.



Conway Schist: very dark gray, finely corrugated, medium-grained, graphitic muscovite schist with garnet and large staurolite crystals.



Conway Schist: white, hard, fine-grained quartzitic schist with low abundance of mica and graphite flakes.



Pegmatite: white, coarse grained, muscovite-biotite-quartz-feldspar pegmatite.

56



Strike and dip orientation and dip angle.

NOTES:

1. Strike and dip orientation and dip angle were determined during a field investigation by a TAMS geologist.
2. Not all dip angles could be measured.

DYNAMIC STABILITY ANALYSIS OF
KNIGHTVILLE DAM
NEW ENGLAND DIVISION, COE
SITE OUTCROP MAP

rock is dark due to the abundance of graphite. The major constituents of the schist are quartz, feldspar and mica; secondary minerals include garnet, staurolite, zoisite and hornblende. The graphite occurs as disseminated flakes and scaly masses within the schist, and can easily be identified by its metallic-greasy luster. The graphite has crystallized with its perfect cleavage planes oriented parallel to the foliation of the rock.

The major constituents of the mica schist are interlocked to form a completely crystalline mass which have been separated into beds. The preferred orientation of the flakes of graphite and layered silicates result in the formation of thin laminations. The rock outcrops are generally thinly bedded.

A band of mica schist containing large crystals of staurolite outcrops along the west valley wall approximately 80 feet above the spillway crest (See Plate 16). The addition of long, opaque staurolite crystals to the mica schist produces a much darker surface than the surrounding outcrops of schist. The staurolite occurs as prismatic crystals with a glassy luster which are randomly oriented with respect to the foliation.

In general, the mica schist is a hard rock that is only slightly weathered. The weathered zone extends less than 1/16-inch into the surface of the outcropping schist. A majority of the outcrops have a hard surface layer of foliation that does not flake or peel. Some of the outcrops are covered with a moss which grows in a yellow-brown medium-grained soil. The moss develops in planar partings of the schist and causes them to split.

One outcrop, approximately 12 feet in length and 8 feet high and exposed nearly 50 feet downstream from the spillway crest along the west valley wall, contains zones of highly to slightly weathered rock. The highly weathered rock

is friable, yielding flakes of foliated schist when the surface is rubbed. The dark, micaceous and graphitic enriched layers appear to be more friable than the nearly lighter, slightly quartzitic enriched layers. A two inch thick slab was easily broken off perpendicular to the foliation; the ensuing fresh surface was almost completely ironstained. Minor crevices and plant partings of the schist, found in small drainage channels in the highly weathered zone, are coated with a white, siliceous cement.

b. Quartzitic Schist - A band of quartzitic schist along a discontinuous line which extends from the west bank of the river channel, along the east wall of the spillway channel, and along the intake tunnel channel before being covered by glacial deposits. The quartzitic schist is a hard, white-gray, fine-grained rock with well-developed planar features. The primary constituents of the quartzitic schist are quartz and albite. The preferred orientation of the mica flakes is parallel to the foliation of the schist.

The quartzitic schist appears to be harder and more dense than the surrounding mica schist. In general, the quartzitic schist does not have the thinly laminated planar partings; instead, there are thin beds of schist broken up by a set of joints aligned transversely to the preferred orientation of the grains.

c. Pegmatite - Outcrops of pegmatites are present along both banks of the downstream river channel and the intake channel (See Plate 16). The pegmatite outcrops are a coarse grained, white, igneous intrusive rock composed principally of quartz, alkali feldspar, and muscovite. Accessory minerals include garnets, biotite, and hornblende.

Large pegmatite boulders are present in the downstream spillway channel, and there is an accumulation of very large pegmatite boulders and rubble found on the east bank of the river channel approximately 70 feet downstream of the outlet tunnel. A number of pegmatite boulders found in the downstream river channel contain large crystals of tourmaline; however, no large tourmaline crystals were observed in the pegmatite outcrops near the dam.

The majority of the pegmatite outcrops near the dam are exposed as sills which parallel the local foliation. The intrusive pegmatite sills have a sharp unweathered, predominantly closed contact with the surrounding schist. Along some of the sills, there is an 1/8-inch spacing between the pegmatite and the intruded schist. Visually no alteration zone could be found in the schist along the contact with the pegmatite, and there are no signs of weakness due to weathering along the observed contacts. Overall, the pegmatites are very hard and very faintly weathered, showing only localized minor discoloration.

A very large sill of pegmatite on the west bank of the downstream river channel has been exposed as a result of erosion by the river. The pegmatite also is found as dikes and lenses which either cut through the planar foliation or are aligned in a sub-parallel direction to the foliation.

4. Structural Geology

The orientations of the exposed metamorphic and igneous rocks near the dam coincide with the regional trend for folds and planar orientation. A well-developed, north-east-trending, northwest-dipping slip cleavage is present in all of the metamorphic outcrops. The strike of the planar bedding which is common to all of the rock types exposed near the dam is N10 to 15°E, steeply inclined to the west with an

average dip of 60 degrees. Local variations in dip were measured, and ranged from about 25 to 75 degrees west.

Examination of two outcrops located near the dam indicate that the schist has been deformed. A change in dip angle in the outcrops occurs along the west bank of the intake channel next to the tunnel. The planar bedding is curvilinear, with the strike appearing to remain N10 to 15°E, but the dip becomes steeper with increasing depth. It appears that the axis to the fold is east of the intake tunnel and tower.

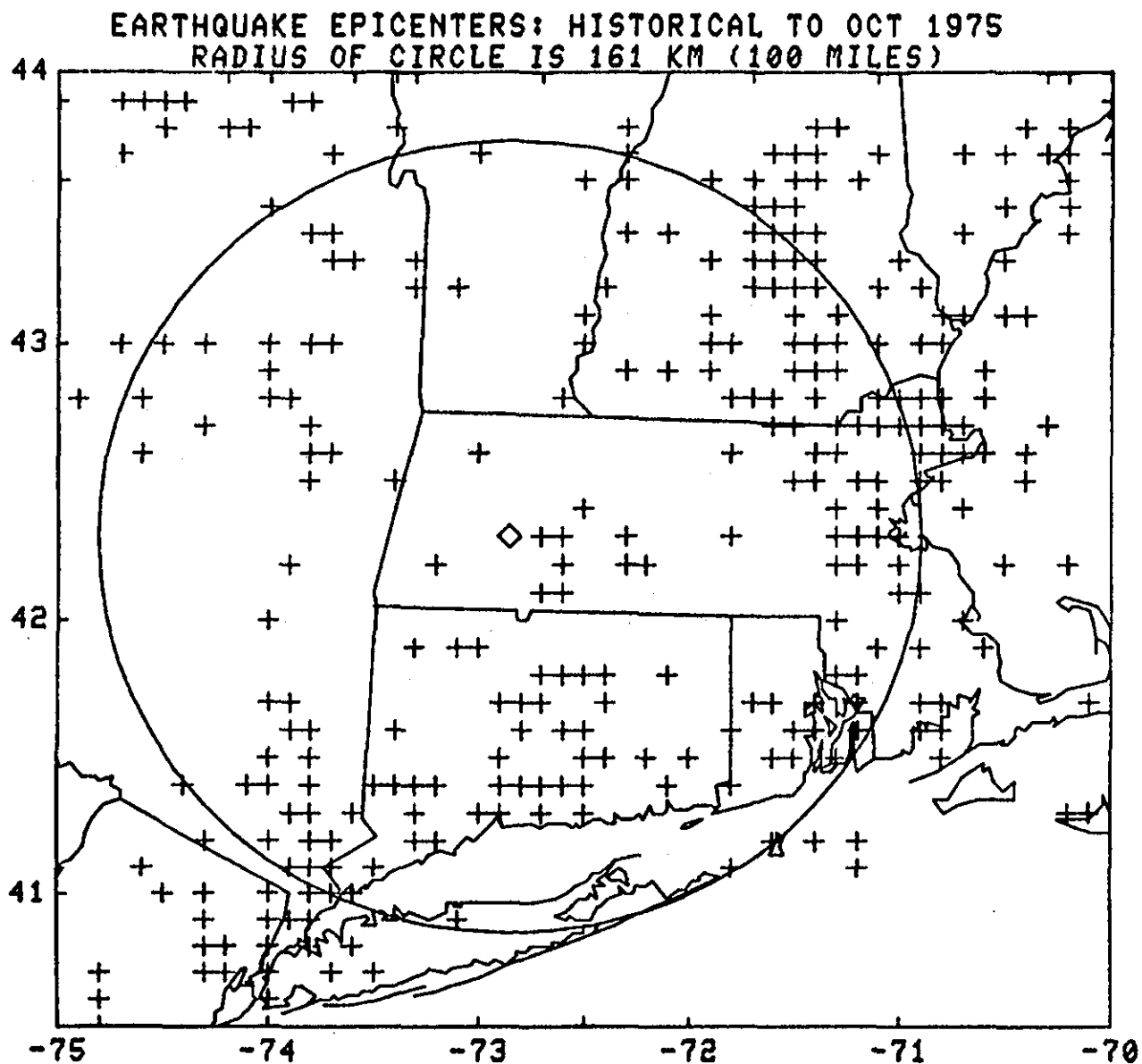
There is no evidence of faulting at the dam. The quartzitic schist is surrounded by the mica schist, and there is no exposed unconformity to suggest that the quartzitic schist is a member of a different formation. Most of the contacts between the two schists in the downstream spillway channel are covered with overburden.

5. Local Seismicity *

To analyze the local seismicity in the vicinity of Knightville Dam, a STUDY area was established and included a region encompassed by a 100 mile radius and its immediate surrounding region. If only the region inside the 100 mile radius had been considered, then the significant seismically active zones of central New Hampshire, northeastern Massachusetts and New York would be excluded in the analysis.

Plates 17 and 18 show the historic earthquake epicenter for the period 1568 to 1975 and the instrumental earthquake epicenters for the period October 1975 to March 1981, respectively. A clustering of epicenters close to the damsite as shown on Figure 17, occurs primarily in the Connecticut Valley region to the east. Although these events are small, they are important because of their proximity to the damsite.

* This is a summary of Professor Toksoz's work which is presented in Appendix B.



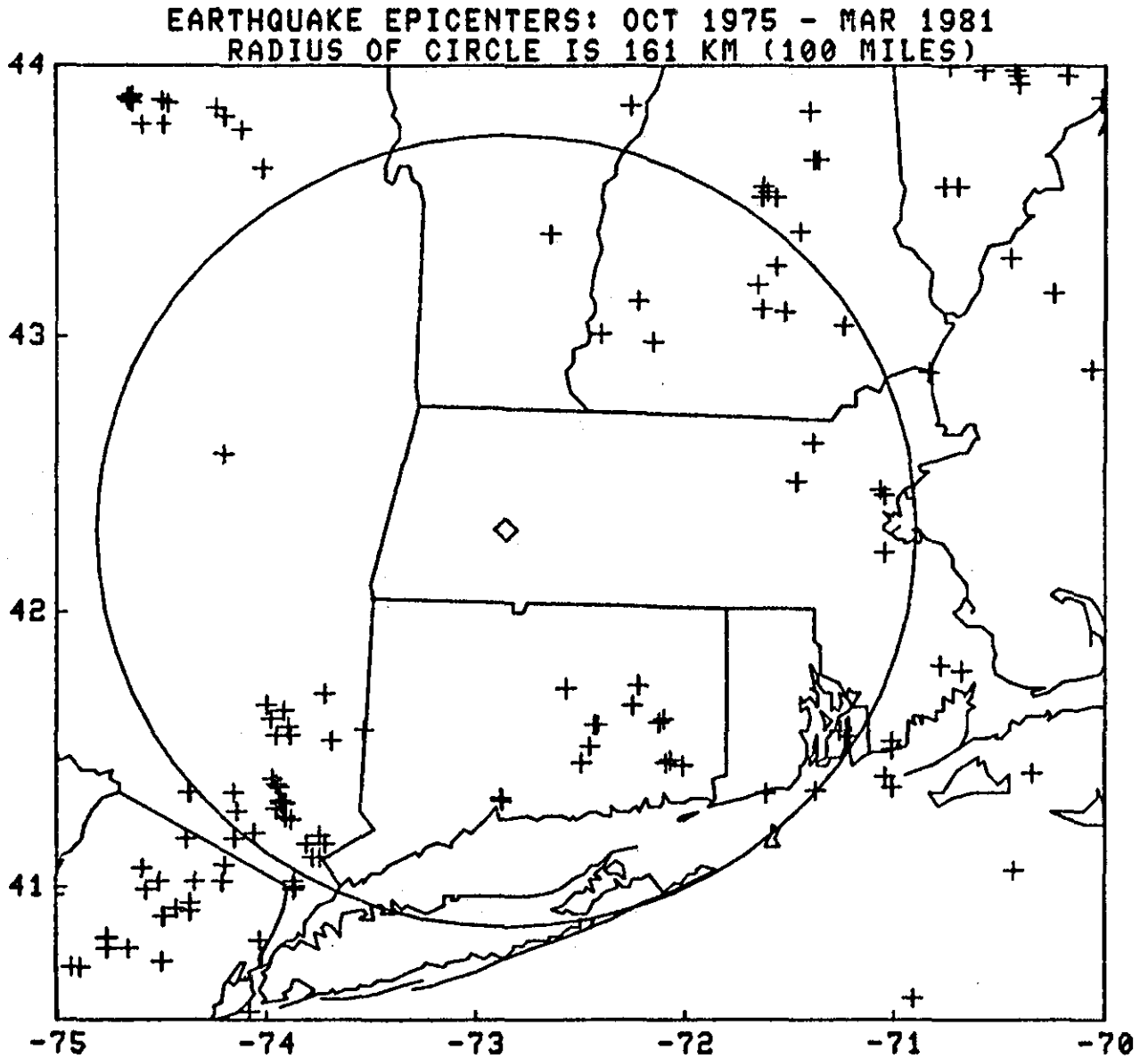


Plate 18 shows that no close events were recorded for the period October 1975 to March 1981. Table 4 summarizes the significant earthquakes within the Knightville Dam STUDY AREA. (A significant earthquake is defined as an event of intensity of at least VII or magnitude of at least 5.0).

Analyses were performed, utilizing the Gutenberg and Richter (1956) statistical relation, to determine the recurrence interval of different intensity and magnitude earthquakes based on the historical and the instrumental data sets. The statistical results indicate the following recurrence intervals for the various earthquakes:

DATA SET: (1568 to Oct. 1975)		DATA SET: (Oct. 1975 to Mar. 1981)	
<u>Intensity</u>	<u>Recurrence Interval (years)*</u>	<u>Magnitude</u>	<u>Recurrence Interval (years)*</u>
V	5	4.0	8
VI	20	5.0	90
VII	80	6.0	1000
VIII	325		
IX	1300		

* For an explanation of the reliability of these data, See Professor Toksoz's Report in Appendix B (Volume 2).

Similar analyses were performed utilizing the earthquake data collected within a 50 km distance of the dam. The results indicate that an intensity V earthquake can be expected to occur within this close region every 70 to 100 years. This return period is considerably longer when compared to the results from the 1568 to 1975 data set; this difference is simply a reflection of the much smaller area of consideration and the fact that the area within 50km of the dam is characterized by a lower rate of seismic activity than that of the entire STUDY AREA.

Table 4

SIGNIFICANT EARTHQUAKES WITHIN THE KNIGHTVILLE DAM STUDY
AREA (A SIGNIFICANT EARTHQUAKE IS ONE OF INTENSITY AT LEAST
VII OR MAGNITUDE AT LEAST 5.0 m_b)

<u>Year</u>	<u>Dis- tance in km</u>	<u>Magni- tude m_b</u>	<u>Int</u>	<u>State</u>	<u>Area</u>
1727	193	-	7	MA	Cape Ann
1737	192	-	7	NY	New York
1755	214	-	8	MA	Cape Ann
1884	212	-	7	NY	New York
1931	141	-	7	NY	Lake George
1940	209	5.4	7	NH	Ossipee
1940	209	5.4	7	NH	Ossipee

V. SELECTION OF DESIGN EARTHQUAKES

A. SEISMIC HAZARD ANALYSIS

In the previous section, the regional and site seismicity was reported and included the history of the earthquake activity and the estimate of the return times for various earthquake activities. These data were used to estimate the accelerations which would be produced by the Maximum Credible and Operating Basis Earthquakes.

The peak ground accelerations at the damsite were computed using relationships proposed by Klimkiewicz (1980) and Nuttli (1979), Nuttli and Hermann (1981), and Battis (1981). The computed values of peak ground accelerations (pga) are a function of earthquake magnitude and distance from the source, and are based on the recorded history of seismic activity in the area.

In New England seismic activity is not associated with known faults, and it is therefore difficult to determine on a geologic basis the largest possible earthquake in the region. Two assumptions were therefore made in the analysis, as follows:

(1) The largest earthquake in the STUDY AREA will occur where there have been high seismic activity based on all historical and instrumental data, and

(2) The Maximum Credible Earthquake in the STUDY AREA will have a source magnitude equal to that of the largest actual event in the STUDY AREA plus a one-half m_b unit.

The peak ground accelerations due to the Maximum Credible Earthquake were computed separately for regional events (those outside the 50 km radius from the dam) and the local events (those inside the 50 km radius). The seismic hazard analysis for this work was performed by Professor Nafi Toksoz, and is presented in Appendix B (Volume 2).

1. Regional Events (50 to 215 km)

a. Maximum Credible Earthquake - The Maximum Credible Earthquake for a regional event was computed and based on the location of large historical events ($\text{MMI} \geq \text{VII}$) in the STUDY AREA. These events occurred at Ossipee, New Hampshire; Cape Ann, Massachusetts; New York, New York; Lake George, New York; E. Haddam, Connecticut; and Torrington, Connecticut events (See Table 5). In addition, a small close event which occurred at Leeds, Massachusetts (March 14, 1893, $\text{MMI} = \text{IV}$), which is approximately 12 km from the damsite, was also included. The maximum credible magnitudes for each of these events were computed by increasing the recorded intensities (or equivalent magnitudes) by a one-half m_b unit (See Table 5).

The computed peak ground accelerations at the damsite from these credible events are shown in the last three columns of Table 5. Using the statistical relationship of Nuttli (1979), a range of accelerations from 20 to 60 cm/sec^2 was obtained; the largest value resulted from the events at Cape Ann, E. Haddam and Torrington. Using the equations of Nuttli and Hermann (1981), the computed accelerations range from 17 to 42 cm/sec^2 , the largest acceleration being produced by the close event at E. Haddam. Finally, using Battis' (1981) equations the largest computed acceleration was 82 cm/sec^2 from the Cape Ann event.

It is important to note that the values determined using Battis equations are the peak ground accelerations (pga). Values calculated by Nuttli and Hermann are sustained acceleration (or the average value for three cycles about the maximum). Sustained acceleration is lower than the peak acceleration, generally by a factor of 1.2 to 1.5. The discrepancy of about a factor of 2 between the two sets is partly

Table 5

ACCELERATION FOR MAXIMUM CREDIBLE EARTHQUAKE
WITHIN THE KNIGHTVILLE STUDY AREA

Area	dist. in km	max. cred. m_b	Int ¹	Accel ²	cm/sec ² Accel ³	Accel ⁴
Ossippe, NH	205	6.0	5	20-50	17	46
Cape Ann, MA	213	6.5	5 1/2	30-60	29	82
NY City, NY	197	6.0	5	20-50	19	48
Lake George, NY	136	5.5	4 3/4	25-45	19	39
E. Haddam, CT	89	5.7	5 1/2	30-60	41	76
Torrington, CT	50	5.0	5 1/2	30-60	35	54
Leeds, MA	12	4.0	5 1/2	30-60	42	37

- 1) Intensity calculated via Klimkiewicz (1980)
- 2) Acceleration from the acceleration-intensity curve of Nuttli (1979).
- 3) Acceleration calculated from the expressions of Nuttli and Hermann (1981)
- 4) Acceleration calculated from the expression of Battis (1981)

due to different models of attenuation. However, based on the recent data collected from the Gaza, New Hampshire event (January 19, 1982, $m_b = 4.7$), Battis' attenuation values are more applicable to New England than those to Nuttli and Hermann, as described subsequently. Thus the maximum pga value (82 cm/sec^2) computed using Battis' curves will be used for analysis from the Cape Ann event ($m_b = 6.5$).

It is important to check the validity of the 82 cm/sec^2 pga and to obtain a measure of its variability such as the standard deviation or 95 percent confidence intervals. This is done by comparing the computed pga value with the observed values of different earthquakes of magnitudes comparable to the "hypothetical" Cape Ann event ($m_b = 6.5$). A discussion of this comparison procedure is presented in Professor Toksoz's report (See Appendix B). The results indicate, based on California earthquake statistical data, that for a mean pga value of approximately 80 cm/sec^2 , the mean value plus one standard deviation can be as high as 125 cm/sec^2 , and the mean value plus two standard deviations is 200 cm/sec^2 .

b. Operating Basis Earthquake - The Operating Basis Earthquake is defined by the U.S. Nuclear Regulatory Commission as "the largest earthquake that reasonably could be expected to affect a structure during the life of the structure". For analysis a nominal life of 100 years is assumed for Knightville Dam. Based on the recurrence interval analyses previously reported the largest event likely to occur in 100 years would have a source intensity (MMI) of 7.5 or equivalent magnitude of $m_b = 5.5$. This event is most likely to occur in the Cape Ann, Massachusetts or Ossipee, New Hampshire seismotectonic zone. Placing such an event at the closest distance of 160 km and using Battis' (1981) attenuation curves, a peak ground acceleration of 32 cm/sec^2 is obtained. If variations with azimuth due to source and lateral heterogeneity are assumed to be similar to those of

the San Fernando earthquake (See Toksoz's Report), a mean plus one standard deviation of 52 cm/sec^2 and a mean plus two standard deviations of 84 cm/sec^2 are obtained.

2. Local Events ($\leq 50 \text{ km}$)

a. Maximum Credible Earthquake - The earthquake within the radius of 50 km of the dam present a problem. These are all historic events. They are generally small. There has been no detailed analysis of the reliability of their assigned intensities. The closest earthquake to the dam (distance = 12 km) is the Leeds, Massachusetts earthquake of 14 March 1893 with intensity of IV. To determine Maximum Credible Earthquake the same criteria as used for the regional events was applied. The intensity was increased by one unit and the peak ground acceleration at the damsite was computed to be less than about 45 cm/sec^2 . At such short distances, however, earthquake source properties (finiteness, rupture propagation, asperities of stress drop across the fault plane) and local geologic heterogeneities can affect the maximum accelerations at a given site. The Gaza, New Hampshire earthquake of 19 January 1982 provided some strong motion data relevant to this problem; this is discussed in the next section.

b. Implications of the Strong Motion Data from the Gaza, New Hampshire Earthquake (January, 1982) - On January 19, 1982, (January 18 local time), an earthquake of $m_b=4.7$ occurred in Gaza, New Hampshire. This earthquake was recorded by the northeastern U.S. seismic network and is presently being studied in detail. The earthquake also triggered the strong motion instruments located at six different sites at distances of 7 to 104 km. These instruments were installed and are operated by the Corps of Engineers. The stations, distances, and recorded accelerations are listed in Table 6. The importance of these data is that for the

Table 6

STRONG MOTION RECORDS FROM
GAZA, N.H. EARTHQUAKE

The Gaza, NH Earthquake of Jan, 19, 1982

Epicenter data: O.T. 00:14:42.5 UTC

Latitude 43.520

Longitude -71.610

Depth 5 km (approx)

Magnitude 4.7 (m_b)

Strong Motion Data

Peak Acceleration Values

	L		V		T		Resolved horiz	
	g	cm/s ²	g	cm/s ²	g	cm/s ²	g	cm/s ²
Franklin Falls Dam, NH								
Distance = 7 km								
Abutment	0.22	218	0.14	136	0.56	544	0.60	586
Crest	0.10	100	0.10	101	0.24	238	0.26	258
Downstream	0.08	77	0.14	136	0.31	307	0.32	317
North Hartland Dam, VT								
Distance = 62 km								
Crest	0.02	23	0.02	17	0.02	22	0.03	32
Union Village Dam, VT								
Distance = 61 km								
Abutment	0.01	6	0.01	6	0.01	5	0.01	8
Crest	0.02	22	0.02	22	0.03	26	0.03	34
Downstream	0.03	34	0.03	34	0.03	26	0.04	43
White River Jtn., VT								
Distance = 61 km								
Basement	0.02	15	0.02	17	0.02	21	0.03	26
North Springfield Dam, VT								
Distance = 75 km								
Downstream	0.03	31	0.02	15	0.02	23	0.03	39
Crest	0.03	31	0.02	15	0.02	15	0.03	34
Ball Mountain Dam, VT								
Distance = 104 km								
Crest	0.01	11	0.02	15	0.01	12	0.02	16

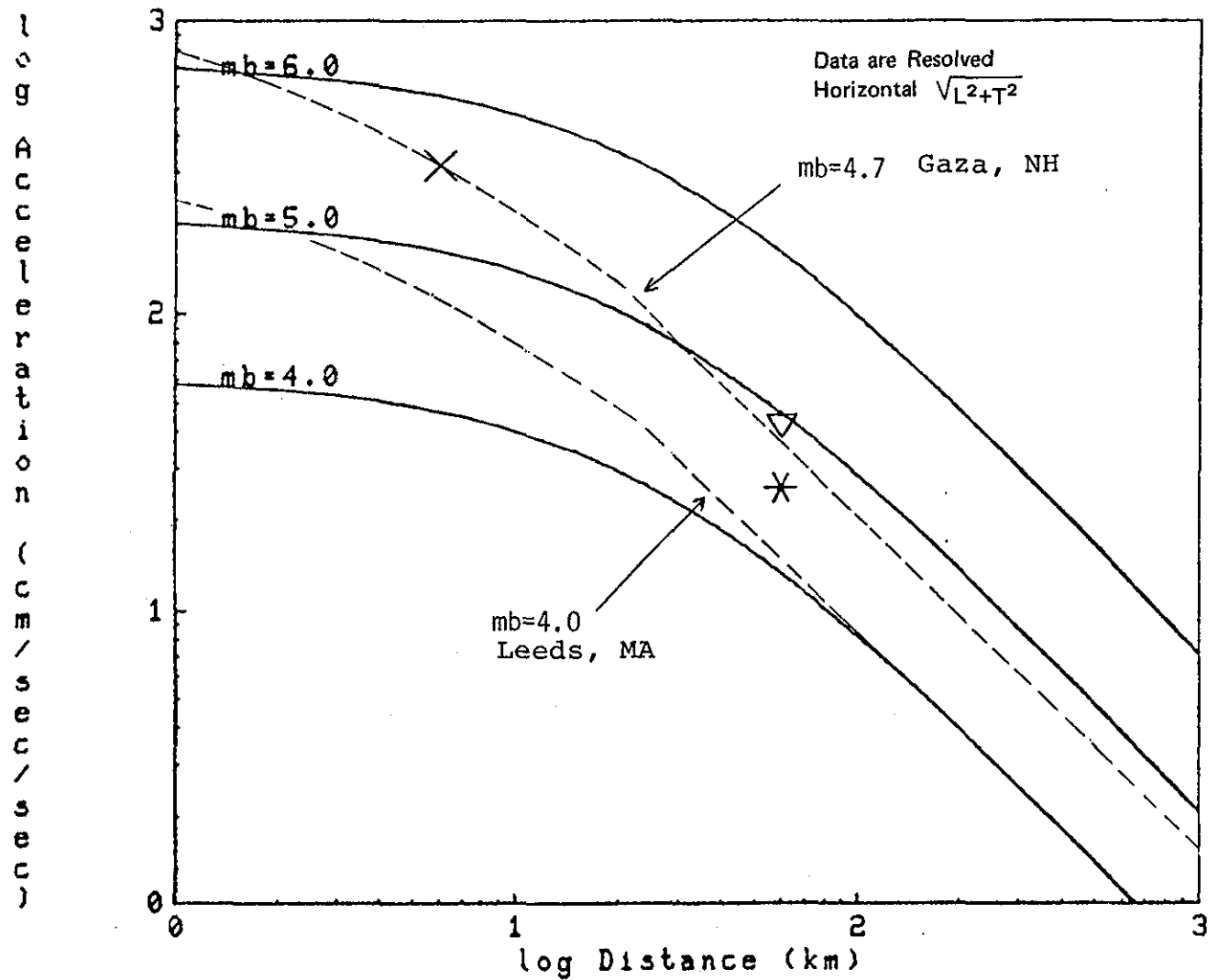
first time strong motion records in New England for an earthquake of known magnitude are available.

The Gaza, New Hampshire earthquake should be given great weight for estimating the peak ground acceleration at Knightville Dam for this project, since the Maximum Credible Earthquake close to the dam is based on the Leeds, Massachusetts event of March 14, 1893. Its size is comparable to the Gaza earthquake ($m_b = 4.0$ vs. 4.7) and the Gaza-Franklin Falls Dam distance (7 km) is also similar to the Leeds-Knightville Dam distance (12 km).

Free-field accelerations are of interest in this study, therefore, data collected at the downstream stations rather than the crest or abutments were used. Further, to obtain the peak horizontal acceleration, the vector sum of the longitudinal and transverse components was computed. The difference between this "resolved" horizontal value and the larger of the two components is not significant as can be seen in Table 10.

The acceleration observations from the Gaza, New Hampshire earthquake have been superposed onto the decay curves of Battis (1981), as shown in Plate 19. The curves are shown to roughly parallel Battis's curves for acceleration versus distance for the Gaza, New Hampshire data and a new curve for $m_b = 4.0$, which corresponds to the Maximum Credible Earthquake at Leeds, Massachusetts. For a distance of 12 km, an acceleration of about 70 cm/sec^2 is obtained. As is shown in Table 6 and Toksoz's Report, at "close-in" distances, accelerations can vary by a factor of 2 to 5 with azimuth, due to source properties and local ground conditions. Given a 70 cm/sec^2 mean value, peak acceleration of $200\text{-}300 \text{ cm/sec}^2$ due to the maximum credible event could be expected.

Battis (1981)



LEGEND

- X Franklin Falls Dam, NH Downstream
- ∇ Union Village Dam, VT Downstream
- * White River Junction, Vt Basement of VA Hospital

c. Operating Basis Earthquake - The frequency-magnitude statistics for the local events is poor due to a few data points. However, the return period of an earthquake $m_b = 4.0$ is about 100 years. Thus, the $m_b = 4.0$ is also the Operating Basis Earthquake, and pga values between 200-300 cm/sec² could also be expected for this event.

B. DESIGN EARTHQUAKES

1. Regional Event

a. Ground Motions - For "regional" model earthquakes, the calculated value of peak ground acceleration due to the Maximum Credible Earthquake is 82 cm/sec². This is due to the model earthquake at Cape Ann, Massachusetts with $m_b = 6.5$. The 82 cm/sec² is in good agreement with other estimates for the general area of New England. It also compares favorably with European data, and after correction for attenuation differences, with peak ground acceleration values from California earthquakes of similar magnitudes (Borrego Mountain earthquake of 1968 and mean of the San Fernando earthquake of 1971). This 82 cm/sec² should be considered the mean value. Mean plus one standard deviation gives 125 cm/sec² and mean plus two standard deviations gives a peak ground acceleration value of 200 cm/sec², on the basis of global data.

For the analysis, a peak ground acceleration value of 200 cm/sec² is selected for the Maximum Credible Earthquake. The choice of the mean plus two standard deviations for the maximum credible peak ground acceleration (instead of mean plus one standard deviation) is based on both the expected scatter of the ground acceleration for a given earthquake, and the uncertainties associated with the distance and the magnitude of the maximum credible earthquake. Since this hypothetical event is distant and of magnitude 6.5, the frequency at peak acceleration will be between 1 and 5 Hz and

duration of shaking at least 10 seconds.

For the Operating Basis Earthquake a peak ground acceleration of 32 cm/sec^2 has been computed. The mean plus one standard deviation is 53 cm/sec^2 and the mean plus two standard deviations is 84 cm/sec^2 . For the previously mentioned reasons, the value of 84 cm/sec^2 has been selected for the peak ground acceleration for the Operating Basis Earthquake. Peak frequency is likely to be between 2 and 6 Hz.

Calculated velocity and displacement values corresponding to peak ground accelerations at the nominal peak frequencies are given in Table 7. All of the data presented is for free field rock motions.

b. Strong Motion Record - Selection of the strong motion records for the design earthquakes was made by Professor Whitman, with corroboration of Professor Toksoz and TAMS' project personnel. Professor Whitman's Report entitled, "Strong Motions for Use in Analysis of Knightville Dam," is presented in Appendix C. One of the major problems which exists in selecting time history series for this work is the lack of suitable strong motion recordings in the Eastern United States.

For the regional event; the N55E component of the Puddingstone Reservoir time series was selected for both the Operating Basis Earthquake (84 cm/sec^2) and the Maximum Credible Earthquake (200 cm/sec^2). This time series is reproduced in Plate 20. This series resulted from the San Fernando, California earthquake ($m_p = 6.4$) of February 1971, and was recorded at the reservoir site, approximately 70 km from the epicenter. The peak acceleration measured at Puddingstone Reservoir was 70 cm/sec^2 . The predominant measured frequencies ranged from 1 to 5 Hz, and the duration of the strongest part of the shaking was approximately 10 seconds. This record can be

Table 7
SUMMARY TABLE OF RECOMMENDED
FREE-FIELD ROCK GROUND MOTIONS

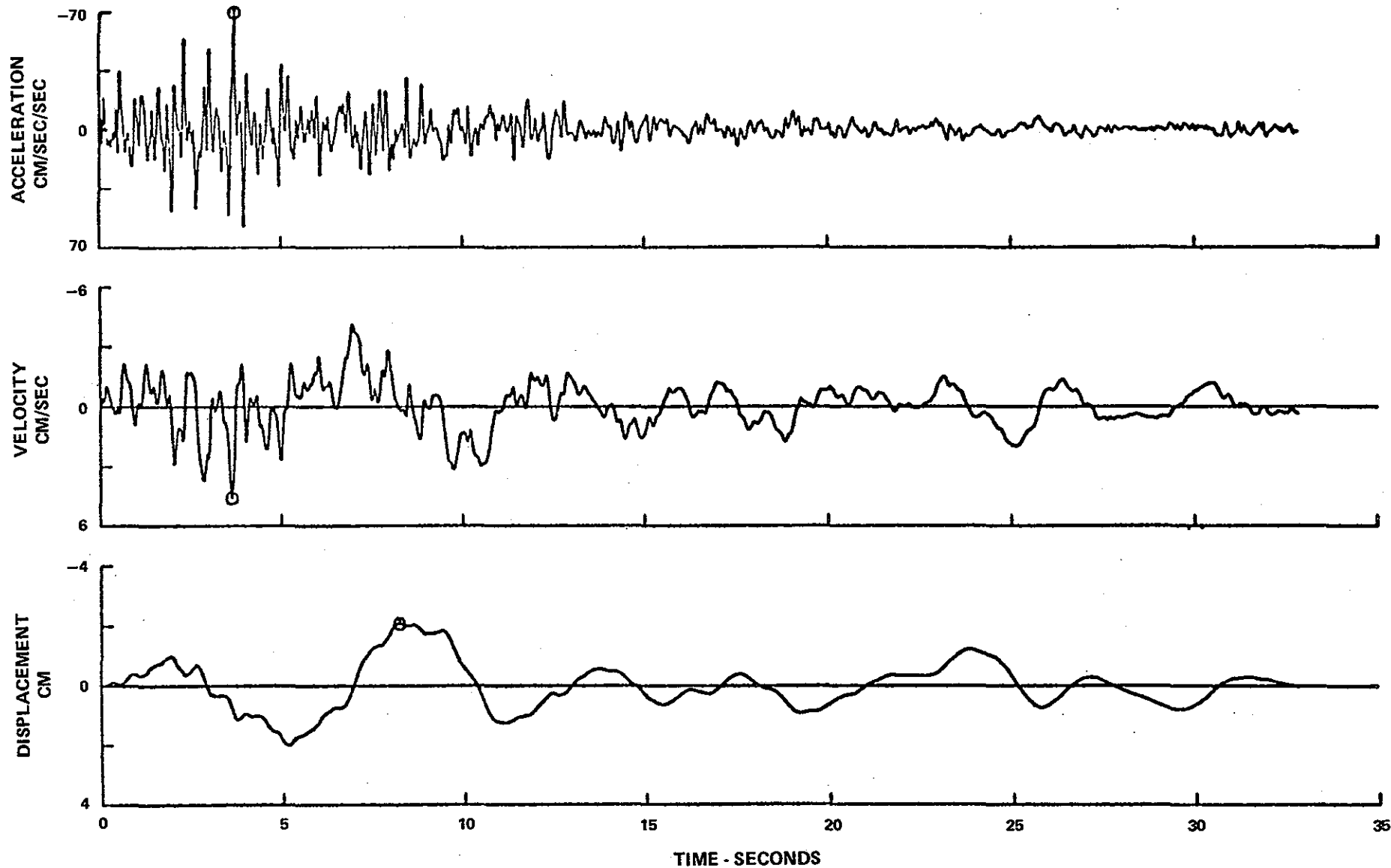
Epicenter Area (Seismotectonic Zone)	<u>Regional</u>	<u>Operating Basis</u>	<u>Local*</u>
	Maximum Credible Earthquake	Earthquake	Maximum Credible Earthquake
	Cape Ann, MA	Cape Ann, MA or Ossipee, NH	Leeds, MA
Nominal Distance to Knightville Dam (kg)	213	213	12
Magnitude (m_b)	6.5	5.5	4.0
Peak Frequency (Hz)	3.0	4.0	12.0
Acceleration at Dam mean cm/sec^2	82.	32.	70.
Acceleration at Dam mean $+1\sigma \text{ cm/sec}^2$	125.	52.	-
Acceleration at Dam mean $+2\sigma \text{ cm/sec}^2$	200.	84.	250.**
(1) Velocity at Dam mean cm/sec	4.35	1.70	0.93
Velocity at Dam mean $+1\sigma \text{ cm/sec}$	6.63	2.76	-
Velocity at Dam mean $+2\sigma \text{ cm/sec}$	10.6	4.46	3.32
(1) Displacement at Dam mean cm	0.23	0.09	0.01
Displacement at Dam mean $+1\sigma \text{ cm}$	0.35	0.15	-
Displacement at Dam mean $+2\sigma \text{ cm}$	0.56	0.24	0.04

* Same value for Maximum Credible and Operating Basis earthquake.
(see text)

** Estimate based on scatter of near field data. (see Appendix B).

(1) Velocity and displacement corresponding to peak acceleration
at listed frequency (these are not peak velocity and peak
displacement).

V-12



DYNAMIC STABILITY ANALYSIS OF
KNIGHTVILLE DAM
NEW ENGLAND DIVISION, COE
PUDDINGSTONE RESERVOIR
STRONG MOTION RECORD

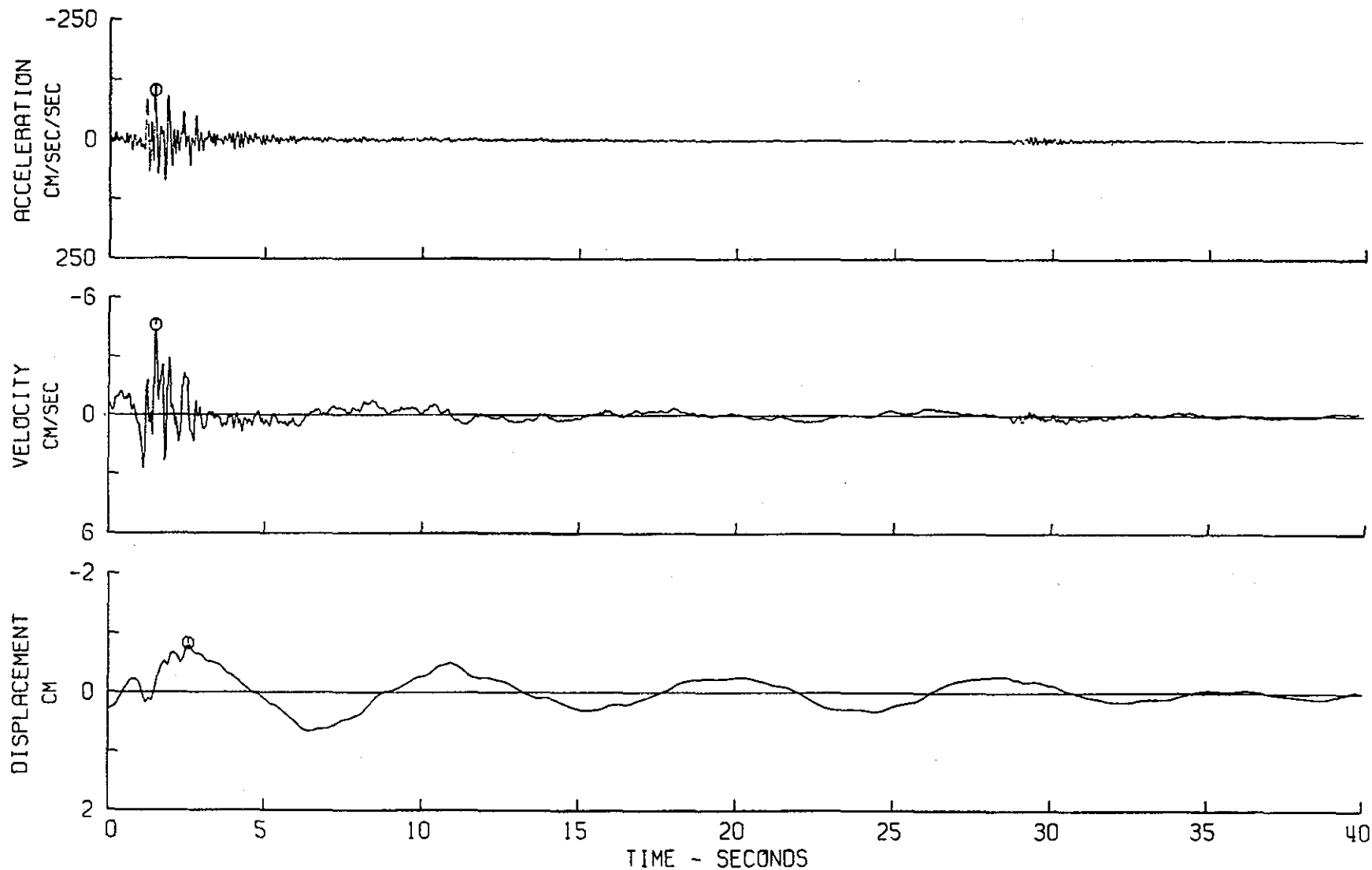
normalized to 84 cm/sec^2 and 200 cm/sec^2 to represent the Operating Basis Earthquake and the Maximum Credible Earthquake, respectively.

2. Local Event

a. Ground Motions - For local events the picture is more complicated. The nearest known event to the Knightville Dam occurred near Leeds, Massachusetts at a distance of 12 km on March 14, 1893. A local Maximum Credible Earthquake based on the central U.S. attenuation models gives a peak ground acceleration of $30\text{-}60 \text{ cm/sec}^2$. However, if the results of the preliminary analysis of the strong motion data from the Gaza, New Hampshire earthquake of January 19, 1982, and a Maximum Credible Earthquake near Leeds, Massachusetts are used, a peak ground acceleration of 70 cm/sec^2 is obtained at the damsite. Given the variability of peak ground accelerations due to source properties and local heterogeneities, peak accelerations of 200 to 300 cm/sec^2 cannot be ruled out. The durations of such motions will be short and the frequencies will be high (10-15 Hz). The return period of the local Maximum Credible Earthquake is less than 100 years. Thus, above values of peak ground acceleration apply for the Operating Basis Earthquake. Corresponding values of ground velocity and displacement are summarized in Table 7. Again, these values are for free field rock motions.

b. Strong Motion Record - For the event, the recommended time series is the S80E component of the record at Golden Park during the San Francisco Earthquake of 22 March 1957. This series is reproduced in Plate 21.

V-14



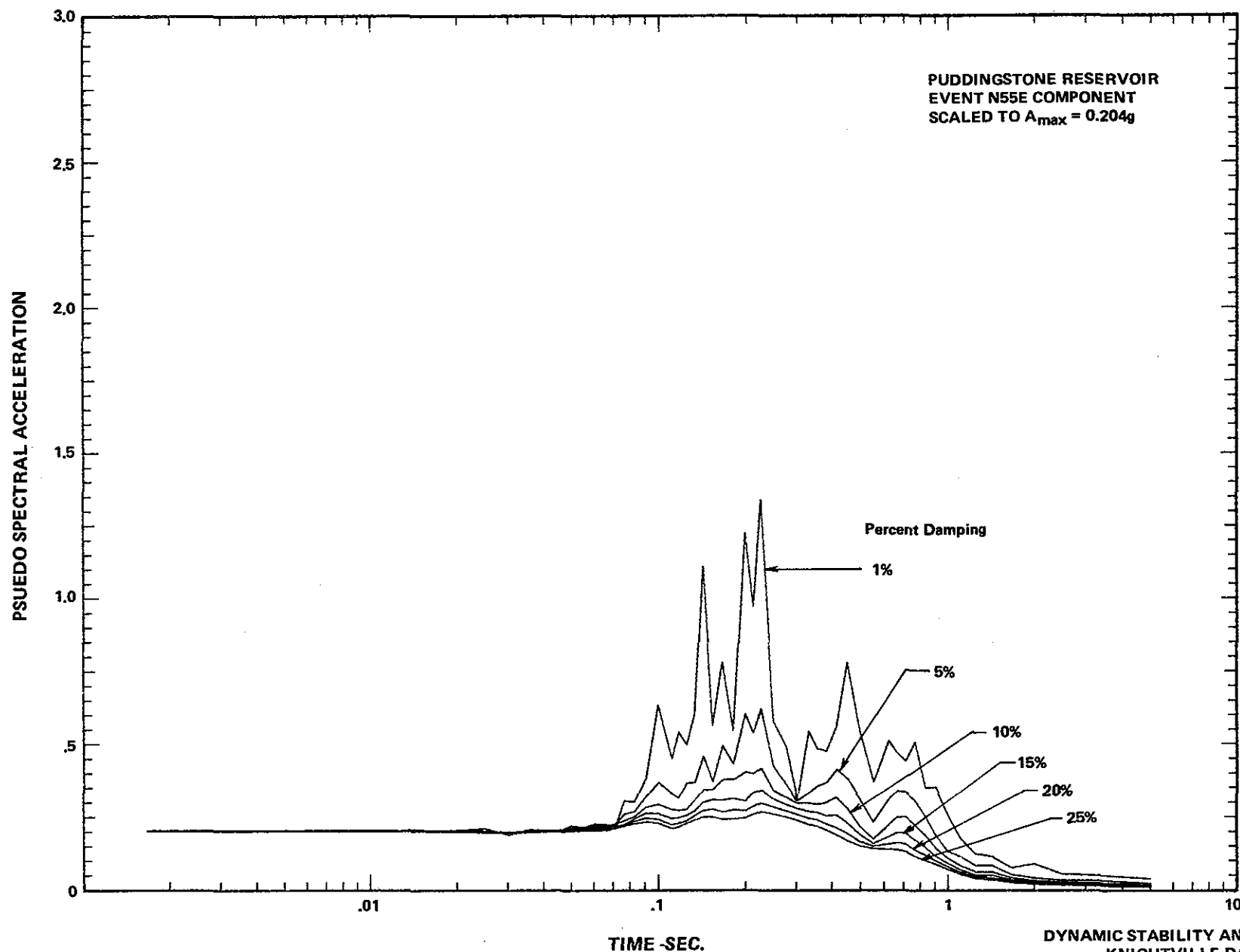
DYNAMIC STABILITY ANALYSIS OF
KNIGHTVILLE DAM
NEW ENGLAND DIVISION, COE
GOLDEN GATE PARK
STRONG MOTION RECORD
PLATE 21

The San Francisco earthquake had $m_b = 4.9$. While this magnitude is larger than the postulated event with $m_b = 4.0$, the durations and frequency contents lie within the range that might be expected from a local event. The peak acceleration at Golden Gate Park was 103 cm/sec^2 . The instrument at Golden Gate Park was founded upon chert with thin interbedded shale, and was about 12 km from the epicenter.

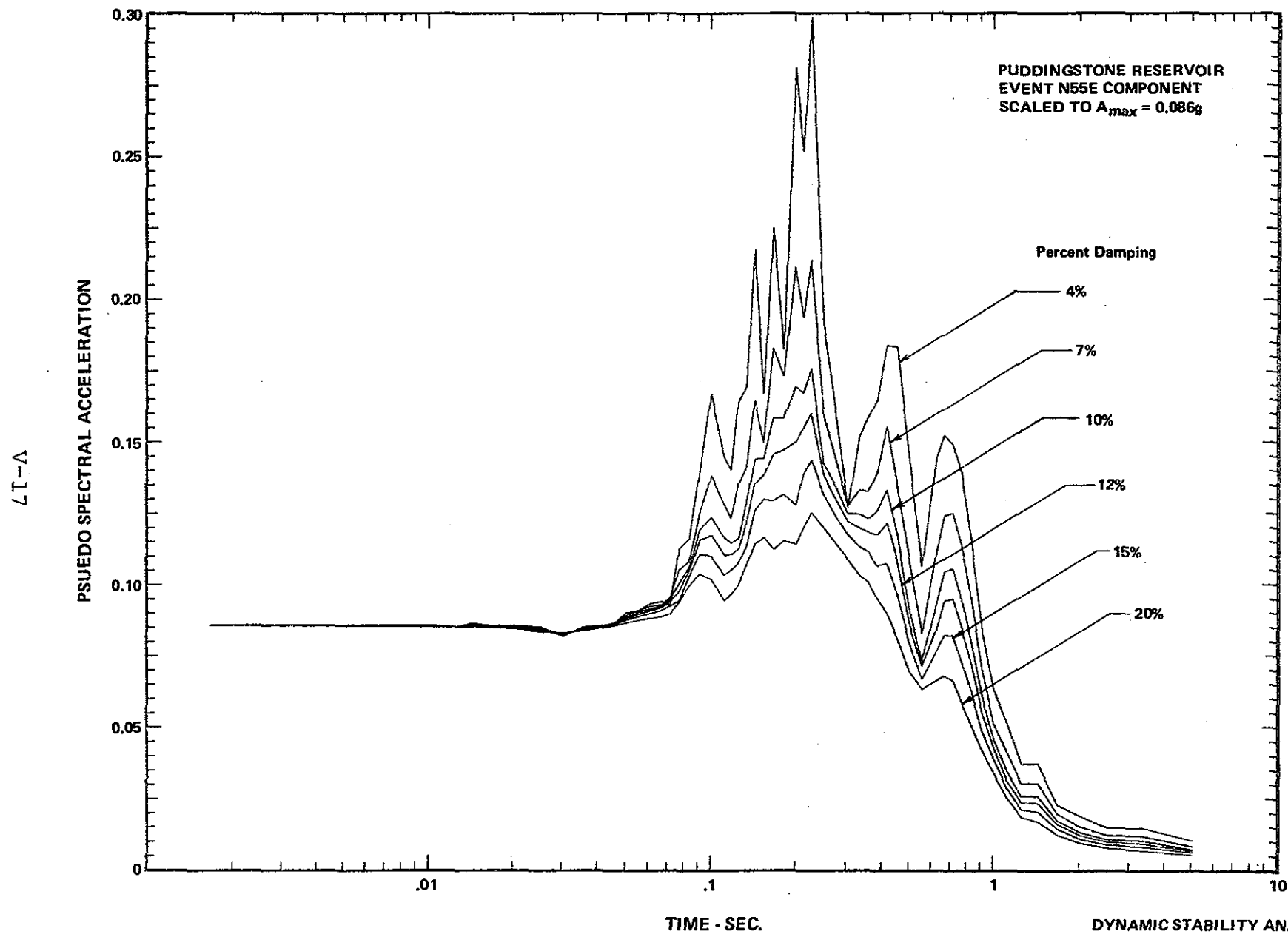
It is anticipated that ground motions from the local events will have less of an effect on the dynamic stability of the dam than the regional events due to the high frequencies and shorter duration of shaking; therefore only the regional event was selected for use in the analysis.

The time series to be used for the regional event was shown in Plate 20; the pseudo-response spectra for various values of damping for both the Maximum Credible and Operating Basis events are shown on Plates 22 and 23.

91-Δ



DYNAMIC STABILITY ANALYSIS OF
KNIGHTVILLE DAM
NEW ENGLAND DIVISION, COE
RESPONSE SPECTRUM
 $A_{max} = 0.204g$



DYNAMIC STABILITY ANALYSIS OF
KNIGHTVILLE DAM
NEW ENGLAND DIVISION, COE
RESPONSE SPECTRUM
 $A_{max} = 0.086g$

VI. STATIC AND DYNAMIC LABORATORY TESTING PROGRAM

A. GENERAL

Prior to construction a laboratory testing program was performed on split spoon and "undisturbed" soil samples obtained during the pre-construction field exploration and sampling program performed at the site. As previously reported, laboratory tests included visual classification, water content, grain-size determination, permeability, strength and consolidation tests. The tests were performed on the dam foundation soils and the potential borrow area soils; the results of the program are presented by the U.S. Army Corps of Engineers (1939).

Laboratory tests were performed on representative samples of embankment obtained during construction of the dam. Hydraulic shell samples were taken at one-hundred foot stations at locations 50, 100, 150, 200 and 250 feet upstream and downstream of the centerline of the dam. Hydraulic core samples were taken at one-hundred foot stations at the centerline, and upstream and downstream at the one-quarter points, and at the theoretical core limits. The laboratory tests performed on these samples included: water content, grain-size, and specific gravity determinations. The results are presented by the U.S. Army Corps of Engineers (1941).

In 1980 a study was made to assess the liquefaction and cyclic mobility potential of the hydraulic core material. The study included a program of exploration and sampling at locations along the crest and a program of laboratory testing. Laboratory testing of "undisturbed" samples was not performed. The laboratory testing program included visual classification, grain-size analyses, water content and specific gravity determinations on selected core samples. The results of the testing program are presented by the U.S. Army Corps of Engineers (1981).

The laboratory testing program for this work was performed on embankment soil samples obtained during the field testing program. The program included split spoon (1-3/8 inch and 3-inch, I.D.), 2.8-inch diameter "undisturbed" stationary piston and 2.8-inch Pitcher-type sampling. The stationary piston and Pitcher-type sampling were performed in the hydraulic core and downstream hydraulic shell, respectively. As previously reported, few Pitcher-type samples were obtained downstream in the relatively cohesionless hydraulic shell.

Selected "undisturbed" samples of the hydraulic core and shell and selected split spoon samples of the hydraulic shell material were delivered to the laboratory. The testing program consisted of index tests, and static and dynamic properties tests on "undisturbed" hydraulic core samples and disturbed and reconstituted hydraulic shell samples. Index tests were performed on representative samples and included: visual classification, Atterberg limits, grain-size analyses, specific gravity tests and water content determinations. Properties tests consisted of one-dimensional consolidation tests, static and dynamic triaxial and resonant column tests.

B. SOIL CLASSIFICATION AND INDEX PROPERTIES

1. Soil Classification

The field testing program included (3) boreholes each at selected locations along the crest and along the downstream slope. The boreholes at the crest encountered 30 to 32 feet of impervious fill, underlain by approximately 125 feet of hydraulic core, which, in turn, is underlain by bedrock.

A soil profile at the downstream locations consists of 8+ feet of riprap, underlain by approximately 60 feet of hydraulic shell material, which, in turn, is underlain by bedrock. The final subsurface exploration logs which show the soil profile encountered at each borehole location are presented in Appendix A.

The hydraulic core material consists primarily of brown silt (ML). The silt exhibits very low to no plasticity and contains approximately 10 to 20 percent fine sand which is typically in the form of horizontal layers; the layers are, in general, less than one-inch thick. Some of the samples contained traces of clay and organic matter. The bulk material is highly dilatant as determined from the shaking test, and has low dry strength.

The downstream hydraulic shell material consists of well-graded angular to subrounded gravelly sand (SW) to sandy gravel (GW). The material contains approximately 5 to 15 percent fine particle sizes (mostly very low to non-plastic silt) and a small amount of mica. The approximate maximum particle size in the shell samples was 2 to 3 inches. According to the U.S. Army Corps of Engineers (1941), the maximum size particles placed for shell construction was 6 inches.

2. Index Properties

Laboratory index tests were performed on representative embankment samples. A compilation of the test results for all samples is presented on the Summary of Laboratory Test Results sheets presented in Appendix D; the results are briefly discussed below.

a. Hydraulic Core - The moisture contents measured in the laboratory on disturbed and "undisturbed" samples range from 25 to 42 percent. These values are plotted versus depth on Plate 24. The lower values were measured on samples from the upper portion (El 600 to El 560) and lower portion (El 560 to El 480) of the core zone. In the central portion

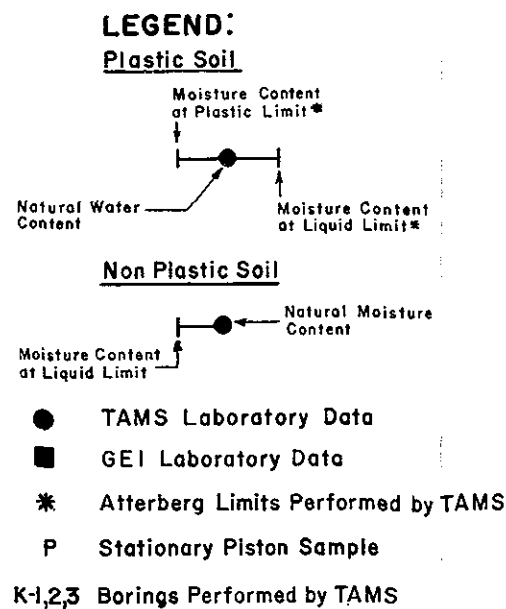
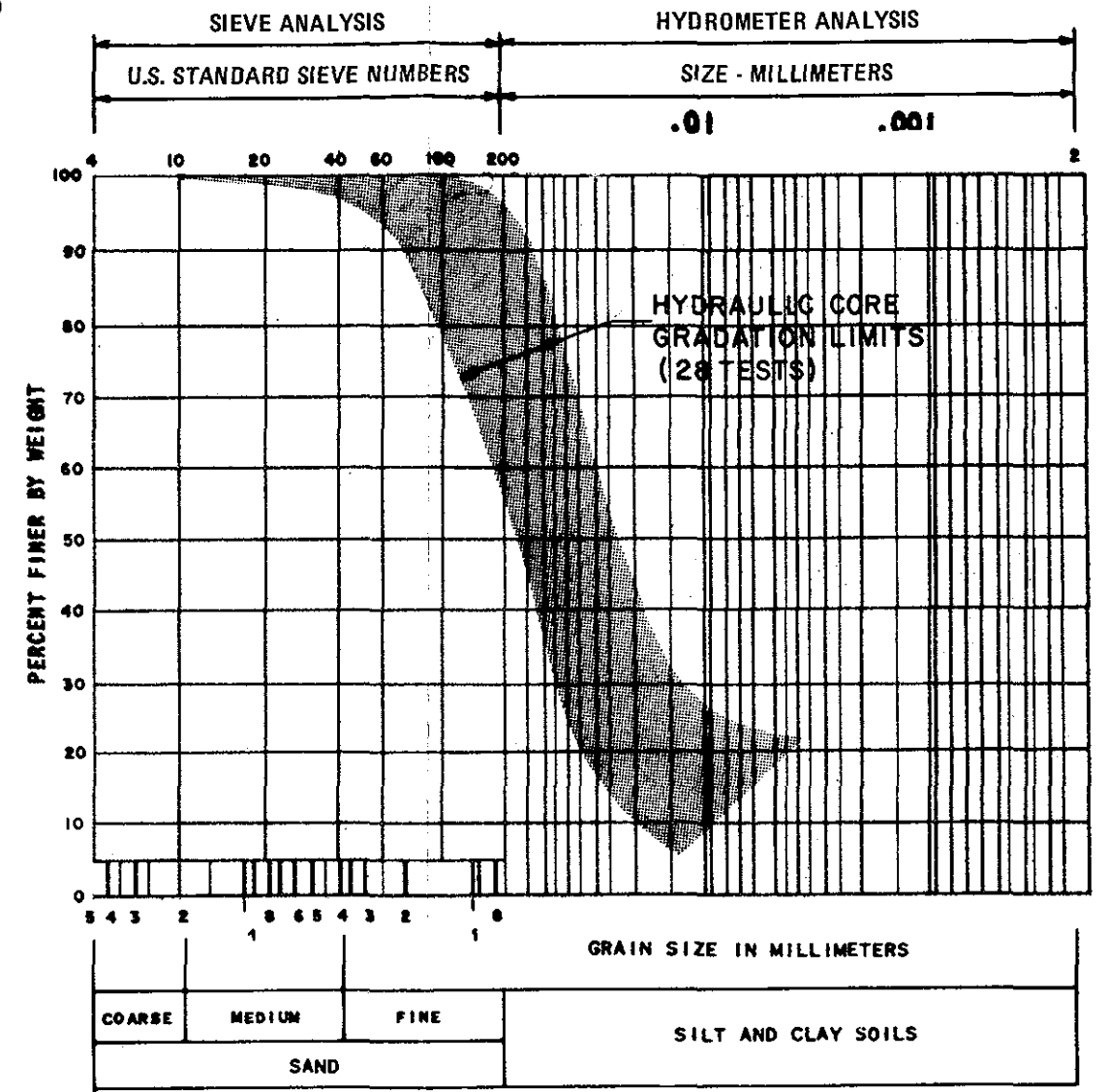
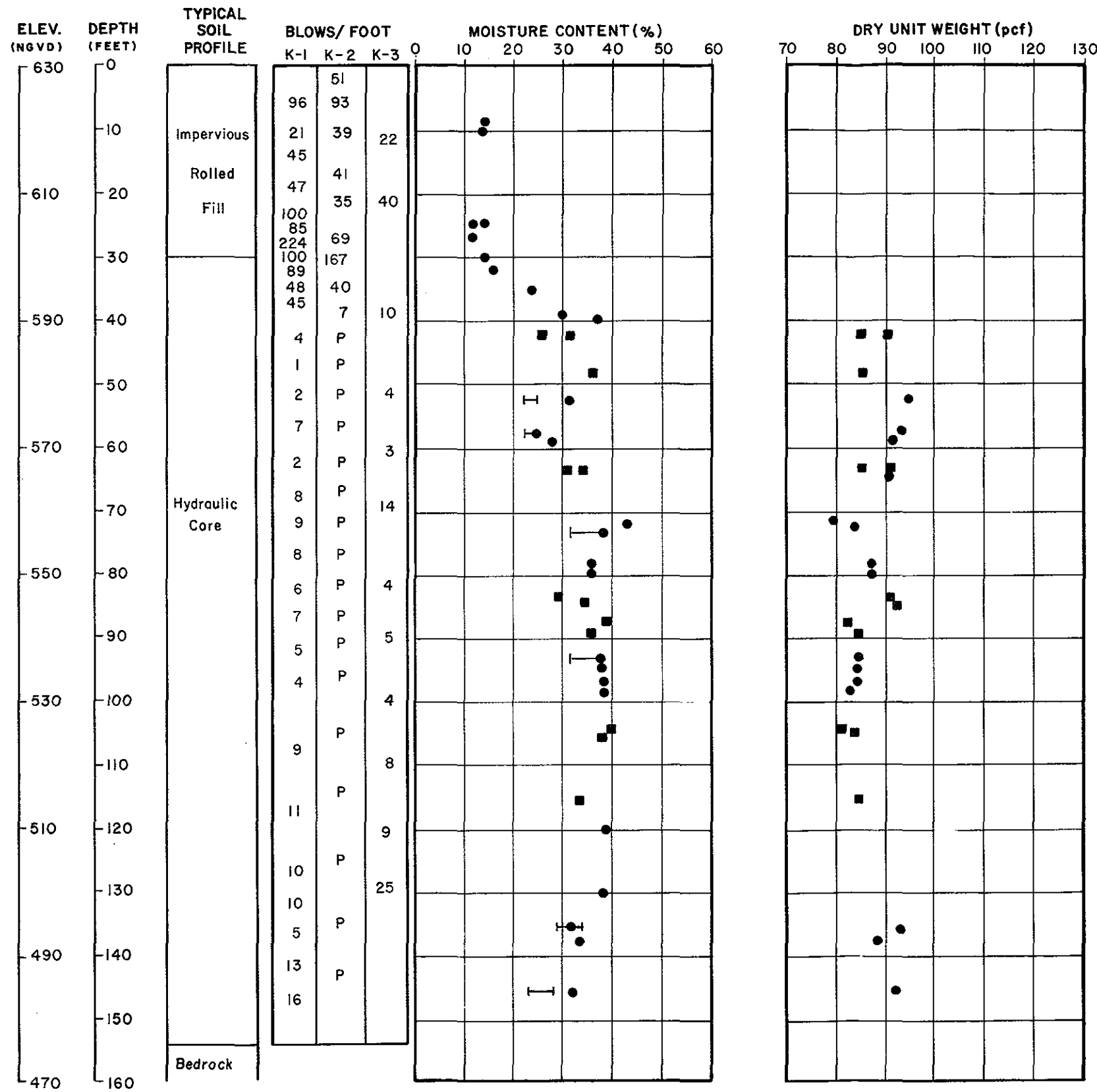


PLATE V-1 from Laboratory Testing Report (May 1982)

DYNAMIC STABILITY ANALYSIS OF
KNIGHTVILLE DAM
NEW ENGLAND DIVISION, COE
ENGINEERING PROPERTIES OF
HYDRAULIC CORE

of the core, between El 560 and El 500, values were typically greater than 35 percent. It is difficult to determine the reasons for this variation. One explanation may be that the samples from the central portion of the core contained fewer fine sand lenses and therefore drained less through the perforated end packers used to seal the sampling tubes.

The dry unit weight values of the "undisturbed" material also plotted versus depth are shown on Plate 24. The dry unit weight values are shown to vary slightly with depth and range between 80 and 95 pcf. The blow count data also plotted on Plate 24 suggest that the lower N-values are due to the lower unit weight values and higher corresponding water contents.

Five Atterberg Limit determinations were made on representative samples of the core material. The liquid limits (LL) vary between 25 to 35 percent, and the plastic limit (PL) from 23 to 30; the material is classified as ML based on the Unified Soil Classification system. Four of the five samples used for the Atterberg Limit determination had natural bulk moisture contents greater than their measured liquid limits (See Plate 24). These data suggest that either the core material has not yet reached full consolidation under the embankment loads or that pore water is being maintained at high elevations by capillary forces. Based on the grain size distribution of the core material, the latter reason seems to be more logical.

The range of grain size curves for the hydraulic core material is shown also on Plate 24. The gradation limits are based on the results of 28 tests; the tests were performed on "undisturbed" and disturbed samples using sieve and hydrometer methods. As shown, the fine fraction (silt and clay) constitutes by weight between 50 to 95 percent of

the core material.

Specific gravity (G_s) determinations were performed on seven core samples. The (G_s) values range from 2.74 to 2.81, and the mean value is 2.78.

b. Hydraulic Shell - Six natural water content determinations were made on representative disturbed and "undisturbed" samples from Borehole K-4. The values of moisture content range from approximately 4 to 11 percent. The values show no correlation with depth, however, the low values do indicate that the downstream slope at this borehole location is not fully saturated.

Dry unit weight determinations were made on the few "undisturbed" (Pitcher-type) hydraulic shell specimens. The results of these tests are summarized below.

SUMMARY OF DRY UNIT WEIGHTS
DOWNSTREAM SHELL MATERIAL

<u>Borehole No.</u>	<u>Sample No.</u>	<u>Depth (ft)</u>	<u>Dry Unit Weight (pcf)</u>
K-5	P-2	34	121.7
K-5	P-9	64	143.8
K-6	P-2	46	138.4

A modified compaction test was performed on the shell mixture, and the results are presented in Appendix C. The results indicate that the maximum density is 141.6 pcf and occurs at an optimum water content of about 5.1 percent. No significant "bleeding" of water occurred during compaction, even for the highest water content utilized (14%). The test was performed in accordance with ASTM Designation D1557-70, Method C.

Two maximum and minimum unit weight determinations (ASTM D2049-69) were made on a mixture of split spoon

samples from Borings K-4 and K-5. The results of the two tests varied by less than one percent; the computed maximum and minimum unit weights were 134.3 pcf and 106.6 pcf, respectively. The maximum density is within the range of unit weights determined from "undisturbed" samples. The difference in unit weight values however could be due to the variations in grain-size characteristics.

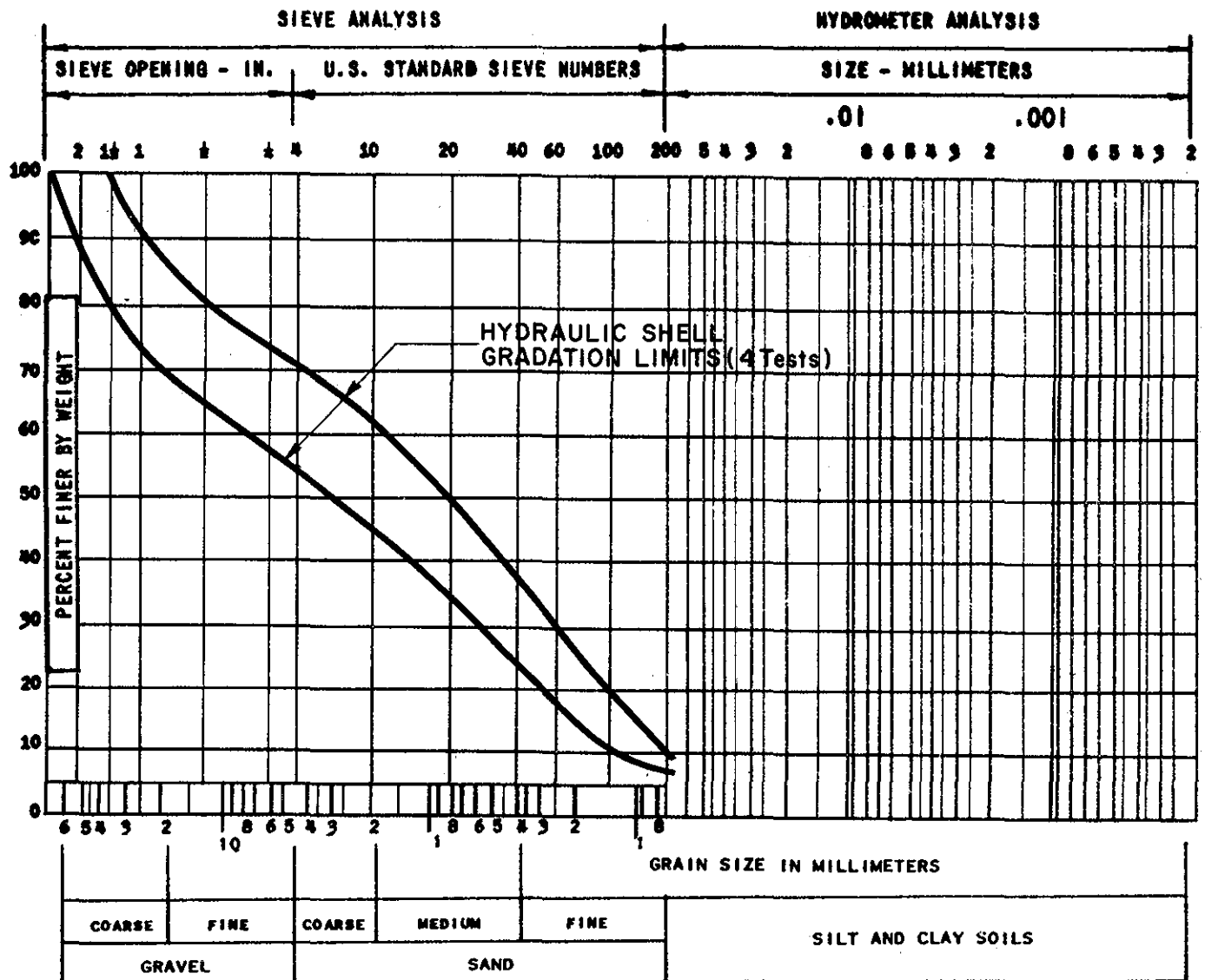
Plate 25 shows the gradation range of the downstream material for samples obtained from boreholes K-4 and K-5. The average value of D_{50} and D_{10} for these samples is approximately 2.0 mm and 0.09 mm, respectively. The latter value is less than half the D_{10} -values determined from grain size analyses on representative samples (at the approximate same location) during construction. The difference is probably due to the I.D. of the samplers which were unable to obtain larger than 3-in diameter particle sizes during sampling for this work.

Two specific gravity (G_s) tests were performed on a mixture of split spoon samples from Borings K-4 and K-5. The computed values are 2.90 and 2.92; these relatively high values may be attributed to the presence of mica.

C. STATIC TESTING PROGRAM

1. General

To determine the static properties of the embankment materials, a total of 23 consolidated-drained (S) and consolidated-undrained (\bar{R}) triaxial shear tests were performed on "undisturbed" core samples and compacted (reconstituted) shell samples. In addition, four one-dimensional consolidation tests were performed on "undisturbed" core specimens. In general, the "undisturbed" hydraulic core samples were recovered in good condition; any densification of the "undisturbed" soil which occurred during transport of the tube was limited to less than 0.5 percent.



Due to the relatively few "undisturbed" (Pitcher-type) hydraulic shell samples available for strength testing, compacted samples were prepared from a mixture of soil from split spoon samples from Boring K-5. The mixture consisted of samples S-4 through S-17, and was "scalped" of its plus 1/2-inch particle sizes. This material was removed in order that the maximum size particles used for compaction of the strength specimens be no greater than 1/6 of the diameter of the specimens. The diameter of all compacted strength test specimens was 2.8 inches. Specimens of larger diameters were not prepared because there was insufficient material for testing larger sizes.

2. Sample Preparation

a. Hydraulic core - Test specimens for static strength tests were obtained by cutting the stationary piston tubes into approximate 8-inch lengths. The specimens were trimmed at the top and bottom to obtain an approximate 7-inch high test specimen, and extruded from the tubes using manual and hydraulic methods. The top, bottom and sides of the sample were carefully examined to determine if silt or sand layers existed within the specimen. The samples were tested without trimming the lateral surface.

b. Hydraulic shell - Specimens for static strength tests were compacted by pressing the materials in a split mold in approximately 5 to 7 layers. Each layer was scarified prior to placement of the next layer in order to assure uniformity of density throughout the specimen and to provide for a good bond between the layers. The material was compacted at its natural water content which ranged between 7 and 9 percent. The desired compacted dry unit weight was 130 pcf. This value was estimated to be the in situ value based on the recorded blow counts, grain size characteristics and unit weight determinations.

3. Consolidated-Undrained Triaxial Compression (\bar{R}) Tests

a. General - A total of eleven isotropically consolidated-undrained triaxial compression (\bar{R}) tests with pore pressure measurements were performed on "undisturbed" core and compacted shell specimens. Two additional anisotropically consolidated-undrained triaxial (\bar{R}) tests were performed on the shell specimens.

b. Procedure -

1. Hydraulic Core: After trimming the specimen, a vacuum pressure of about 10 psi was applied to the top of the specimen as the specimen was extruded directly into a membrane. This procedure was used to assure that the sandy silt material would not fail under its own weight when removed from the sampling tube. The specimen was placed in the triaxial cell and consolidated to isotropic pressures ranging from 10 to 80 psi. Each specimen was allowed to consolidate for approximately 16 hours, or until a negligible amount of pore fluid exited from the sample.

A back pressuring technique, which incorporates simultaneous incrementing of back pressure and cell pressure was used to saturate the specimen. A back pressure of 100 psi was used for all tests. Skempton's B-parameter was checked at the top and bottom of the specimen; a minimum value of 0.95 was considered acceptable as an indication of full saturation.

Upon completion of the back pressure saturation procedure, the sample was loaded using a stress-controlled device. Loading was performed by incrementing the deviator stress ($\sigma_1 - \sigma_3$) by 3 to 9 psi at approximate 10 minute intervals. The rate of loading was governed by the time required for the

pore pressures to stabilize under each load increment. Pore pressures were measured at the top and bottom of the specimen at the end of each load increment. When failure seemed imminent, the rate of loading was decreased to prevent rapid failure of the specimen. All samples were tested to a maximum axial strain of 20 percent.

At the completion of each test, the specimen was unloaded, removed from the cell, cut into halves, and the angle of shear failure (if any) was recorded. Photographs of the cut specimen were taken to provide a pictorial record of each failure. Grain size analyses and/or Atterberg Limits were performed on half sections of the failed specimens.

2. Hydraulic Shell: The procedure used to perform the \bar{R} tests on the compacted shell specimens is primarily the same as that used for core specimens. For these specimens, however, back pressure saturation was performed prior to the consolidation stage.

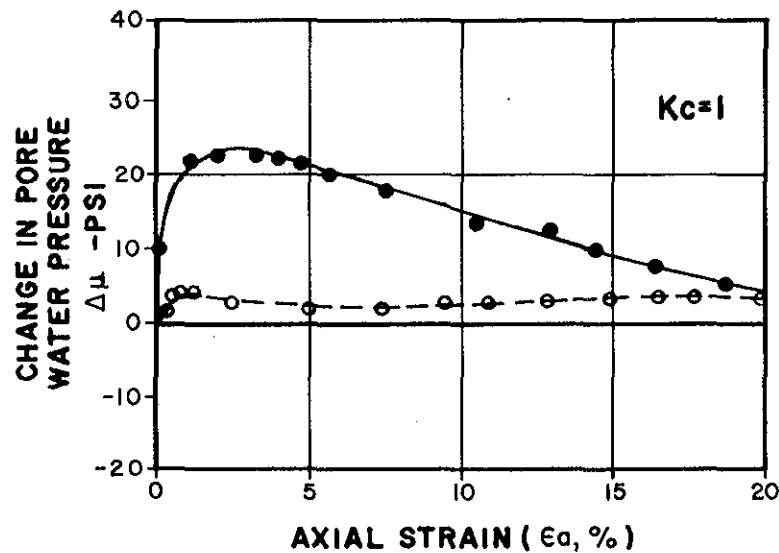
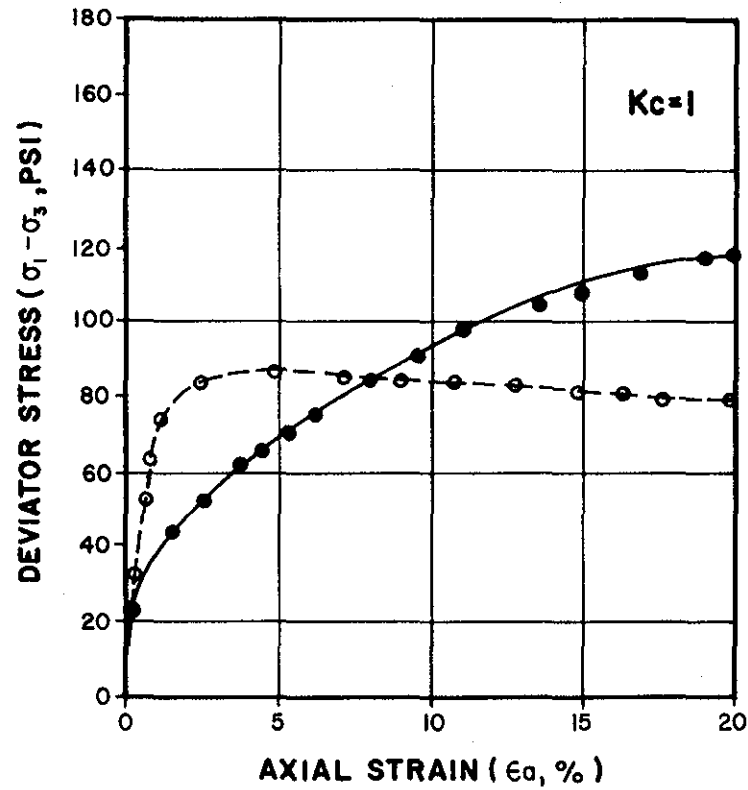
Two anisotropically consolidated-undrained triaxial tests with pore pressure measurements were performed on compacted samples of the shell mixture. The test specimens were set up in the triaxial cell and consolidated to an initial isotropic stress of approximately 7 psi. The specimen was back pressure saturated until a B-value of 0.95 was attained. The specimen was then anisotropically consolidated in increments maintaining a consolidation stress ratio $K_C = \bar{\sigma}_{1C} / \bar{\sigma}_{3C}$ of 2 for each increment. The specimen was monotonically loaded in undrained shear using a strain controlled device. The strain rate used during the tests was 0.2 percent per minute. During shear vertical loads were monitored with a proving ring, and pore pressures were monitored with pressure transducers at the top and bottom of the specimen.

c. Results - The results of the stress and strain controlled \bar{R} tests performed are presented in Appendix D. For each test the following are plotted versus axial strain: deviator stress ($\sigma_1 - \sigma_3$); pore pressure (u); and effective principal stress ratio ($\bar{\sigma}_1/\bar{\sigma}_3$). In addition, the properties of the triaxial specimens and a sketch of the type and angle of failure (if any) are also presented.

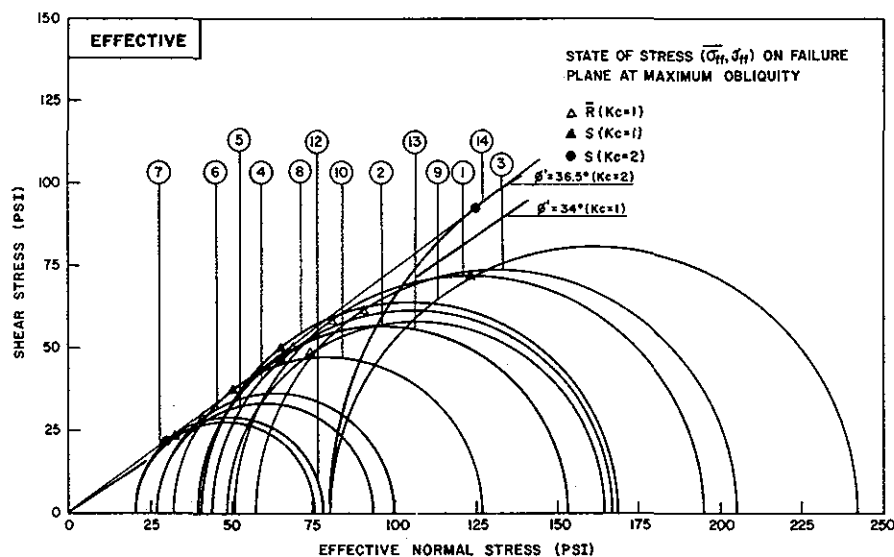
A typical plot of deviator stress and excess pore pressure vs strain curves for \bar{R} tests on the "undisturbed" core material for a $K_C=1$ is shown on Plate 26. The undrained stress-strain curve is characteristic of an insensitive soil. The peak stress (maximum deviator stress) is typically attained at 20 percent strain, and in no case was there a rapid loss in strength beyond the peak stress condition. The pore pressure curve shows an increase in pore water pressure at low strain and a gradual decrease at larger strains.

Similar curves for \bar{R} tests performed on the compacted shell material initially consolidated to $K_C=1$ are shown also on Plate 26. As shown, the maximum value of deviator stress and pore water pressure was reached at between 1 and 5 percent strain; these values remained essentially constant with increasing strain. The test results shown were typical for all \bar{R} tests ($K_C=1$) performed on this material.

The results of the \bar{R} tests are presented in the form of Mohr-Coulomb strength envelopes on Plates 27 and 28 for tests performed on "undisturbed" core specimens and compacted shell specimens, respectively. On each Plate, the effective strength data are plotted in the upper diagram and the total strength data are plotted in the lower diagram. A summary table also is presented on each Plate and gives the pertinent data for each test.



	DESIGNATION	$\bar{\sigma}_{sc}$ (psi)
CORE	—●—	50
SHELL	—○—	40



SUMMARY OF STATIC STRENGTH LABORATORY TEST DATA
FOR "UNDISTURBED" HYDRAULIC CORE SAMPLES

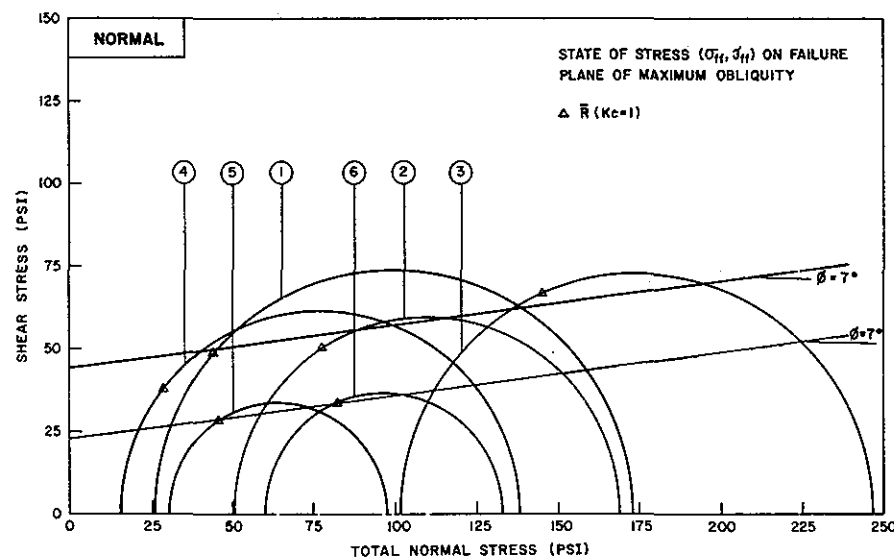
TEST NO.	BORING NO.	SAMPLE NO.	SAMPLE DESCRIPTION (1)	TYPE OF TEST (2)	$(\sigma_1 - \sigma_3)_f$ (psi)	σ_{3f} (psi)	u_f (psi)	$\bar{\sigma}_{3f}$ (psi)	α_f (degrees)	wi (%)	γ_d (pcf)	ϵ_f (%)	Kc
1	K-2	SP-16	BROWN SILT, SM. F. SAND, TR. CLAY	\bar{R}	147	25	-25	50	50	31.4	92.4	20	1
2	K-2	SP-16	BROWN SANDY SILT	\bar{R}	118	50	3	47	55	34.4	88.4	20	1
3	K-2	SP-17	BROWN SILT, SM. SAND	\bar{R}	147	100	43	57	59	32.0	92.0	20	1
4	K-2	SP-3	BROWN SANDY SILT	\bar{R}	122	15	-28	43	—	30.3	95.0	20	1
5	K-2	SP-4	BROWN SILT AND F. SAND	\bar{R}	66	30	3	27	62	24.5	93.0	20	1
6	K-2	SP-4	BROWN SILT AND F. SAND	\bar{R}	72	60	33	27	63	28.1	91.0	20	1
7	K-2	SP-11	BROWN SILT, TR. SAND	S	55	—	—	20	55	37.7	84.2	20	1
8	K-2	SP-11	BROWN SILT, SM. F. SAND	S	128	—	—	40	—	38.3	84.1	20	1
9	K-2	SP-12	BROWN SILT, TR. SAND	S	162	—	—	80	—	38.9	83.3	20	1
10	K-2	SP-8	BROWN SANDY SILT	\bar{R}	93	40	8	32	63	35.3	86.7	20	1
11	K-2	SP-12	BROWN SILT, SM. F. SAND	\bar{R}	73	50	25	25	58	37.7	84.7	20	1
12	K-2	SP-7	BROWN MICACEOUS SANDY SILT	S	56	—	—	20	—	42.5	79.9	20	2
13	K-2	SP-7	BROWN MICACEOUS SILT, SM. F. SAND	S	113	—	—	40	—	38.6	84.1	20	2
14	K-2	SP-8	BROWN SILT, SM. F. SAND	S	234	—	—	80	53	35.7	87.5	20	2

NOTES

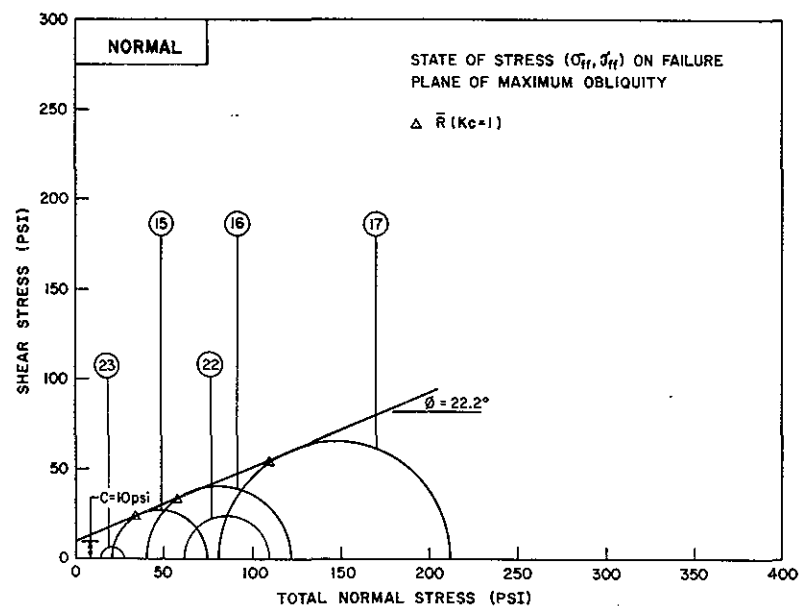
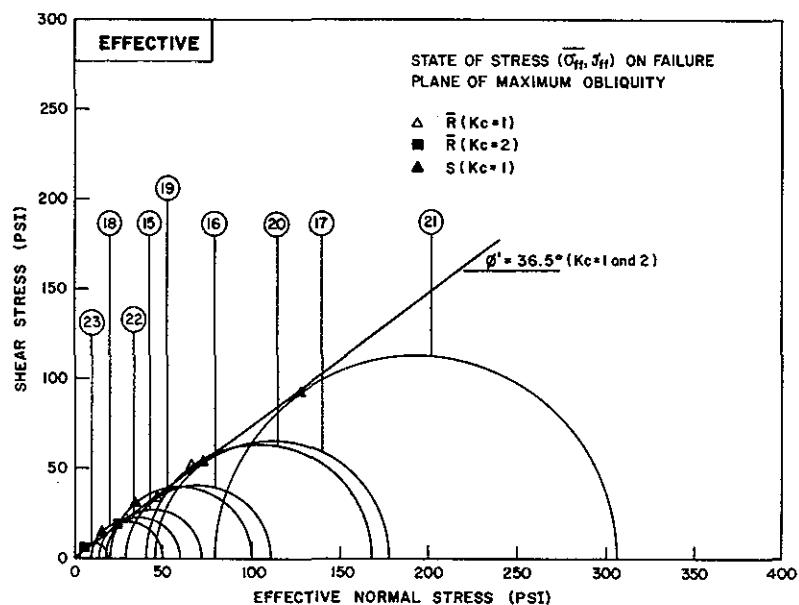
- (1) UNLESS OTHERWISE STATED ALL SAMPLES CONTAIN A TRACE TO SOME AMOUNT OF MICA.
- (2) \bar{R} = CONSOLIDATED UNDRAINED TRIAXIAL COMPRESSION TEST WITH PORE PRESSURE MEASUREMENTS.
S = CONSOLIDATED DRAINED TRIAXIAL COMPRESSION TEST.

LEGEND

- $(\sigma_1 - \sigma_3)_f$ = DEVIATOR STRESS AT FAILURE
 σ_{3f} = TOTAL MINOR PRINCIPAL STRESS AT FAILURE
 u_f = PORE PRESSURE AT FAILURE
 $\bar{\sigma}_{3f}$ = EFFECTIVE MINOR PRINCIPAL STRESS AT FAILURE
Kc = RATIO OF MAJOR TO MINOR PRINCIPAL STRESS AT THE END OF CONSOLIDATION
- α_f = ANGLE OF TEST SPECIMEN FAILURE PLANE
wi = INITIAL MOISTURE CONTENT
 γ_d = INITIAL DRY UNIT WEIGHT
 ϵ_f = PERCENT STRAIN AT FAILURE



DYNAMIC STABILITY ANALYSIS OF KNIGHTVILLE DAM NEW ENGLAND DIVISION, COE RESULTS OF STATIC STRENGTH TESTS OF "UNDISTURBED" CORE MATERIAL



SUMMARY OF STATIC STRENGTH LABORATORY TEST DATA
FOR COMPACTED HYDRAULIC SHELL SAMPLES

TEST NO.	BORING NO.	SAMPLE NO. ⁽¹⁾	SAMPLE DESCRIPTION	TYPE OF TEST ⁽²⁾	$(\sigma_1 - \sigma_3)_f$ (psi)	σ_{3f} (psi)	u_f (psi)	$\bar{\sigma}_{3f}$ (psi)	α_f (degrees)	wi (%)	γ_d (pcf)	ϵ_f (%)	Kc
15	K-5	C	BROWN SAND, SM. GRAVEL, SM. SILT	\bar{R}	54	20	2	18	—	9.0	129.0	20	1
16	K-5	C	BROWN SAND, SM. GRAVEL, SM. SILT	\bar{R}	81	40	11	29	—	9.0	129.7	20	1
17	K-5	C	BROWN SAND, SM. GRAVEL, SM. SILT	\bar{R}	133	80	35	45	—	8.4	130.8	20	1
18	K-5	C	BROWN SAND, SM. GRAVEL, SM. SILT	S	39	—	—	10	—	8.7	129.1	20	1
19	K-5	C	BROWN SAND, SM. GRAVEL, SM. SILT	S	80	—	—	20	—	8.1	129.5	19.5	1
20	K-5	C	BROWN SAND, SM. GRAVEL, SM. SILT	S	128	—	—	40	—	8.7	129.5	20	1
21	K-5	C	BROWN SAND, SM. GRAVEL, SM. SILT	S	226	—	—	80	—	8.9	129.3	20	1
22	K-4,5	C	BROWN GRAVELLY SILTY SAND	\bar{R}	45	57	43	14	—	—	125.5	20	2
23	K-4,5	C	BROWN GRAVELLY SILTY SAND	\bar{R}	11	14	10	4	—	—	127.8	20	2

NOTES

- (1) ALL SAMPLES FROM BOREHOLE K-5 WERE COMBINED AND SCREENED OF PLUS 1/2-INCH MATERIAL
C = COMBINED SAMPLE.
- (2) \bar{R} = CONSOLIDATED UNDRAINED TRIAXIAL COMPRESSION TEST WITH PORE PRESSURE MEASUREMENTS.
S = CONSOLIDATED DRAINED TRIAXIAL COMPRESSION TEST.

LEGEND

- $(\sigma_1 - \sigma_3)_f$ = DEVIATOR STRESS AT FAILURE
 σ_{3f} = TOTAL MINOR PRINCIPAL STRESS AT FAILURE
 u_f = PORE PRESSURE AT FAILURE
 $\bar{\sigma}_{3f}$ = EFFECTIVE MINOR PRINCIPAL STRESS AT FAILURE
Kc = RATIO OF MAJOR TO MINOR PRINCIPAL STRESS AT THE END OF CONSOLIDATION

- α_f = ANGLE OF TEST SPECIMEN FAILURE PLANE
wi = INITIAL MOISTURE CONTENT
 γ_d = INITIAL DRY UNIT WEIGHT
 ϵ_f = PERCENT STRAIN AT FAILURE

DYNAMIC STABILITY ANALYSIS OF
KNIGHTVILLE DAM
NEW ENGLAND DIVISION, COE
RESULTS OF STATIC STRENGTH
TESTS OF COMPACTED SHELL MATERIAL

From the Mohr-Coulomb strength envelope the effective angle of shearing resistance under initial isotropic stress condition ($K_c=1$) is 34 degrees and 36.5 degrees with zero strength at zero normal stress for the hydraulic core and hydraulic shell materials, respectively. Similarly, for the initial anisotropic conditions, $K_c=2$, the value of the effective angle of friction for both materials is 36.5 degrees with zero shear strength at zero normal stress.

The Mohr-Coulomb strength envelope in terms of total stress can be represented for the hydraulic core material by two lines each having an angle of 7 degrees and a shear strength at zero normal stress of 23 and 39 psi. The variations in cohesion intercept is difficult to explain; it may be due to variations in sample composition and structure, especially the content and orientation of mica particles.

The failure envelope in terms of total stress for the hydraulic shell material can be defined by an angle of 22 degrees, and a shear strength of approximately 10 psi at zero normal stress. Two of the five tests produced results with substantially lower strengths. The difference in results may be due to the fact that these tests were performed using constant rate of strain as opposed to constant rate of stress; the samples were prepared using vibratory air hammer as opposed to static compaction; and/or the samples may have contained different quantities of mica which would effect the strength.

The envelopes presented in each Plate are based on the stress developed at twenty percent axial strain. The tests indicate that on all isotropically consolidated samples, the maximum strength was reached at twenty percent strain. For the two anisotropically consolidated samples, the maximum strength was reached at two to three percent axial strain.

4. Consolidated-Drained Triaxial Compression (S) Tests

a. General - Four isotropically consolidated-drained triaxial compression (S) tests were performed on compacted hydraulic shell specimens. Three S tests were performed also on "undisturbed" hydraulic core specimens consolidated to initial anisotropic conditions.

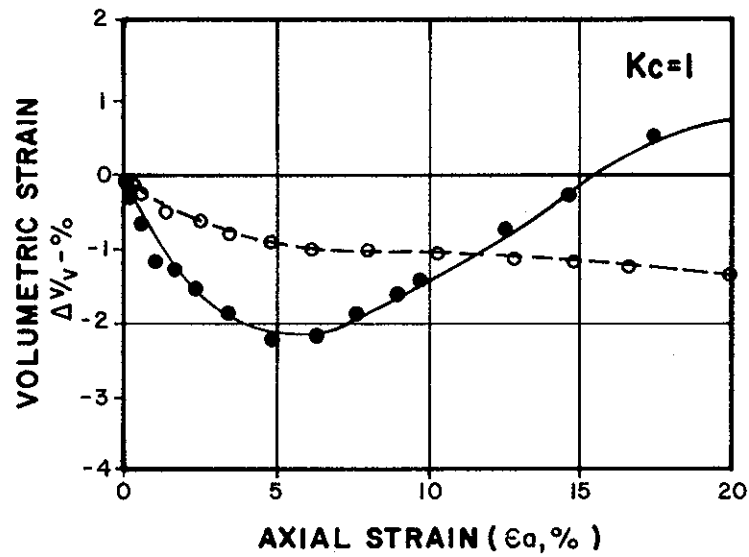
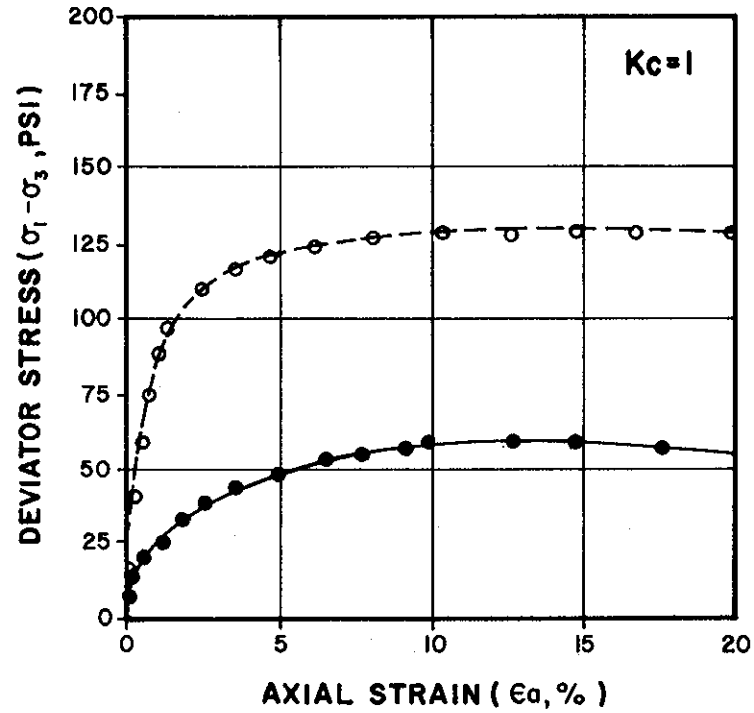
b. Procedure - The S testing procedure used in this program is similar to the procedure used for performing the \bar{R} tests. However, during these tests the specimen was permitted to drain at top and bottom, and volume change measurements were made for each application of vertical load.

c. Results - The results of the isotropic and anisotropic S tests are presented in Appendix D. A typical set of stress and volumetric strain vs axial strain curves for S tests ($K_c=1$) on the "undisturbed" core material is shown on Plate 29. Also shown on this Plate are typical S test results on the compacted shell specimens.

For the core material, the drained test results show some decrease in volume followed by a slight tendency for dilation near and at failure. For the compacted shell material, the volumetric strain and deviator stress reached high values at low axial strains and increased slightly with increasing axial strain.

The results of the isotropic S tests are also presented in the form of a Mohr-Coulomb strength envelope on Plates 27 and 28. For the isotropic consolidated hydraulic core material, the S test results are similar to those shown for the \bar{R} tests, with the effective angle of friction equal to 34 degrees and zero shear strength at zero normal stress.

The strength parameters from anisotropic S tests are shown also on Plate 27 and 28. For the hydraulic core material consolidated to initial $K_c=2$ conditions, the



	DESIGNATION	$\bar{\sigma}_{sc}$ (psi)
CORE	—●—	20
SHELL	—○—	40

effective angle of friction is 36.5 degrees with zero shear strength at zero normal stress which is slightly higher than that for isotropic conditions. For the hydraulic shell material the effective angle of shearing resistance is 36.5 degrees for both isotropic and anisotropic consolidation.

5. One-Dimensional Consolidation Tests

Four one-dimensional consolidation tests were performed on "undisturbed" core specimens to assist in determining the static properties of this material. Results of these tests are presented in Appendix D.

Each of the hydraulic core specimens were trimmed and placed in a floating ring type consolidometer. The specimens were loaded incrementally (LIR=1) to a minimum 32 ksf stress following back pressure saturation to 100 psi. At the end of the loading cycle, the sample was incrementally unloaded to 0.5 ksf. Drainage was permitted at both top and bottom of the sample.

The values of Compression Index (C_c) computed from the "straight-line" portion of the e -log p plots show a relationship with initial moisture content. Representative samples tested from the upper and lower portions of core have relatively low computed values of C_c ; these same samples have relatively low values of initial moisture content. Samples tested from the central portion of the zone have relatively high values of both C_c and natural water content. These results are summarized below:

SUMMARY OF C_c -VALUES FOR "UNDISTURBED" CORE MATERIAL

<u>Sample*</u>	<u>Depth(feet)</u>	<u>Natural Water Content (percent)</u>	<u>C_c</u>
SP-3	53.5	31.8	0.12
SP-7	72.5	39.4	0.25
SP-11	93.5	41.3	0.30
SP-16	135.5	32.2	0.12

*Samples from Borehole K-2

The computed values of coefficient of consolidation (c_v) range between 10^{-1} and 10^{-2} cm^2/sec . There is no apparent correlation between water content or depth and the computed values of c_v .

D. DYNAMIC TESTING PROGRAM

1. General

A dynamic testing program was conducted to determine the behavior of the embankment soils under dynamic loading. The program consisted of twenty-three cyclic load triaxial ($\overline{\text{CR}}$) tests, six resonant column (RC) tests and three small strain triaxial (E) tests. The results of the dynamic testing program not shown herein, are presented in Appendix E.

2. Sample Preparation

a. Hydraulic core - Prior to cutting and trimming of the test specimens, measurements were made to determine if compression of the sample occurred during transportation. The tube samples were handled and shipped in an upright vertical position. Prior to sealing the tubes in the field, the top expandable packer was placed tightly against the inner tube wall in contact with the top surface of the sample. If any densification of the soil occurred, an air space would result between the bottom of the packer and the top surface of the sample. This air space was measured and the percent compression was computed by dividing the space measurement by the length of the sample in the tube. The cutting and trimming procedures for the dynamic test program specimens were the same as the procedure followed for the static test program specimens.

b. Hydraulic shell - Reconstituted samples of the shell material were prepared from a mixture of soil from split-spoon samples from Borings K-4 and K-5. Compacted specimens were made by placing seven to eight 0.4-in-thick

layers of material in a split compaction mold. The material was placed at a water content of about 8 percent. The density of the sample was controlled by placing a predetermined weight of material in each layer. A three-inch thick steel plate was placed on top of each layer and impacted vertically with a vibratory air hammer until the layer thickness reached 0.4 in. The impact energy could be varied by controlling the air pressure to the air hammer.

The majority of $\overline{CR-R}$ and CR tests on the shell mixture were performed at a consolidated dry unit weight of between 130 and 133 pcf.

3. Cyclic Triaxial ($\overline{CR-R}$ and CR) Tests

a. General - Two (2) isotropic and nine (9) anisotropic consolidated-undrained cyclic load triaxial (\overline{CR}) tests were performed on undisturbed core samples. Four (4) of these tests were followed by a monotonic load phase ($\overline{CR-R}$). Fourteen (14) anisotropically consolidated-undrained cyclic load triaxial tests were performed on compacted samples of the shell mixture. Two (2) of these tests were followed by a monotonic load phase.

The values of K_c ($\bar{\sigma}_{1c}/\bar{\sigma}_{3c}$) used during consolidation for the "undisturbed" hydraulic core specimens were 1.0 and 1.5. The values used for the reconstituted hydraulic shell specimens were 1.5 and 2.0. These values were based on the ratios of major to minor principal stresses computed from preliminary stability computations made prior to testing.

b. Procedure -

1. Hydraulic Core: The specimen was set up in the triaxial cell and consolidated to an initial isotropic stress of 0.5 kg/cm^2 . The specimen was back pressure saturated

to obtain a Skempton B-value of at least 0.95.

The specimens were consolidated in increments to the desired isotropic or anisotropic consolidation stresses. Primary consolidation of the specimens under each increment of load was typically complete within 5 minutes. The final consolidation stresses remained on the specimen for at least 3 hours before cyclic loading, and in most tests, the final consolidation stresses remained on the specimen for over 16 hours.

A symmetrical cyclic deviator stress was applied under undrained conditions. The load cycles were applied at a frequency of 0.4 Hz. The first half cycle of load was compressive, and typically 20 load cycles were applied.

Axial load, pore pressure at the ends of the specimen, and axial deformation were recorded continuously during cyclic loading. At the completion of cyclic loading, the specimen was returned to the approximate consolidation shear stress which existed prior to cyclic loading. Pore pressures reached equilibrium in less than one second after completion of cyclic loading.

Specimens which did not exceed a compressive strain of 5% after 20 load cycles were monotonically loaded in undrained shear. Drainage of the specimen was not allowed after cyclic loading. The excess pore pressures generated by cyclic loading remained in the sample until the start of monotonic loading. A strain controlled loading device was used to apply monotonic loads.

After completion of each test, the specimen was weighed and sliced vertically into two sections. One section was used for a water content determination to determine the dry weight of the specimen. The other section was partially

air-dried, photographed, described, and finally used for index testing. Grain size analyses were performed on material from the portion of the specimen where the strains tended to concentrate.

2. Hydraulic Shell: Consolidation, saturation, cyclic loading, and monotonic loading of compacted samples followed the same procedures used for "undisturbed" samples described in the previous section with the following differences:

- The specimens consolidated very rapidly under each increment of load, usually reaching the end of primary consolidation in a few seconds.
- The final consolidation stresses remained on the sample for at least 16 hours before cyclic loading.
- The number of cycles applied during cyclic loading was not limited to 20. The maximum number of load cycles applied was 95. Two CR-tests were followed by an R-phase and these had axial strains after cyclic loading of 0.05% and 6.31%, respectively.
- After completion of each test, the entire specimen was oven dried to obtain an accurate dry weight measurement.

c. Results - A summary of the CR and CR-R triaxial test results for the "undisturbed" hydraulic core and the re-constituted hydraulic shell specimens is presented in Tables 8 and 9. Tests on each material were run at two minor principal stresses ($\bar{\sigma}_{3C}$) and two consolidation ratios ($K_C = \bar{\sigma}_{1C} / \bar{\sigma}_{3C}$). For the hydraulic core specimens, $\bar{\sigma}_{3C}$ -values equal to 2.5 and 5.0 kg/cm² were used and K_C -values were equal to 1.0 and 1.5. Similarly for the hydraulic shell specimens, $\bar{\sigma}_{3C}$ -values of 1.0 and 4.0 kg/cm² and K_C -values of 1.5 and 2.0 were used.

Table 8
Summary of Cyclic Load
Triaxial Test Data
(Hydraulic Core)

Test No. (1)	Boring/Sample Nos. (2)	Depth of Test Specimen ft	Dry Unit Weight				Water Content		Consolidation Stresses				Consolidation Stress Ratios		Back Pressure u_c kg/cm ²
			In Tube		In Cell		In Tube as measured in lab %	In Cell after con- solidation %	Principal Stresses		On Failure Plane ⁽⁴⁾		$\frac{\bar{\sigma}_{1c}}{\bar{\sigma}_{3c}}$	$\frac{\tau_{fc}}{\bar{\sigma}_{fc}}$	
			in ⁽³⁾ field pcf	as delivered to lab pcf	initial pcf	after con- solidation pcf			Vertical $\bar{\sigma}_{1c}$ kg/cm ²	Lateral $\bar{\sigma}_{3c}$ kg/cm ²	$\bar{\sigma}_{fc}$ kg/cm ²	τ_{fc} kg/cm ²			
CR-1	K-2/SP-2A	47.5	85.0	85.0	85.7	89.5	36.1	33.4	3.75	2.50	2.77	0.51	1.50	0.18	8.00
CR-R-2	K-2/SP-1B	42.5	84.7	84.7	85.4	90.9	31.0	32.1	3.75	2.50	2.77	0.51	1.50	0.18	8.00
CR-3	K-2/SP-13B	106.5	81.0	81.0	81.2	88.6	40.7	34.1	7.50	5.00	5.53	1.02	1.50	0.18	4.00
CR-4 ⁵⁾	K-2/SP-5A	63.0	84.9	85.1	85.3	-	34.2	-	-	-	-	-	-	-	-
CR-5	K-2/SP-5B	63.7	90.6	90.9	89.0	93.7	31.0	30.2	3.75	2.50	2.77	0.51	1.50	0.18	8.00
CR-6	K-2/SP-9B	83.3	90.9	91.2	89.5	95.7	29.3	28.8	7.50	5.00	5.53	1.02	1.50	0.18	8.00
CR-R-7	K-2/SP-9C	84.0	87.4	87.7	87.1	91.7	34.6	31.7	5.00	5.00	5.00	0	1.00	0	8.00
CR-R-8A	K-2/SP-10A	87.8	82.3	82.5	80.9	87.6	39.0	34.9	7.50	5.00	5.53	1.02	1.50	0.18	8.00
CR-R-8B	K-2/SP-10A	87.8	-	-	-	87.7	-	34.8	7.50	5.00	5.53	1.02	1.50	0.18	8.00
CR-R-8C	K-2/SP-10A	87.8	-	-	-	87.9	-	34.6	7.50	5.00	5.53	1.02	1.50	0.18	8.00
CR-R-9	K-2/SP-14A	116.5	84.6	85.0	84.3	89.9	32.7	33.2	7.50	5.00	5.53	1.02	1.50	0.18	8.00
CR-10	K-2/SP-10C	89.1	84.9	85.0	85.1	91.0	35.9	32.2	5.00	5.00	5.00	0	1.00	0	8.00

- Notes: 1) The symbol CR represents an undrained cyclic triaxial test. The symbol CR-R represents an undrained cyclic triaxial test (CR) followed by an undrained, monotonically loaded triaxial test (R). Tests CR-R-8A, B, and C were performed on the same specimen.
- 2) The letters A, B, and C after sample number refer to top, middle, and bottom sections of tube, respectively.
- 3) The dry unit weight in the field was determined by multiplying the dry unit weight, as received in the laboratory, by a factor to account for settlement of soil in the tube during transportation.
- 4) Stresses are given on an assumed failure plane inclined 62.5° to the horizontal. (ϕ assumed equal to 35°). The subscript f represents the failure plane.
- 5) The specimen for Test CR-4 inadvertently failed during consolidation stage.

Table 8
(Continued)

Test No. 1)	Cyclic ²⁾ Shear Stress on Failure Plane ³⁾ τ_{fy} kg/cm ²	Cyclic Stress Ratios			No. of Load Cycles Applied	Induced Pore Pressure After Cyclic Loading kg/cm ²	Compressive Strain During Cyclic Loading						Compressive Strain at Start of Monotonic Loading %	Shear Stresses on Failure Plane During Monotonic Loading		Maximum Induced Pore Pressure During Monotonic Loading kg/cm ²
			On Failure Plane				Accumulated Strain				Number of Cycles to Reach 5% & 10% Accumulated Com- pressive Strain (or Double Ampli- tude Strain) ¹³⁾			Peak kg/cm ²	at 20% strain kg/cm ²	
			$\frac{\tau_{fy}}{\bar{\sigma}_{fc}}$	$\frac{\tau_{fc} + \tau_{fy}}{\bar{\sigma}_{fc}}$			Cycle 5	Cycle 10	Cycle 15	Cycle 20	5% Strain	10% Strain				
CR-1	0.61	0.30	0.22	0.41	17	(7)	3.83	9.24	(4)	-	7	11	-	-	-	
CR-R-2	0.50	0.24	0.18	0.37	20	1.52	0.45	0.82	1.24	1.73	>20	>20	2.07	1.83 ⁵⁾	1.75	
CR-3	1.13	0.28	0.20	0.39	15	(7)	3.14	8.18	13.40	-	7	12	-	-	-	
CR-4 ⁶⁾	-	-	-	-	-	(7)	-	-	-	-	-	-	-	-	-	
CR-5	0.56	0.27	0.20	0.39	20	1.87	1.67	3.40	5.26	7.70	15	>20	-	-	-	
CR-6	0.84	0.21	0.15	0.34	20	3.45	2.15	3.98	5.85	7.39	14	>20	-	-	-	
CR-R-7	0.40	0.10	0.08	0.08	19 ⁹⁾	1.37	0.17	0.18	0.18	0.17	>19	>19	-0.02	2.42	2.35 ¹⁰⁾	
CR-R-8A ¹²⁾	0.36	0.09	0.06	0.25	20	0.72	-	-	-	0.04	>20	>20	-	-	-	
CR-R-8B ¹²⁾	0.50	0.12	0.09	0.28	20	1.07	-	-	-	0.05	>20	>20	-	-	-	
CR-R-8C ¹²⁾	0.67	0.16	0.12	0.31	20	1.82	0.03	0.12	0.19	0.32	>20	>20	0.38	2.75 ¹¹⁾	3.15	
CR-R-9	0.91	0.22	0.16	0.35	20	3.37	0.71	1.59	2.74	3.90	>20	>20	4.56	2.57	3.81	
CR-10	0.63	0.15	0.13	0.13	15 ⁸⁾	(7)	0.41	0.66	8.58	-	14	16	-	-	-	

Notes:

- 1) The symbol CR represents an undrained cyclic triaxial test. The symbol CR-R represents an undrained cyclic triaxial test (CR) followed by an undrained, monotonically loaded triaxial test (R).
- 2) A maximum of 20 cycles were applied at a frequency of 0.4 Hz.
- 3) The failure plane is assumed to be inclined at an angle of 62.5° to the horizontal. The subscript f represents the failure plane.
- 4) The deformation transducer jammed during cycle 11. The downward piston travel (equivalent to a strain of about 20%) was reached at the start of cycle 18.
- 5) Axial piston travel was reached at 12.9% strain. The shear stress on the failure plane was still increasing when the test was terminated.
- 6) Specimen for Test CR-4 inadvertently failed during consolidation stage.
- 7) The piston reached the end of its travel after cyclic loading. Since the specimen was "hanging" from the piston, pore pressure data is not reported.
- 8) Double amplitude strains are reported. The upward piston travel was reached during cycle 16.
- 9) Double amplitude strains are reported. The maximum compressive strain was 0.06% and the maximum tensile strain was 0.16%.
- 10) The shear stress is reported at an axial strain of 18.8%. The peak shear stress occurred at a strain of 17.5%.
- 11) Axial piston travel was reached at 16.8% strain. The shear stress on the failure plane was still increasing when the test was terminated.
- 12) Test CR-R-8A, B and C were performed on the same specimen at three different cyclic stress ratios. The pore pressure generated by each test was dissipated before cyclic loading at higher cyclic stress ratios.
- 13) Accumulated compressive strain or double amplitude strain is reported, whichever occurred first.

Table 9

Summary of Cyclic Load
Triaxial Test Data
(Hydraulic Shell)

Test No. (2)	Dry Unit Weight In Cell ³⁾		Water Content In Cell After Consolidation	Consolidation Stresses				Consolidation Stress Ratios		Back Pressure u_c kg/cm ²
	initial	after con- solidation		Principal Stresses		On Failure Plane ⁽⁴⁾		$\frac{\bar{\sigma}_{1c}}{\bar{\sigma}_{3c}}$	$\frac{\tau_{fc}}{\bar{\sigma}_{fc}}$	
				Vertical $\bar{\sigma}_{1c}$ kg/cm ²	Lateral $\bar{\sigma}_{3c}$ kg/cm ²	 $\bar{\sigma}_{fc}$ kg/cm ²	 τ_{fc} kg/cm ²			
	pcf	pcf	%							
CR-R-11	131.0	132.4	12.6	1.50	1.00	1.11	0.20	1.50	0.18	9.00
CR-12	128.2	129.5	13.7	1.49	1.00	1.10	0.20	1.49	0.18	9.00
CR-13	128.8	130.0	13.5	1.50	1.00	1.11	0.20	1.50	0.18	9.00
CR-R-14	128.1	130.3	13.4	2.00	1.00	1.21	0.41	2.00	0.34	9.00
CR-15	129.6	131.4	13.0	2.00	1.00	1.21	0.41	2.00	0.34	9.00
CR-16	129.1	131.0	13.1	2.00	1.00	1.21	0.41	2.00	0.34	9.00
CR-17	127.2	133.7	12.2	6.03	4.00	4.43	0.83	1.51	0.19	9.00
CR-18	125.8	131.6	12.9	6.03	4.00	4.43	0.83	1.51	0.19	9.00
CR-19	125.4	132.5	12.6	6.03	4.00	4.43	0.83	1.51	0.19	9.00
CR-20	125.3	133.4	12.3	8.05	4.00	4.86	1.66	2.01	0.34	9.00
CR-21	126.1	132.9	12.4	8.00	4.00	4.85	1.64	2.00	0.34	9.00
CR-22	124.7	132.0	12.8	8.01	4.00	4.85	1.64	2.00	0.34	9.00
CR-23	129.5	135.2	11.7	8.03	4.00	4.86	1.65	2.01	0.34	9.00
CR-24	123.2	125.3	15.3	2.00	1.00	1.21	0.41	2.00	0.34	9.00

- Notes: 1) The shell material consists of a mixture of selected split-spoon samples from Borings K-4 and K-5.
 2) The symbol CR represents an undrained cyclic triaxial test. The symbol CR-R represents an undrained cyclic triaxial test (CR) followed by an undrained, monotonically loaded test (R).
 3) All samples were compacted in the laboratory in eight layers. Each layer was about 2.2 cm thick and compacted with a vibratory air hammer impacting on the top of the layer.
 4) Stresses are given on an assumed failure plane inclined 62.5° to the horizontal (ϕ assumed equal to 35°). The subscript f represents the failure plane.

Table 9
(Continued)

Test No. 1)	Cyclic ²⁾ Shear Stress on Failure Plane ³⁾ kg/cm ²	Cyclic Stress Ratios			No. of Load Cycles Applied	Induced Pore Pressure After Cyclic Loading kg/cm ²	Compressive Strain During Cyclic Loading						Compressive Strain at Start of Monotonic Loading %	Shear Stresses on Failure Plane During Monotonic Loading		Maximum Induced Pore Pressure During Monotonic Loading kg/cm ²
		$\frac{\sigma_d}{2\sigma_{3c}}$	On Failure Plane				Accumulated Strain				Number of Cycles to Reach 5% & 10% Accumulated Com- pressive Strain (or Double Ampli- tude Strain) ⁵⁾			Peak kg/cm ²	at 20% strain kg/cm ²	
			$\frac{\tau_{fy}}{\sigma_{fc}}$	$\frac{\tau_{fc}+\tau_{fy}}{\sigma_{fc}}$			Cycle 5	Cycle 10	Cycle 15	Cycle 20	5% Strain	10% Strain				
CR-R-11	0.24	0.29	0.22	0.40	19	0.30	0.00	0.01	0.00	-	>19	>19	0.05	1.66	1.41	0.33
CR-12	0.41	0.50	0.37	0.55	5 ⁸⁾	(4)	8.89	-	-	-	4	5	-	-	-	-
CR-13	0.33	0.40	0.30	0.48	13 ⁸⁾	(4)	0.23	3.41	-	-	10	12	-	-	-	-
CR-R-14	0.34	0.42	0.28	0.62	20	0.60	0.84	1.55	2.41	5.28	20	>20	6.31	0.67	0.67 ⁶⁾	0.56
CR-15	0.41	0.50	0.34	0.68	20	(4)	0.69	1.55	5.98	18.76	14	18	-	-	-	-
CR-16	0.28	0.35	0.23	0.57	95	0.66	0.18	0.26	0.33	0.40	81	89	-	-	-	-
CR-17	1.18	0.36	0.27	0.45	1	(4)	-	-	-	-	2	2	-	-	-	-
CR-18	0.66	0.20	0.15	0.34	16	(4)	0.36	1.32	9.01	-	14	16	-	-	-	-
CR-19	0.44	0.14	0.10	0.29	63	3.20	0.07	0.14	0.20	0.28	59	64	-	-	-	-
CR-20	0.82 ⁷⁾	0.25	0.17	0.51	$\frac{1}{2}$	(4)	-	-	-	-	<1	<1	-	-	-	-
CR-21	0.33	0.10	0.07	0.41	77 ⁸⁾	2.86	0.02	0.06	0.10	0.14	64	71	-	-	-	-
CR-22	0.49	0.15	0.10	0.44	9	(4)	0.05	-	-	-	10	10	-	-	-	-
CR-23	0.51	0.19	0.13	0.46	39	(4)	0.39	0.86	1.39	2.31	26	31	-	-	-	-
CR-24	0.28 ⁷⁾	0.34	0.23	0.57	$\frac{1}{2}$	(4)	-	-	-	-	<1	<1	-	-	-	-

Notes:

- 1) The symbol CR represents an undrained cyclic triaxial test. The symbol CR-R represents an undrained cyclic triaxial test (CR) followed by an undrained, monotonically loaded triaxial test (R).
- 2) Load cycles were applied at a frequency of 0.4 Hz.
- 3) The failure plane is assumed to be inclined at an angle of 62.5° to the horizontal. The subscript f represents the failure plane.
- 4) The piston reached the end of its travel after cyclic loading. Since the specimen was "hanging" from the piston, pore pressure data is not reported.

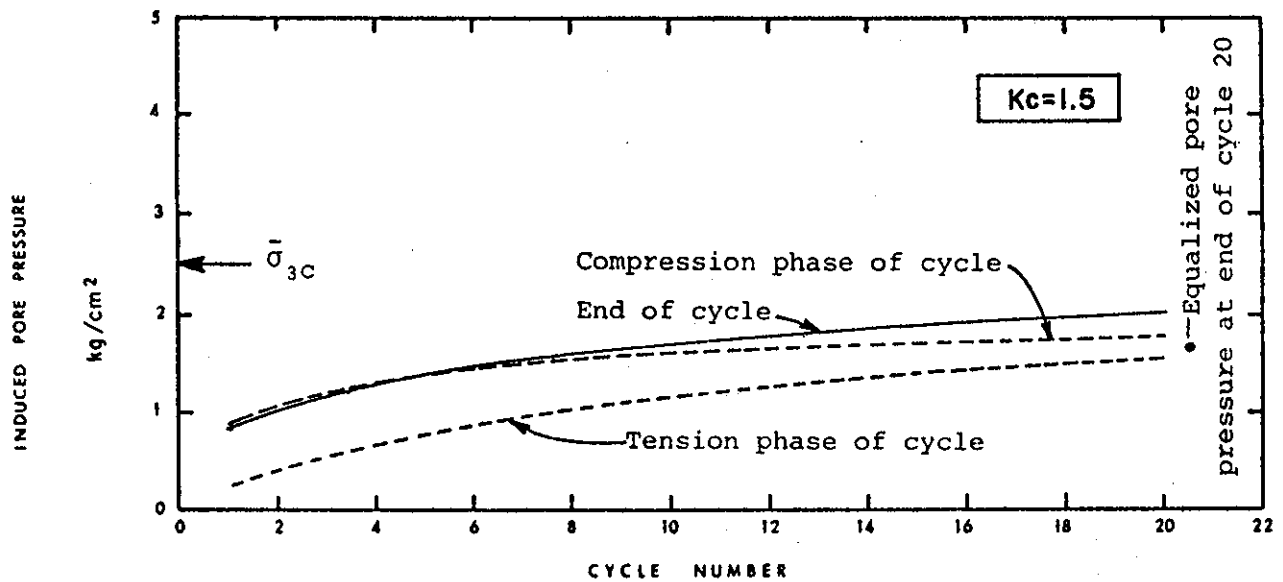
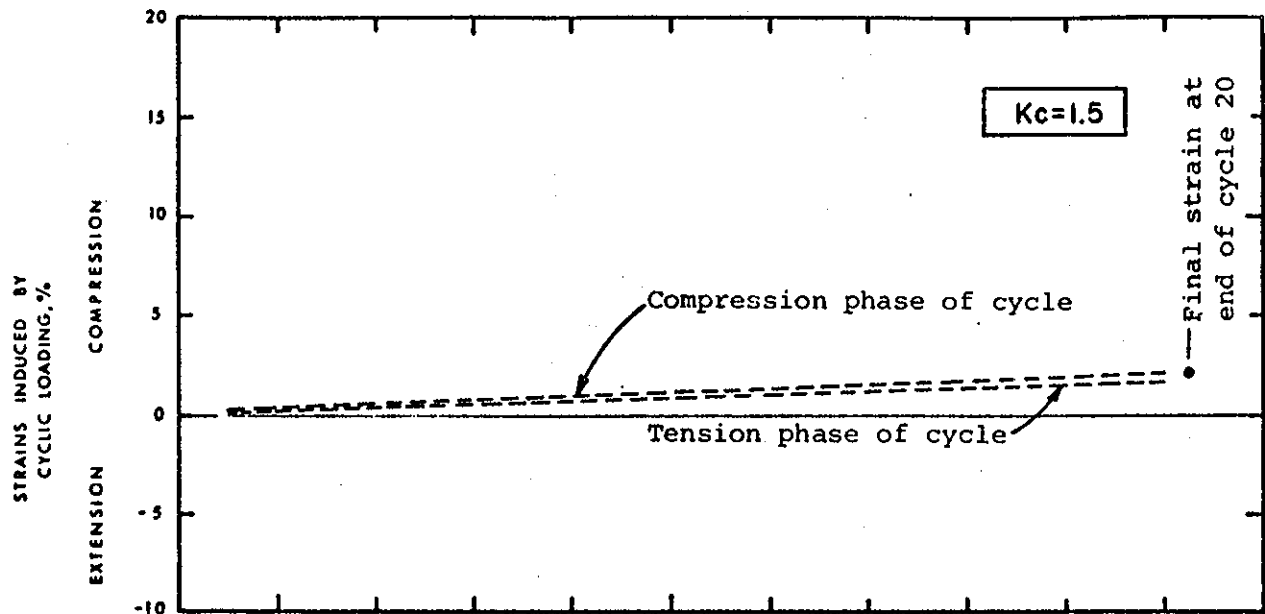
- 5) Accumulated compressive strain or double amplitude strain is reported, whichever occurred first.
- 6) The shear stress is reported at a strain of 17.9%.
- 7) The specimen failed during the compression phase of the first load cycle. The reported value of τ_{fy} was the maximum value attained during application of the compression load.
- 8) Double amplitude strains are reported.

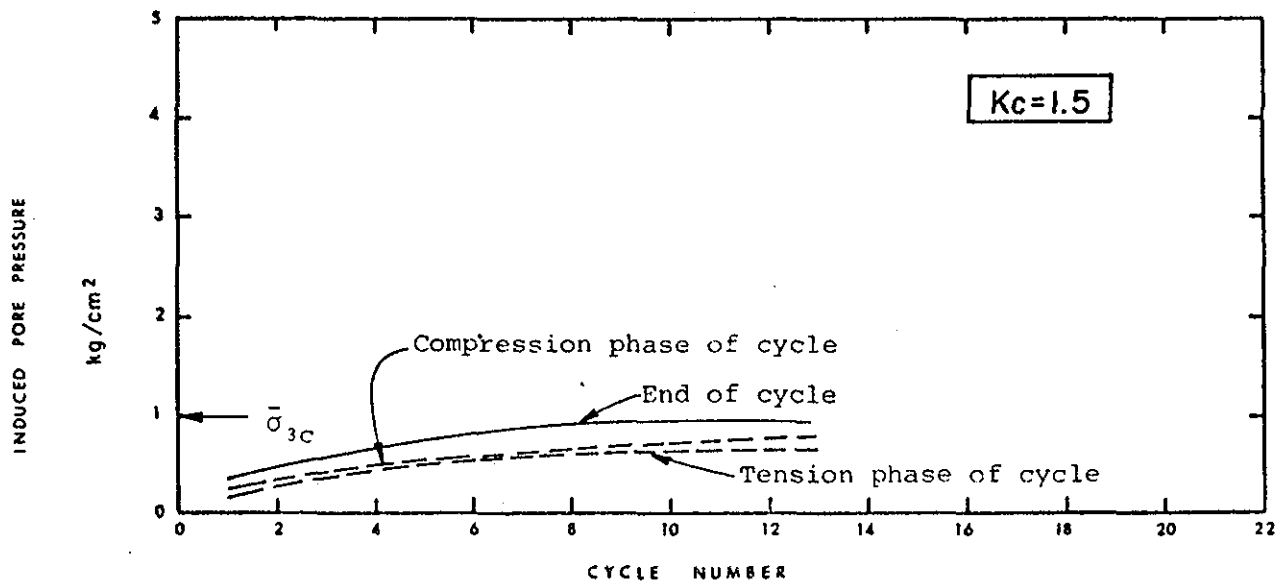
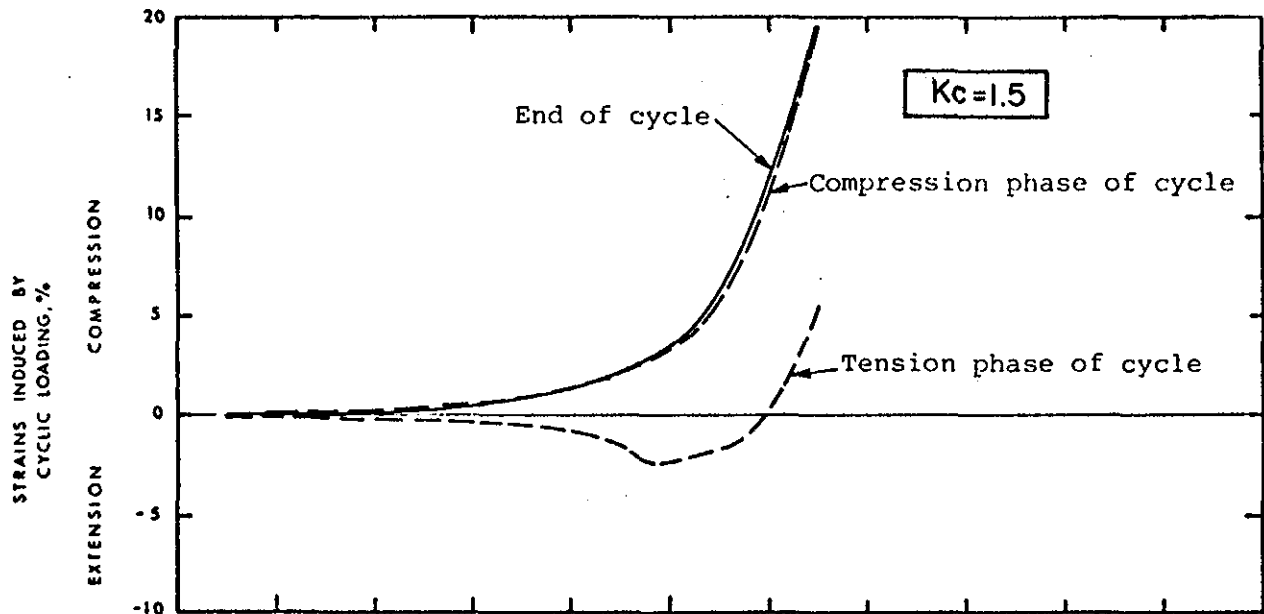
In addition to the saturation and consolidation information presented in the Tables, each Table also lists the following cyclic load-monotonic load triaxial data:

- (1) the cyclic shear stress on the failure plane (τ_{fy} , kg/cm²);
- (2) the cyclic deviator stress ratio ($\sigma_d/2\bar{\sigma}_{3c}$)
- (3) the cyclic shear stress ratio on the failure plane (τ_{fy} / σ_{fc})
- (4) the total shear stress ratio on the failure plane [$(\tau_{fc} + \tau_{fy}) / \sigma_{fc}$];
- (5) the number of load cycles applied during each test (N);
- (6) accumulated compressive strain during cyclic loading at the end of 5, 10, 15 and 20 cycles of loading;
- (7) the number of cycles to reach 5 percent and 10 percent accumulated compressive axial strain; and
- (8) the results of the monotonic \bar{R} tests.

Plates 30 and 31 show typical test results for the hydraulic core and hydraulic shell specimens consolidated to K_c -values of 1.5. The upper portion shows the accumulated strains induced by cyclic loading and the bottom portion shows the induced pore pressure and the value of the initial effective consolidation stress ($\bar{\sigma}_{3c}$). Accumulated strain and induced pore pressure are plotted versus the number of cyclic stress applications.

In order to facilitate a more direct comparison between the results of the cyclic load test data and the results of the dynamic response analysis, the laboratory curves relating axial strain versus number of cycles for the "undisturbed" core and reconstituted shell samples were transformed





into the graphs shown in Plates 32 and 33 using the procedure outlined by Serff, Seed, Makdisi and Chang (1976). These Plates show the relationship between the cyclic shear resistance (τ_{fy}), corresponding to either 5 or 10 percent axial strain in 3, 5 and 10 cycles, and the normal stress on the failure plane (τ_{fc}) during consolidation. The effect of the initial static state of stress on this relationship is shown for two values of α which is defined as follows:

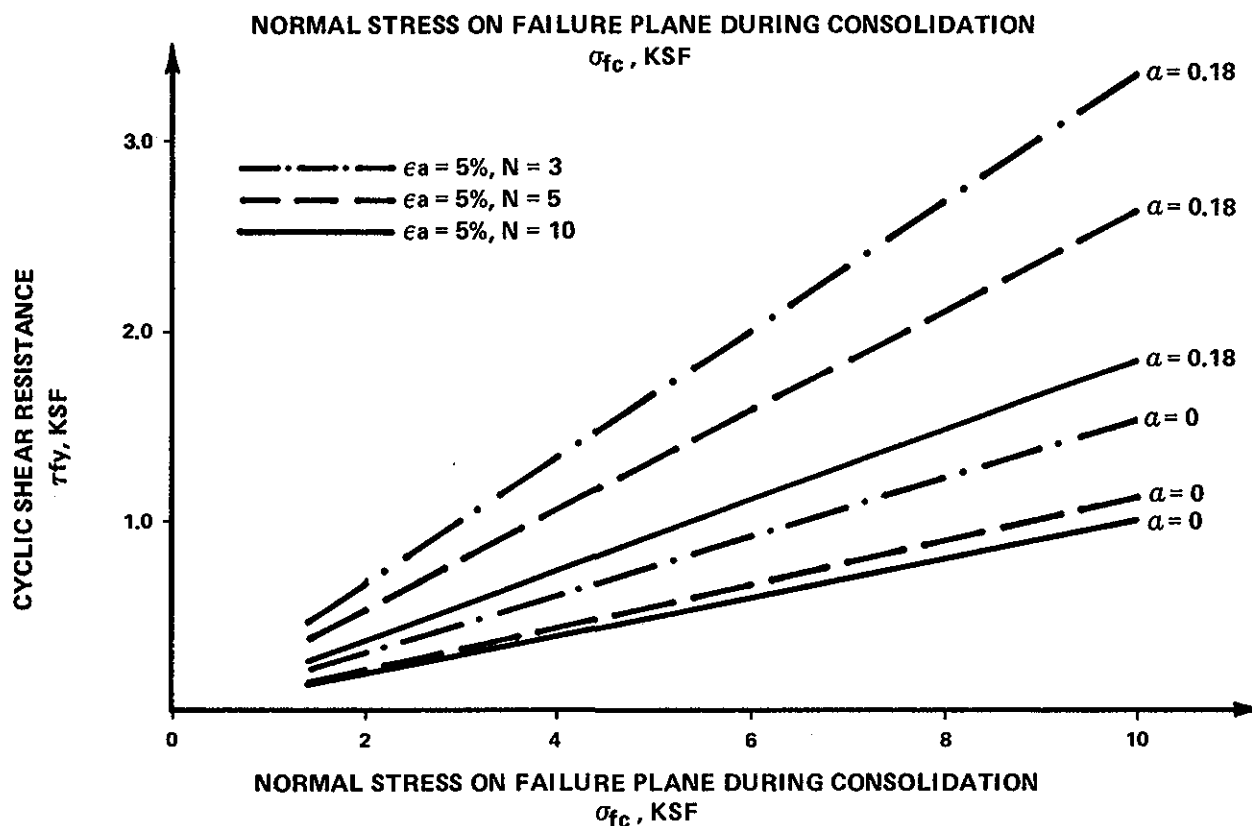
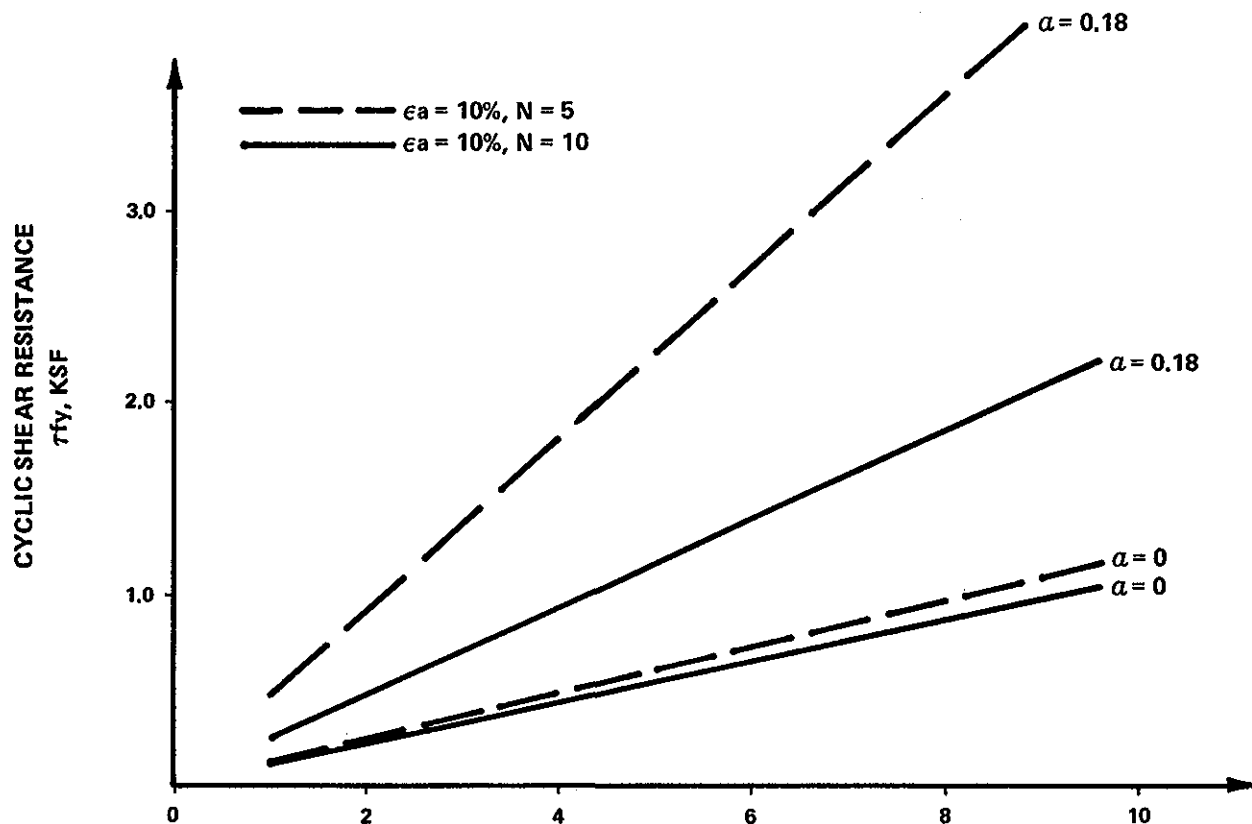
$$\alpha = \frac{\tau_{xy}}{\bar{\sigma}_{fc}} = \frac{\tau_{fc}}{\bar{\sigma}_{fc}}$$

where $\tau_{xy} = \tau_{fc}$ = shear stress on failure plane during consolidation

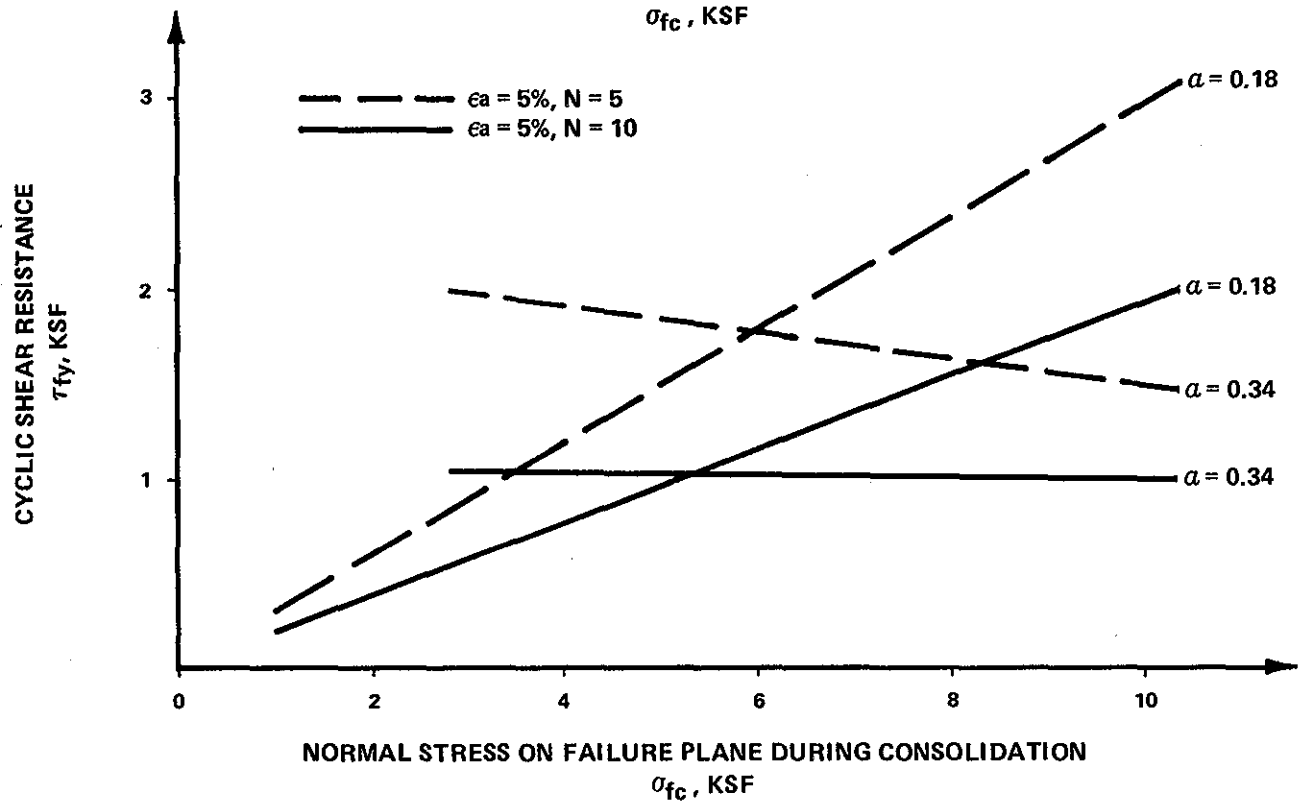
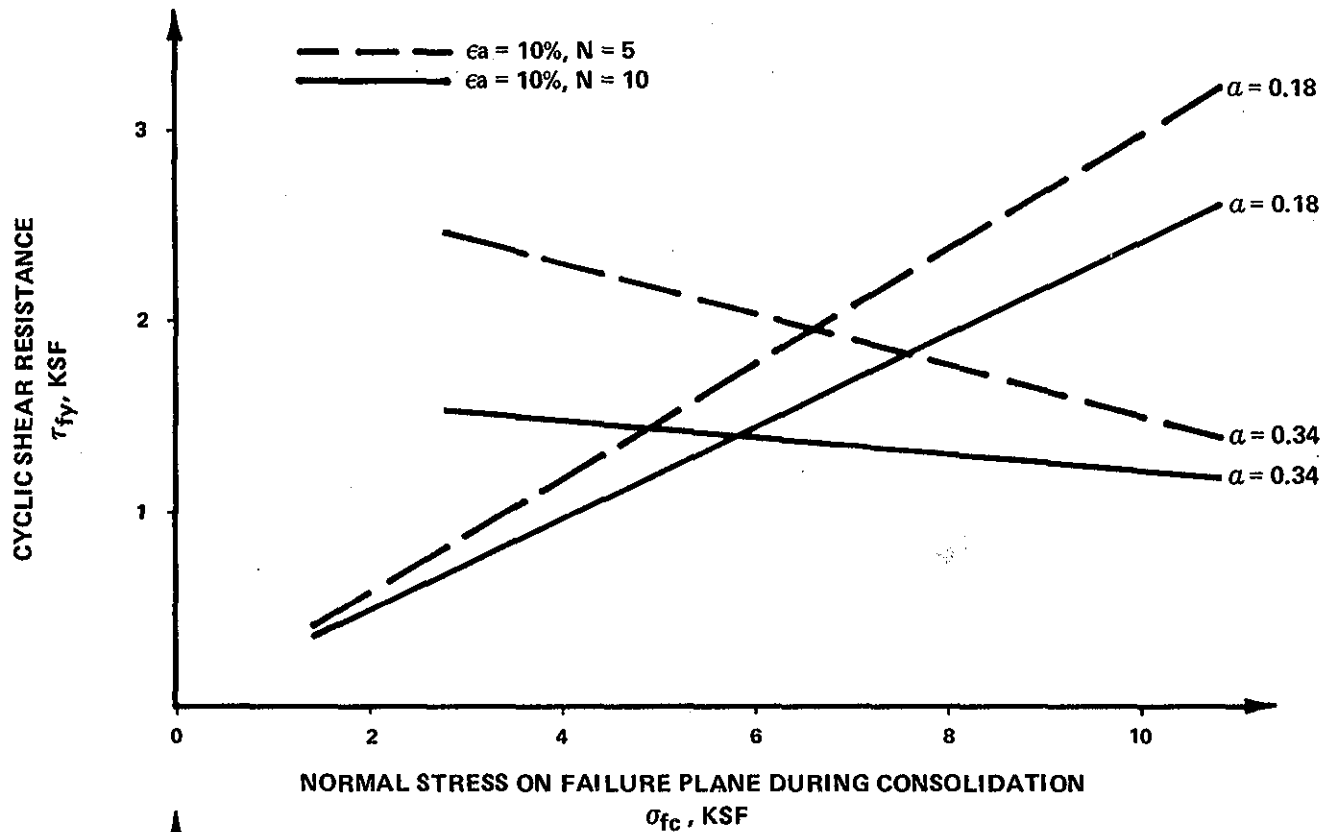
$\bar{\sigma}_{fc}$ = effective normal stress on failure plane during consolidation

In the dynamic response analysis, maximum values of dynamic shear strength (τ_{max}) are generated along horizontal surfaces within each soil element and each horizontal surface is assumed to be the potential failure surface for the element (or layer). In the cyclic triaxial test, however, the failure surface is generally oriented at an angle of $45+\phi/2$ degrees, and therefore these results must be modified to account for the differences in failure plane orientation.

According to Serff, et. al., (1976), for laboratory specimens consolidated to initial isotropic conditions ($K_C = 1$ and $\alpha = 0$), the maximum cyclic shear stress measured on a horizontal failure surface is about 65 percent of the maximum shear stress measured in the triaxial test, whereas for values of $K_C > 1.5$ ($\alpha > 0.18$), the shear stresses obtained from the simple cyclic shear test and the cyclic triaxial test



DYNAMIC STABILITY ANALYSIS OF
KNIGHTVILLE DAM
NEW ENGLAND DIVISION, COE
CYCLIC STRESS CONDITIONS
CAUSING 5 & 10% AXIAL STRAIN
(HYDRAULIC CORE)

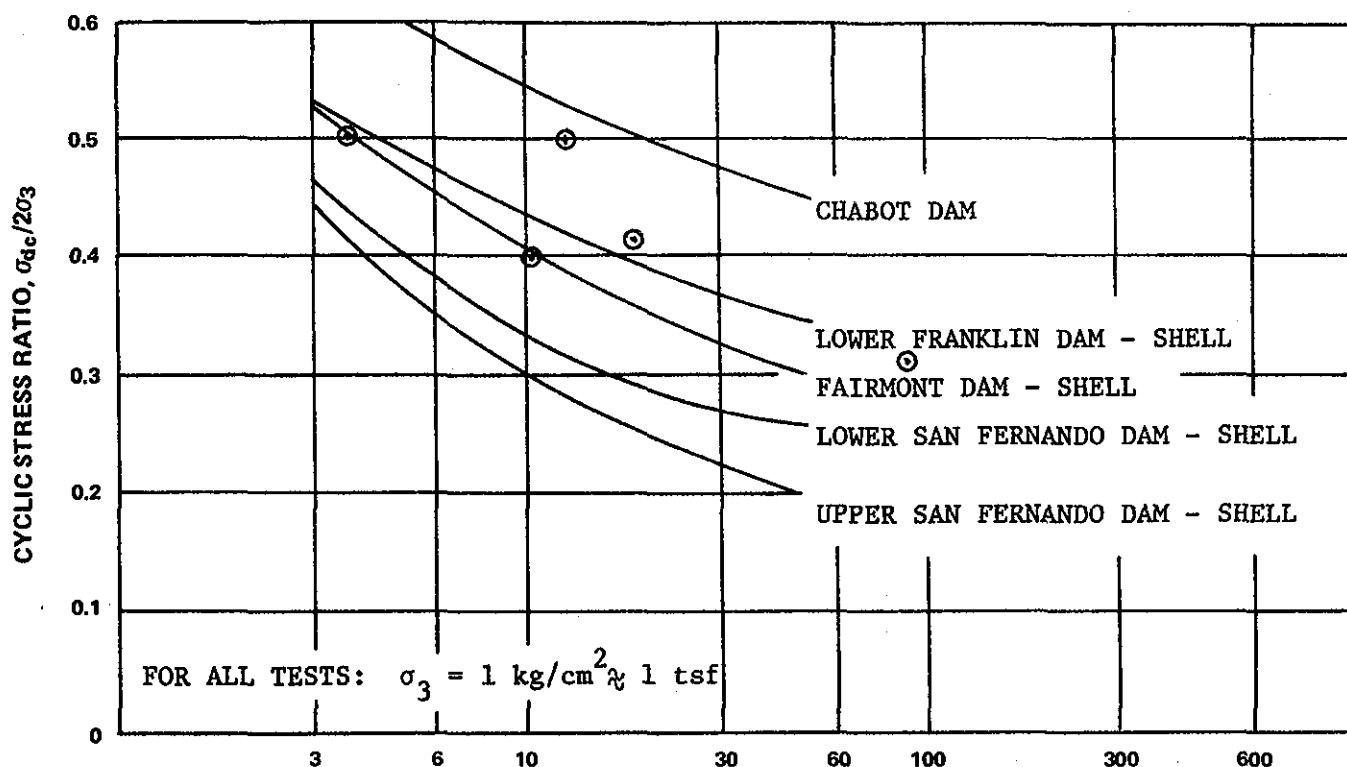


DYNAMIC STABILITY ANALYSIS OF
KNIGHTVILLE DAM
NEW ENGLAND DIVISION, COE
CYCLIC STRESS CONDITIONS
CAUSING 5 & 10% AXIAL STRAIN
(HYDRAULIC SHELL)

are approximately the same. To account for these differences at low values of K_c , the results of the isotropically consolidated ($\alpha = 0$) cyclic triaxial tests performed for this work were reduced by 65 percent; these reduced values are plotted in Plate 32. (No $K_c = 1$ data are available for the shell material, and therefore the shell data were not reduced).

In Plate 32, it is shown that the hydraulic core samples consolidated to initially low values of K_c the cyclic shear resistance (τ_{fy}) increases with increasing values of α . For the shell samples (See Plate 33), which were initially consolidated to higher values of K_c , the opposite trend is true. Similar results showing these trends have been reported by Castro (1976), and can be attributed to the effects of initial shear stress at the time of consolidation on cyclic load test results and/or the effects of mica within the specimen.

As previously reported, cyclic triaxial tests were performed on reconstituted shell samples rather than "undisturbed" samples because of the difficulties associated with obtaining "undisturbed" samples of the relatively coarse grained shell. Previous studies have shown that the cyclic shear resistance measured on undisturbed shell material can be 95 to 100 percent greater than the resistance measured on reconstituted samples, and correction factors as high as 1.8 have been used on strength data obtained using reconstituted samples (Marcuson and Krinitzsky, 1976). To determine if a similar correction factor would be required in this study, the results of the cyclic triaxial were compared to the results of similar tests performed on "undisturbed" shell materials in other studies. This comparison, shown on Plate 34, indicates that the Knightville Dam results on reconstituted samples are in close agreement with results obtained elsewhere, and therefore, no correction factor was applied to these results.



NUMBER OF CYCLES REQUIRED TO CAUSE $\pm 5\%$ STRAIN

⊙ Data for Hydraulic Shell @ $\sigma_3 = 1 \text{ kg/cm}^2$ (Knightville Dam.)

DAM	(g) PEAK ACCELERATION	(mi) DISTANCE	MAGNITUDE	HEIGHT (FT)
CHABOT	0.35	20	8-1/4	135
LOWER FRANKLIN	0.20	20	6-1/2	103
FAIRMONT	0.20	20	6-1/2	121
LOWER SAN FERNANDO	0.55 (0.20)	5 (20)	6-1/2 (6-1/2)	142
UPPER SAN FERNANDO	0.55 (0.20)	5 (20)	6-1/2 (6-1/2)	82

(after Seed, Makdisi, de Alba 1977)

DYNAMIC STABILITY ANALYSIS OF
KNIGHTVILLE DAM
NEW ENGLAND DIVISION, COE
COMPARISON OF LABORATORY
TEST RESULTS

4. Resonant Column (RC) Tests

a. General - Two (2) resonant column (RC) tests were performed on "undisturbed" core samples, one (1) RC-test was performed on an "undisturbed" Pitcher sample of the shell material and three (3) RC-tests were performed on compacted samples of the same mixture of shell material used for cyclic triaxial tests.

Resonant column tests were performed to determine shear moduli and damping ratios of the soil at shear strains of approximately 10^{-6} to 10^{-4} mm/mm.

b. Procedure - The specimen was set up in the resonant column cell and consolidated to an initial isotropic stress of 0.5 kg/cm^2 . The specimen was back pressure saturated so that volume changes under each increment of consolidation load could be measured accurately with a burette. A high B-value was not required for the resonant column test because shear modulus and damping characteristics are not sensitive to degree of saturation.

Sinusoidal torsional vibrations were applied to the "free" end of the sample by means of an electromagnetic field inducing torsional forces to four permanent magnets which, in turn, were rigidly attached to the top cap assembly of the sample. The magnets induced a cyclic torque to the "free" end of the sample and the frequency of the cyclic torque was changed until a state of resonance was attained. The amplitude of vibration was monitored using an accelerometer attached to the top cap. The accelerometer output was displayed on an oscilloscope from which frequencies were measured. The output amplitude was measured using a digital voltmeter. Resonance was defined as that frequency for which the acceleration attained a maximum value.

The single amplitude shear strain, γ_{sa} , at resonance was computed from the acceleration amplitude, frequency, and the radius of the sample. The values reported are those which occurred at the top outer periphery of the sample where they are a maximum. The shear strains ranged from about 10^{-6} to 10^{-4} mm/mm.

The shear wave velocity, V_s , was determined as a function of the resonant frequency, the rotational moments of inertia of the sample and the top cap assembly, and the sample height.

Damping ratios at resonance were determined from the rate of vibration decay after excitation power to the magnets was cut off. The decaying trace of the accelerometer output was recorded on the oscilloscope and subsequently photographed for measurements of peak to peak output decay. (A typical photograph of the damped oscillations is shown in Appendix E).

The test was repeated using successively higher electrical inputs to the electromagnetic system which increases the rotational movement, making possible the determination of shear modulus and damping at higher strain levels. The sample was then consolidated to a next higher consolidation stress and additional data on shear modulus and damping were made.

c. Results - The results of the resonant column tests are presented in tabular form in Appendix E. The results of these tests are used to determine the relationship of shear modulus (G) and damping (ν) with shear strain for the response analysis.

In order to obtain the variation in shear modulus and damping over the range of shear strain required for a dynamic analysis (0.0001 to 1 percent), the results of the resonant

column and small strain cyclic triaxial tests (as discussed below) were combined. The shear modulus ratio (G/G_{\max}) defined as the ratio of the shear modulus (G) at any strain to the maximum shear modulus (G_{\max}), is plotted on Plates 35 and 36 for the "undisturbed" hydraulic core and reconstituted shell materials, respectively. It has been reported that for a given value of shear strain, a variation in shear modulus results from the influence of mean effective stress, $\bar{\sigma}_m$ (Bureau of Reclamation, 1976). This variation was also observed herein, and the upper and lower limits of the variation for the materials are shown on the Plates.

As previously reported, cross-hole and down-hole shear wave velocity measurements were made in the core, shell and impervious rolled fill zones. These measurements were used to compute values of G_{\max} using the following relation:

$$G_{\max} = (V_s^2) \gamma_t / g$$

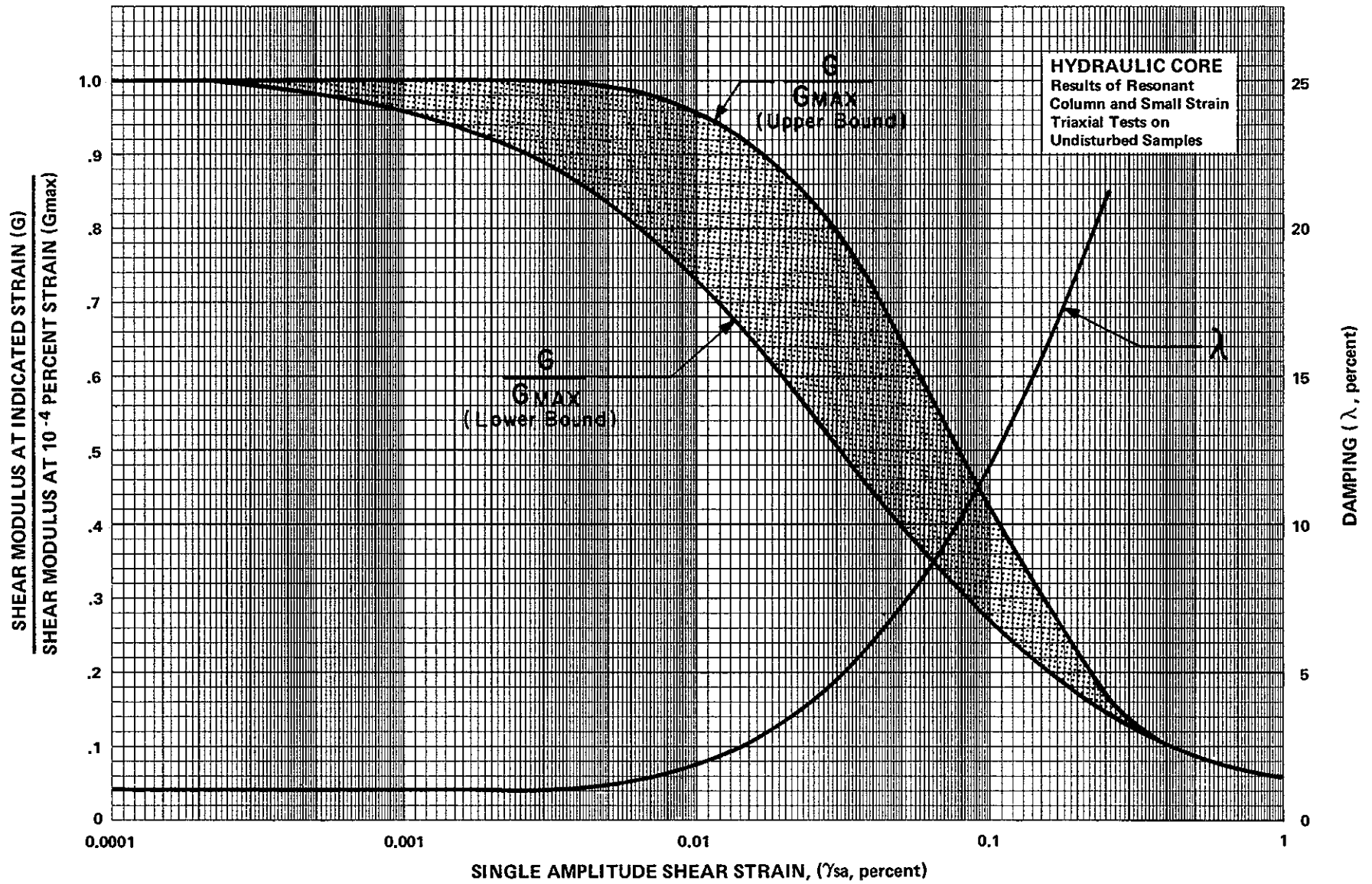
where G_{\max} = shear modulus at low strains, i.e.,
@ 10^{-4} percent (psf)

γ_t = total unit weight of soil (pcf)

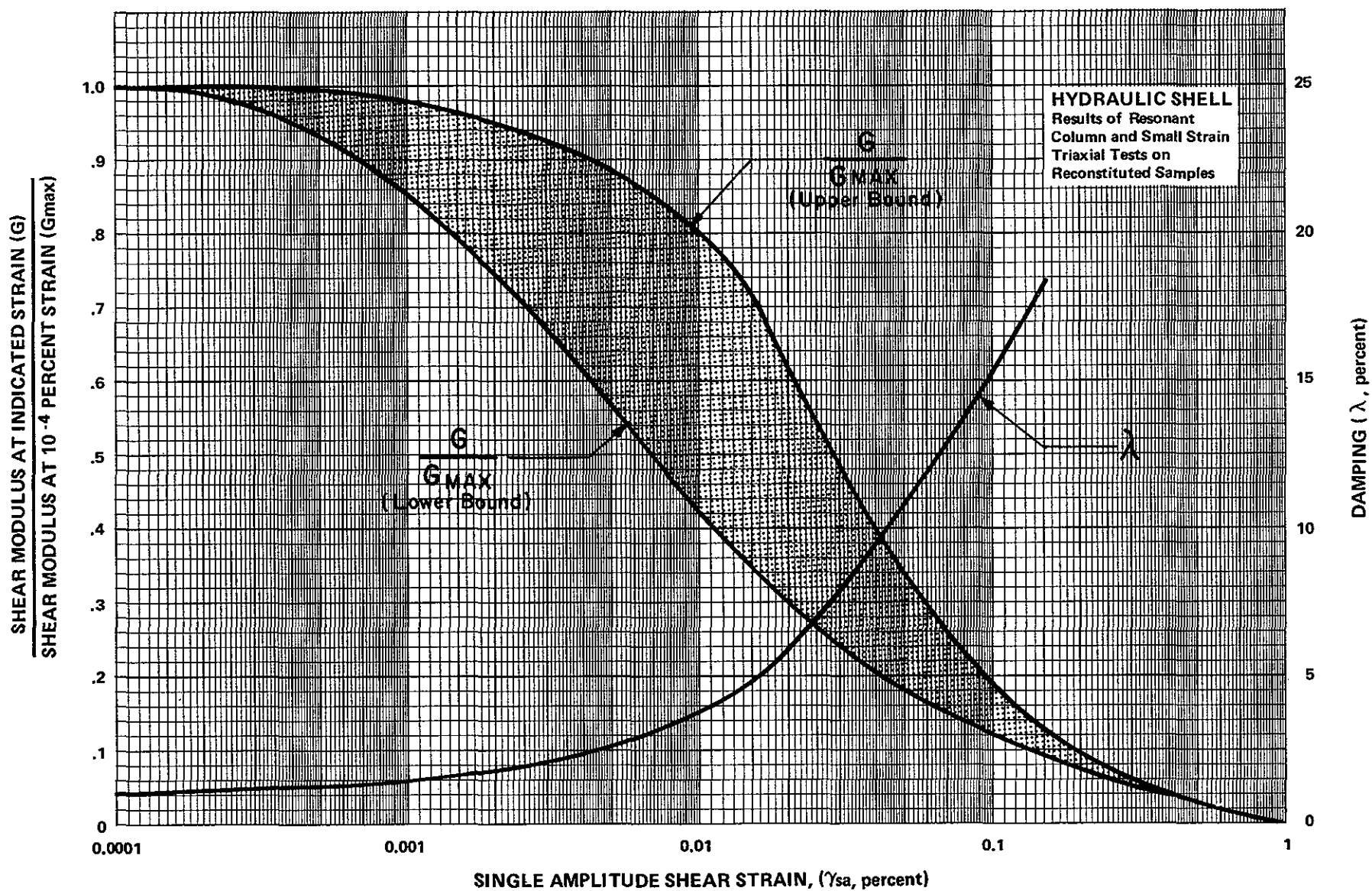
g = acceleration of gravity (ft/sec²)

V_s = shear wave velocity (ft/sec)

The values of damping versus shear strain for the core and shell are also shown on Plates 35 and 36. These values were also obtained from the dynamic tests and are considered to be average curves, since damping is also strongly influenced by values of the mean effective confining stress ($\bar{\sigma}_m$).



DYNAMIC STABILITY ANALYSIS OF
KNIGHTVILLE DAM
NEW ENGLAND DIVISION, COE
SHEAR MODULUS AND DAMPING
vs STRAIN (HYDRAULIC CORE)



DYNAMIC STABILITY ANALYSIS OF
KNIGHTVILLE DAM
NEW ENGLAND DIVISION, COE
**SHEAR MODULUS AND DAMPING
vs STRAIN (HYDRAULIC SHELL)**

5. Small Strain Triaxial Tests

a. General - Two small strain triaxial compression (E) tests were performed on "undisturbed" core samples; one E test was performed on a compacted sample of the shell mixture. The E tests were performed to determine the shear modulus and damping ratios of the soil at shear strains between about 1×10^{-4} and 5×10^{-3} mm/mm.

b. Procedure - The specimen was set up in the triaxial cell, consolidated to an initial isotropic stress of 0.5 kg/cm^2 , and back pressure saturated. The anisotropic consolidation stresses were applied to the specimen in increments.

A small symmetrical cyclic deviator stress was applied under undrained conditions. The load cycles were applied at a frequency of about 0.025 Hz. Axial load and axial strains were recorded continuously with a strip chart recorder during cyclic loading. The cyclic deviator stress applied to the specimen was controlled during each cycle so that the double amplitude strains of the specimen would be approximately the same for each load cycle. Cyclic loading was continued until the applied cyclic deviator stress did not change significantly from one cycle to the next.

After cyclic loading, the excess pore pressure in the specimen was measured. The drainage valve to the specimen was then opened to allow excess pore pressures to dissipate.

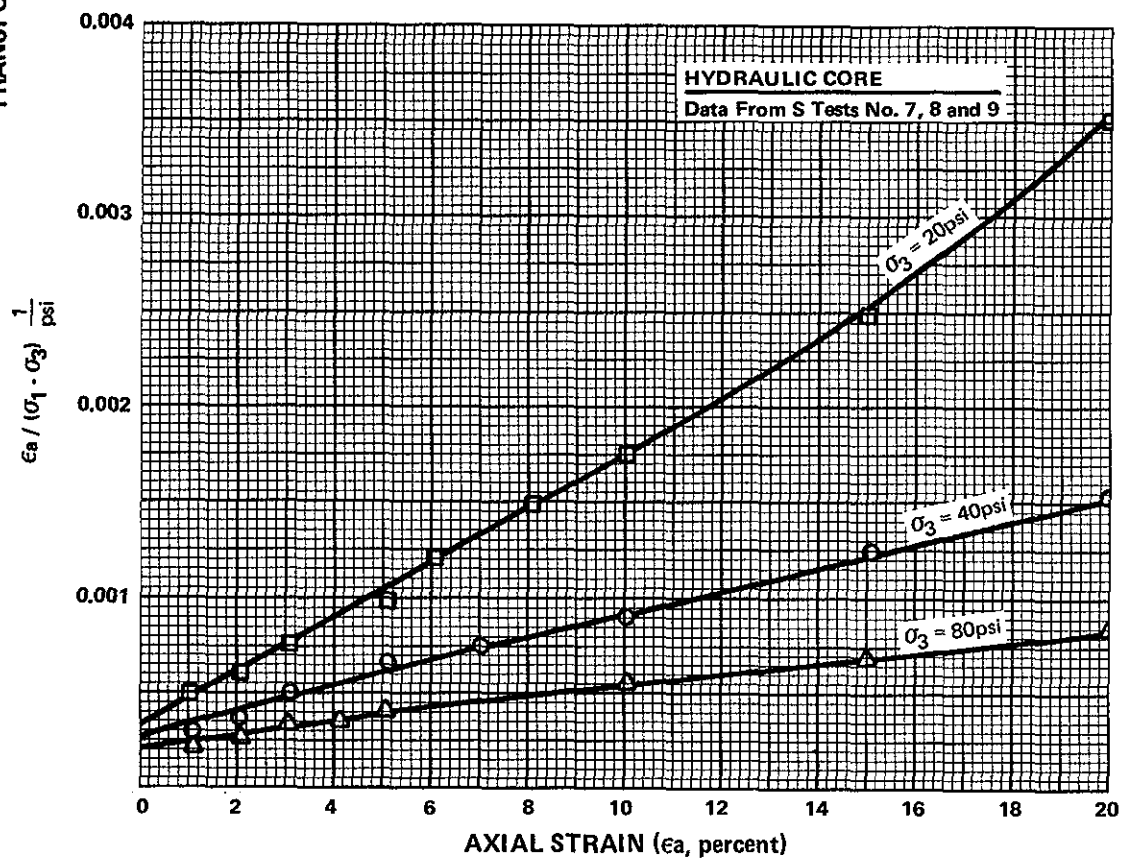
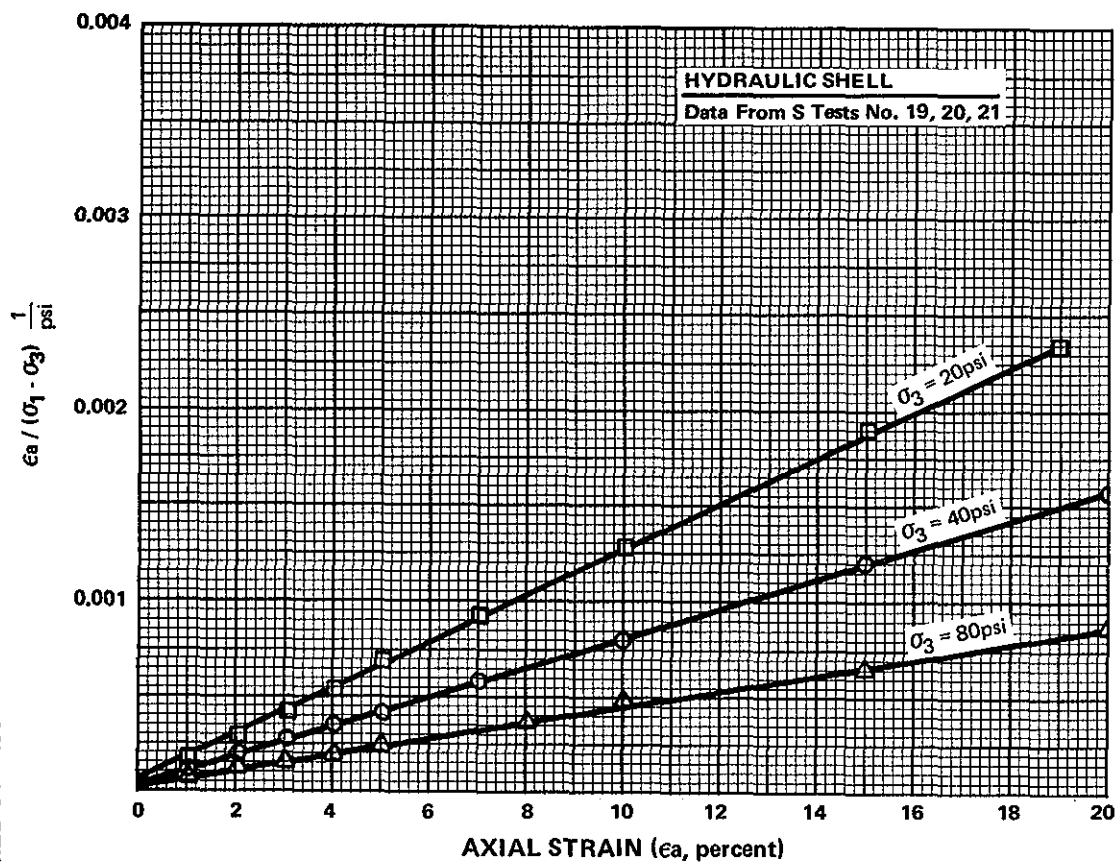
The above cyclic load procedure was repeated at higher strain levels.

The cyclic deviator stress was plotted vs axial strain for the last (or near to last) load cycle in each determination.

The stress-strain hysteresis loop was used to determine the secant elastic modulus, E_s , and damping ratio, D , for the soil at a particular strain level. The methods used to determine secant elastic modulus and damping ratio are schematically shown in Appendix E along with the formula used to compute secant shear modulus, G_s , and the single amplitude cyclic shear strain, γ_{sa} .

c. Results - The results of E tests performed on the hydraulic core and shell specimens are presented in Appendix E. The results include values of shear modulus (G) and damping (λ) for the various values of shear strain. Since the results of the E tests are for shear strains which are slightly larger than those resulting from the RC tests, these data were used to develop the G/G_{max} and versus γ_{sa} relationships shown in Plates 35 and 36.

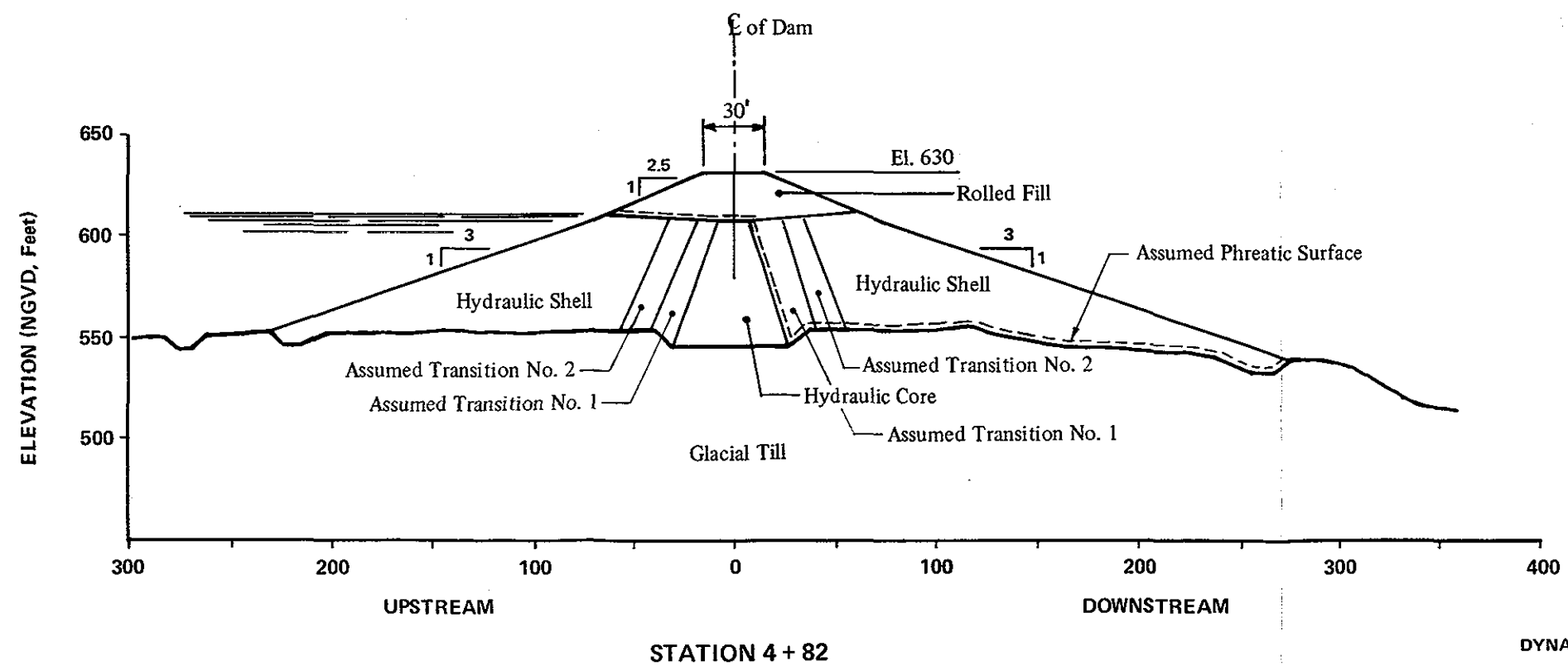
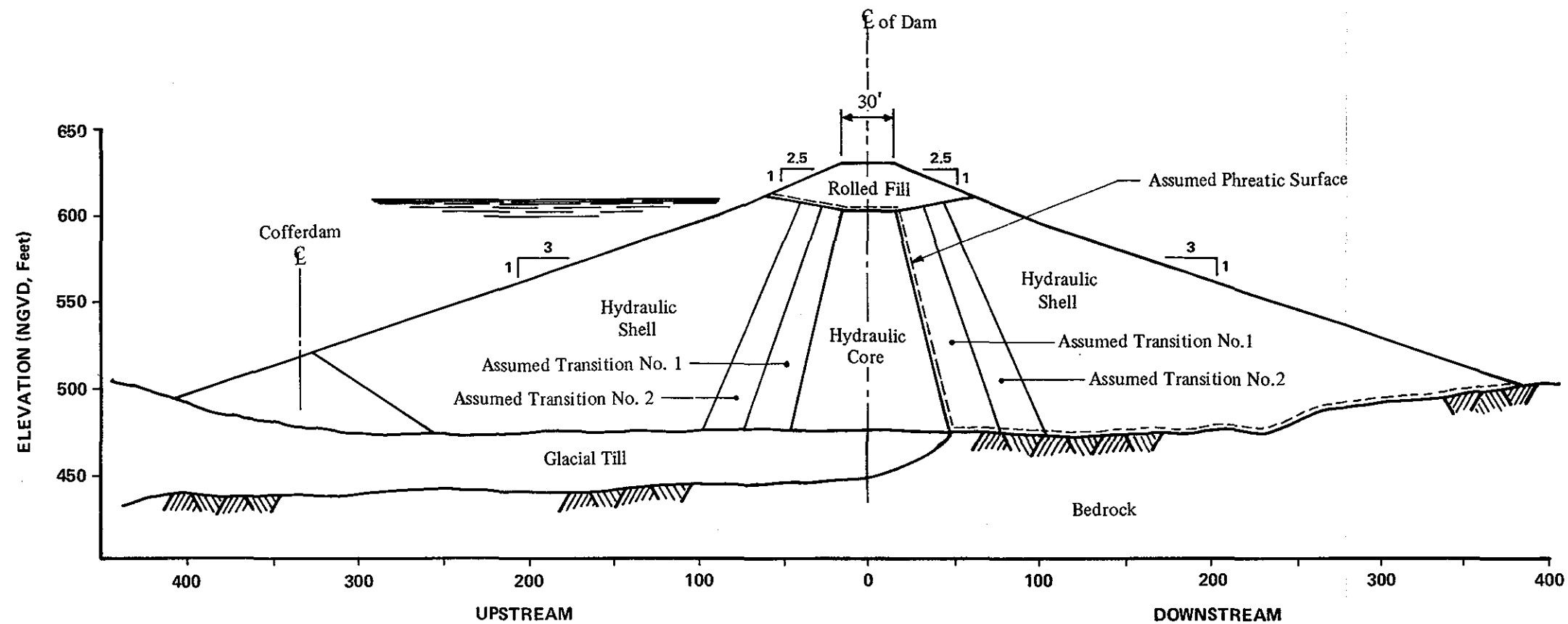
TRANSFORMED STRESS



Station 4+82, as shown on Plate 37. Station 8+50 was selected because it represents the approximate maximum section of the dam. According to the original contract drawings, the dam is approximately 160 feet high at this location and is underlain by a relatively shallow glacial till deposit on the upstream side and by bedrock on the downstream side. The embankment at Station 4+82 is approximately 80 feet high and is underlain by a thick deposit of compact glacial till on both the upstream and downstream sides. The latter section was chosen for analysis in order that the effects of the thick till foundation on the dynamic response of the dam could be determined.

The core and shoulders of the dam were constructed approximately to El 605 using the hydraulic fill method of construction. This method was used to separate the fine and coarse fractions of the borrow material for the core and shell zones, respectively. As a result, the outer portions of the shell contain coarser particle sizes than the portion of the shell located nearest to the core. To account for this variation in particle size with position, two transition zones within the shells, both upstream and downstream of the core, were incorporated in the analysis. The location of these zones were based on grain-size data in the shells collected during construction of the dam (U.S. Army Corps of Engineers, 1941). The "assumed" transition zones are shown in Plate 37; other reasons for utilizing these zones are discussed in a following section.

The static state of stress analysis is an effective stress analysis, therefore, seepage forces must be included to obtain the effective stress in the soil prior to earthquake. At Knightville Dam, normal operational procedures require that the reservoir be drained immediately after filling. In view of the short period of storage and the low value of permeability of the core ($\approx 10^{-4}$ cm/sec), it is unlikely that steady seepage conditions have ever developed within the core. For this reason, seepage forces were not included in the analyses.



DYNAMIC STABILITY ANALYSIS OF
KNIGHTVILLE DAM
NEW ENGLAND DIVISION, COE
EMBANKMENT CROSS-SECTION
USED FOR DYNAMIC ANALYSIS

In the analysis, the reservoir level was assumed to be at the top of the hydraulic core (El 605) and the phreatic surface through the dam was assumed as shown on Plate 37. Static (and dynamic) analyses were not performed for partial pool and/or no pool conditions, because these conditions are considered to be less critical with respect to the stability of the dam under earthquake shaking.

The finite element grids used in the analysis for the embankment sections at Stations 8+50 and 4+82 are shown in Plates 38 and 39, respectively.

D. STRESS-STRAIN AND MATERIAL PROPERTIES

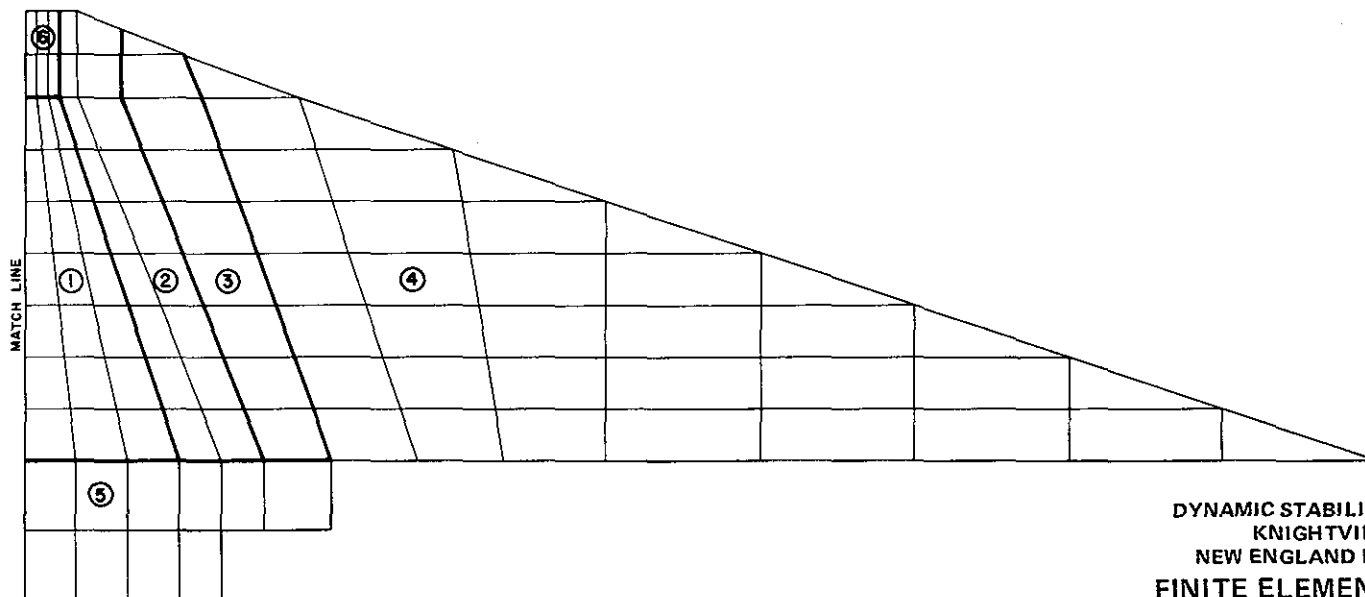
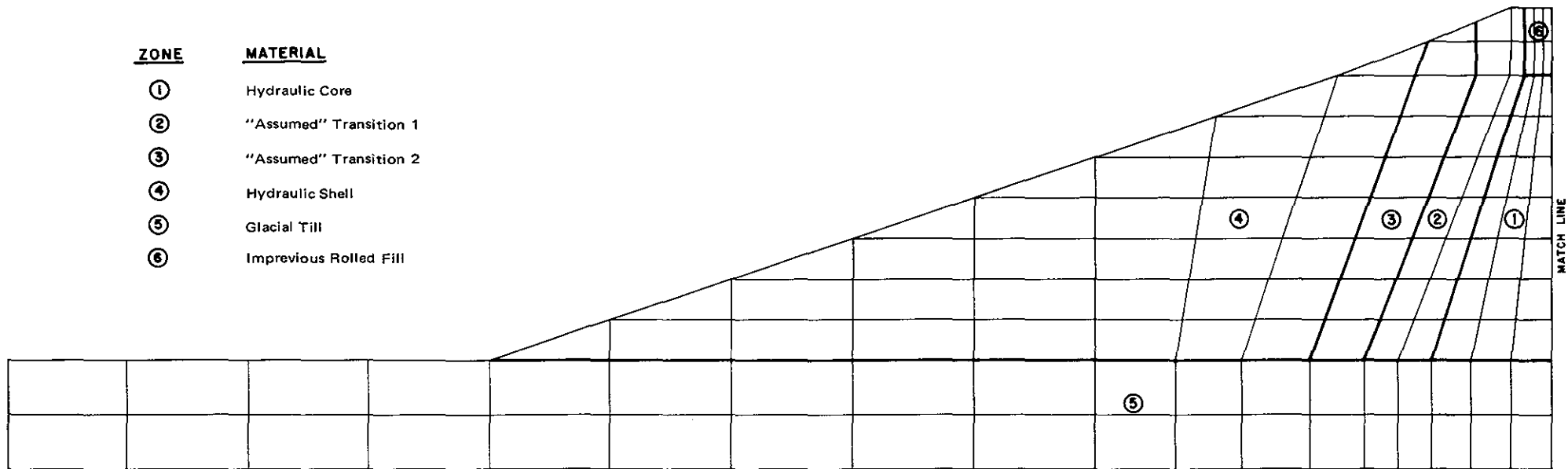
In order to successfully determine the stresses within an embankment, it is necessary to accurately model the non-linear behavior of soil under load. In the FEADAM program, the non-linear behavior of each soil element is modelled utilizing a successive increment procedure. In each increment the stress-strain behavior of the soil is considered to be linear and governed by the generalized Hooke's Law of elastic deformation for plane strain conditions (Duncan, et al. 1980). By using Hooke's Law it is possible to model the non-linearity, stress-dependency, and inelasticity of the soil by varying the values of Young's modulus and bulk modulus with confining stress.

The relationship between initial Young's modulus (E_i) and stress used in the program is based on the hyperbolic stress-strain behavior exhibited by most soils. The expression has been derived elsewhere (Kulhawy, Duncan, and Seed, 1969), and is as follows (for primary loading only):

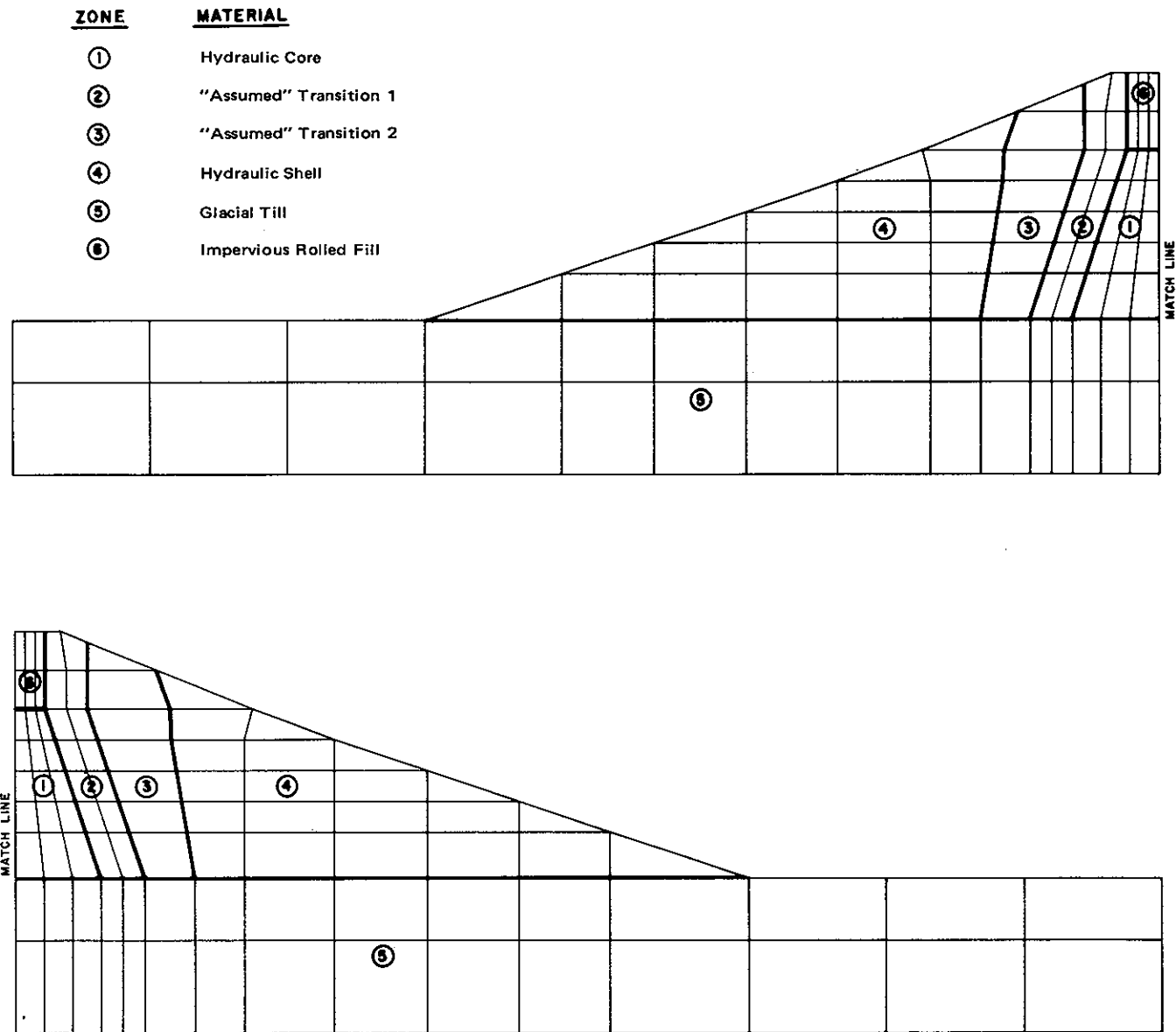
$$E_i = \left[1 - \frac{R_f (1 - \sin \phi) (\sigma_1 - \sigma_3)}{2C \cdot \cos \phi + 2\sigma_3 \cdot \sin \phi} \right]^2 K \cdot P_a \left\{ \frac{\sigma_3}{P_a} \right\}^n$$

ZONE**MATERIAL**

- ① Hydraulic Core
- ② "Assumed" Transition 1
- ③ "Assumed" Transition 2
- ④ Hydraulic Shell
- ⑤ Glacial Till
- ⑥ Impervious Rolled Fill



DYNAMIC STABILITY ANALYSIS OF
KNIGHTVILLE DAM
NEW ENGLAND DIVISION, COE
FINITE ELEMENT GRID USED
FOR FEADAM AND FLUSH
STATION 8 + 50



DYNAMIC STABILITY ANALYSIS OF
 KNIGHTVILLE DAM
 NEW ENGLAND DIVISION, COE
 FINITE ELEMENT GRID USED
 FOR FEADAM AND FLUSH
 STATION 4 + 82

Similarly, the relationship between bulk modulus (B) and confining stress (σ_3) used to determine volume change under load is defined by Duncan, Wong and Ozawa (1980) as follows:

$$B = K_b P_a \left(\frac{\sigma_3}{P_a} \right)^m$$

To solve the constitutive equations, each of the parameters is required as input for the analysis. The definition and function of these parameters are presented in Table 10.

Table 10

SUMMARY OF THE HYPERBOLIC PARAMETERS
(From Duncan, Wong and Ozawa, 1980)

Parameter	Name	Function
K, K_{ur}	Modulus number	Relate E_i and E_{ur} to σ_3
n	Modulus exponent	
C	Cohesion intercept	Relate $(\sigma_1 - \sigma_3)_f$ to σ_3
$\phi, \Delta\phi$	Friction angle parameters	
R_f	Failure ratio	Relates $(\sigma_1 - \sigma_3)_{ult}$ to $(\sigma_1 - \sigma_3)_f$
K_b	Bulk modulus number	Value of B/P_a at $\sigma_3 = P_a$
m	Bulk modulus exponent	Change in B/P_a for ten-fold increase in σ_3

NOTE: The values of strength parameters (C, ϕ) and principal stresses (σ_1, σ_3) to be used in the equations must be consistent with the type of strength tests performed, i.e., R, \bar{R} , S-tests.

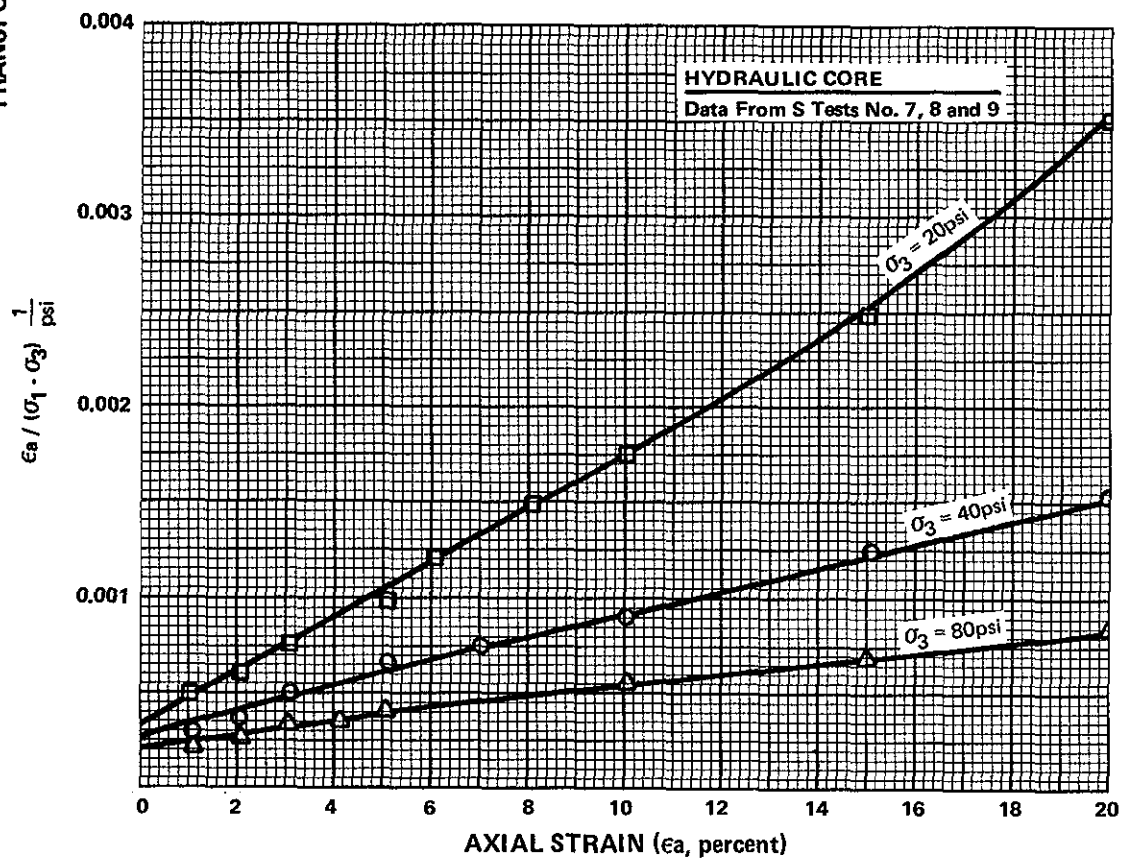
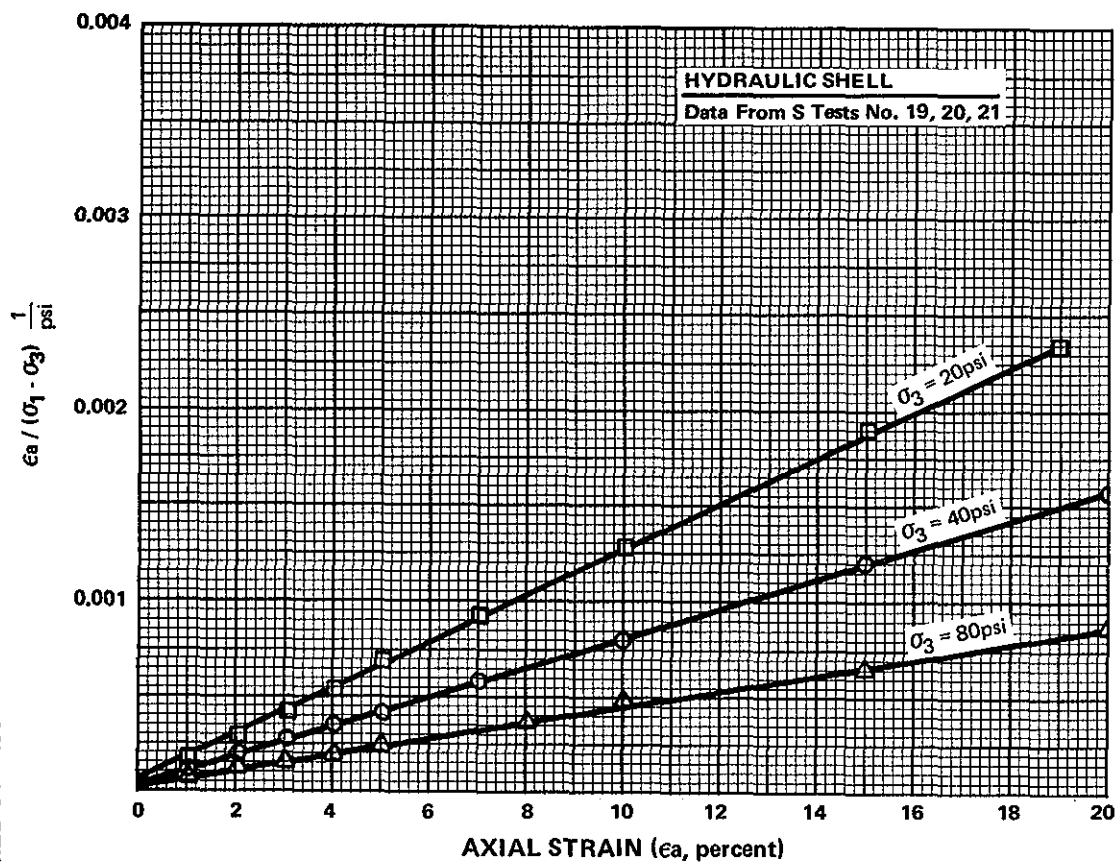
In order to compute the values of Modulus number (K) and exponent (n), transformed hyperbolic stress-strain relations were plotted using the consolidated-drained triaxial (S) test results for the "undisturbed" hydraulic core and re-constituted hydraulic shell specimens, as shown on Plate 40. From these plots values of E_i/P_a and σ_3/P_a (P_a equals atmospheric pressure) are plotted to determine the values of K and n, as shown on Plate 41. In this procedure the value of E_i is taken as the inverse of the intercept of the transformed stress value, $(\sigma_1 - \sigma_3)/\epsilon_a$ at zero percent strain, and n is the slope of the line.

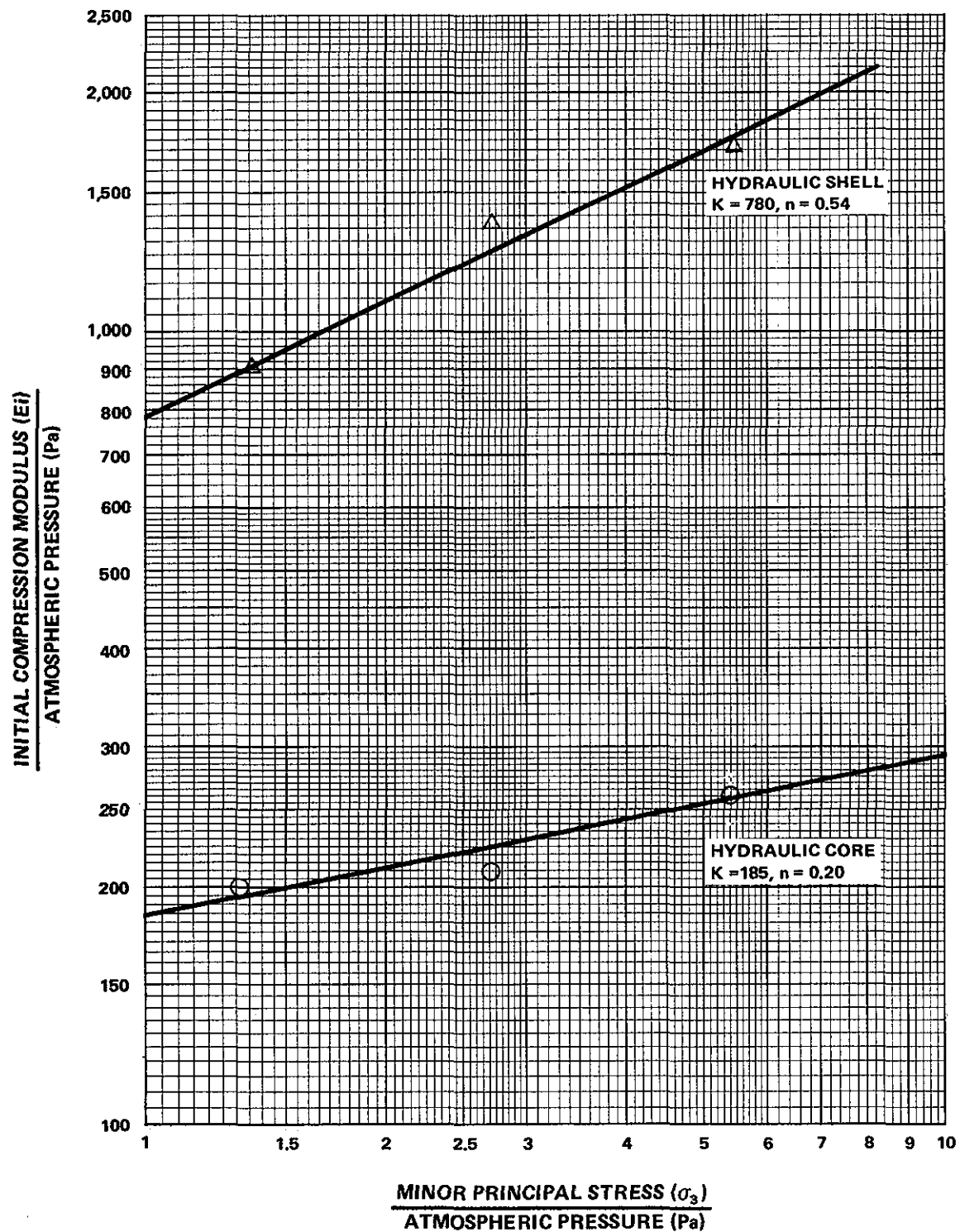
Duncan, Byrne, Wong and Mabry (1980) describe the procedure for computing the bulk modulus (B) from the volume change data obtained from consolidated-drained triaxial tests. The results of this procedure are plotted on Plate 42.

Table 11 provides a summary of the soil properties used in the FEADAM analysis. Since laboratory tests were performed on core and shell samples only, the values for the other embankment and foundation zones listed in Table 11 were obtained, as discussed below.

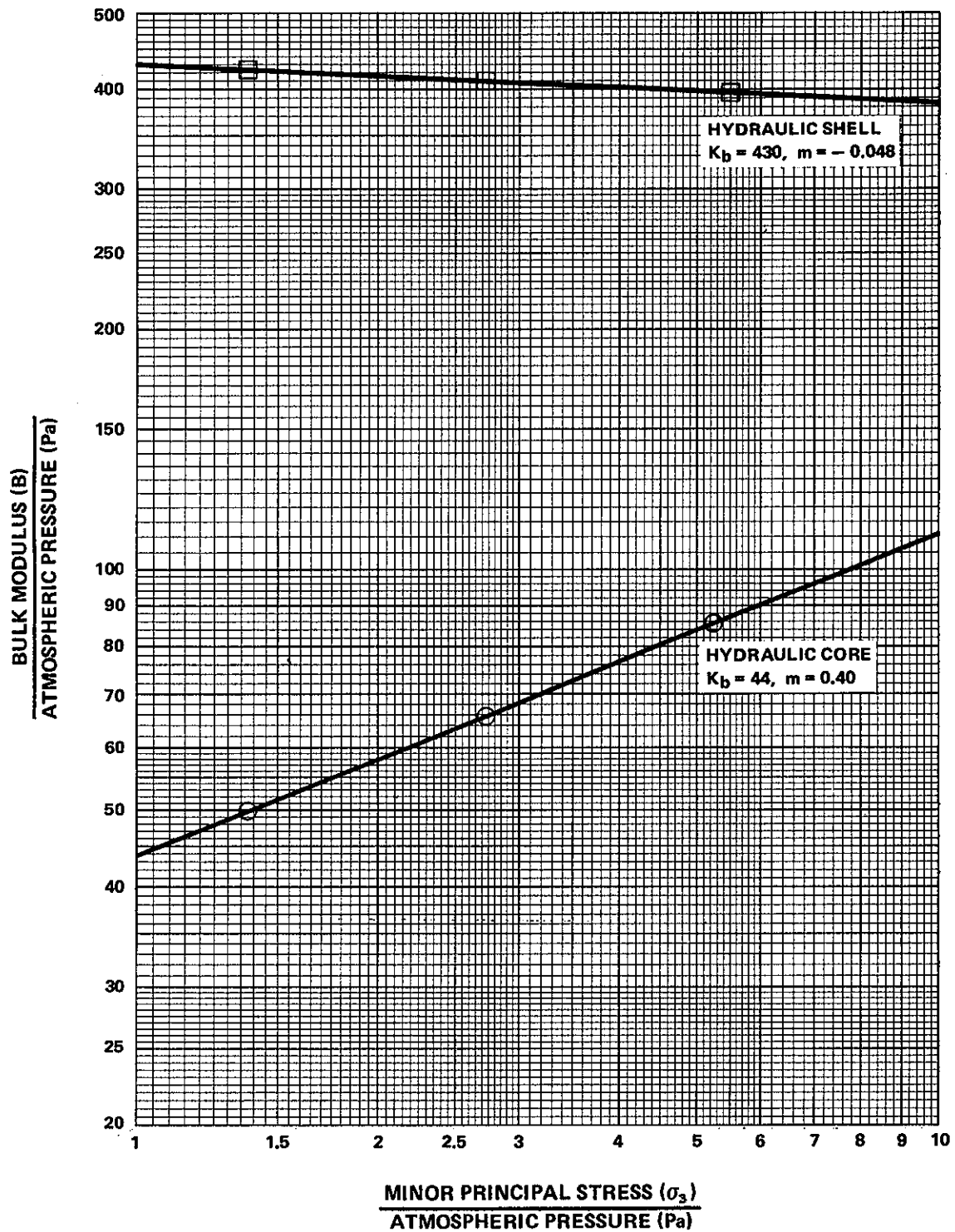
During the pre-construction investigation, borehole and laboratory test data were obtained for the glacial till foundation (See U.S. Army Corps of Engineers, 1939). Values of initial void ratio computed for this material ranged between 0.3 and 0.4; these values indicate that the pre-construction material was in a relatively dense state. In order to adequately model this material in the FEADAM analysis, high values of unit weight and friction were assumed; these assumed values are consistent with values obtained on similar materials and the pre-construction test data shown on Plate 15. The elastic and bulk moduli parameters were assumed based on the values presented by Kulhawy, et. al. (1969, Tables 2 and 4) and Duncan, et. al. (1980, Table 5).

TRANSFORMED STRESS





DYNAMIC STABILITY ANALYSIS OF
KNIGHTVILLE DAM
NEW ENGLAND DIVISION, COE
DETERMINATION OF
ELASTIC PARAMETERS



DYNAMIC STABILITY ANALYSIS OF
 KNIGHTVILLE DAM
 NEW ENGLAND DIVISION, COE
 DETERMINATION OF
 BULK MODULUS PARAMETERS

TABLE 11
SOIL PARAMETERS USED IN NON-LINEAR
STATIC ANALYSIS - FEADAM

SOIL PARAMETER	SYMBOL	VALUES USED IN ANALYSIS							
		Impervious Rolled Fill*	Hydrau- lic Core	Hydrau- lic Shell	Upstream Tran- sitions		Downstream Tran- sitions		Glacial Till
					#1	#2	#1	#2	
Saturated Unit Weight	γ_s (pcf)	120*	116	147	147 140*	147 140*	147 140*	147 140*	155
Buoyant Unit Weight	γ_b (pcf)	---	54	85	85	85	85	85	90
Cohesion	C (psf)	2,600	0	0	0	0	0	0	0
Friction Angle	ϕ (degrees)	25	36	41†	41	41	41	41	45
Elastic Modulus Parameters	K	300	185	780	383	581	383	581	1,600
	n	0.76	0.20	0.54	0.31	0.42	0.31	0.42	0.20
Bulk Modulus Parameters	K_b	430	44	430	172	301	172	301	952
	m	0.05	0.40	0.05	0.26	0.13	0.26	0.13	0.20
Failure Ratio	R_f	0.90	0.76	0.91	0.91	0.91	0.91	0.91	0.67

* Moist Unit Weight

† A slightly higher value of ϕ was chosen to reflect the plus
½-inch size particles not used for preparing laboratory test specimens.

The "assumed" values shown in Table 11 for the upstream and downstream transitions were based on the values obtained from the laboratory tests on the core and shell samples. The assumed values of unit weight, cohesion and friction for the transitions were equivalent to those computed in the laboratory for the hydraulic shell. However, the elastic and bulk moduli parameters were computed by a linear interpretation of the core and shell values.

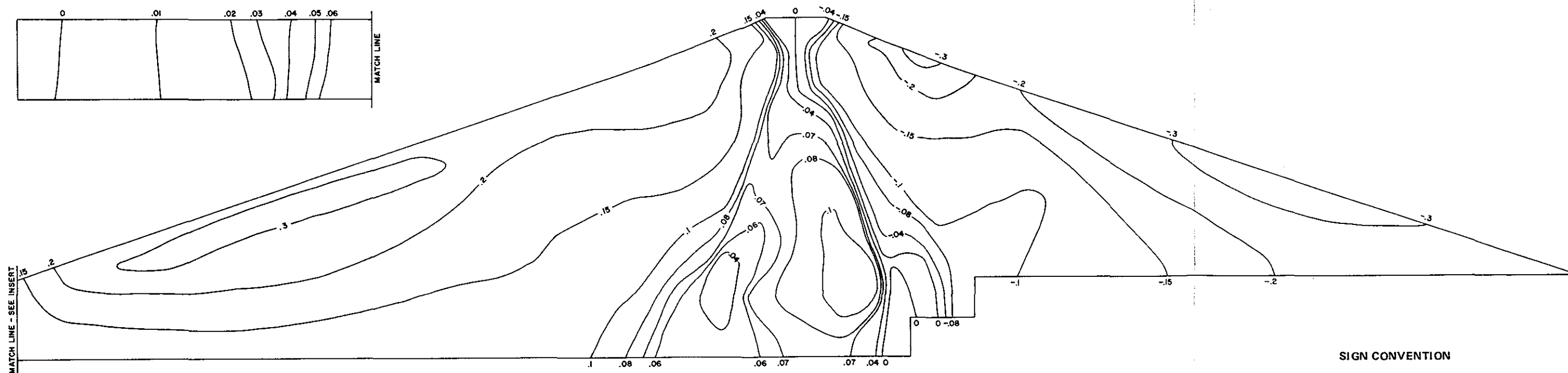
The values shown in Table 11 for the impervious rolled fill zone were based on visual classification and laboratory index tests performed on split spoon samples obtained during the field exploration program. The results indicate that this zone contains varying amounts of silts and clays (See Subsurface Exploration Logs in Appendix A). As a result a relatively low value of unit weight and angle of internal friction were assumed for this zone, and a reasonable value of cohesion (2600 psf) was assumed. For the elastic and bulk moduli parameters, the assumed values were based on the references previously reported for the glacial till.

E. RESULTS OF STATIC ANALYSIS

The results of the analysis for each of the embankment sections are shown on Plates 43 through 46. Plate 43 shows contours for equal values of $\alpha = \tau_{xy} / \bar{\sigma}_y$ (shear stress on a horizontal plane, τ_{xy} or τ_{fc} , divided by the effective vertical stress, $\bar{\sigma}_y$), and $\bar{\sigma}_y$ within the embankment and foundation for the section at Station 8+50. Similarly, Plate 44 shows contours of equal value of $K_c = \bar{\sigma}_{1c} / \bar{\sigma}_{3c}$ (principal consolidation stress ratio) and $\bar{\sigma}_x$ (effective horizontal stress). Plates 45 and 46 show the contours of these same values for the embankment section located at Station 4+82.

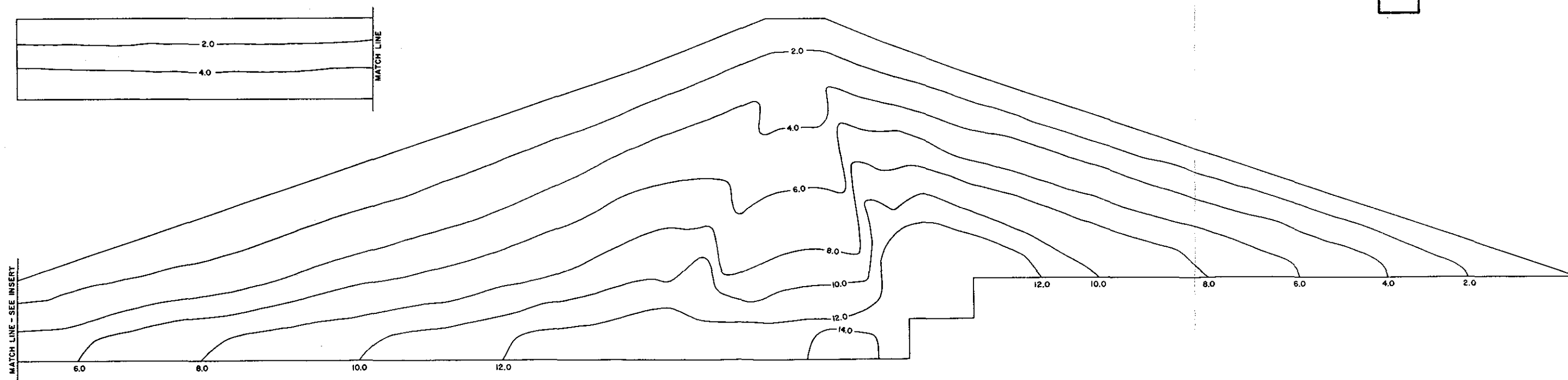
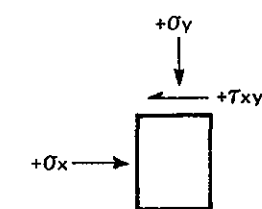
The static stresses and ratios of static stresses shown on the Plates are consistent with stresses computed for dams of similar geometry (See Marcuson and Krinitzsky, 1976). It should be noted that these computed static stresses are assumed to exist in the dam just prior to the seismic event. In actuality the stresses probably differ since the embankment has, since construction, undergone numerous loading and unloading cycles which would be extremely difficult to model in the analysis.

As previously mentioned, two upstream and downstream transition zones were used in the analysis. Preliminary FEADAM analyses were performed without these zones, and the results showed that at the assumed upstream and downstream core/shell contacts, relatively high and unsafe static stresses existed. The high values were considered to be a manifestation of the analyses since only one set of elastic stress-strain properties (K , n , K_p , m) were used to characterize the voluminous upstream and downstream shells. Therefore, in order to eliminate this unreasonable condition, transitions were assumed for the analysis. This assumption was considered to be appropriate based on the variation in particle size within the shell, as previously discussed.

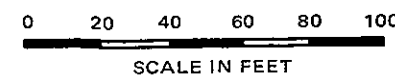


CONTOURS OF $\alpha = \tau_{xy} / \bar{\sigma}_y$

SIGN CONVENTION



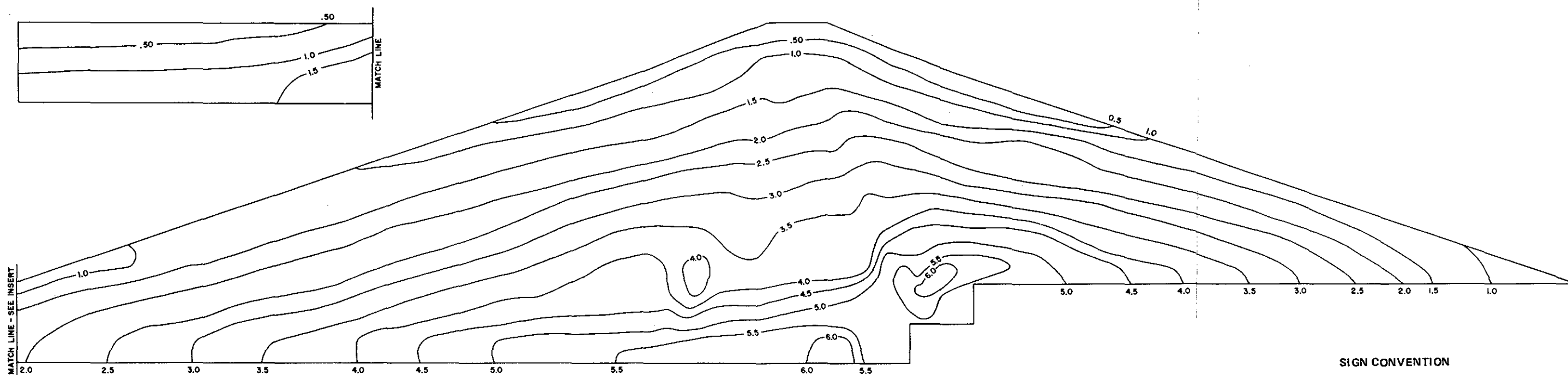
CONTOURS OF $\bar{\sigma}_y$ (KSF)



DEFINITIONS

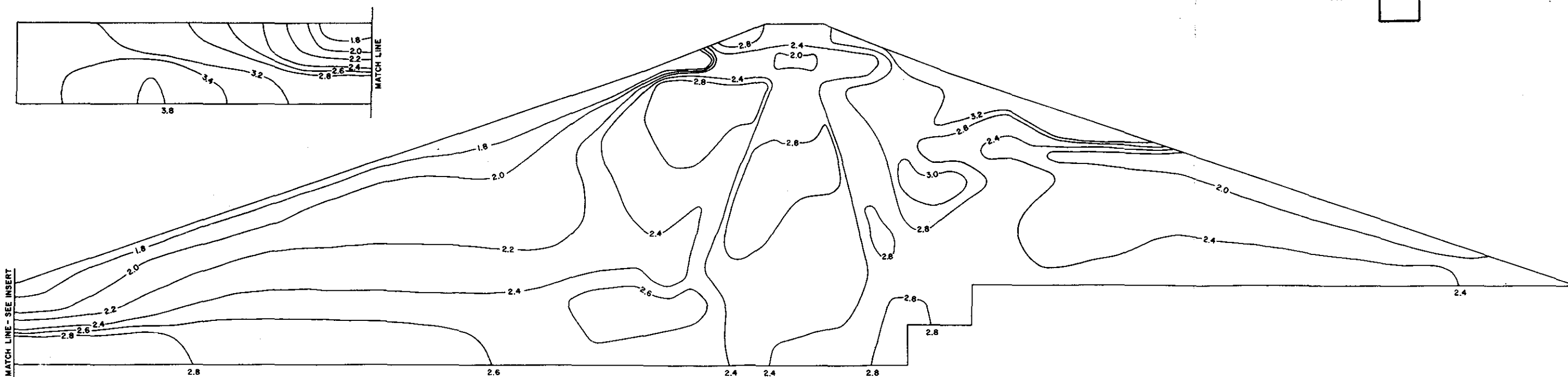
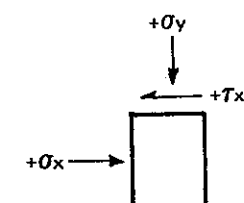
- (1) τ_{xy} = Static shear stress on a horizontal plane.
- (2) $\bar{\sigma}_y$ = Vertical effective overburden stress on a horizontal plane.
- (3) σ_x = Horizontal stress on vertical plane.

DYNAMIC STABILITY ANALYSIS OF
KNIGHTVILLE DAM
NEW ENGLAND DIVISION, COE
RESULTS FROM FEADAM
STATION 8 + 50



CONTOURS OF $\bar{\sigma}_x$ (KSF)

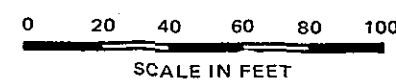
SIGN CONVENTION



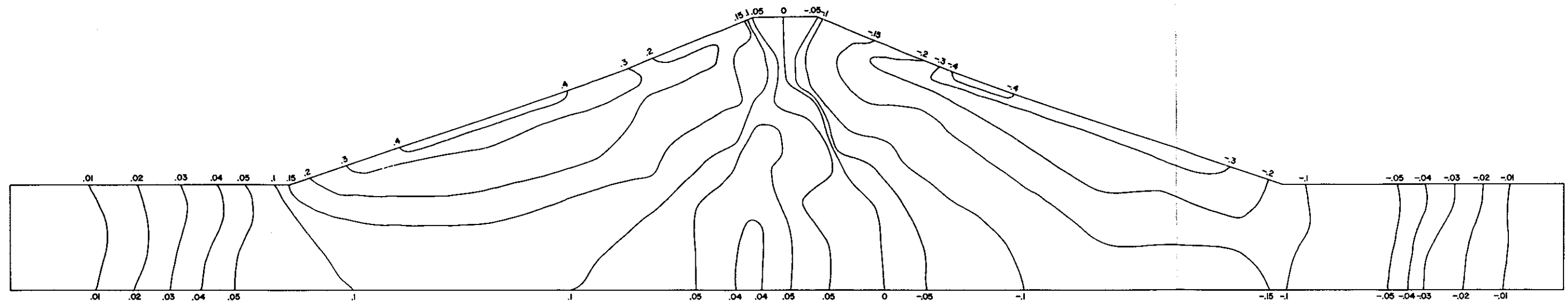
CONTOURS OF $K_c = \bar{\sigma}_{1c} / \bar{\sigma}_{3c}$

DEFINITIONS

- (1) $\bar{\sigma}_x$ = Effective horizontal stress on a vertical plane
- (2) $\bar{\sigma}_{1c}$ = Effective major principal stress at the end of consolidation.
- (3) $\bar{\sigma}_{3c}$ = Effective minor principal stress at end of consolidation.

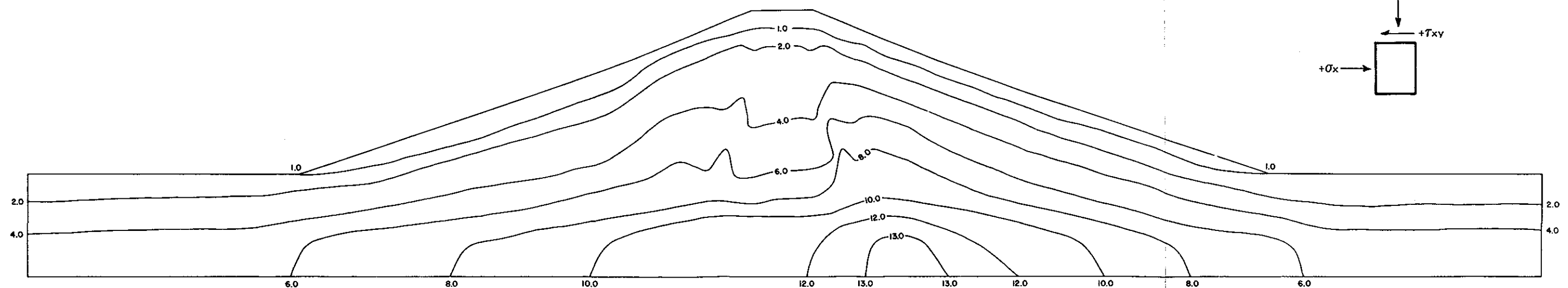
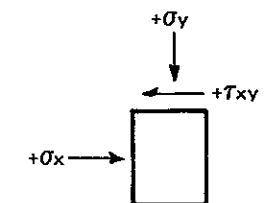


DYNAMIC STABILITY ANALYSIS OF
KNIGHTVILLE DAM
NEW ENGLAND DIVISION, COE
RESULTS FROM FEADAM
STATION 8 + 50



CONTOURS OF $\alpha = \tau_{xy} / \bar{\sigma}_y$

SIGN CONVENTION



CONTOURS OF $\bar{\sigma}_y$ (KSF)

DEFINITIONS

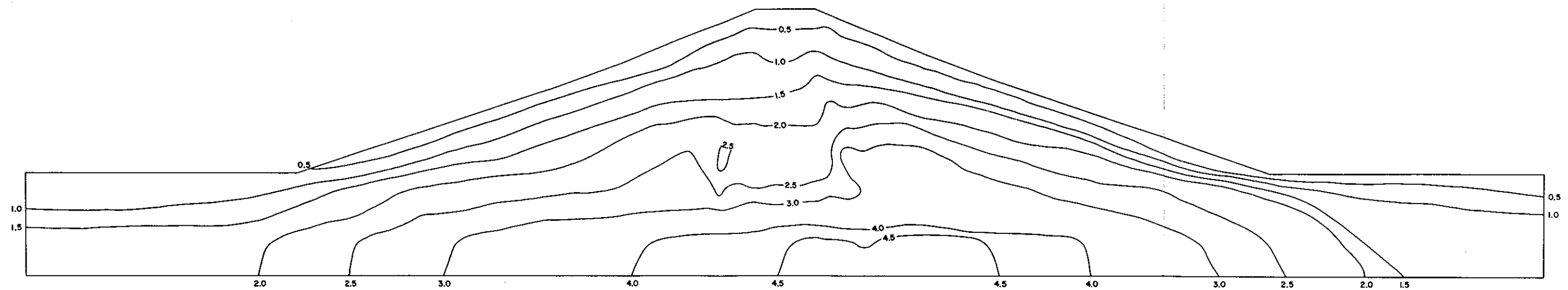
- (1) τ_{xy} = Static shear stress on a horizontal plane
- (2) $\bar{\sigma}_y$ = Vertical effective overburden stress on a horizontal plane.
- (3) σ_x = Horizontal stress on vertical plane.

0 20 40 60 80 100
SCALE IN FEET

DYNAMIC STABILITY ANALYSIS OF
KNIGHTVILLE DAM
NEW ENGLAND DIVISION, COE
RESULTS FROM FEADAM
STATION 4 + 82

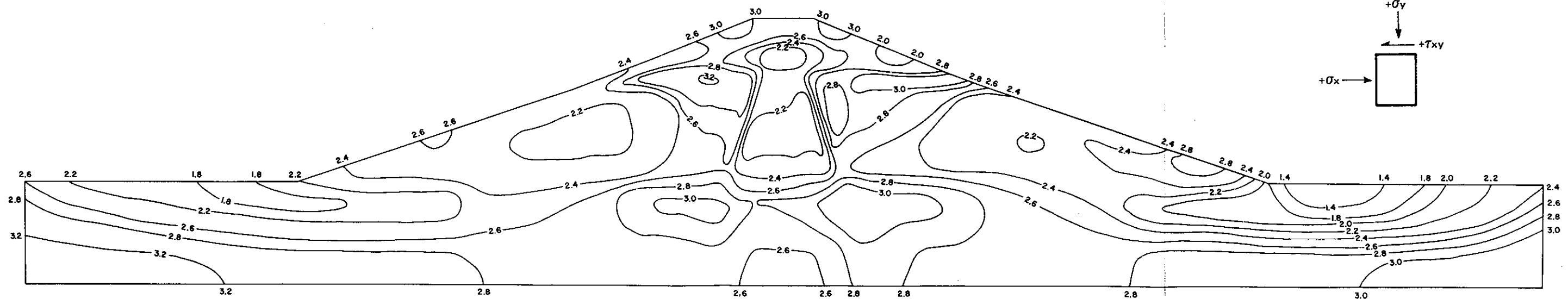
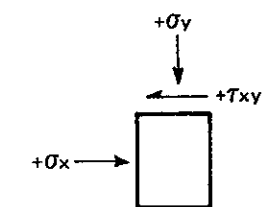
VII-17

PLATE 45



CONTOURS OF $\bar{\sigma}_x$ (KSF)

SIGN CONVENTION



CONTOURS OF $K_c = \bar{\sigma}_{1c} / \bar{\sigma}_{3c}$

0 20 40 60 80 100
SCALE IN FEET

DEFINITIONS

- (1) $\bar{\sigma}_x$ = Effective horizontal stress on a vertical plane
- (2) $\bar{\sigma}_{1c}$ = Effective major principal stress at the end of consolidation.
- (3) $\bar{\sigma}_{3c}$ = Effective minor principal stress at end of consolidation.

VIII. DYNAMIC ANALYSIS

A. GENERAL

There are several methods available for evaluating the dynamic response and/or liquefaction potential of embankment dams subject to an earthquake. These methods include:

- Simplified analyses based on the observed performance of actual sites subject to known earthquake activity, and
- Computer analyses to determine the dynamic stresses in the dam and to compare these stresses with the cyclic shear resistance obtained from laboratory tests.

The methods utilized in this study include a "simplified" semi-empirical analysis using standard penetration test data, and computer analyses using both a one-dimensional program entitled SHAKE and a two-dimensional finite element program entitled FLUSH. A description of each method and the results obtained are presented herein.

B. FAILURE CRITERION

In 1978, the American Society of Civil Engineers Committee on Soil Dynamics published a list of standardized definitions of terms related to liquefaction. According to the Committee (ASCE, 1978), liquefaction is defined as follows:

"the act or process of transforming any substance into a liquid as a consequence of increased pore pressure and reduced effective stress."

The liquefaction potential of a soil is determined from either large scale cyclic load tests performed in the field or cyclic load tests performed in the laboratory.

In either type of test, liquefaction is considered to occur when the pore water pressures generated during cyclic loading increase and are maintained very near or at the level of the confining pressure (σ_3) applied to the soil. Having determined the soil response to cyclic tests, it is then possible to assess the seismic stability of the dam.

It is also possible to assess the overall stability of the dam by using a strain potential assessment procedure. In this procedure, the cyclic shear resistance of the soil, or the level of cyclic stress required to produce a given amount of strain in a specified number of cycles (ASCE, 1978), is measured in the laboratory on samples consolidated to different initial static stress conditions. This resistance is then compared to the average dynamic shear stress induced by the earthquake. If the earthquake stresses exceed the cyclic resistance for a given strain potential limit, then the soil is considered to have failed or liquefied. On the other hand, if the reverse occurs, the soil element is considered stable. According to Serff, et al. (1976), the strain potential assessment procedure offers greater guidance in assessing embankment performance under seismic shaking.

For the one- and two-dimensional computer analyses of Knightville Dam, the strain potential criterion was used. A cyclic resistance corresponding to a five percent axial strain was set as the strength criterion, this value is consistent with the values recommended and/or used by others (Serff, et al. (1976); Seed, et al. (1973); Marcuson, et al. (1979)).

C. SIMPLIFIED ANALYSIS - SEED AND IDRIS PROCEDURE

1. General - During the past few years, simplified procedures have been developed to assess the liquefaction potential of soils. These procedures are considered "simplified" because they are based on field borehole data and do not require sophisticated computer analyses. One

popular procedure proposed by Seed and Idriss (1971 and 1981), requires that standard penetration resistance values obtained at a site underlain by sand be compared with a comprehensive collection of resistance values taken at various sites underlain by similar soil deposits where liquefaction or no liquefaction was known to have taken place.

The SEED and IDRIS PROCEDURE has been used in this study to assess the liquefaction potential of the hydraulic core at Knightville Dam by using the standard penetration test (SPT) data obtained from the crest boreholes. The procedure was not used, however, to assess the liquefaction of the hydraulic shell, since the SPT-values obtained from the downstream boreholes in the shell are not considered to be representative.

2. Method of Analysis - As previously mentioned the simplified analysis is based on actual performance records collected at "liquefied" and "non-liquefied" sites. The procedure was first published by Seed and Idriss (1971) and was based on the performance records available at that time. Since then, more field data has become available and these data are incorporated into the empirical charts presented in the new procedure (Seed and Idriss, 1981) and discussed herein.

In the analysis, the value of cyclic shear stress ratio on a horizontal surface at some depth required to cause liquefaction is defined as follows:

$$\frac{(\tau_h)_{avg}}{\bar{\sigma}_o} = 0.65 \times \frac{A_{max}}{g} \times \frac{\sigma_o}{\bar{\sigma}_o} \times r_d$$

where $(\tau_h)_{avg}$ = average cyclic shear stress developed on a horizontal surface

A_{max} = maximum acceleration

$\bar{\sigma}_o$ = initial (pre-earthquake) effective overburden pressure on layer under consideration

σ_o = initial (pre-earthquake) total overburden pressure

r_d = a stress reduction factor

In this expression the 0.65 factor is used to convert the value of maximum shear stress to an equivalent average stress level, and the r_d factor is a measure of the soils ability to deform under load. The variation of r_d with depth is shown on Plate 47.

Values of cyclic stress ratio known to be associated with liquefaction or no liquefaction in the field for various magnitude earthquakes have been plotted as a function of the modified standard penetration resistance (N_1), which is the measured penetration resistance corrected to an effective overburden pressure of one ton per square foot, based on the results of Gibbs and Holtz (1957). (See Plate 47) The value of N_1 is computed, as follows:

$$N_1 = C_N \times N$$

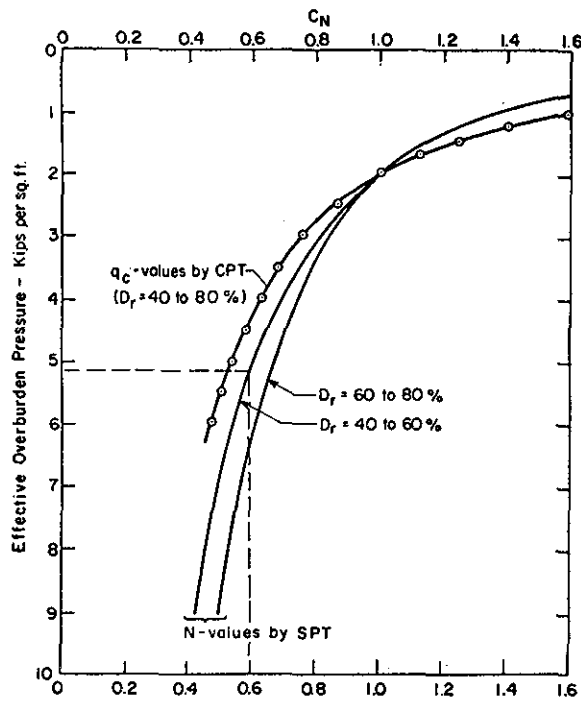
where N_1 = modified standard penetration resistance

C_N = correction factor for effective overburden pressure

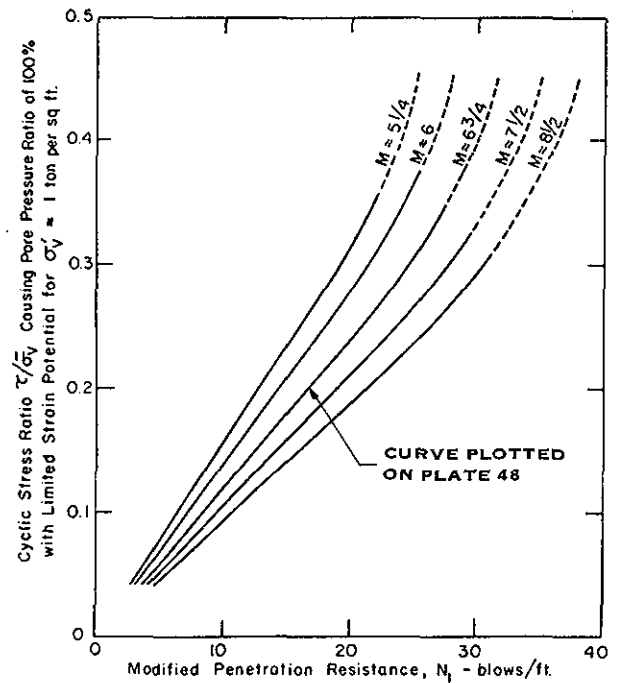
N = standard penetration resistance from field program (blows/foot)

Plate 47 shows the relationship of modified penetration (N_1) and average cyclic stress ratio ($\tau_h/\bar{\sigma}_v$ or $(\tau_h)_{avg}/\bar{\sigma}_0$) for various magnitude earthquakes. Values which plot above a given earthquake magnitude curve would indicate liquefaction potential; values that plot below a given curve would indicate no liquefaction potential. Thus for any given value of maximum ground acceleration, the possibility of liquefaction can be obtained with the aid of this chart.

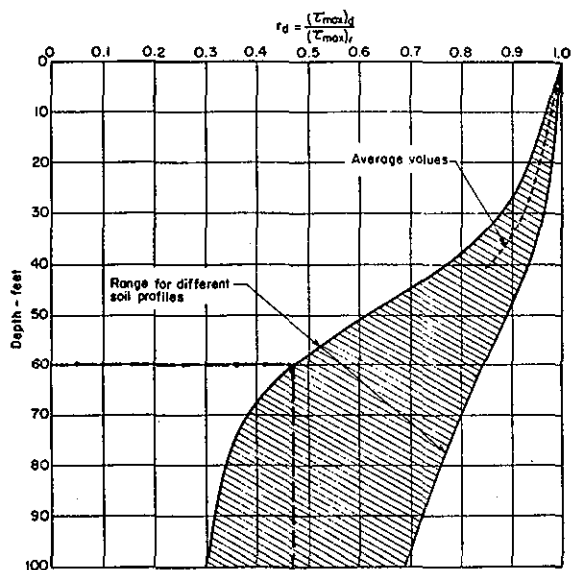
3. Results of Simplified Analysis - Plate 48 shows the results of the simplified analysis performed for the core; Plate 47 provides a sample calculation utilizing this simplified procedure. For the analysis an A_{max} value of 0.20g was used; this value corresponds to the maximum peak ground acceleration of the base rock for the Maximum Credible Event. As



(a) CHARTS FOR DETERMINATION OF C_N



(b) CHART FOR EVALUATION OF LIQUEFACTION POTENTIAL FOR DIFFERENT MAGNITUDE EARTHQUAKES



(c) RANGE OF VALUES OF r_d FOR DIFFERENT SOIL PROFILES

SAMPLE CALCULATION

- Hydraulic core, Depth = 60ft.
- $\bar{\sigma}_v = \gamma_m(\text{cap}) h_{\text{cap}} + \gamma_b(\text{core}) h_{\text{core}}$
- $\bar{\sigma}_v (60\text{ft}) = 4.9\text{ksf}$
- For $D_r = 40$ to 60% , $C_N = 0.6$ (see(a))
- At 60feet, Average $N = 5$ blows/foot (see Plate 48)
- $N_1 = C_N N = 3$; for silty sands add 7.5, therefore $N_1 = 10.5$ blows/ft.
- r_d (lower bound) = 0.47 (see(c))

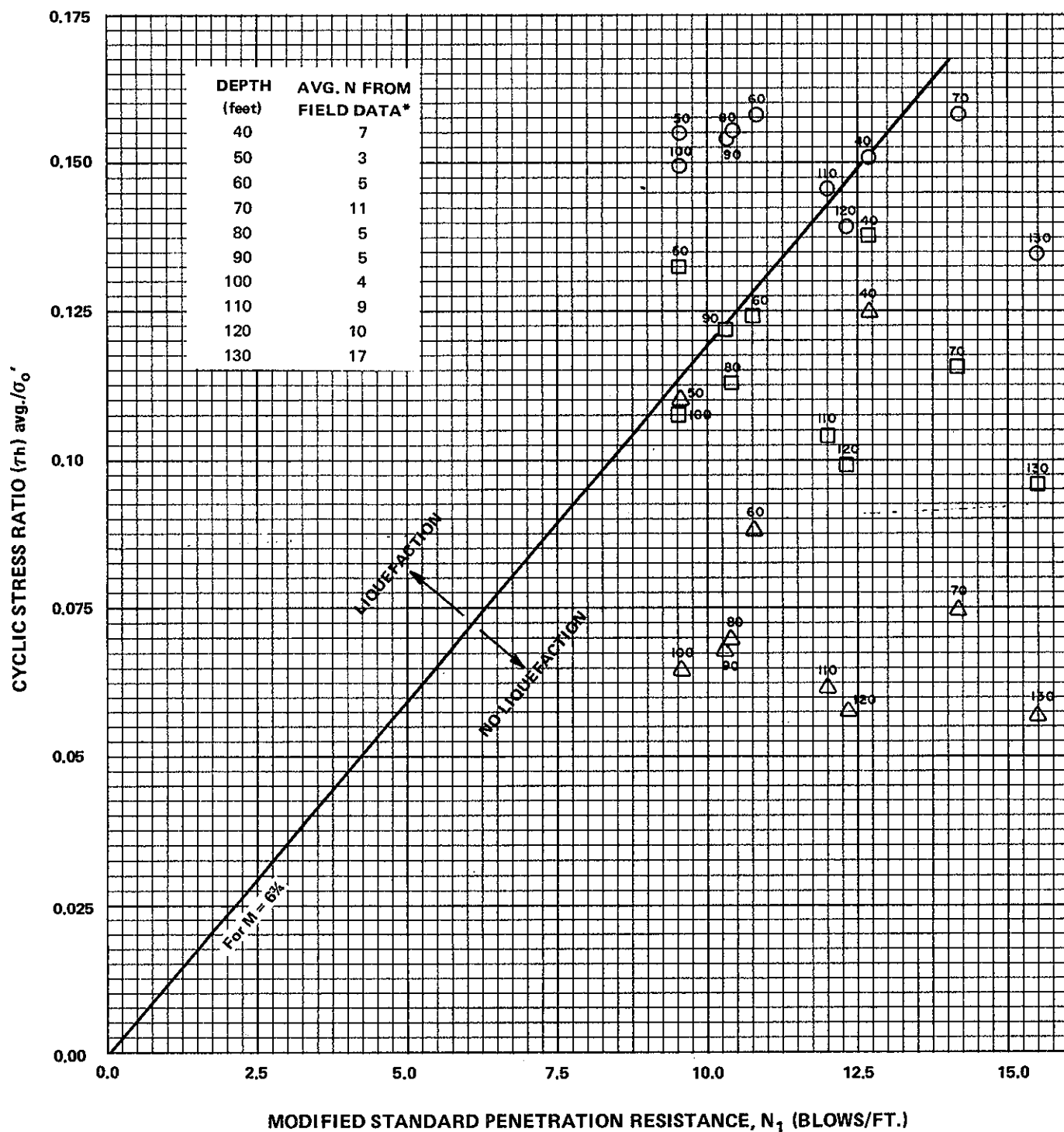
$$\tau/\bar{\sigma}_v = 0.65 \frac{A_{\text{max}}}{g} \frac{\sigma_v}{\bar{\sigma}_v} r_d$$

$$A_{\text{max}} = 0.2g$$

$$\tau/\bar{\sigma}_v = 0.158 \text{ (see Plate 48)}$$

(a) & (b) from Seed and Idriss (1981)

(c) from Seed and Idriss (1971)



* NOTE: For Sandy Silts
 $N_1 = C_N N + 7.5$
 (See Seed and Idriss, 1981)

DYNAMIC STABILITY ANALYSIS OF
 KNIGHTVILLE DAM
 NEW ENGLAND DIVISION, COE
 LIQUEFACTION POTENTIAL OF
 CORE BASED ON
 SIMPLIFIED PROCEDURE

previously reported, this event is likely to occur at Cape Ann, Massachusetts, and have a magnitude of 6.5. The maximum peak ground acceleration used for analyses of the Operating Basis Earthquake was 0.086g, corresponding to a magnitude 5.5 event which is also likely to occur at Cape Ann.

The results shown on Plate 48 indicate that for the lower bound curve and mean curve of r_d (See Plate 47), almost all of the cyclic stress ratios ($\tau_h/\bar{\sigma}_v$) plot below the liquefaction boundary curve (assumed $M = 6 \frac{3}{4}$), indicating that no liquefaction is likely to occur at the depths shown. However, if the upper bound curve of r_d is used, then there is the potential for liquefaction within the core at depths ranging from 50 to 110 feet.

A similar analysis was performed for the Operating Basis Earthquake. For this event, all of the data plot below the $M = 5\frac{1}{2}$ boundary curve, indicating that there is little likelihood of liquefaction in the core due to this event. As previously mentioned, a Simplified Analysis was not performed for the shell.

The results of the Simplified Analysis are ambivalent and depend on the value of r_d chosen for the analysis. Also the empirical charts shown in Plate 47 depend on the reliability of field data and do not take into account other significant factors such as the duration of shaking. In addition the simplified results are only useful for a preliminary evaluation of liquefaction potential and only applicable to the embankment section investigated. In recognition of the limitations of the Simplified Analysis the results of a detailed laboratory investigation and several different response analyses using more sophisticated computer techniques were performed in this study; the results are presented in the following sections.

D. ONE-DIMENSIONAL ANALYSIS

1. General - A one-dimensional response analysis was performed to evaluate the response of the dam and foundation to the earthquake events. The procedure used for the analysis, utilizes strain-dependent values of shear moduli and damping. Although the results obtained from a one-dimensional analysis are not directly applicable to a dam, due to the assumptions outlined below, this procedure was used in order to compute, relatively quickly and economically, the response of the embankment to the Operating Basis and Maximum Credible Events and to compare the results with the Simplified Analysis and the Two-Dimensional Analysis results.

2. Method of Analysis - The one-dimensional computer program used for this analysis is named SHAKE. The program was developed by the University of California at Berkeley for earthquake response analysis of horizontally layered sites. (Schnabel, Lysmer and Seed, 1972). A listing of the computer program has been presented as an Attachment to the Dynamic Response Analysis Report; a general description of the output is presented in Appendix F.

The program is used to compute the dynamic response of an assumed system of homogeneous, viscoelastic soil layers of infinite lateral extent to vertically travelling shear waves. In the program, non-linearity of shear modulus and damping is accounted for by use of equivalent linear soil properties to obtain values of modulus and damping compatible with the effective shear strains computed in each horizontal soil layer. According to Schnabel, et al. (1972), the following assumptions are made in the analysis: (1) the soil layers are finite in the horizontal direction, (2) the response in the soil layers is caused by the upward propagation of shear waves from the underlying rock, and (3) the strain dependence of modulus and damping is accounted for by an equivalent linear procedure.

In this analysis, the Puddingstone Reservoir strong motion record was scaled to the Operating Basis and Maximum Credible Events. In SHAKE the motions are represented by a time series of horizontal acceleration. These motions are used by the program to compute the maximum values of dynamic stresses and shear strains, and the dynamic stress and acceleration time histories at the middle of each layer, and the maximum values of acceleration at the top of each soil layer.

3. $K_2(\text{Max})$ Determination - For granular soils

it has been shown that the value of shear modulus (G) is a function of void ratio (or relative density), confining pressure and strain amplitude (Seed and Idriss, 1970). The expression used to relate shear modulus to these important parameters is:

$$G = 1000 K_2 (\bar{\sigma}_m)^{\frac{1}{2}}$$

where G = shear modulus (psf)
 $\bar{\sigma}_m$ = mean effective confining pressure (psf)
 K_2 = constant which depends on void ratio
 and strain amplitude

The program SHAKE uses this expression to compute values of G for varying shear strain.

The value of K_2 is a maximum at very low shear strains, and is determined using the computed value of G from shear wave velocity measurements ($G_{\text{max}} = V_s^2 \rho$). Table 12 presents the values of $K_{2(\text{max})}$ which were computed using the field data. Also shown in the Table are the values of $K_{2(\text{max})}$ which were computed from the resonant column (RC) laboratory test data using the value of shear modulus computed at 10^{-4} percent strain for each test specimen.

Based on the data presented in Table 12, the average value of $K_{2(\text{max})}$ for the hydraulic core was estimated to be about 33. For the hydraulic shell, average values of 115 and 70 were computed from the field investigation and resonant column testing, respectively. Seed and Idriss (1970)

Table 12
DETERMINATION OF $K_2(\text{MAX})$ FROM FIELD DATA
AND LABORATORY TEST DATA FOR
SHAKE ANALYSES

FIELD

<u>Material</u>	<u>Depth (feet)</u>	<u>V_s (fps)</u>	<u>G_{max} (ksf)</u>	<u>$\bar{\sigma}_m$ (psf)</u>	<u>$K_2(\text{max})$</u>
Core	70	900	2,936	5,454	39
Shell	40	1,240	6,590	3,276	115

LABORATORY (RC TESTS)

<u>Material</u>	<u>$\bar{\sigma}_c$ (psf)</u>	<u>G_{max} (ksf)</u>	<u>K 2 (max)</u>
Core	14,340	4,140	35
Core	7,380	3,010	35
Core	2,050	1,430	32
Shell	6,780	6,900	84
Shell	3,380	4,550	78
Shell	13,520	6,620	57

$$(1) \quad G_{\text{max}} = \rho V_s^2, \quad \gamma_{\text{core}} = 116 \text{ pcf}, \quad \gamma_{\text{shell}} = 145 \text{ pcf}$$

$$(2) \quad G_{\text{max}} = K_2(\text{max}) \cdot 1,000 \cdot (\bar{\sigma}_m)^{\frac{1}{2}};$$

$$\bar{\sigma}_m (\text{field}) = \bar{\sigma}_c (\text{lab}) \quad (\text{assumed})$$

$$(3) \quad \bar{\sigma}_m = \frac{(1 + 2 K_o) \bar{\sigma}_v}{3}, \quad K_o (\text{core \& shell}) = 0.42 \quad (\text{assumed})$$

(4) Water level in core assumed at El 560; moist conditions assumed in shell during V_s measurement investigation.

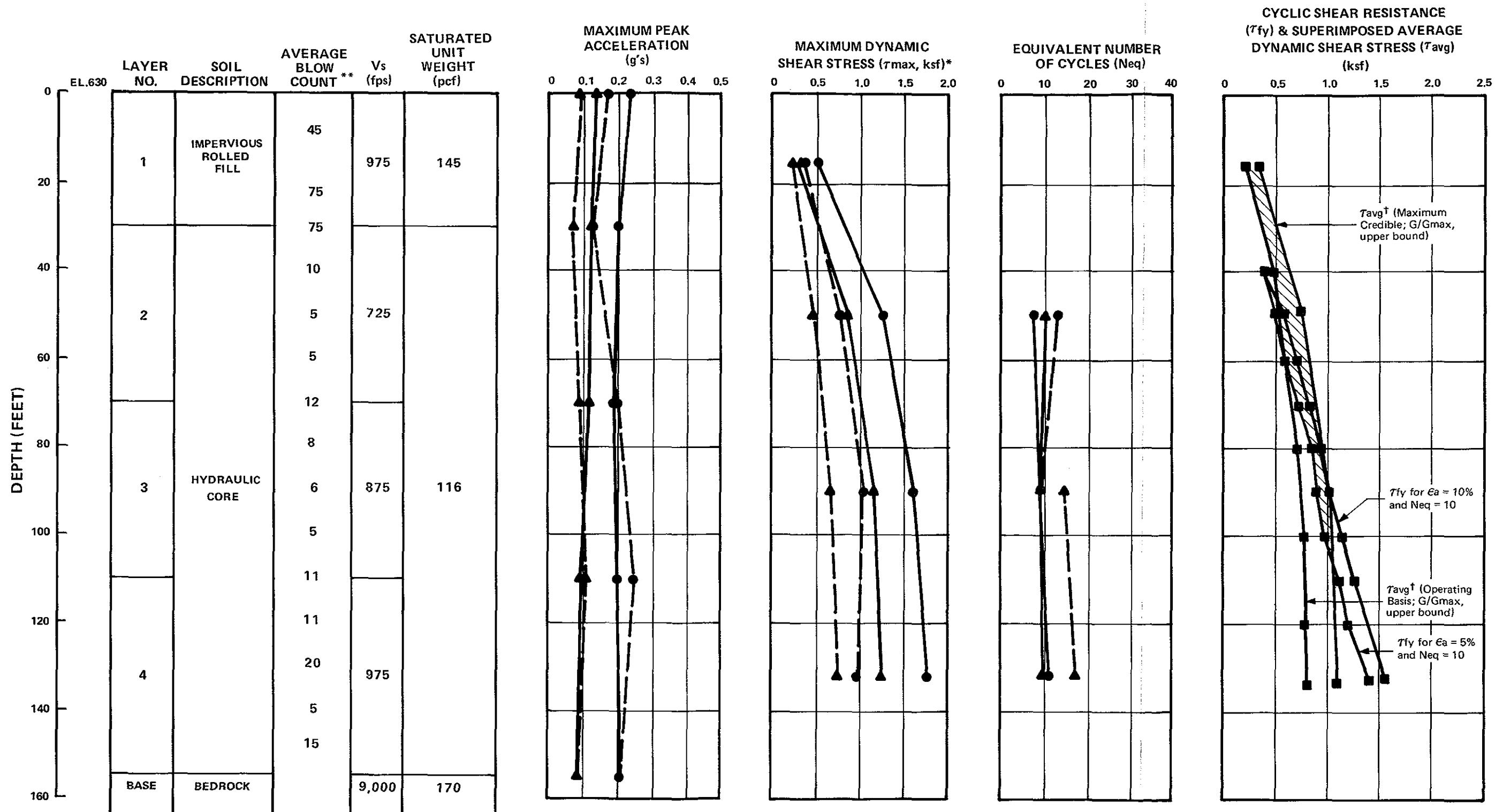
show $K_{2(max)}$ values for sand at different relative densities; for dense sands, the values of K_2 determined at very low strain from laboratory tests ranged between 50 and 75. Based on Seed and Idriss' findings, a value of 70 for $K_{2(max)}$ was used in the analysis for the hydraulic shell. $K_{2(max)}$ values for the rolled fill, till and riprap were obtained from Seed and Idriss (1970).

In the SHAKE program two of the pertinent input data required are the G/G_{max} and damping ratio reduction curves for the materials being considered in the analysis. The program is limited however to the use of only one reduction curve each for G/G_{max} and damping (Schnabel, et al. 1972). This means that the variation in G/G_{max} and damping ratio as a function of shear strain is the same for each material. The absolute value of shear modulus however changes since G is computed from G_{max} values input for each material. The analyses performed for this work used the G/G_{max} reduction curve applicable to the hydraulic core for all the materials in the vertical soil column taken at the crest sections (See Plate 35); for the upstream sections, the G/G_{max} reduction curve applicable to the shell material was used for all materials in the soil column (See Plate 36). The values of $K_{2(max)}$ and the corresponding G/G_{max} reduction curves used in the analyses are as follows:

<u>Material</u>	<u>$K_{2(max)}$</u>	<u>G/G_{max} Reduction Curve Used</u>
Core	33	Core
Shell	70	Shell
Rolled Fill	127	Core
Till	140	Shell and Core [†]
Riprap	16	Shell

4. Results of One-Dimensional Analysis - The results of the one-dimensional SHAKE analysis are shown on Plates 49 through 52 for vertical soil profiles through the

[†] For upstream vertical soil column, shell curve used; for crest vertical soil column, core curve used



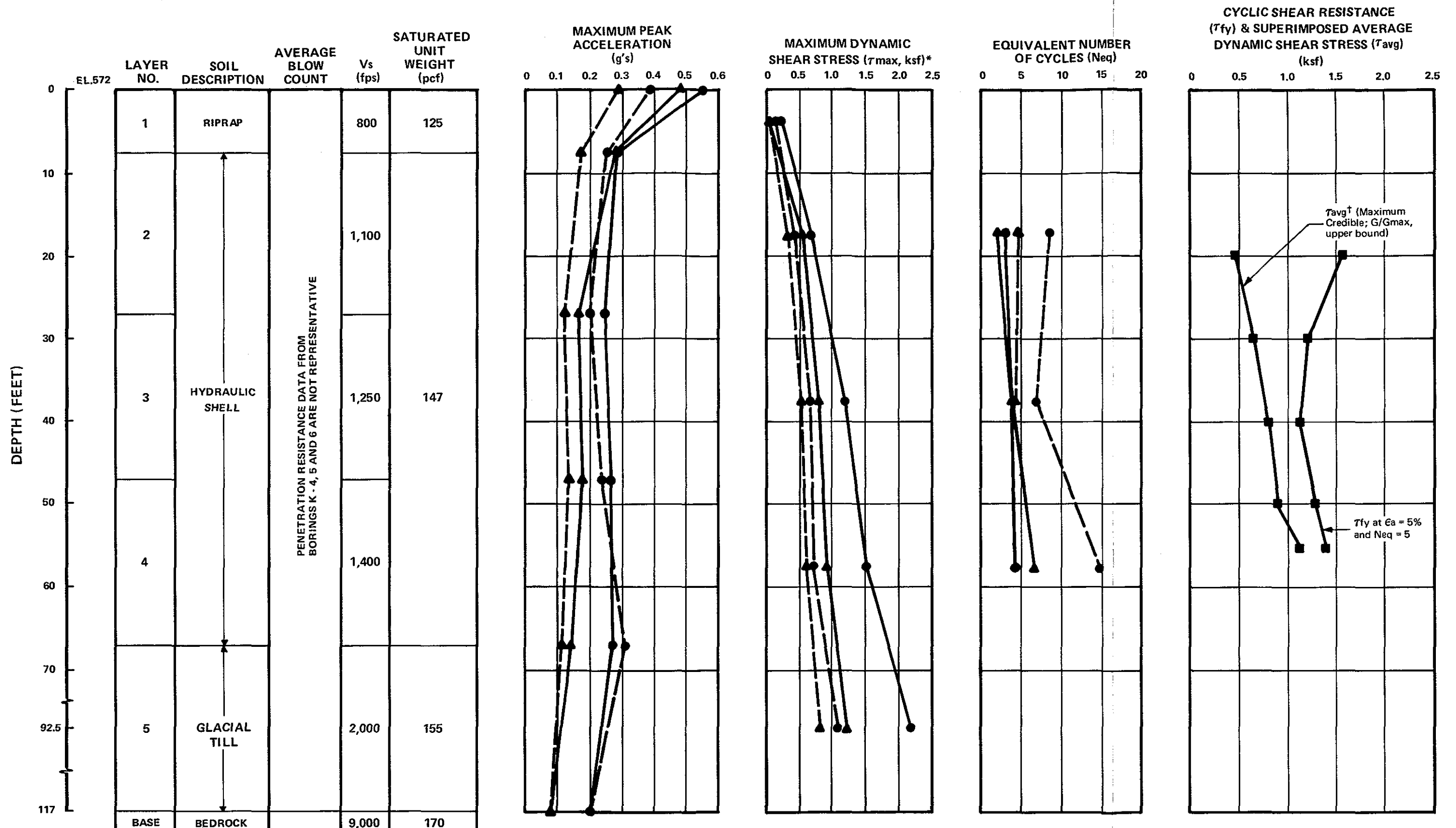
LIQUEFIED ZONE FROM MAXIMUM CREDIBLE EVENT
(For τ_{fy} at $\epsilon_a = 5\%$, $N_{eq} = 10$)

- MAXIMUM CREDIBLE EARTHQUAKE; G/Gmax, UPPER BOUND
- MAXIMUM CREDIBLE EARTHQUAKE; G/Gmax, LOWER BOUND
- ▲—▲ OPERATING BASIS EARTHQUAKE; G/Gmax, UPPER BOUND
- ▲—▲ OPERATING BASIS EARTHQUAKE; G/Gmax, LOWER BOUND

* τ_{max} = MAXIMUM DYNAMIC SHEAR STRESS COMPUTED FROM SHAKE
 $\dagger \tau_{avg} = 0.65 \times \tau_{max}$

** AVERAGE BLOW COUNT BASED ON VALUES OBTAINED FROM BOREHOLES K - 1 AND K - 3

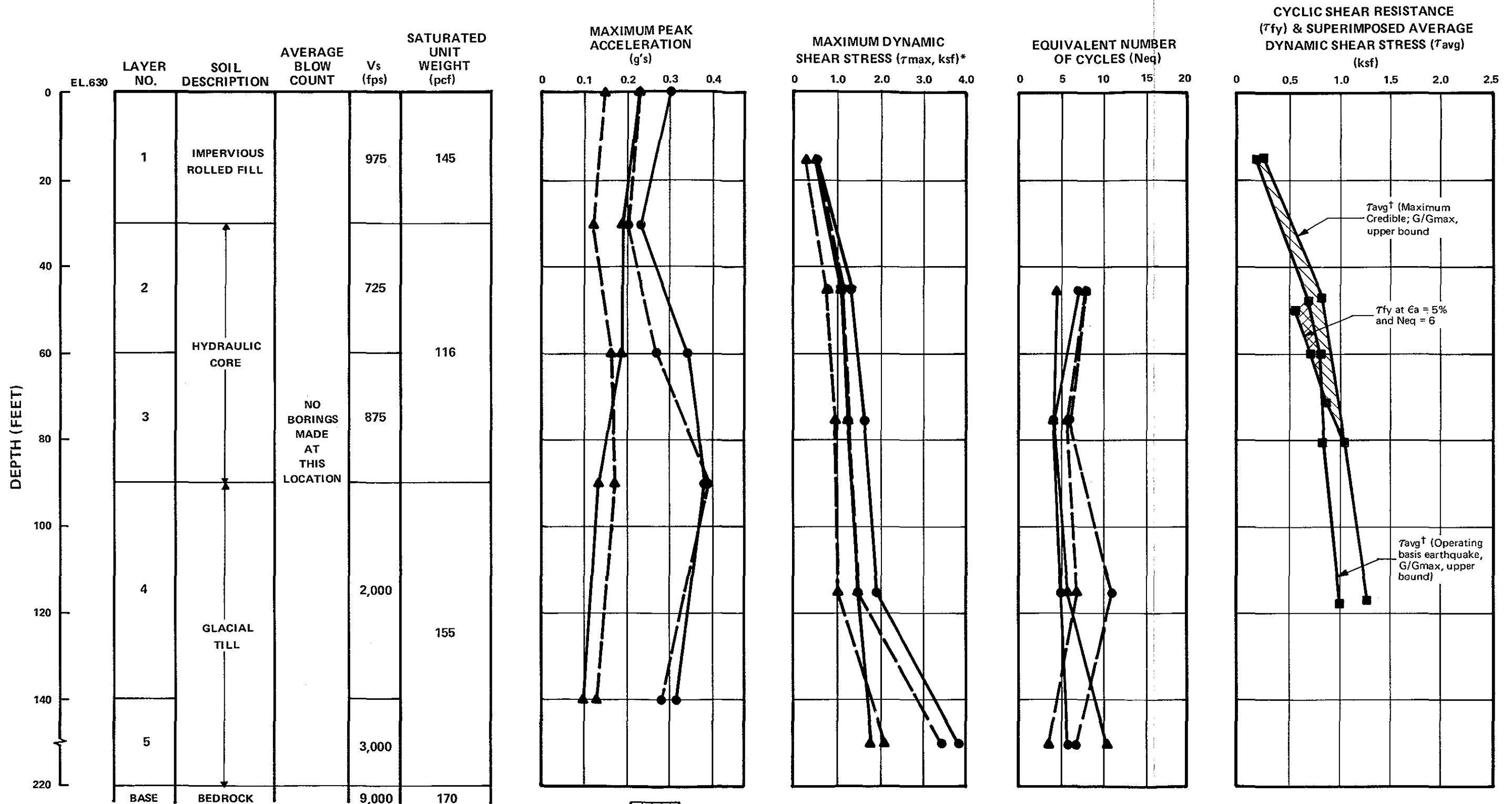
DYNAMIC STABILITY ANALYSIS OF
 KNIGHTVILLE DAM
 NEW ENGLAND DIVISION, COE
 RESULTS OF ONE DIMENSIONAL
 ANALYSIS USING SHAKE
 STATION 8+50; CREST



- MAXIMUM CREDIBLE EARTHQUAKE; G/Gmax, UPPER BOUND
- MAXIMUM CREDIBLE EARTHQUAKE; G/Gmax, LOWER BOUND
- ▲—▲ OPERATING BASIS EARTHQUAKE; G/Gmax, UPPER BOUND
- △—△ OPERATING BASIS EARTHQUAKE; G/Gmax, LOWER BOUND

* τ_{max} = MAXIMUM DYNAMIC SHEAR STRESS COMPUTED FROM SHAKE
 $\dagger \tau_{avg} = 0.65 \times \tau_{max}$

DYNAMIC STABILITY ANALYSIS OF
 KNIGHTVILLE DAM
 NEW ENGLAND DIVISION, COE
 RESULTS OF ONE DIMENSIONAL
 ANALYSIS USING SHAKE
 STATION 8+50; UPSTREAM SLOPE
 PLATE 50



- MAXIMUM CREDIBLE EARTHQUAKE; G/Gmax, UPPER BOUND
- MAXIMUM CREDIBLE EARTHQUAKE; G/Gmax, LOWER BOUND
- ▲—▲ OPERATING BASIS EARTHQUAKE; G/Gmax, UPPER BOUND
- ▲—▲ OPERATING BASIS EARTHQUAKE; G/Gmax, LOWER BOUND

LIQUEFIED ZONE FROM MAXIMUM CREDIBLE EVENT

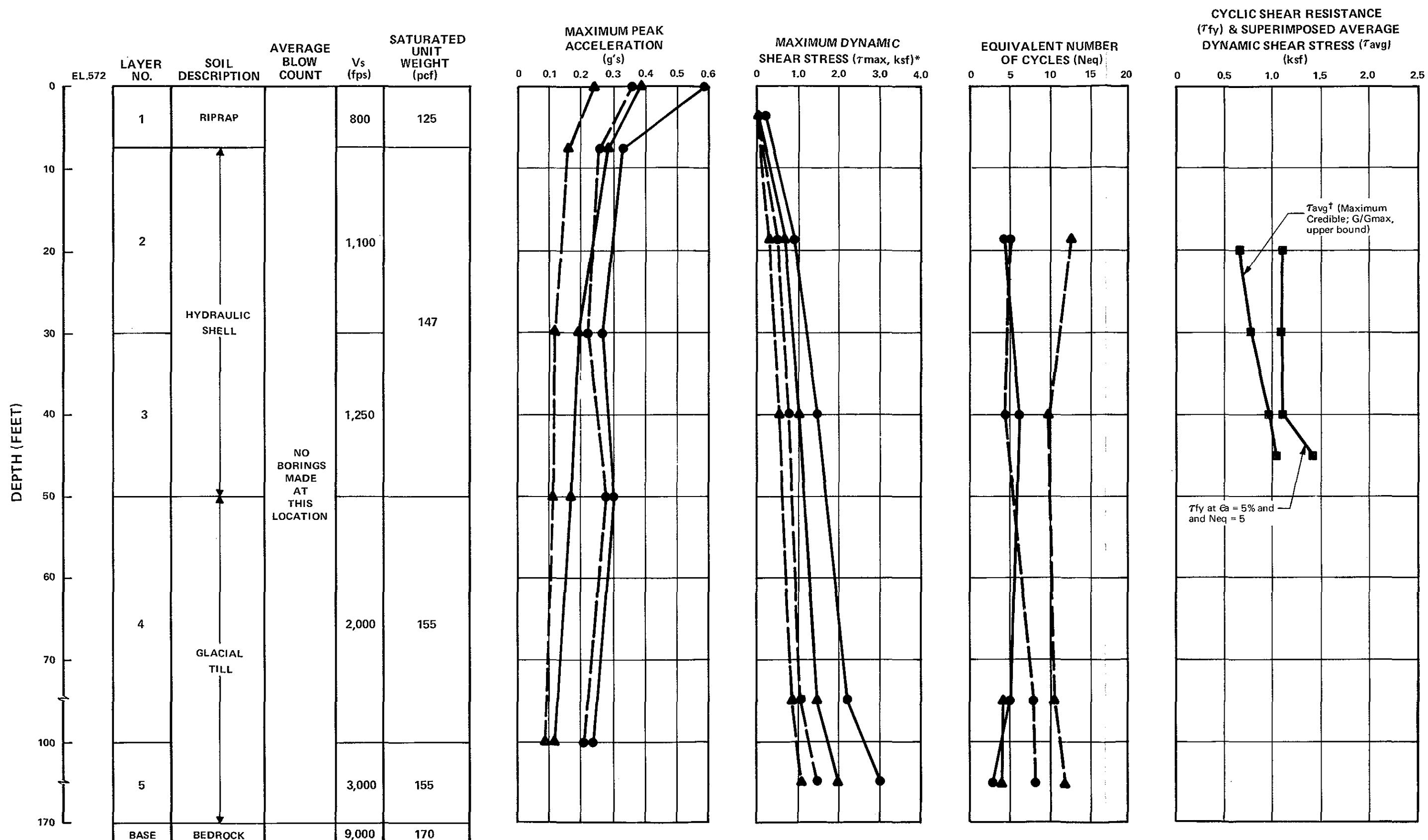
LIQUEFIED ZONE FROM OPERATING BASIS EVENT

* τ_{max} = MAXIMUM DYNAMIC SHEAR STRESS COMPUTED FROM SHAKE

† $\tau_{avg} = 0.65 \times \tau_{max}$

DYNAMIC STABILITY ANALYSIS OF
KNIGHTVILLE DAM
NEW ENGLAND DIVISION, COE

RESULTS OF ONE DIMENSIONAL
ANALYSIS USING SHAKE
STATION 4+82; CREST



- MAXIMUM CREDIBLE EARTHQUAKE; G/Gmax, UPPER BOUND
- MAXIMUM CREDIBLE EARTHQUAKE; G/Gmax, LOWER BOUND
- ▲—▲ OPERATING BASIS EARTHQUAKE; G/Gmax, UPPER BOUND
- ▲—▲ OPERATING BASIS EARTHQUAKE; G/Gmax, LOWER BOUND

* τ_{max} = MAXIMUM DYNAMIC SHEAR STRESS COMPUTED FROM SHAKE

\dagger $\tau_{avg} = 0.65 \times \tau_{max}$

DYNAMIC STABILITY ANALYSIS OF
KNIGHTVILLE DAM
NEW ENGLAND DIVISION, COE
RESULTS OF ONE DIMENSIONAL
ANALYSIS USING SHAKE
STATION 4+82; UPSTREAM SLOPE

crest and through the upstream slope at Stations 8+50 and 4+82. Some of the pertinent program input data are also shown on each Plate; these data include soil layer number, soil layer thickness, average shear wave velocity, and the unit weight. In the analysis, the G/G_{\max} reduction curves, i.e., the upper bound curve and the lower bound curve (See Plates 36 and 37) were used to determine the influence of stiffness reduction on the response of the dam to seismic shaking.

On each Plate are shown the computed maximum value of peak acceleration at the top of each soil layer and the maximum value of dynamic shear stress (τ_{\max}) induced at the middle of each soil layer by the Operating Basis and Maximum Credible Events.

Also shown on each Plate is the equivalent number of uniform cycles (N_{eq}) computed from the shear stress time series obtained for each of the various soil layers. The N_{eq} values were computed using the procedure proposed by Seed, Idriss, Makdisi and Banerjee (1975), using the laboratory weighting curves presented therein for an average equivalent uniform shear stress (τ_{avg}) which is taken as 65 percent of the maximum shear stress. This procedure was used to facilitate comparison of the non-uniform cyclic shear stress pattern induced by the earthquake and the uniform shear stress series used during cyclic load testing of laboratory specimens.

The results of the one-dimensional analysis indicate that the largest values of maximum acceleration and maximum dynamic shear stress generally occur from the Maximum Credible Event. This is expected since the peak acceleration of the Maximum Event (0.204g) is more than twice the peak acceleration of the Operating Event (0.086g). The results also show that for each earthquake event, the largest values of acceleration and shear stress also occur when the upper bound

values of G/G_{\max} for the corresponding materials are used in the analysis.

To evaluate the seismic stability using the results of the one-dimensional analysis or any other procedure, it is necessary to establish a criterion which could be used to assess the failure. As stated previously, a "strain potential" failure criterion of five percent axial strain is adopted for the dynamic analysis of Knightville Dam. In general, embankments which undergo less than 5 percent strain are considered to be safe against earthquake threat whereas those which experience more than 5 percent strain are considered to be unsafe. (Marcuson, et al. 1980).

Plates 49 and 51 show the comparison of the average dynamic shear stress (τ_{avg}) induced on the soil during earthquake and the cyclic shear resistance (τ_{fy}) of the soil for a vertical soil column through the crest. The cyclic shear resistance was obtained from the cyclic load test data previously shown on Plates 32 and 33. The Plates show that within the upper 70 feet of hydraulic core at Station 8+50 and within the upper 60 feet of core at Station 4+82, the average cyclic shear stress induced by the Maximum Credible Event (0.204g) is greater than the cyclic shear resistance at 5 percent strain for an average value of equivalent cycles. According to the failure criterion, this condition is considered to be unsafe.

Plates 50 and 52 show the results of similar comparisons for vertical soil columns taken at the upstream shell locations. At both embankment sections, the results show that the cyclic shear resistance (τ_{fy}) is greater than the average superimposed dynamic stress (τ_{avg}) from the Maximum Credible Event. No comparison is made for the Operating Basis Event, since the average stresses induced by this event are smaller than those from the Maximum Credible Event.

A comparison is also made of cyclic shear resistance and the superimposed dynamic shear stress from the Operating Basis Event on Plates 49 and 51 for the vertical columns through the hydraulic core. Both plates show that sufficient cyclic shear resistance is available at five percent strain and an average value of equivalent cycles, therefore the hydraulic core is considered safe from shaking caused by the Operating Basis Event.

E. TWO-DIMENSIONAL FINITE ELEMENT ANALYSIS

1. General - A two-dimensional finite element method (FEM) was used to compute the dynamic response of the embankment to base motions resulting from the Maximum Credible and Operating Basis events. The advantages of this type of analysis over the simplified and one-dimensional analyses are that the FEM allows for the inclusion of irregular and sloping boundaries, such as for a dam, and permits the use of different soil properties for each embankment and foundation soil element.

In the previous analyses it was determined that the dynamic shear stresses in the hydraulic core would exceed the cyclic shear resistance determined from cyclic load tests for the five percent "strain potential" criterion. Since it has been reported that one-dimensional analyses can seriously overestimate the dynamic response of an embankment (Marcuson, Hadala and Franklin, 1980), it was decided to perform the two-dimensional finite element analysis.

2. Method of Analysis - The finite element program used to examine the dynamic response of the embankment is entitled FLUSH and includes a post processing program STRAIN. The former is a modified version of the program named LUSH, developed by Lysmer, et al. (1974); the modified version includes the use of viscous boundaries to include three-dimensional effects and the use of transmitting boundaries to minimize the required number of elements (Lysmer, et. al. 1975). A general description of the

of the sample output is presented in Appendix F. FLUSH was essentially written to compute acceleration time histories and spectra, and/or relative displacements between nodal points, whereas STRAIN computes time histories of shear stress and shear strain induced in each element during the earthquake.

The solution technique and other assumptions used in the program are explained by Lysmer, et al. (1975). Basically, the program formulates a system of matrices and solves the equation of motion for an undamped system as follows:

$$[M] \{\ddot{U}\} + [K] \{U\} = -\{m\} \ddot{y} - \{V\} + \{F\} + \{T\}$$

where $\{U\}$ and $\{\ddot{U}\}$ are the nodal point displacement and acceleration, respectively; $[M]$ and $[K]$ are the mass and stiffness matrices, respectively; \ddot{y} is the given input acceleration time history; and $\{m\}$, $\{V\}$, $\{F\}$ and $\{T\}$ are as described in the above reference.

3. Input Parameters - Plates 38 and 39 show the finite element mesh used for the two-dimensional analysis of embankment sections at Stations 8+50 and 4+82, respectively. As previously mentioned, the same mesh was used in the static state of stress analysis, in order that the results of the static and dynamic analyses could be conveniently applied.

In the FLUSH program, the input parameters include, dam and foundation geometry, total unit weight of soil (γ_t) maximum values of shear moduli (G_{max}), shear moduli reduction curves (G/G_{max} vs. γ_{sa}), damping curves (λ vs. γ_{sa}), the assumed phreatic surface, and the strong motion record.

Plates 35 and 36 show the relationship between shear moduli reduction factor (G/G_{max}) and damping (λ) versus shear strain for the hydraulic core and hydraulic shell, respectively. In the FEM analysis, the program uses an equivalent linear method and iterates to obtain modulus and damping

versus strain compatibility. The results of the SHAKE analyses indicated that higher values of maximum dynamic shear stress result when using the upper bound G/G_{\max} versus shear strain curves. The upper bound curves were therefore used in the FEM analysis to characterize the embankment zones, as follows:

<u>EMBANKMENT ZONE</u>	G_{\max}^* (ksf)	G/G_{\max} <u>CURVE USED IN ANALYSIS</u>
Hydraulic Core	2,935	Core
Hydraulic Shell	4,015	Shell
Transition #1	3,295	Shell
Transition #2	3,655	Shell
Impervious Rolled Fill	4,375	Shell
Glacial Till	20,000	Shell

* These values were computed using the $K_2(\max)$ values used in the SHAKE analyses. The G_{\max} values for the transitions were assumed as interpolated values between those computed for the core and shell.

For the analysis, a total of four FLUSH computer runs were made. Two runs were made for each embankment section (Stations 8+50 and 4+82) for both the Maximum Credible and Operating Basis Events.

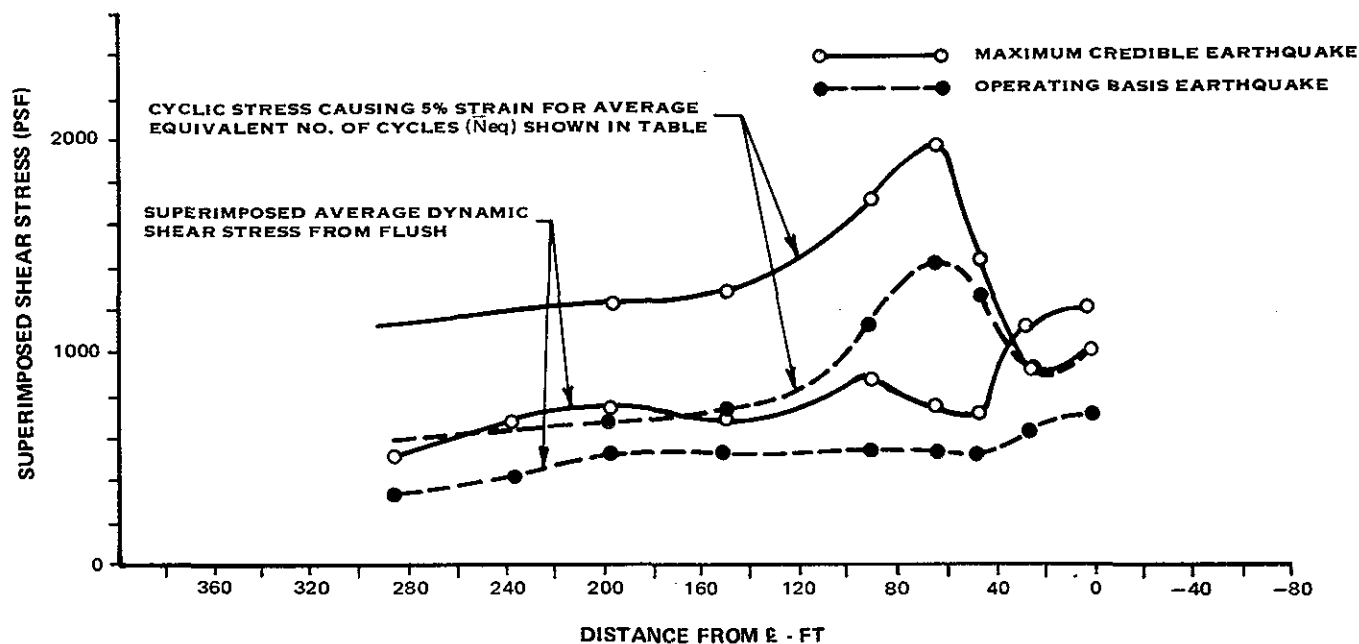
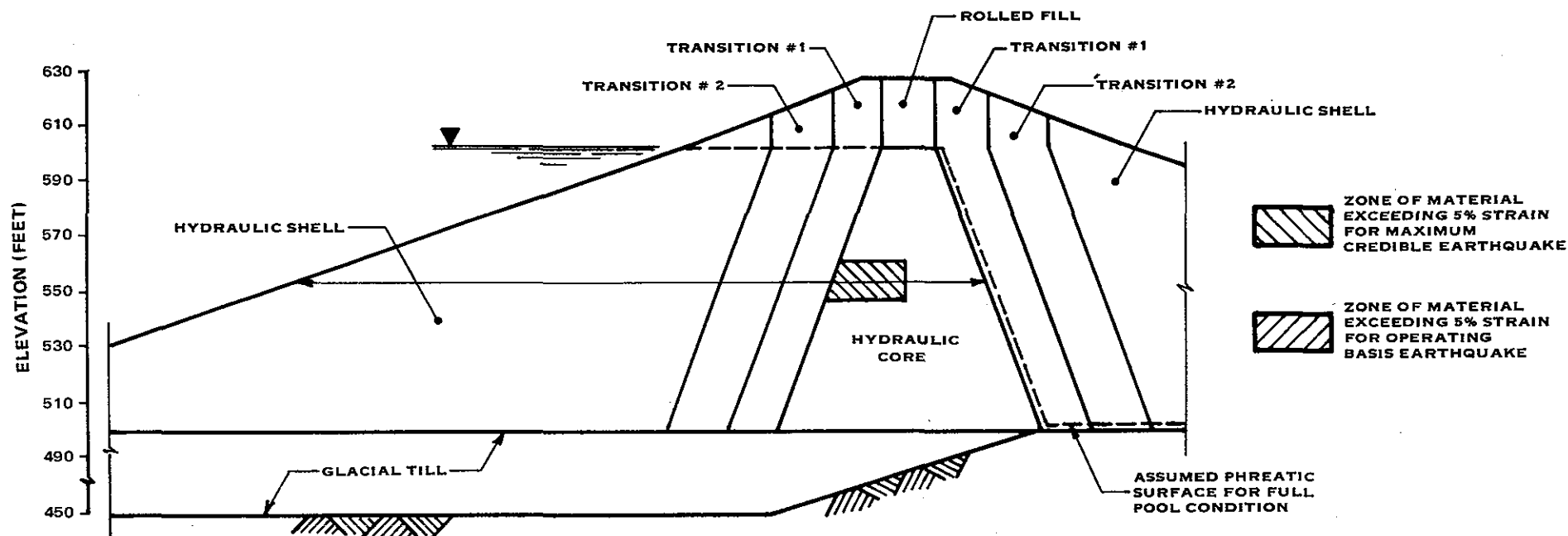
4. Results of Two-Dimensional Analysis - In the finite element analysis, the modulus and damping values of each element are not known at the outset, and an iterative procedure is required. The strain in each element is first estimated and the strain-dependent values of modulus and damping are obtained for that element. The analysis is then conducted and the values of shear strain are computed. Based on the computed shear strains, new values of modulus and damping are obtained and the analysis is repeated. Proceeding in this manner, the analysis is continued until the values of modulus and damping are compatible with the strain developed in each element (Seed, et al. 1973). For each of the four FLUSH analyses performed for this work, a total of five iterations were required to achieve strain compatibility. Compatibility was considered to be achieved when the new value of either shear

modulus or damping was no more than 5 percent of the values of the previous iteration.

The portion of the response analysis which is important to this study is the value of dynamic shear stress computed on a horizontal plane within each soil element. Generally (Seed, et al. 1973), the average dynamic shear stress is assumed to be 65 percent of the maximum dynamic shear stress obtained from FLUSH. This average superimposed dynamic stress was compared to the cyclic shear resistance of the soil for five (5) percent axial strain and an average equivalent number of uniform stress cycles (\bar{N}_{eq}). The equivalent number of uniform stress cycles was computed using the dynamic stress histories obtained from the FLUSH program in accordance with the procedure presented by Seed, et al. (1975).

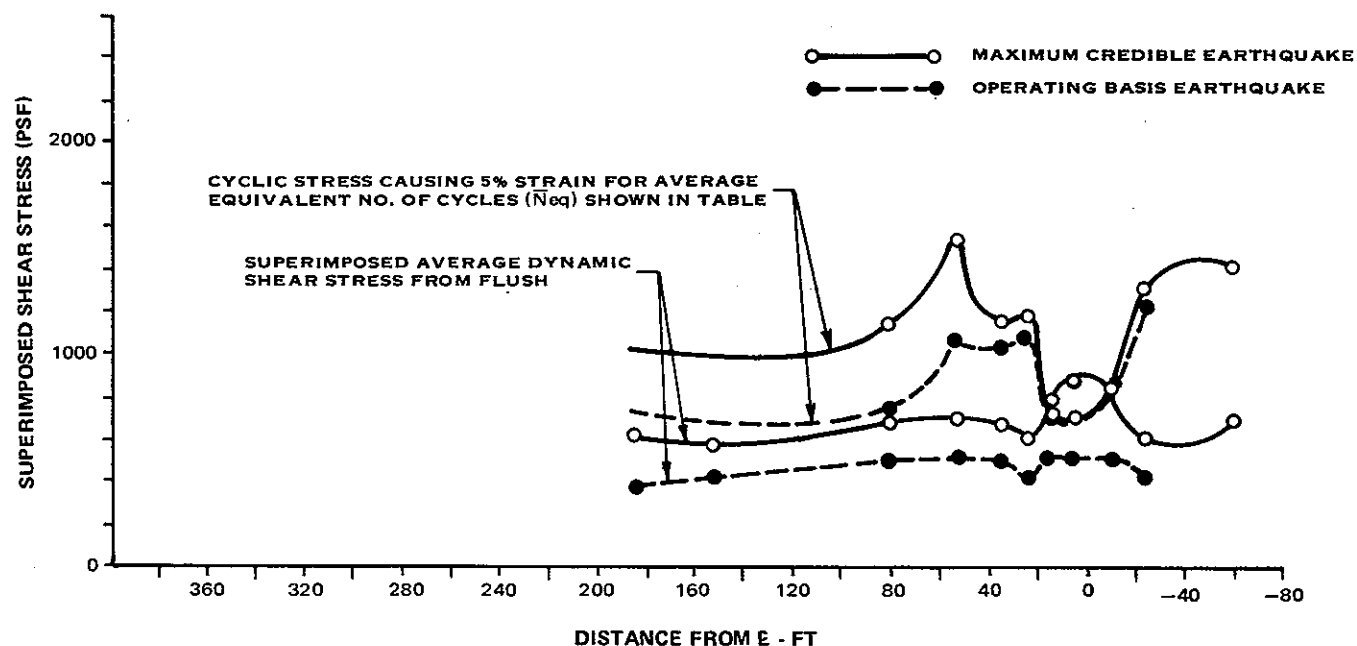
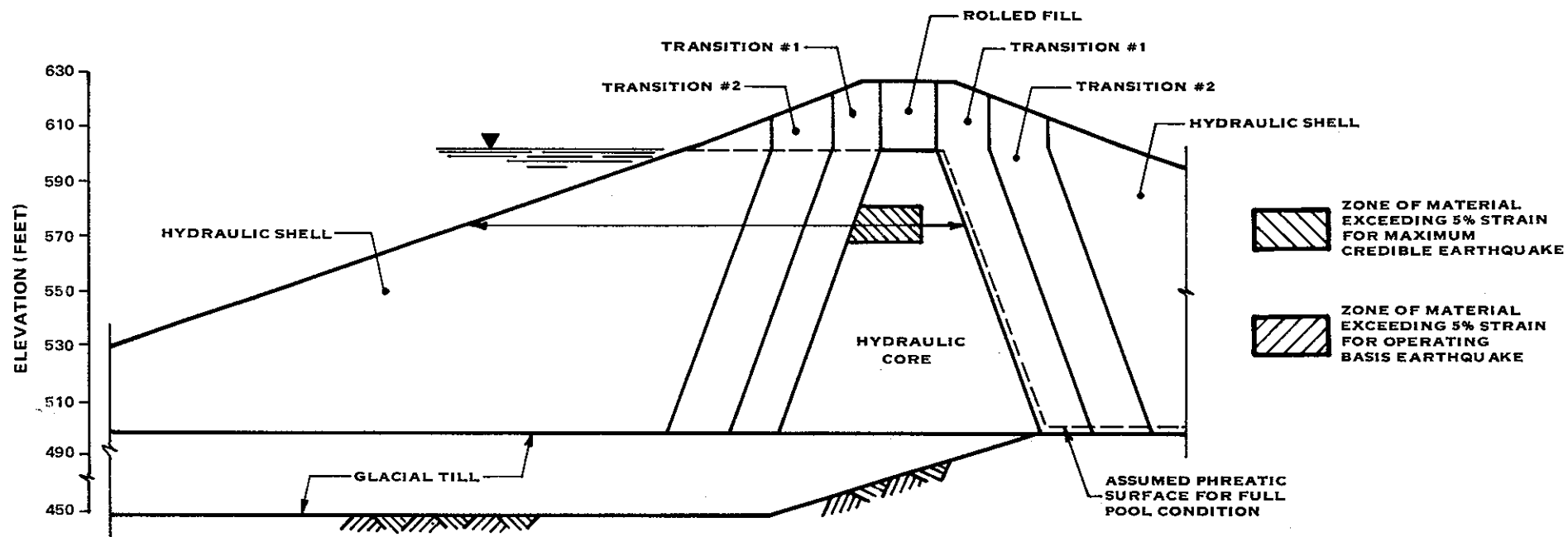
For each of the embankment sections investigated in this analysis, a comparison of stresses was made along horizontal planes through the dam. For the embankment at Station 8+50, the comparison was made along planes at Elevations 555, 575, and 590; for the embankment at Station 4+82, along planes at Elevations 567 and 585.

The results of the comparison are shown for the two earthquakes in Plates 53 through 57. In the upstream hydraulic shell at both embankment sections the cyclic shear resistance at 5 percent strain for the indicated average equivalent number of uniform stress cycles is greater than the superimposed average dynamic shear stress from either the Maximum Credible or Operating Basis Events. For the hydraulic core, however, the results are different. Within portions of the core at Station 8+50, the superimposed average dynamic shear stresses are greater than the cyclic shear resistance for the Maximum Credible Event. For the Operating Basis Event the superimposed average dynamic shear stress in the core is less than the cyclic shear resistance. At Station 4+82 portions of the



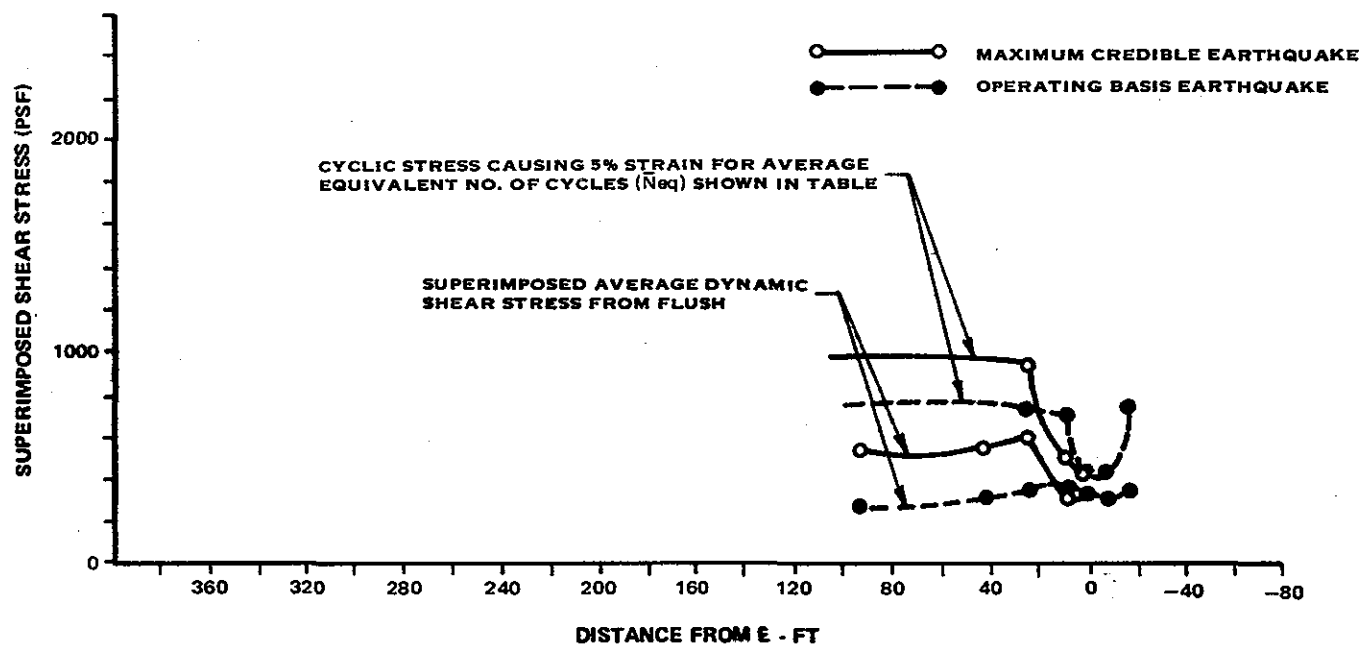
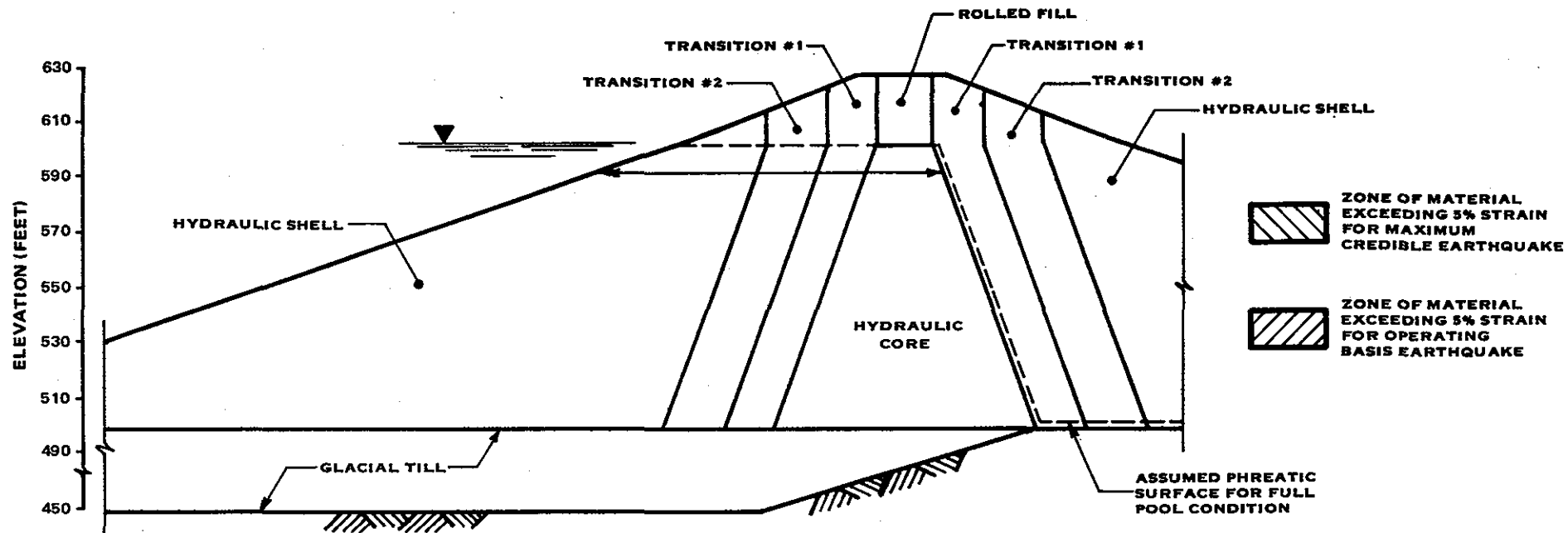
ZONE	N_{eq}	
	MAXIMUM CREDIBLE	OPERATING BASIS
HYDRAULIC CORE	7	7
TRANSITION No.1	7	9
TRANSITION No.2	5	9
HYDRAULIC SHELL	5	10

DYNAMIC STABILITY ANALYSIS OF
KNIGHTVILLE DAM
NEW ENGLAND DIVISION, COE
AVG. SUPERIMPOSED SHEAR STRESS
vs CYCLIC SHEAR RESISTANCE
AT EL. 555; STATION 8 + 50



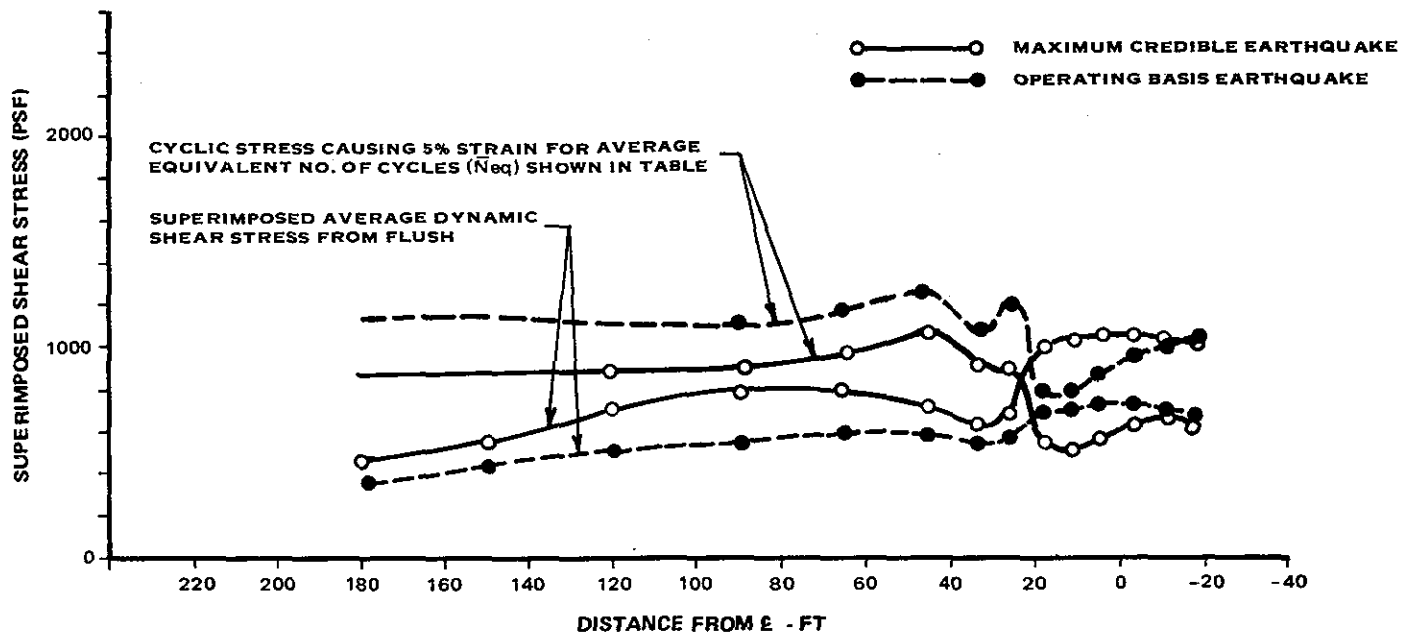
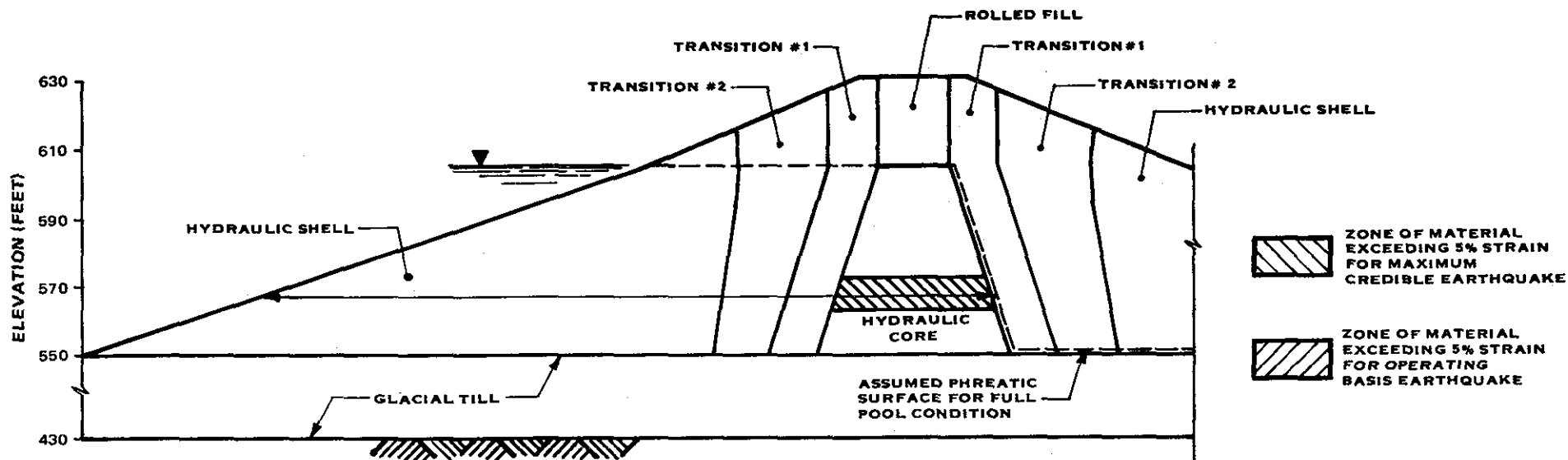
ZONE	\bar{N}_{eq}	
	MAXIMUM CREDIBLE	OPERATING BASIS
HYDRAULIC CORE	7	7
TRANSITION No.1	7	9
TRANSITION No.2	5	9
HYDRAULIC SHELL	5	10

DYNAMIC STABILITY ANALYSIS OF
KNIGHTVILLE DAM
NEW ENGLAND DIVISION, COE
AVG. SUPERIMPOSED SHEAR STRESS
vs CYCLIC SHEAR RESISTANCE
AT EL. 575; STATION 8 + 50



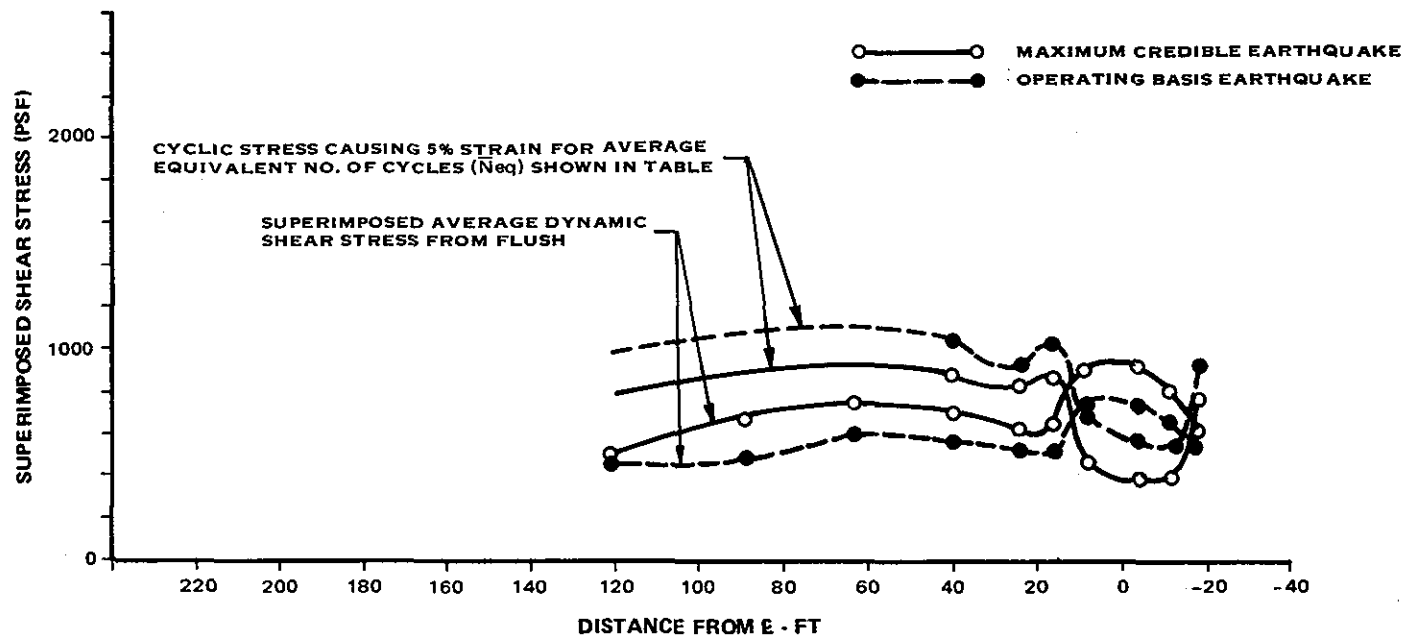
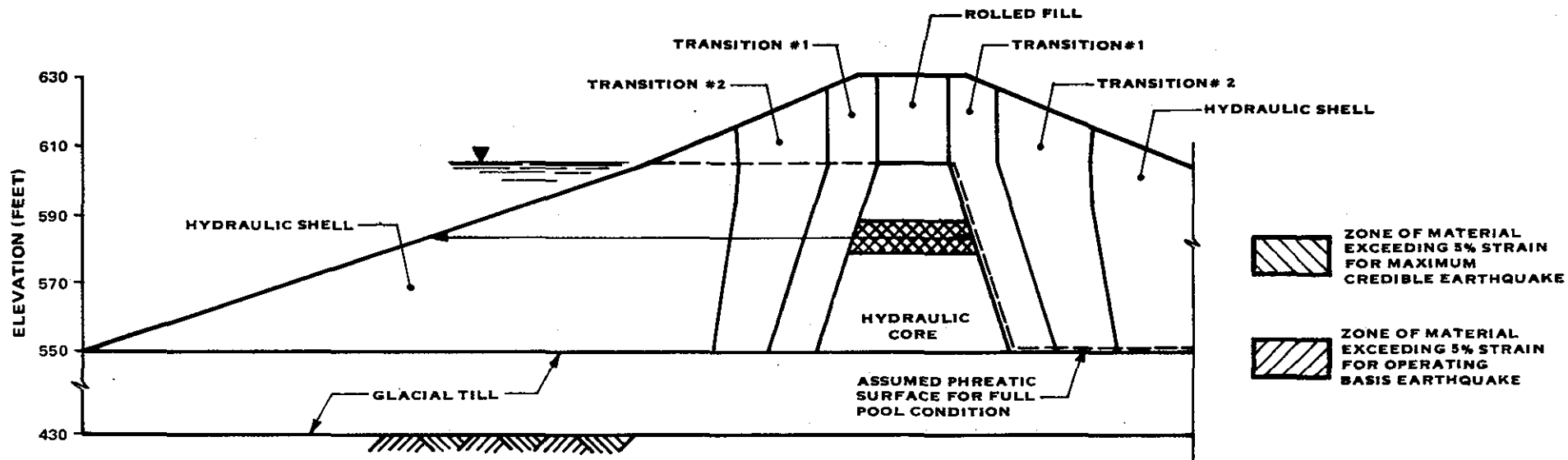
ZONE	N_{eq}	
	MAXIMUM CREDIBLE	OPERATING BASIS
HYDRAULIC CORE	7	7
TRANSITION No.1	7	9
TRANSITION No.2	5	9
HYDRAULIC SHELL	5	10

**DYNAMIC STABILITY ANALYSIS OF
KNIGHTVILLE DAM
NEW ENGLAND DIVISION, COE
AVG. SUPERIMPOSED SHEAR STRESS
vs CYCLIC SHEAR RESISTANCE
AT EL. 590; STATION 8 + 50**



ZONE	N_{eq}	
	MAXIMUM CREDIBLE	OPERATING BASIS
HYDRAULIC CORE	8	3
TRANSITION No.1	8	5
TRANSITION No.2	7	5
HYDRAULIC SHELL	7	5

DYNAMIC STABILITY ANALYSIS OF
KNIGHTVILLE DAM
NEW ENGLAND DIVISION, COE
AVG. SUPERIMPOSED SHEAR STRESS
VS CYCLIC SHEAR RESISTANCE
AT EL. 567; STATION 4 + 82

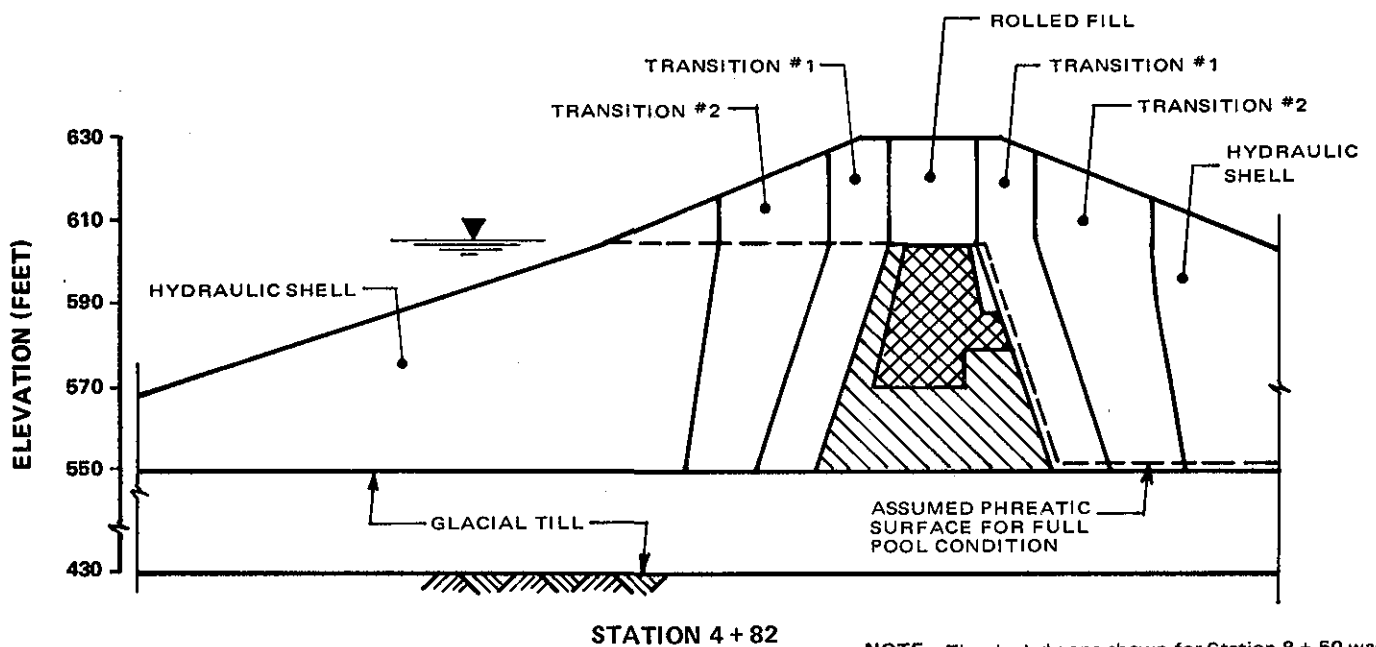
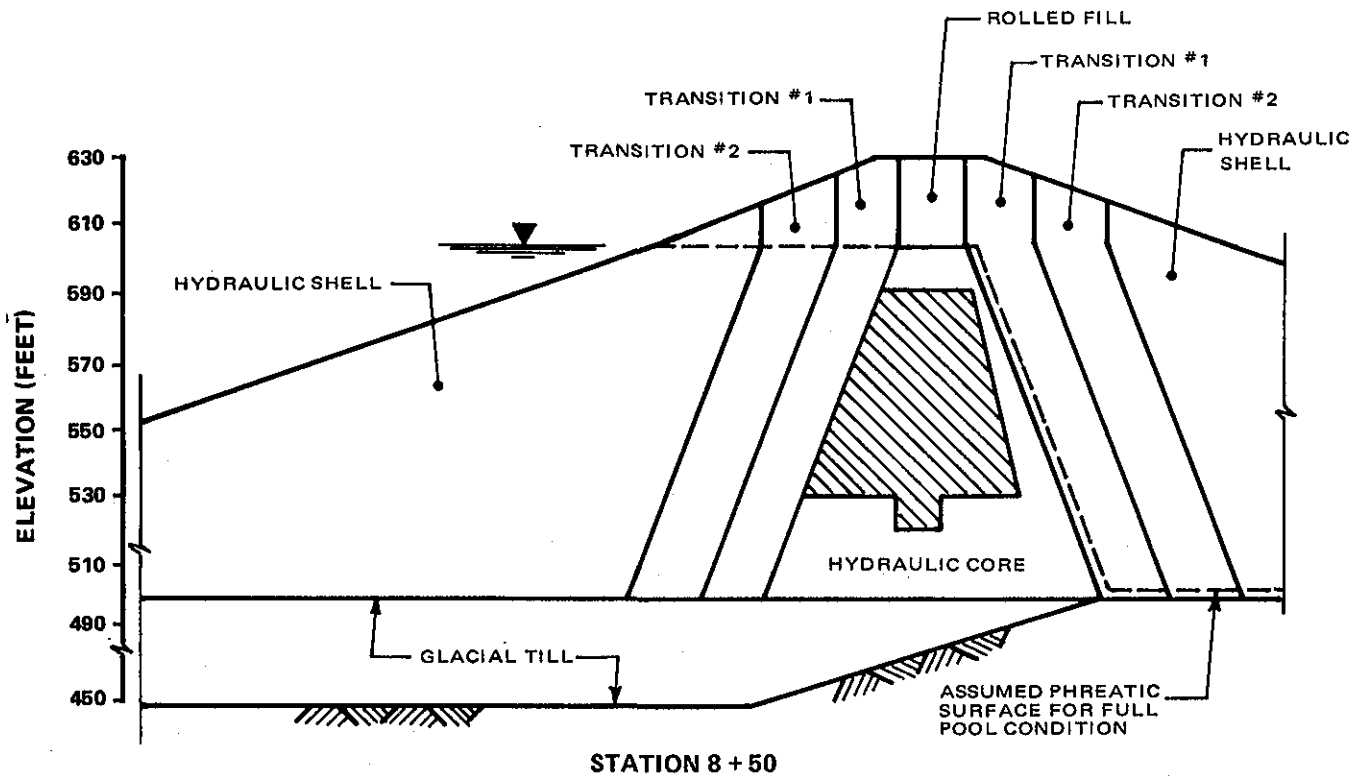



ZONE	N_{eq}	
	MAXIMUM CREDIBLE	OPERATING BASIS
HYDRAULIC CORE	8	3
TRANSITION No.1	8	5
TRANSITION No.2	7	5
HYDRAULIC SHELL	7	5

DYNAMIC STABILITY ANALYSIS OF
KNIGHTVILLE DAM
NEW ENGLAND DIVISION, COE
AVG. SUPERIMPOSED SHEAR STRESS
VS CYCLIC SHEAR RESISTANCE
AT EL. 585; STATION 4 + 82

core exhibit the same behavior during both events as those at Station 8+50 when subjected to the Maximum Credible Event. In each of the Plates, no shear stresses are shown downstream of the core since it is assumed that the downstream shell is not saturated and therefore not susceptible to liquefaction.

Plate 58 summarizes the results obtained for various levels within the embankment, as shown in Plates 53 through 57, as well as, for other levels not shown on the Plates. The Plate shows for each earthquake event, the zones in which the strain potential criterion is not met. The results indicate that the hydraulic core at both embankment sections is susceptible to liquefaction. These results are consistent with those obtained from the one-dimensional and simplified analyses.



 Zone of Material Exceeding 5% Axial Strain for Maximum Credible Earthquake

 Zone of Material Exceeding 5% Axial Strain for Operating Basis Earthquake

NOTE: The shaded zone shown for Station 8 + 50 was partially developed using engineering judgment, since the superimposed dynamic stresses were not computed for all elements in the core.

DYNAMIC STABILITY ANALYSIS OF
KNIGHTVILLE DAM
NEW ENGLAND DIVISION, COE
ZONE OF LIQUEFACTION
DETERMINED FROM FLUSH
STATIONS 8 + 50 & 4 + 82

PLATE 58

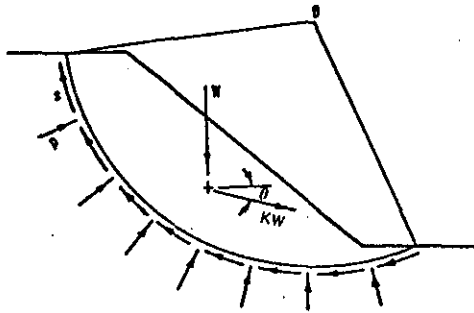
IX. SEISMIC STABILITY AND PERMANENT DEFORMATION ANALYSIS

A. GENERAL

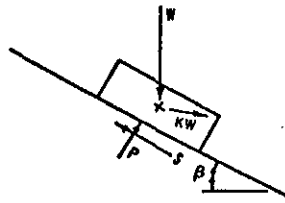
Before the 1960's, the seismic design of slopes and embankments was based on the pseudo-static method of analysis. Generally, if a factor of safety computed from the pseudo-static analysis was greater than unity, the embankment dam was considered to be safe. In 1965, Newmark proposed that the seismic stability of embankments be based on deformations rather than pseudo-static factors of safety, since slope and embankment failures had occurred in cases for which the computed psuedo-static factors of safety were greater than unity.

The basic concept of Newmark's procedure is shown in Plate 59. The concept is based on the assumption that a potential sliding mass behaves as a rigid body and that the resistance to sliding is unsymmetrical, i.e., the block can slide downslope more easily than upslope. In Plate 59(a) is shown a case of potential sliding under earthquake loading, which is analogous to Newmark's simple rigid sliding block model (Plate 59(b)). The force polygon shown on Plate 59(c) represents the forces acting on the inclined rigid block. For the condition shown, the base is undergoing an acceleration to the left and upward, the shearing resistance, S , has reached its limiting value, and movement of the block occurs down the slope (Franklin and Chang, 1977).

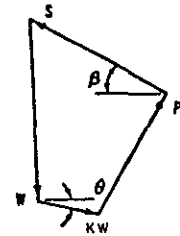
In order to compute the permanent displacement of the sliding block, or of an equivalent embankment slope which has failed due to earthquake loading, Newmark proposed the procedure illustrated in Plate 59(d). In this illustration, A_g represents the acceleration of the rectangular pulse (base) and k_g is the yield acceleration of the block. The permanent displacement which occurs due to the pulse is the relative displacement of the sliding block with respect to the base. Since



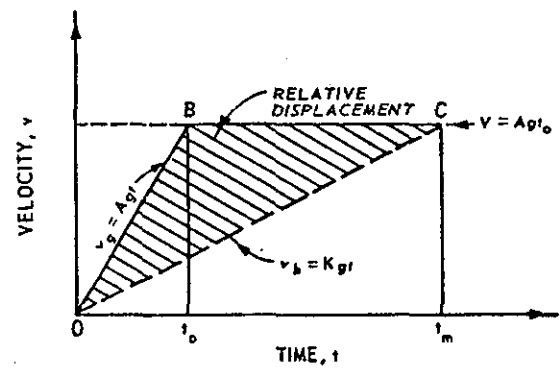
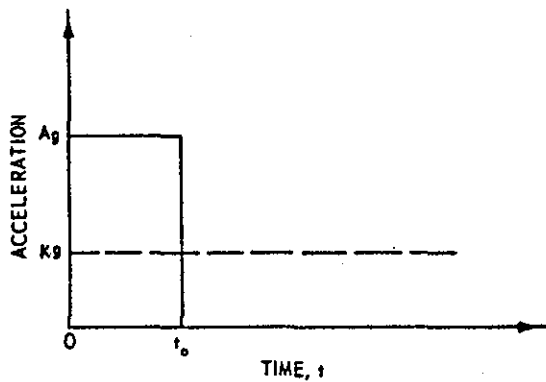
(a) POTENTIAL SLIDING MASS



(b) SLIDING BLOCK MODEL



(c) FORCE POLYGON FOR F.S. = 1.0



(d) NEWMARK'S DISPLACEMENT CONCEPTS

the absolute displacements of the base and block are given by the areas under their respective velocity versus time curves, the relative velocity is given by the area between the two curves. This area is shown shaded in Plate 59(d).

Since Newmark's work, many investigators have proposed methods for determining the permanent deformation of potential sliding masses in earth dams (Seed, 1981; Makdisi and Seed, 1977; Franklin and Chang, 1977; Sarma, 1973; Ambraseys and Sarma, 1967; Hendron and Fernandez, 1977). All of the methods are generally based on Newmark's work.

In order to assess the seismic stability of the embankment sections studied herein and compute the amount of permanent displacement which could occur along potential sliding surfaces as a result of the seismic events, two methods of analysis were used. These methods are discussed in the following.

B. MAKDISI AND SEED SIMPLIFIED METHOD

1. General - In 1977, Makdisi and Seed published a simplified procedure for estimating the embankment deformation resulting from earthquake loadings. This procedure developed because, at the time, there was a need for a simple, yet rational approach to the seismic design of embankments. The method utilizes the concept proposed by Newmark (1965). However, the primary assumption of the Newmark procedure as previously discussed is that the sliding mass is a rigid block, whereas in the simplified method, the dam is assumed to act as a deformable earth structure.

The simplified method involves three steps and utilizes design curves based on cases previously analyzed. Following the procedure developed by Makdisi and Seed (1977), the three steps in the analysis are as follows:

(1) Determine the coefficient of yield acceleration (k_y) along potential sliding surfaces for a factor of safety of unity;

(2) Determine the induced crest acceleration (\ddot{U}_{\max}) in the embankment from a simplified procedure proposed by Seed and Makdisi (1979) or from a dynamic response analysis and determine the maximum average yield acceleration ($K_{\max}g$) at any depth, and

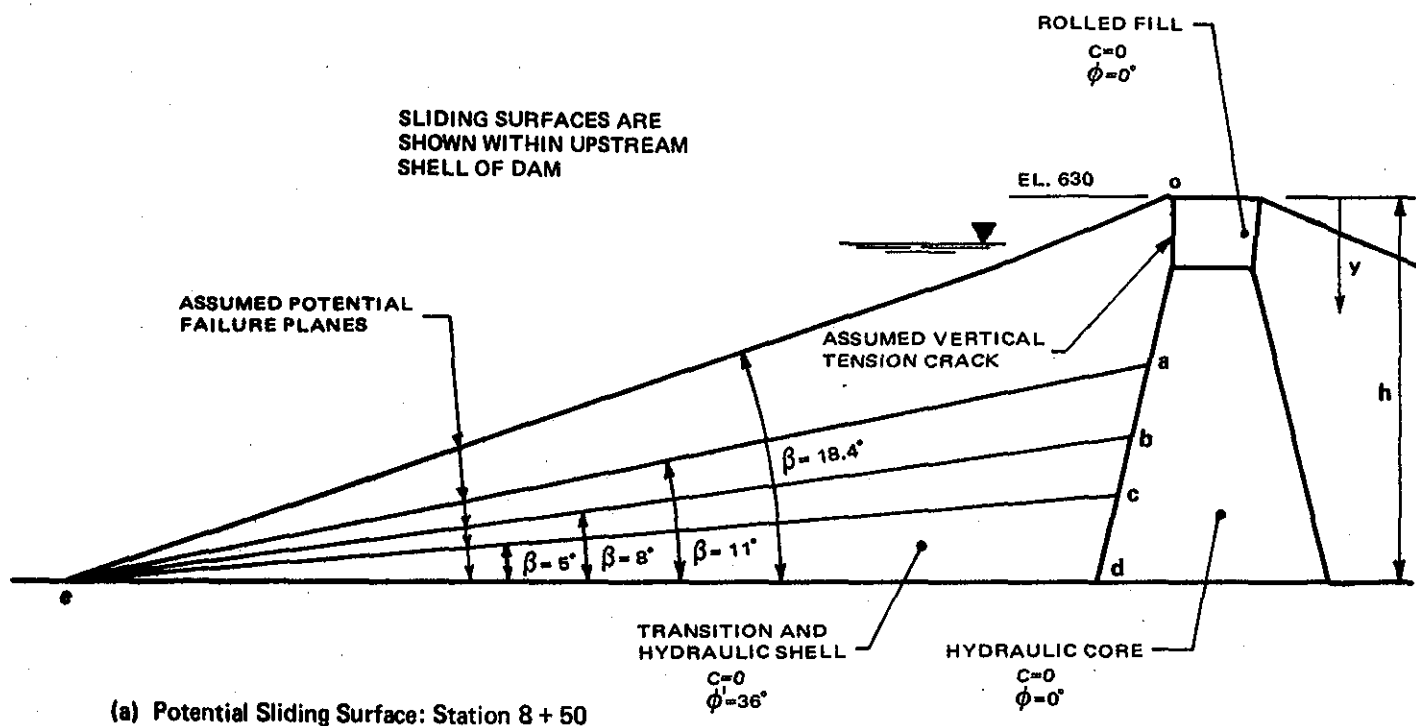
(3) Compute the magnitude of displacement (U) along the critical failure plane utilizing the design curves presented in the reference.

Each of the steps used in the analysis is described below.

2. Step #1: Critical Yield Acceleration Determination - The shearing resistance between the sliding mass and the underlying base is evaluated in terms of a critical acceleration, $k_y g$, which is the level of base acceleration that would provide a factor of safety of unity, and make sliding imminent (Hynes-Griffin, 1979). For the Makdisi and Seed Simplified Analysis, any static stability analysis method (Bishop, 1955; Morgenstern and Price, 1965; Sarma, 1973) can be used to determine the critical acceleration along potential failure surfaces. For this simplified deformation analysis, a series of potential wedge-type sliding masses were analyzed as shown on Plate 60(a). The failure surface of each sliding mass was assumed to extend along the upstream face of the core and to cut through the upstream shell material to the toe of the embankment at an angle β . The assumed shear strengths along the failure surfaces were as follows:

<u>Material</u>	<u>C</u> <u>(psf)</u>	<u>ϕ</u> <u>(degrees)</u>
Core and Rolled Fill	0	0
Shell	0	36

The zero strength values assumed for the core and rolled fill zones were based on the conservative assumption that liquefaction and cracking would respectively occur in each. For the shell, a value of 36 degrees was used rather than



β (DEGREES)	k_y
0	0.44
5	0.36
8	0.33
11	0.29
18.4	0.19

(b) Determination of Coefficient of Yield Acceleration (k_y)

DEFINITIONS

y = distance from crest of dam to center of mass of sliding surface.
h = total height of embankment section.

SAMPLE CALCULATION

- For surface "ocb", $\beta = 5^\circ$
 $\gamma(\text{avg}) = 146\text{pcf}$
 $\gamma'(\text{avg}) = 86.9\text{pcf}$ } See (1)
- $k_y = \frac{\gamma'}{\gamma} \tan(\phi' - \beta)$
 $k_y = \frac{86.9}{146} \tan(36 - 5)$
 $k_y = 0.36$

(1) Unit weights are computed on a weighted average basis

DYNAMIC STABILITY ANALYSIS OF
KNIGHTVILLE DAM
NEW ENGLAND DIVISION, COE
SEISMIC STABILITY ANALYSIS
USING MAKDISI AND SEED
SIMPLIFIED PROCEDURE

full value of friction ($\phi = 41^\circ$) used in the static stress analysis because it was assumed that seepage forces exist in the shell due to drainage from the liquefied core and would thereby reduce the value of effective friction along the assumed failure surfaces.

The values of yield acceleration for the wedges shown on Plate 60(a) were computed from the expression:

$$F.S. = \left[\frac{1 - K \frac{\gamma}{\gamma'} \tan \beta}{\tan \beta + K \frac{\gamma}{\gamma'}} \right] \tan \phi'$$

where

- F.S. = factor of safety
- K = horizontal earthquake acceleration coefficient
- γ = average total unit weight of sliding block
- γ' = average submerged unit weight of sliding block
- β = angle of failure surface
- ϕ' = effective friction angle of shell material

In the analysis a factor of unity is used for earthquake conditions; the above expression can therefore be rearranged to compute the coefficient of critical yield acceleration (k_y) directly, as follows:

$$k_y = \frac{\gamma}{\gamma'} \tan (\phi' - \beta)$$

The values of k_y computed for each of the sliding blocks shown are given in Plate 60(b). The computed values range from 0.44 for a failure along the base ($\beta = 0^\circ$) to 0.19 for a very shallow surface failure ($\beta = 18^\circ$), which represents the critical k_y .

3. Step #2: Determination of Earthquake Induced Acceleration - To compute the permanent deformations of a potential sliding mass, the time histories of earthquake-induced

average accelerations must be determined. The one- or two-dimensional analyses provide the maximum value of acceleration and the time series of accelerations for each layer or soil element. In the deformation analysis, the time series obtained at locations along the sliding surface are averaged to obtain a time history of average accelerations, which is then considered to be the base motion for that sliding mass.

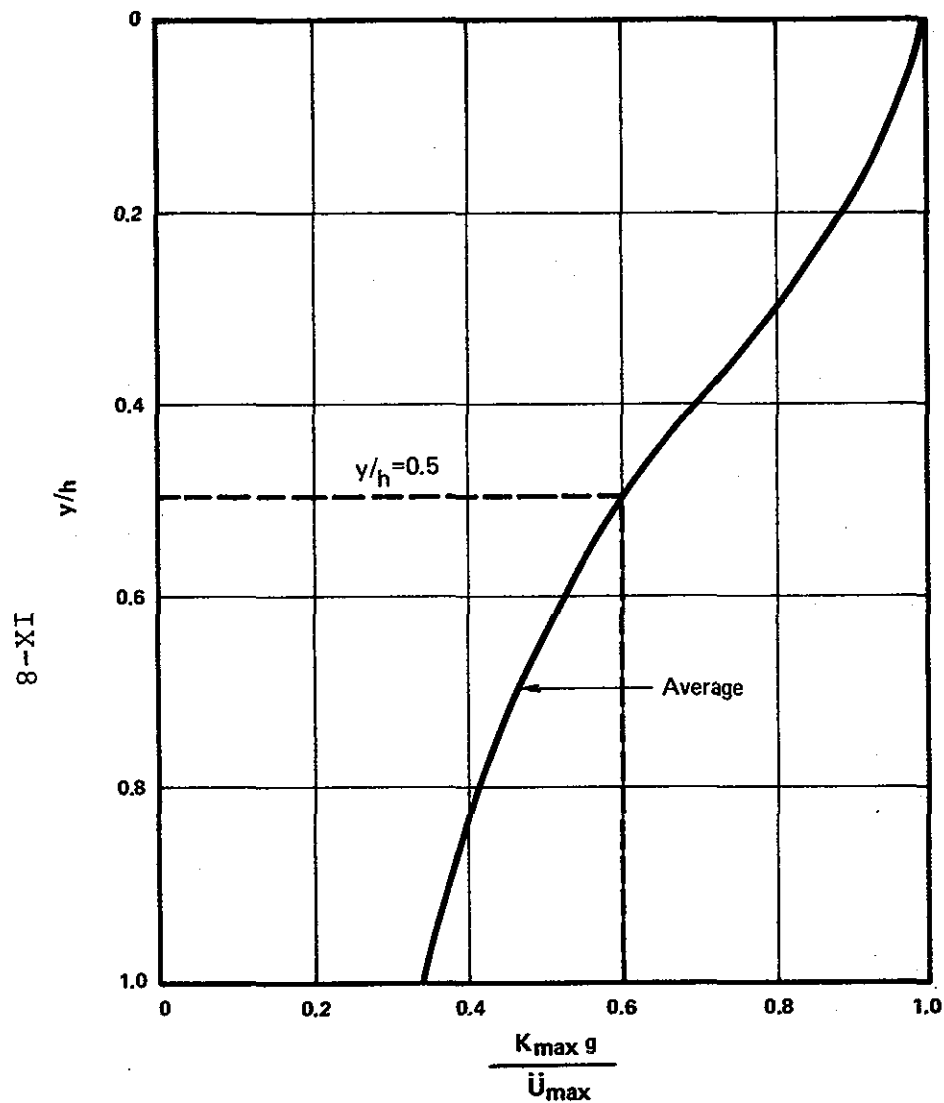
The maximum value of the average acceleration for a sliding surface at any depth can be determined from the relationship developed by Makdisi and Seed (1977). The variation of effective peak acceleration, $K_{\max} g$, with depth of base, y , of the potential slide mass is shown by a curve on Plate 61(a) in terms of the maximum acceleration ratio, which is defined as the ratio of maximum crest acceleration, \ddot{U}_{\max} , and the maximum average acceleration, K_{\max} . This curve was used to determine the permanent displacement of the embankment as described in Step #3, and as illustrated on the Plate.

4. Step #3: Determination of Permanent Displacement - According to Makdisi and Seed (1977), the factors which control the amount of permanent deformation induced by an earthquake along a potential sliding surface are as follows:

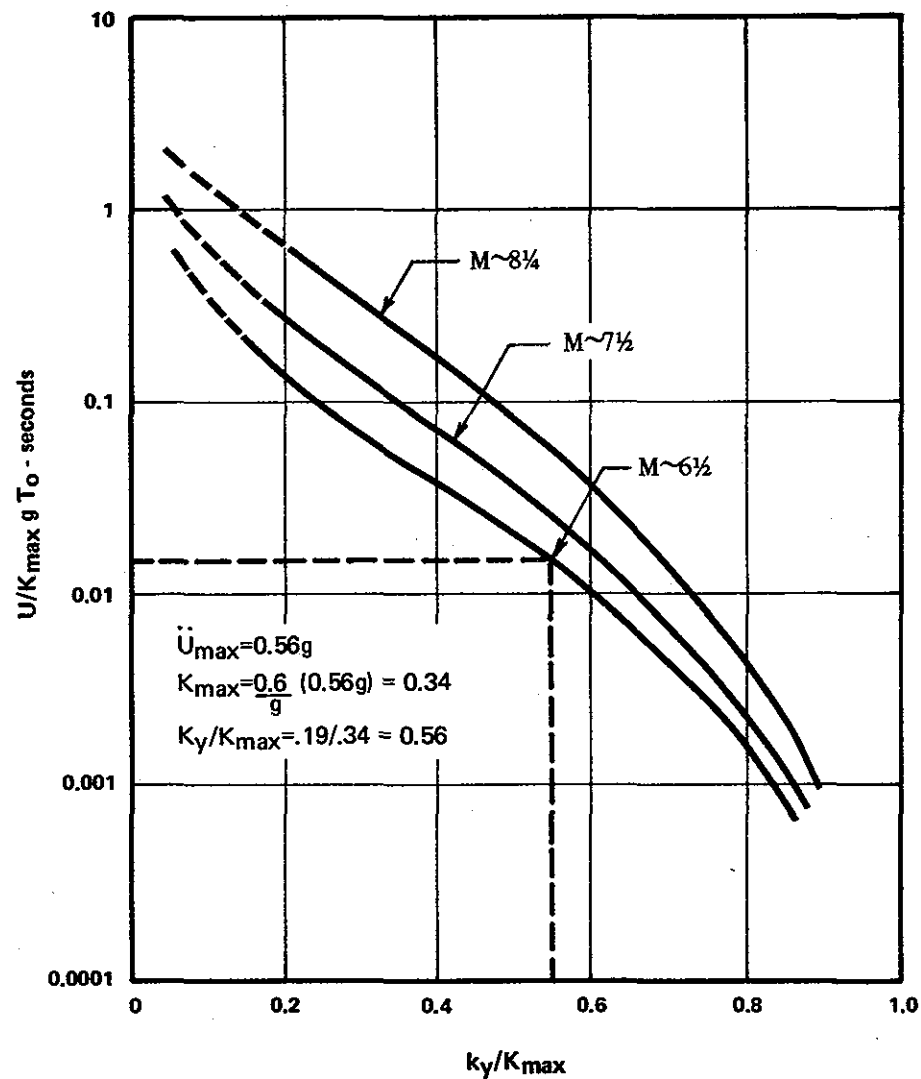
a) the amplitude of induced average accelerations, which is a function of the base motion, the amplifying potential of the embankment material, and the location of the sliding mass within the embankment;

b) the frequency content of the average acceleration time-history, which is governed by the embankment height and stiffness characteristics, and is usually dominated by the first natural frequency of the embankment;

c) the duration of significant shaking, which is a function of the magnitude of the specified earthquake.



(a) Variation of Effective Peak Acceleration, k_{max} , with Depth of Base of Potential Slide Mass



(b) Computed Displacements of Embankment Dams

(after Makdisi and Seed, 1977)

DYNAMIC STABILITY ANALYSIS OF
KNIGHTVILLE DAM
NEW ENGLAND DIVISION, COE
INDUCED PERMANENT DEFORMATION
SIMPLIFIED ANALYSIS

To consider each of these factors in the simplified deformation procedure, Makdisi and Seed performed finite element analyses of embankments ranging between 75 and 150 feet in height and having varying slopes and material properties. The embankments were subjected to ground accelerations representing three different earthquake magnitudes ($6\frac{1}{2}$, $7\frac{1}{2}$ and $8\frac{1}{4}$) and the corresponding deformations were computed. The results of their studies are presented in Plate 61(b).

The two charts presented on Plate 33 were used in determining the permanent displacement of Knightville Dam, by following the sequence described below.

First, the coefficient of average maximum yield acceleration for the critical sliding surface was determined. As stated previously the critical surface was shallow having a $k_y = 0.19$ (See Plate 60(b)).

Since the critical surface extends from the crest to the toe of the dam the y/h equals 0.5 (y is defined as the vertical distance below the crest of the dam to the center of mass of the sliding mass). Accordingly, the value of $K_{\max} g / \ddot{U}_{\max}$ from Plate 61(a) is equal to 0.60.

Next the induced crest acceleration, \ddot{U}_{\max} , was computed using a simplified technique developed by Makdisi and Seed (1981) which utilizes a strain-dependent iterative procedure. The crest acceleration for the embankment section at Station 8+50 was computed to be 0.56g; and the first natural period of the dam, T_0 , was computed to be 0.38 seconds.

The final step in the analysis is to compute the permanent deformation along the critical sliding surface using the graph on Plate 61(b). A sample calculation of the procedure is shown on the Plate.

The approximate permanent displacement, U, induced by the Maximum Credible Earthquake can be determined from the curve shown for M = 6½ earthquake on Plate 33(b) and the response characteristics of the embankment given above. Accordingly the permanent displacement of the embankment section at Station 8+50 is computed to be 0.60 inches.

This value of deformation, although small, can only be considered as an "order of magnitude" value since the actual value of displacement is dependent on many factors not considered in the analysis. A more sophisticated, but not necessarily more accurate method of computing displacement, is presented below.

C. SARMA STABILITY/COE DEFORMATION ANALYSES

1. General - The second method of analysis used to assess the seismic stability and permanent deformation of the dam combined the Sarma-type stability analysis for determining the values of critical yield acceleration and a slightly modified version of the permanent displacement analysis presented by the Waterways Experiment Station, Corps of Engineers (Franklin and Chang, 1977).

2. Sarma Stability Analysis - Sarma proposed a stability analysis of embankments and slopes to determine the critical earthquake acceleration required to bring a mass of soil to a state of limit equilibrium. A description of the method and the assumptions made are presented by Sarma (1973, 1974, 1975).

The computer program SAM4 was used to perform the Sarma analysis. The input parameters include geometry of slope and potential failure surface, phreatic surface, unit weights, and shear strength values. The analysis can be performed using either total or effective stress. It is difficult,

however, to use effective stresses because of the problem of estimating cyclic pore pressures; therefore total stress analyses were used.

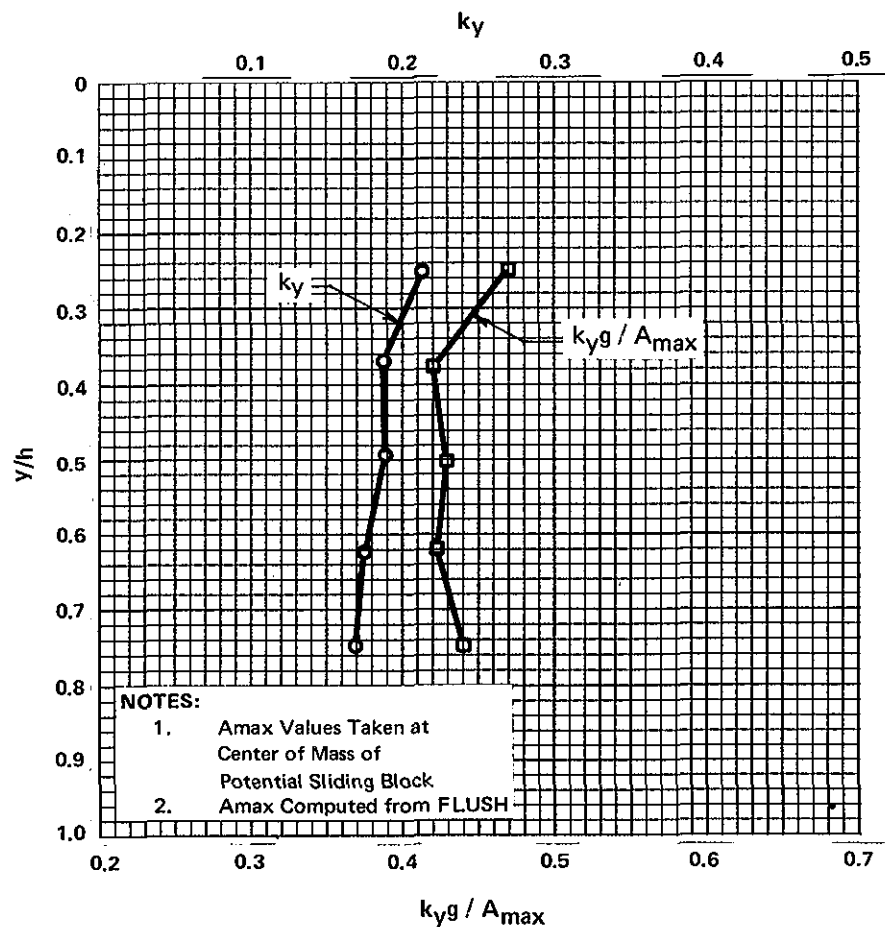
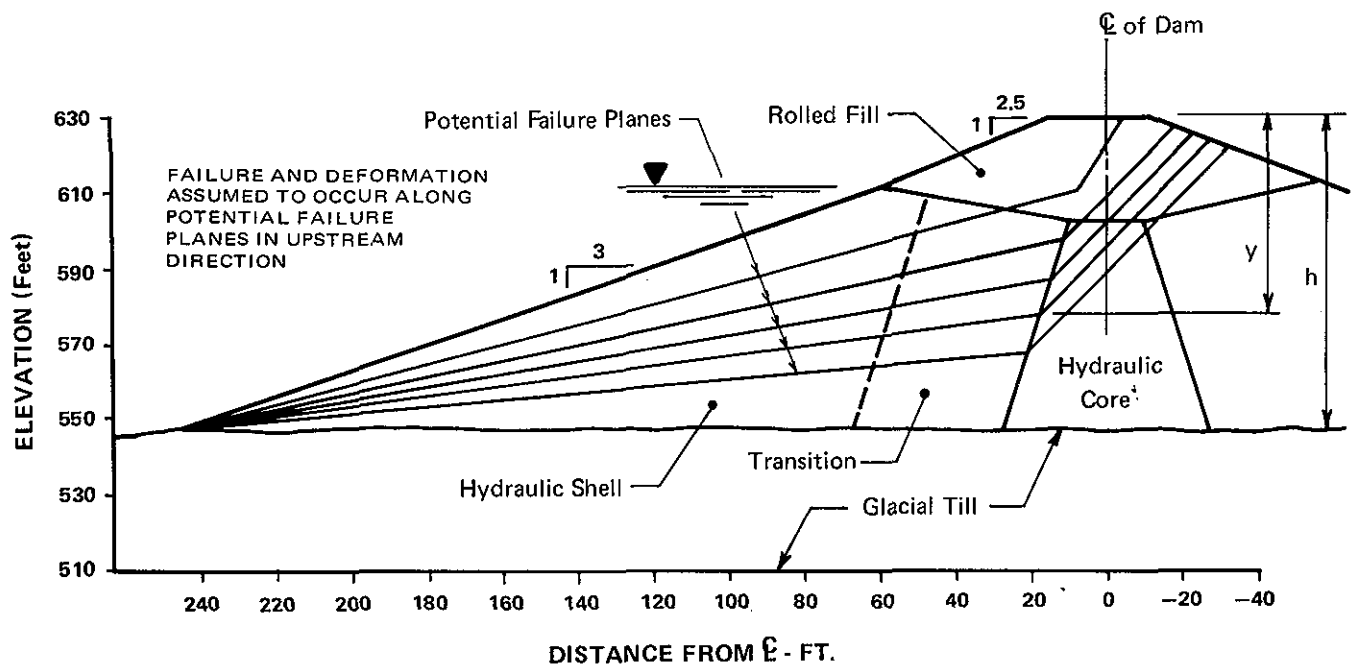
Table 13 gives a summary of the strength parameters which were used in the Sarma analysis, and Plates 62 and 63 show the potential sliding surfaces which were examined.

Table 13
SELECTED STRENGTH PARAMETERS

<u>Material Type</u>	<u>Undrained</u>		<u>Drained</u>	
	<u>(ϕ)</u>	<u>C(psf)</u>	<u>(ϕ)</u>	<u>C(psf)</u>
Core	0	0	--	--
Upstream Shell	--	--	36	0
Rolled Fill	--	--	25	0
Transitions 1 and 2	22	1,440	36	0

The shearing resistance of the core material along the sliding base was assumed to be zero; this assumption is conservative and is based on the results of the dynamic response analysis. The material in the upstream hydraulic shell was assumed to have a reduced drained friction angle of 36 degrees as previously discussed. In each of the transition zones, a composite shear strength envelope was used, that is, at any effective confining pressure the smaller of the undrained and drained strength was used. This strength envelope conservatively takes into account possible dissipation of shear-induced negative pore pressures that might occur in the field but cannot occur in an undrained test in the laboratory.

The coefficients of critical accelerations, k_y , for each of the potential surfaces analyzed, obtained from the Sarma Method are presented in Plates 62 and 63. The use of these results is discussed in the next section.



3. Permanent Deformation - The method used to determine the permanent deformation of Knightville Dam is a procedure developed by Franklin and Chang (1977) with a modification made by TAMS.

Generally, the positive acceleration of an accelerogram is assumed to act in the most critical direction of the system. Using Newmark's approach, the positive acceleration of the earthquake motion and the direction of yield acceleration are normally assumed to act horizontally in the downslope direction. TAMS' procedure assumes that the positive and negative accelerations of a given accelerogram each acts in the downslope direction, and that the accumulated total permanent deformation is calculated for each direction independently. The direction which results in the greater permanent deformation for the given yield acceleration is the critical deformation.

The deformation resulting from a given accelerogram for given yield accelerations was determined using a computer program, YDBH9, developed by TAMS. A general description of the program output is presented in Appendix F.

The program has been developed incorporating the following assumptions:

1. the sliding mass above the failure surface(s) will act as a rigid body during the earthquake.
2. the resistance to sliding is elastoplastic and unsymmetrical along the failure surface(s) during the earthquake. Once the stress reaches the plastic range, the mass will start to move and the resistance will remain unchanged throughout the duration of the earthquake.
3. the yield acceleration is constant throughout the duration of the earthquake and the seismic force acts horizontally in the downslope direction.

4. two cases of earthquake direction are assumed:

case a: the permanent downslope displacement for any given yield acceleration is computed by double integrating the positive acceleration of the base accelerogram.

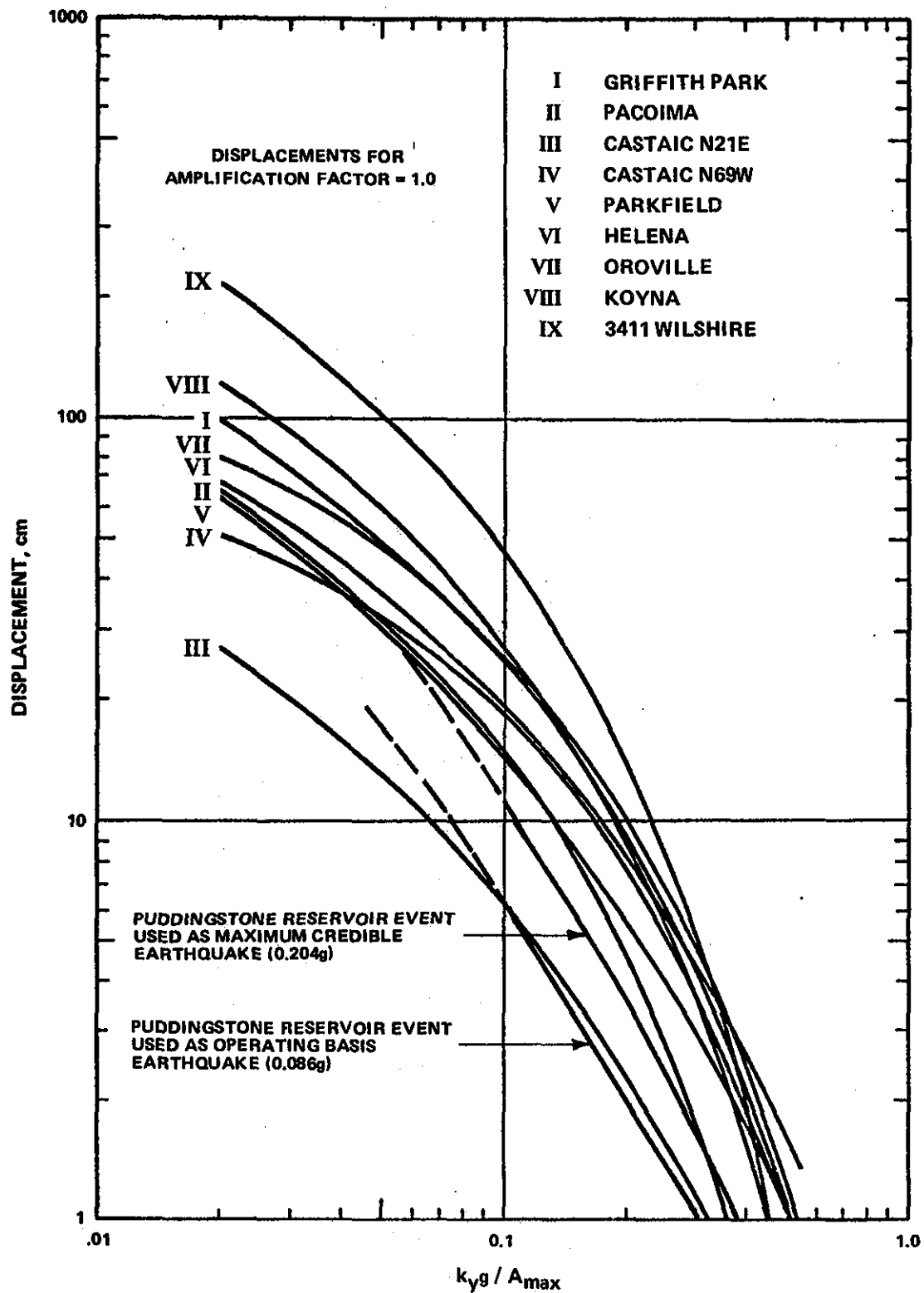
case b: the permanent downslope displacement for any given yield acceleration is computed by double integrating the negative acceleration of the base accelerogram.

The larger value of the two cases is selected as the permanent displacement for the given yield acceleration.

The embankment deformation was determined on the basis of the Puddingstone Reservoir accelerogram scaled to 0.20g and 0.086g; critical permanent displacements were computed for several ratios of yield acceleration and maximum acceleration. The computed deformations are given on Plate 64 in graphical form along with deformations computed from other earthquake records. It can be seen that the deformations expected at Knightville Dam are within the range of values obtained from other dams.

The permanent deformation of the two sections were computed using the coefficient of yield accelerations, k_y , determined as a function of depth ratio for potential failure surfaces. The ratio of critical yield acceleration to maximum acceleration for the given event was calculated also as a function of depth ratio. These results are shown in the lower portion of Plates 62 and 63.

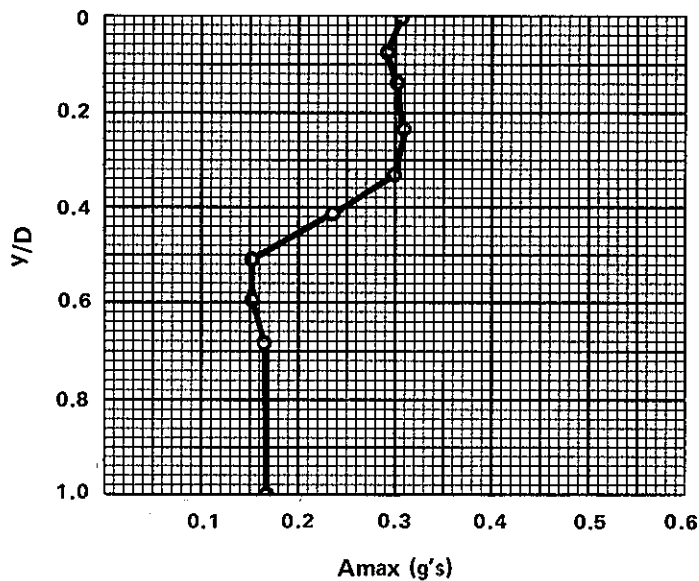
Generally, the maximum acceleration is determined as the average maximum along the potential failure surface. In this analysis however, the maximum acceleration used occurs at the center of mass for the potential failure block and it is assumed that the shape of the accelerogram is not changed. The acceleration at the center of mass was not computed



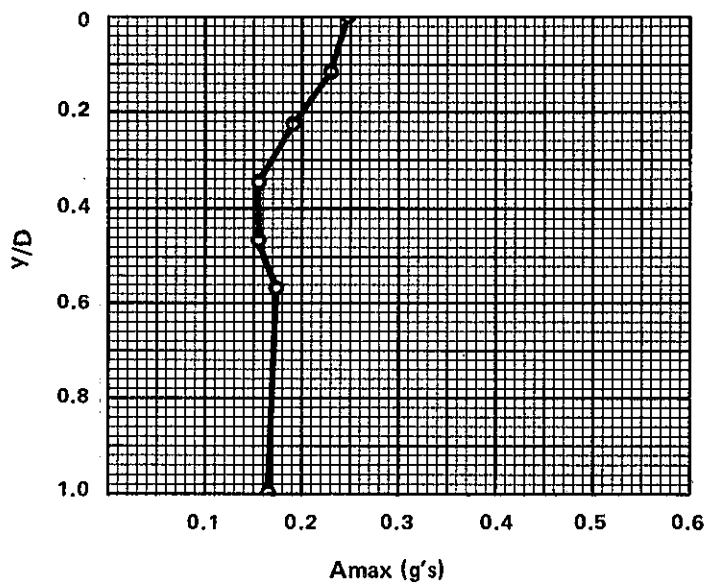
(after Hynes - Griffin, M.E., personal notes 1982)

directly but was interpolated from values obtained at surrounding locations as determined in the FLUSH analysis. Plates 65 and 66 show the relationship of maximum accelerations for the Maximum Credible Earthquake as a function of depth ratio at two locations in each cross-section.

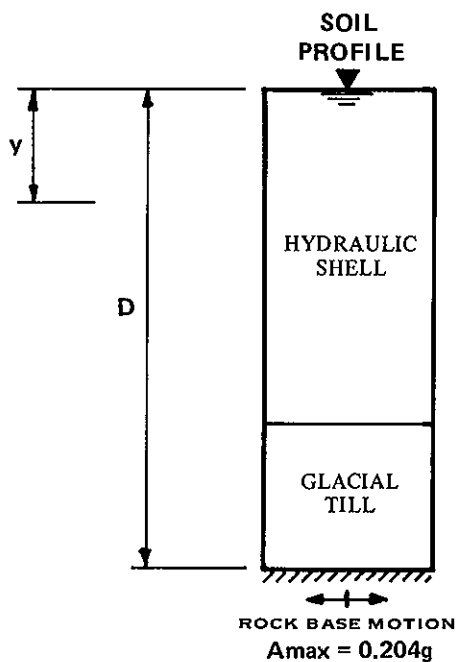
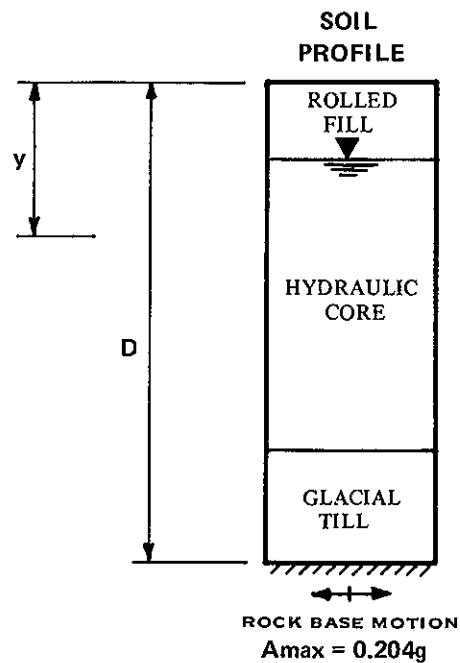
The potential failure surface which will yield the largest permanent deformation occurs where the ratio $k_y g/A_{\max}$ is a minimum. It can be seen in Plates 62 and 63 that this occurs at a ratio of 0.77 and 0.42 for Stations 8+50 and 4+82, respectively. Entering the curves on Plate 36 with the critical $k_y g/A_{\max}$ values indicate that the permanent displacement for the critical potential failure surface is likely to be less than 0.5 inch. This value is about equal to the value computed using the simplified procedure.



(a) Centerline

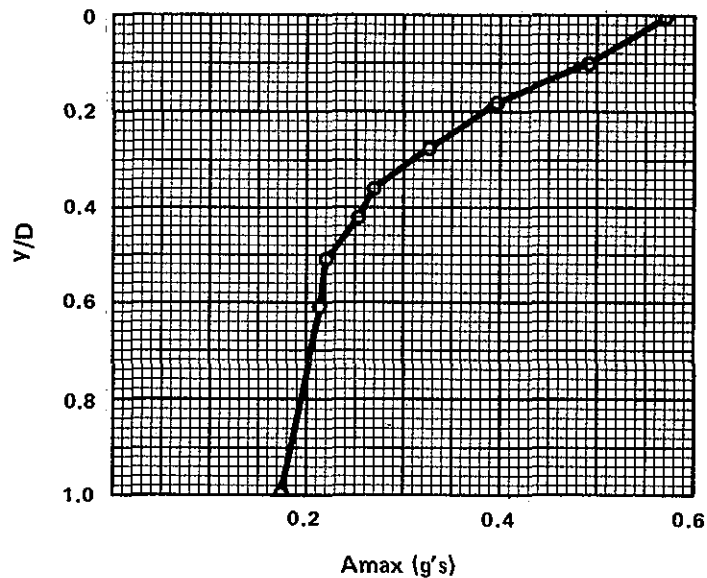


(b) 125 feet upstream Centerline

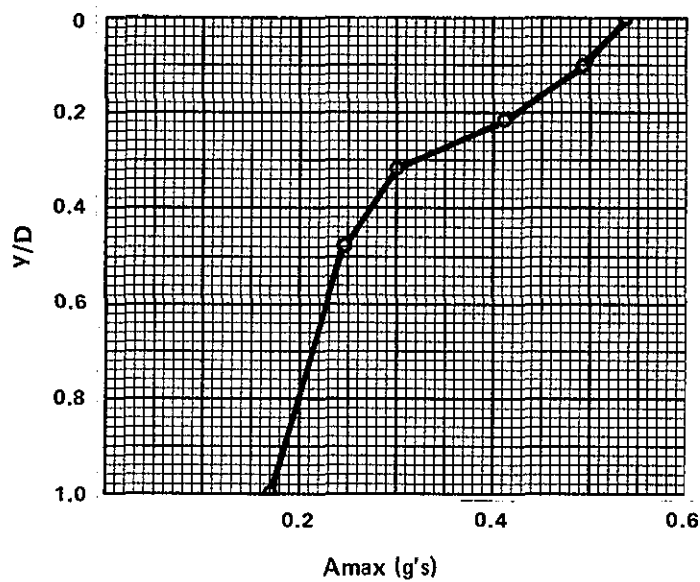


▼ Water Level Assumed in Analysis

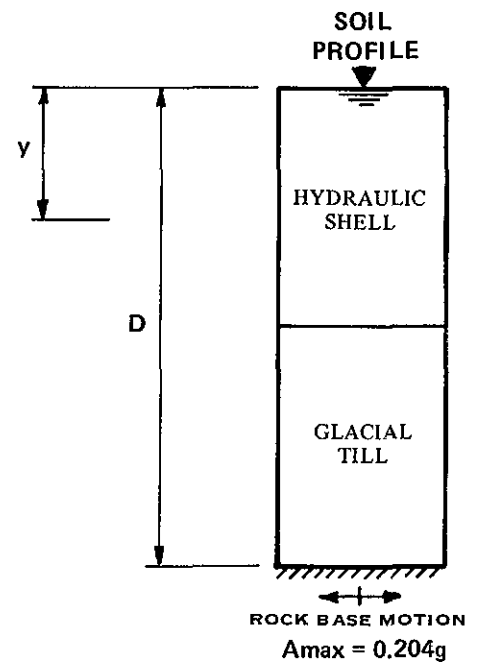
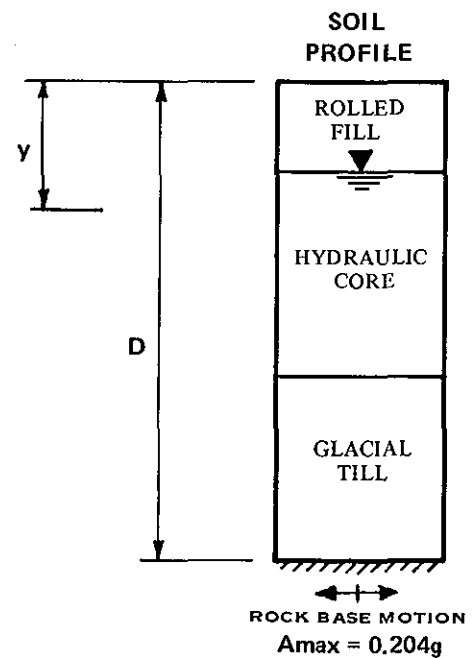
NOTE: Results Obtained from FLUSH Analyses



(a) Centerline



(b) 105 feet upstream of Centerline



▼ Water Level Assumed in Analysis

NOTE: Results Obtained from FLUSH Analyses

X. SUMMARY, CONCLUSIONS AND RECOMMENDATIONS

A. SUMMARY AND CONCLUSIONS

The following tables summarize the results obtained from the analyses described above.

1. Liquefaction Potential

EARTHQUAKE	MAXIMUM CREDIBLE				OPERATING BASIS			
SECTION	STA. 8+50		STA. 4+82		STA. 8+50		STA. 4+82	
ZONE	Core	Shell	Core	Shell	Core	Shell	Core	Shell
Seed-Idriss Simplified								
Lower boundary " r_d " curve	○	--	--	--	○	--	-	--
Mean " r_d " curve	●	--	--	--	○	--	-	--
Upper boundary " r_d " curve	●	--	--	--	○	--	-	--
One-Dimensional (SHAKE)								
Upper Boundary- G/G _{max} vs. γ_{sa}	●	○	●	○	○	--	○	--
Two-Dimensional (FLUSH)	●	○	●	○	○	○	●	○

LEGEND:

- No liquefaction
- Liquefaction occurring in a portion of the zone
- Total liquefaction

2. Permanent Deformation

	MAXIMUM CREDIBLE EARTHQUAKE					
	STA. 8+50			STA. 4+82		
	k_y	Critical $k_{yg/A_{max}}$	δ	k_y	Critical $k_{yg/A_{max}}$	δ
Makdisi-Seed Simplified	0.19	0.56	0.6 in	---	---	----
Sarma/COE Method	0.19	0.77	<0.5 in	0.19	0.42	<<0.5 in

Based on the results of the dynamic analyses presented in this report the following conclusions can be drawn regarding the liquefaction potential, stability and permanent deformation of Knightville Dam when subjected to the Maximum Credible and Operating Basis Earthquakes.

- There is little possibility that the shells of the dam would liquefy during the postulated earthquakes.
- If the core of the dam is below the phreatic surface, substantial portions of the core could liquefy when subjected to the Maximum Credible Earthquake.
- The upper portion of the hydraulic core of the dam could liquefy under the Operating Basis Earthquake, especially in areas where the embankment is founded on thick glacial till deposits (the left abutment).
- Liquefaction of the core under the Maximum Credible and Operating Basis Events could cause subsidence of the core which would result in the collapse of the overlying rolled fill cap. The determination of the degree of subsidence cannot be made utilizing the present state-of-the-art procedures.
- In the event that portions of the core were to liquefy, the overall stability of the dam would not be impaired since the core is contained by the shells which will remain stable.
- For the Maximum Credible and Operating Basis Earthquake the maximum permanent deformation of the embankment is not expected to exceed one inch.

The analytical techniques used for the assessment of dynamic dam behavior involve the use of mathematical models that are based on simplifying assumptions. In addition, the significant properties of the soil used in the analytical methods are determined on the basis of an incomplete knowledge of soil behavior. It would be hardly worthwhile to utilize more exact mathematical models in view of the difficulty in determining non-linear properties of the materials comprising the embankment. However, in view of the valid assessment of the seismic stability of earth dams as obtained from analytical procedures during recent years, it is reasonable to expect that the results obtained for Knightville Dam are representative of the probable performance of the dam during future earthquakes.

B. RECOMMENDATIONS

Based on the conclusions stated above it is recommended that the present flood control operation of the reservoir be continued without change. This type of operation would reduce the risk of damage to the dam in the event of a major earthquake. There are two reasons for the reduced risk:

1. The present operation consists of water release from the reservoir very soon after it has been stored, therefore there is little time for the core to become saturated; an unsaturated material is not susceptible to liquefaction.

2. If the full reservoir level is maintained only for a short period of time, the risk of simultaneous occurrence of the Maximum Credible Earthquake is minimal.

The dynamic response analysis reported herein is based on material properties determined at the crest centerline and 180 ft downstream of the centerline between Stations 7+40 and 7+76. If in the future a change in reservoir operation is contemplated, an additional field and laboratory investigation should be performed to confirm that the soil properties determined at these stations are representative of the remainder of

the embankment. If major differences in soil characteristics are found to exist, it may be necessary to retrofit the dam so that its stability will not be impaired by seismic events after the change in reservoir operation is put into effect. Such modifications may include:

- Densification and/or strengthening of the hydraulic core using methods such as: vibroflotation, electro-osmosis, chemical grouting, compaction piles, and pumping.
- Widening of the crest and flattening of the slopes combined with heightening of the dam.
- Increasing the amount of available freeboard by constructing a parapet wall along the upstream embankment crest edge.
- Replacement of existing "stiff" rolled fill section with a more flexible material that would be able to deform without cracking.

REFERENCES

- Ambraseys, N.N. and Sarma, S.K. (1967), "Response of Earth Dams to Strong Earthquakes," Geotechnique, Vol. 17, No. 3.
- ASCE (1978), "Definition of Terms Related to Liquefaction," Journal of the Geotechnical Engineering Division, ASCE, Vol. 104, GT 9, September.
- Bain, G.W. and Meyerhoff, H.A. (1942), The Flow of Time in the Connecticut Valley, Geologic Imprints.
- Battis, J. (1981), "Regional Modification of Acceleration Attenuation Functions," Bulletin, Seismological Society of America, No. 71, 1309-1321.
- Billings, M.P. (1941), "Pegmatites of Massachusetts," U.S. Geological Survey Cooperative Project Bulletin No. 5, (also, Massachusetts Department of Public Works Bulletin, Vol. 5, pp. 22).
- Bishop, A.W. (1955), "The Use of the Slip Circle in the Stability Analysis of Slopes," Geotechnique, Vol. 5, No. 1, pp. 7-17.
- Bureau of Reclamation (1976), "Dynamic Analysis of Embankment Dams," Bureau of Reclamation Engineering and Research Center, Denver, Colorado.
- Castro, G. and Poulos, J. (1976), "Factors of Affecting Liquefaction and Cyclic Mobility," ASCE Specialty Conference on Liquefaction Problems in Geotechnical Engineering, Philadelphia, September, pp. 105-139.
- Duncan, J.M., Byrne, P., Wong, R.S. and Mabry, P. (1980), "Strength, Stress-Strain and Bulk Modulus Parameters for Finite Element Analysis of Stresses and Movements in Soil Masses," Engineering Research Center Report No. UCB/FT/80-01, Department of Civil Engineering, University of California, Berkeley.

REFERENCES (Cont'd)

- Duncan, J.M., Wong, R.S., and Ozawa, Y. (1980), "A Computer Program for Finite Element Analysis of Dams," Engineering Research Center Report No. UCB/BT/80-02, Department of Civil Engineering, University of California, Berkeley.
- Emerson, B.K. (1917), "Geology of Massachusetts and Rhode Island," U.S. Geological Survey Bulletin 597, (including preliminary geologic map of Massachusetts and Rhode Island, scale 1:250,000).
- Fenneman, N.M. (1938), Physiography of Eastern United States, McGraw-Hill Book Company, Inc., pp. 343-390.
- Fischer, J.A. and Cox, F.L. (1967), "The Seismicity of Massachusetts," Proceedings, Conference on Economic Geology in Massachusetts, University of Massachusetts, Amherst.
- Franklin, A.G., and Chang, F.R. (1977), "Permanent Displacements of Earth Embankments by Newmark Sliding Block Analysis," Miscellaneous Paper S-71-17, U.S. Army Engineer Waterways Experiment Station, Vicksburg, Mississippi.
- Gibbs, H.J., and Holtz, W.G. (1957), "Research on Determining the Density of Sands by Spoon Penetration Testing," Proceeding, Fourth International Conference on Soil Mechanics and Foundation Engineering, London.
- Gurley, R.C. (1967), "Geology in the Design and Construction of the Littleville Dam, Massachusetts," Proceedings, Conference on Economic Geology in Massachusetts, Amherst, Massachusetts.
- Gutenberg, B. and Richter, C.F. (1942), "Earthquake Magnitude, Intensity and Acceleration," Bulletin, Seismological Society of America, No. 32, pp. 163-191.

REFERENCES (Cont'd)

- Hall, B.A. (1970), "Stratigraphy of the Southern End of the Munsungun Anticlinorium, Maine," Maine Geological Survey, Bulletin 22, Department of Economic Department, Augusta, Maine, pp.5-9.
- Harris, C.W. (1981), "Methods of Evaluating Dynamic Embankment Response," Bureau of Reclamation Technical Memorandum, No. 222-TS-1.
- Hatch, N.L., Jr. (1968), "Isoclinal Folding Indicated by Primary Sedimentary Structures in Western Massachusetts," U.S. Geological Survey Professional Paper 600-D, pp. D108-114.
- Hendron, A.J., Cording, F.J., and Aiyer, A.K. (1971), "Analytical and Graphical Methods for the Analysis of Slopes in Rock Masses," NCG Technical Report No. 36, University of Illinois.
- Hendron, A.J. and Fernandez, G. (1977), "Report on the Dynamic Stability of Chatuge and Nutterly Dams," University of Illinois.
- Hunt, C.B. (1967), Physiography of the United States, W.H. Freeman and Company, San Francisco, A., pp. 166-204.
- Hynes-Griffin, M.E. (1979), "Dynamic Analysis of Earth Embankments for the Richard B. Russel Dam and Lake Project," Report to U.S. Army Engineer District, Savannah; U.S. Army Waterways Experiment Station, Vicksburg, Mississippi.
- Jackson, R.A. (1975), "Structural Geology and Stratigraphy of the Huntington Area, Massachusetts," Contribution No. 21, Geology Dept., University of Massachusetts, Amherst, Massachusetts.
- Jahns, R.H. and Willard, M.E. (1942), "Late Pleistocene and Recent Deposits in the Connecticut Valley, Massachusetts," American Journal of Science, Vol. 240, No. 3, pp. 161-191.

REFERENCES (Cont'd)

- Jahns, R.H. (1947), "Geologic Features of the Connecticut Valley, Massachusetts, as Related to Floods," U.S. Geological Survey-Water Supply Paper 996.
- Johnson, J. (1977), "New England Upland Section," Internal Report, School of Civil Engineering, Purdue University, West Lafayette, Indiana (No. 52).
- Jorgansen, N. (1971), A Guide to New England's Landscape, Barre Publishers, Barre, Massachusetts, pp. 250.
- Klimkiewicz, G. (1980), Earthquake Ground Motion Alternation Models for the Northeastern United States, M.S. Thesis, Boston College, Chestnut Hill, Ma., pp. 165.
- Kulhawy, F.H., Duncan, J.M. and Seed, H.B. (1969), "Finite Element Analysis of Stresses and Movements in Embankments During Construction," Geotechnical Engineering Report, No. TE-69-4, Department of Civil Engineering, University of California, Berkeley.
- Ladd, C.C. (1975), "Foundation Design of Embankments Constructed on Connecticut Valley Varved Clays," Research Report R75-7, Geotechnical Publication 343, M.I.T., Cambridge, Massachusetts.
- Lysmer, J., Udaka, T., Seed, H.B. and Hwang, R. (1974) "LUSH - A Computer Program for Complex Response Analysis of Soil-Structure Systems," Earthquake Engineering Research Center Report, No. EERC 74-4, Department of Civil Engineering, University of California, Berkeley.

REFERENCES (Cont'd)

- Lysmer, J., Udaka, T., Tsai, C.F. and Seed, H.B. (1975), "FLUSH - A Computer Program for Approximate 3-D Analysis of Soil-Structure Interaction Problems," Earthquake Engineering Research Center Report No. EERC 75-30, Department of Civil Engineering, University of California, Berkeley.
- Makdisi, F.I. and Seed, H.B. (1977), "A Simplified Procedure for Estimating Earthquake - Induced Deformations in Dams and Embankments," Earthquake Engineering Research Center Report No. UCB/EERC-77/19, Department of Civil Engineering, University of California, Berkeley.
- Makdisi, F.I., Seed, H.B. and Idriss, I.M. (1978), "Analysis of Chabot Dam During the 1906 Earthquake," ASCE Specialty Conference on Earthquake Engineering and Soil Dynamics, Pasadena, Vol. II, pp. 569-588.
- Marcuson III, W.F., and Krinitzsky, E.L. (1976), "Dynamic Analysis of Fort Peck Dam," Technical Report No. S-76-1, U.S. Army Waterways Experiment Station, Vicksburg, Mississippi.
- Marcuson III, W.F., Dennis, W.D., and Cooley, L.A. (1978), "Effect of Load Form and Sample Reconstitution on Test Results," ASCE Specialty Conference on Earthquake Engineering and Soil Dynamics, Pasadena, Vol. II, pp. 588-600.
- Marcuson III, W.F., Hadaka, P.F. and Franklin, A.G. (1980), "Current Methods of Dynamic Analysis for Seismic Stability of Earth Dams," International Society of Engineering Geology, Vol. 16, pp. 19-28.
- Morgenstern, N.R. and Price, V.E. (1965), "The Analysis of the Stability of General Slip Surfaces," Geotechnique, Vol. 15, No. 1, pp. 79-93.

REFERENCES (Cont'd)

- Murphy, D.J., Koutsoftas, D., Covey, J.N. and Fisher, J.A. (1978), "Dynamic Properties of Hard Glacial Till," ASCE Specialty Conference on Earthquake Engineering and Soil Dynamics, Pasadena, Vol. II, pp. 636-657.
- Nuttli, O.W. (1979), "The Relation of Sustained Maximum Ground Acceleration and Velocity to Earthquake Intensity and Magnitude," State-of-the-Art for Assessing Earthquake Hazard in the U.S., Report 16, WES, Corps of Engineers, Vicksburg, Mississippi, pp. 100.
- Nuttli, O.W. and Hermann, R.B. (1981), "Consequences of Earthquake in the Mississippi Valley, ASCE, Preprint No. 81-519.
- Ozawa, Y. and Duncan, J.M. (1973), "ISBUILD: A Computer Program for Analysis of Static Stresses and Movement in Embankments," Geotechnical Engineering Report No. TE-73-4, Department of Civil Engineering, University of California, Berkeley.
- Pessl, F. and Schafer, J.P. (1968), "Two-Till Problem in Naugatuck-Torrington Area, Western Connecticut," Trip B-1 of Guidebook for Fieldtrips in Connecticut, New England Intercollegiate Geological Conference, 60th Annual Meeting, Yale University, New Haven, Connecticut, pp. 9-17.
- Quinn, A.W. (1967), "Deposits of the 'Mineral Belt' of Western Massachusetts," Proceedings, Conference on Economic Geology in Massachusetts, Amherst, Massachusetts.
- Raisz, Erwin (1967), "Geologic Block Diagram of Part of Massachusetts," Proceedings, Conference on Economic Geology in Massachusetts, Amherst, Massachusetts.
- Roberts, W.S. (1976), "Regionalized Feasibility Study of Cold Weather Earthwork," Special Report 76-2, Corps of Engineers, U.S. Army, Cold Region Research and Engineering Laboratory, Hanover, New Hampshire, pp. 190.

REFERENCES (Cont'd)

- Sarma, S.K. (1973), "Stability Analysis of Embankments and Slopes," Geotechnique, Vol. 23, No. 3, pp. 423-433.
- Sarma, S.K., and Bhave, M.V. (1974), "Critical Acceleration versus Static Factor of Safety in Stability of Earth Dams and Embankments," Geotechnique, Vol. 24, No. 4, pp. 661-665.
- Sarma, S.K. (1975), "Seismic Stability of Earth Dams and Embankments," Geotechnique, Vol. 25, No. 4, pp. 743-761.
- Schnabel, P.B., Lysmer, J. and Seed, H.B. (1972), "A Computer Program for Earthquake Response Analysis of Horizontally Layered Sites," Earthquake Engineering Research Center Report No. EERC 72-12, Department of Civil Engineering, University of California, Berkeley.
- Seed, H.B. and Goodman, R. (1964), "Earthquake Stability of Slopes of Cohesionless Soils," Journal of the Soil Mechanics and Foundations Division, ASCE, No. SMG, pp. 43-73.
- Seed, H.B. Et Al. (1970), "Soil Moduli and Damping Factors for Dynamic Response Analysis," Earthquake Engineering Research Center Report No. EERC 70-10, Department of Civil Engineering, University of California, Berkeley.
- Seed, H.B. and Peacock, W.H. (1971), "Test Procedures for Measuring Soil Liquefaction Characteristics," Journal of the Soil Mechanics and Foundation Division, ASCE, Vol. 97, No. SM8, pp. 1099-1119.
- Seed, H.B. and Idriss, I.M. (1977), "Simplified Procedure for Evaluating Soil Liquefaction Potential," Journal of the Geotechnical Engineering Division, ASCE, Vol. 97, No. SM9, pp. 1249-1273.

REFERENCES (Cont'd)

- Seed, H.B., Lee, K.L., Idriss, I.M. and Makdisi, F.I. (1973), "Analysis of the Slides in the San Fernando Dams During the Earthquake of February 9, 1971," Earthquake Engineering Research Center Report No. EERC 73-2, Department of Civil Engineering, University of California, Berkeley.
- Seed, H.B., Idriss, I.M., Makdisi, F.I. and Banerjee, N. (1975), "Representation of Irregular Stress Time Histories By Equivalent Uniform Stress Series in Liquefaction Analysis," Earthquake Engineering Research Center Report No. EERC 75-29, Department of Civil Engineering, University of California, Berkeley.
- Seed, H.B. (1976), "Evaluation of Soil Liquefaction Effects on Level Ground During Earthquakes," ASCE Specialty Conference on Liquefaction Problems in Geotechnical Engineering, Philadelphia, pp. 1-105.
- Seed, H.B., Makdisi, F.I. and DeAlba, P. (1977), "The Performance of Earth Dams During Earthquakes," Earthquake Engineering Research Center Report No. UCB/EERC-77/20, Department of Civil Engineering, University of California, Berkeley.
- Seed, H.B. and Makdisi, F.I. (1979), "Simplified Procedure for Evaluating Embankment Response," Journal of the Geotechnical Engineering Division, ASCE Vol. 105, No. GT12, pp. 1427-1435.
- Seed, H.B. (1981), "Earthquake-Resistant Design of Earth Dams," Proceedings International Conference on Recent Advances in Earthquakes Engineering and Soil Dynamics, Vol. 3, pp. 1157-1173.
- Seed, H.B. (1981), "Stability of Slope and Embankment Dams During Earthquakes," Session No. 7, International Conference on Recent Advances in Geotechnical Earthquake Engineering and Soil Dynamics, St. Louis, Missouri.

REFERENCES (Cont'd)

- Seed, H.B. and Idriss, I.M. (1981), "Evaluation of Liquefaction Potential of Sand Deposits Based on Observations of Performance in Previous Earthquakes," From Preprint 81-544, ASCE National Conference Session No. 24, In-Situ Testing to Evaluate Liquefaction Susceptibility, St. Louis, Missouri.
- Serff, N., Seed, H.B., Makdisi, F.I., and Chang, C.Y. (1976), "Earthquake Induced Deformation of Earth Dams," Earthquake Engineering Research Center Report No. EERC 76-4, Department of Civil Engineering, University of California, Berkeley.
- Slemmons, D.B. and Glass, C.E. (1978), "Remote Sensing Analysis of Fault-Related Structures in New England and Related Seismic Hazards at Corps of Engineers Projects," for NED, August, 1978.
- Slemmons, D. B., Sanders, C., and Whitney, R. A. (1980), "Low-Sun Angle Aerial Reconnaissance of Faults and Lineaments of Southern New England," Report to U.S. Army Corps of Engineers, New England Division, July.
- Stanley, R.S. (1968), "Metamorphic Geology of the Collinsville Area," Trip D-4 of Guidebook for Fieldtrips in Connecticut, New England Intercollegiate Geological Conference, 60th Annual Meeting, Yale University, New Haven, Connecticut, pp. 17.
- Stoeck, P.L. (1975), "Petrology and Contact Effect of the Hatfield Pluton of Belchertown Tonalite in the Whaley-Northampton Area, Western Massachusetts," Contribution No. 7, Geology Department, University of Massachusetts, Amherst, Massachusetts.
- Thornbury, W.D. (1965), Regional Geomorphology of the United States, John Wiley and Sons, Inc., New York, pp. 152-175.
- U.S. Army Corps of Engineers (1939), Analysis of Design, Knightville Dam, Westfield River, Massachusetts.
- U.S. Army Corps of Engineers (1941), Final Report on Construction, Contract No. W-699-eng-848, September 1, 1938 to December 13, 1941, by Geo. M. Brewster and Son, Inc.

REFERENCES (Cont'd)

- U.S. Army Corps of Engineers, (1980), Liquefaction and
and Cyclic Mobility Potential, Completed New England
Dams, PHASE I - Investigation, September.
- U.S. Army Corps of Engineers (1981), Liquefaction and
Cyclic Mobility Potential, Completed New England
Dams, PHASE II - Investigation, 2 Volumes,
February.
- Williams, H., Turner, F.J. and Gilbert, C.M. (1954),
Petrography, W.H. Freeman and Company, San Francisco,
California.